MODELING THE EMISSIONS OF NITROUS OXIDE (N_2O) AND METHANE (CH_4) FROM THE TERRESTRIAL BIOSPHERE TO THE ATMOSPHERE

by

Yuexin Liu

B.S., Beijing University
(1988)

Submitted to the Department of
Earth, Atmospheric and Planetary Sciences
in partial fulfillment of the requirements for the degree of

Doctor of Philosophy in Global Change Science

at the

MASSACHUSETTS INSTITUTE OF TECHNOLOGY

August 1996

Author .....
Center for Meteorology and Physical Oceanography
Joint Program on the Science and Policy of Global Change
August 9, 1996

Certified by .....
Ronald G. Prinn
TEPCO Professor of Atmospheric Chemistry
Thesis Supervisor

Accepted by .....
Thomas H. Jordan
Head, Department of Earth, Atmospheric, and Planetary Sciences

MODELING THE EMISSIONS OF NITROUS OXIDE (N_2O) AND METHANE (CH_4) FROM THE TERRESTRIAL BIOSPHERE TO THE ATMOSPHERE

by

Yuexin Liu

Submitted to the Department of
Earth, Atmospheric and Planetary Sciences
on August 9, 1996, in partial fulfillment of the
requirements for the degree of
Doctor of Philosophy in Global Change Science

Abstract

The overall goals of this thesis are to examine quantitatively the controls which climate has on natural emissions of N_2O and CH_4 from the terrestrial biosphere to the atmosphere and to explore the feedbacks between climate and the N_2O and CH_4 cycles. A process-oriented global model for soil N_2O emissions and a more empirically based global model for wetland CH_4 emissions have been developed to address these goals. These emission models are capable of quantifying the natural emission changes due to climate change and the feedback of the natural emissions onto the climate system.

The global emission model for N_2O, which focuses on soil biogenic N_2O emissions, has a $2.5° \times 2.5°$ spatial resolution. The model can predict daily emissions for N_2O, N_2, NH_3 and CO_2 and daily soil uptake of CH_4. It is a process-oriented biogeochemical model including all those soil C and N dynamic processes for decomposition, nitrification, and denitrification in Li et al.'s [*1992a, b*] site model. The model takes into account the spatial and temporal variability of the driving variables, which include vegetation type, total soil organic carbon, soil texture, and climate parameters. Climatic influences, particularly temperature and precipitation, determine dynamic soil temperature and moisture profiles and shifts of aerobic-anaerobic conditions.

The methane emission model is developed specifically for wetlands and has a spatial resolution of $1° \times 1°$. There are three components for the global wetland methane emission model: high latitude wetlands, tropical wetlands and wet tundra. For high latitude wetlands (i.e. northern bogs), the emission model uses a two-layer hydrological model [*Frolking, 1993*] to predict the water table level and the bog soil temperature, which are then used in an empirical formula to predict methane emissions. For tropical wetlands (i.e. swamps and alluvial formations), a two-factor model (temperature and water availability) is used to model the methane flux by taking into account the temperature and moisture dependence of activity of methanogens. Methane emis-

sions from wet tundra are calculated by assuming a constant small methane flux and an emission season defined by the time period when the surface temperature is above the freezing point. The hydrological model and the two-factor model are driven by surface temperature and precipitation, which links methane emission with climate.

For present-day climate and soil data sets the N_2O emission model predicts an annual flux of 11.3 Tg-N/year (17.8 Tg N_2O/year). The spatial distribution and seasonal variation of the modeled current N_2O emissions are similar to climate patterns, especially the precipitation pattern. Chemical transport model experiments using the modeled soil N_2O emissions plus prescribed other (minor) emissions show good agreement with observations of trends of surface N_2O mixing ratios and the N_2O interhemispheric gradient [*Prinn et al., 1990*]. Sensitivity experiments suggest that soil organic carbon content, precipitation and surface temperature are the dominant factors in controlling global N_2O emissions.

The global CH_4 emission model predicts an annual flux of 127 Tg CH_4/year for present-day climate and wetland conditions, which is in the middle of the range of recent estimates for natural wetland emissions [*Bartlett and Harriss, 1993; Reeburgh et al., 1993; IPCC, 1994*]. Global methane emissions have two strong latitudinal bands with one in the tropics and the other in the northern high latitudes. There are strong seasonal cycles for the high latitude CH_4 emissions and hence for the global total emission amount.

The emission models for N_2O and CH_4 have been applied to two extreme climatic cases: that associated with doubling current CO_2 levels and that during the last glacial maximum. While predicted equilibrium climates from three climate models (MIT 2D, GISS and GFDL GCMs) have been used in both cases, predicted soil organic carbon from terrestrial ecosystem model [TEM, *Melillo et al., 1993*] have been used in the "doubled-CO_2" case and CLIMAP data [*1981*] have been used in the "ice age" case. Results indicate that equilibrium climate changes due to doubling CO_2 would lead to a 34% increase in N_2O emissions and a 54% increase in natural wetland CH_4 emissions. Temperature increases seem to dominate the contribution to increases in N_2O and CH_4 emissions. Geographical coherence of predicted changes in surface temperature and precipitation is significant in determining the predicted changes in global emissions. Ice age soil N_2O emissions and wetland CH_4 emissions are predicted to be significantly smaller (about 50% of current emissions).

Finally, the emission models were coupled with 2D climate and chemistry models developed at MIT [*Sokolov and Stone, 1995; Wang, Prinn and Sokolov, 1996*]. Model results indicate that changes in natural N_2O and CH_4 emissions corresponding to long term climate changes are significant. Predicted N_2O and CH_4 emissions indicate significant sensitivity to outputs from the climate (surface temperature and precipitation) and TEM (total soil organic carbon) models. Fully interactive runs show that there is a significant positive feedback between emissions and climate.

Thesis Supervisor: Ronald G. Prinn
Title: TEPCO Professor of Atmospheric Chemistry

Acknowledgements

Completion of this dissertation has depended on the advice, help and support of many people. First and foremost, I would like to thank my advisor, Ron Prinn, for his numerous discussions and invaluable advice and encouragement which have allowed me to pursue the interdisciplinary and challenging topics in this work.

I have benefited greatly from my experience at MIT. I would like to thank the faculty of the Center for Meteorology and Physical Oceanography for their help with my doctoral education. They have created a great learning environment. I especially wish to acknowledge my committee for their contribution to my education and their criticism and advice: Mario Molina, Alan Plumb and Reginald Newell.

I have been most fortunate to have worked with a diverse group of people and to have received tremendous help from them. I would like to sincerely thank Andrei Sokolov and Chien Wang for the coupled-climate-chemistry model; Xiangming Xiao for the offline outputs of the terrestrial ecosystem model; Amram Golombek for the 3-D chemical transport model; Peter Stone for the ice age data; Changsheng Li and Steve Frolking for DNDC model and bog hydrology model; Bob Boldi for his software SPLOT; and NCAR, GISS and CDIAC for providing variety of data sets.

This research was conducted within the MIT Center for Global Change Science and the MIT Joint Program on Science and Policy of Global Change. Interactions with people from different backgrounds were the most important part of my education at MIT. I would like to thank the Global Change Joint Program and Center for Global Change Science faculty, research scientists and fellow graduate students for day-to-day discussions, advice, support and company, especially Andrei Sokolov, Chien Wang, Xiangming Xiao, Zili Yang, Jean Fitzmaurice, Gary Holian, Mort Webster in the Global Change Joint Program; and Natalie Mahowald, John Graham, Xianqian Shi, Gary Kleiman and Jin Huang in the Center for Global Change Science. All my friends at MIT have helped me one way or another in finishing this thesis.

Finally but most importantly, I would like to thank my wife, Cecilia Xie, whose constancy of love has sustained me to enjoy these years and look forward to others.

This research was supported by the MIT Joint Program on the Science and Policy of Global Change and by grants from NSF (ATM-92-16340), NASA (NAGW-474, NAG1-1805), DOE/NIGEC (901214-HAR), and EPRI (WO 3441-04).

Contents

List of Figures

List of Tables

Chapter 1

Introduction

Nitrous oxide (N_2O) and methane (CH_4) are important trace gases in the atmosphere as a result of both their radiative and chemical effects. On a molecule per molecule basis and in a time horizon of 20 years, the relative potential of cumulative thermal absorption for N_2O is about 290 times as large as CO_2 and that for CH_4 is about 60 times as large as CO_2 [*IPCC, 1994*]. N_2O is the primary source for stratospheric NO, which is involved in a catalytic cycle in depleting stratospheric ozone. CH_4 plays an important role in atmospheric chemistry through its reaction with OH and ensuing chemical feedbacks.

Both N_2O and CH_4 are steadily increasing in the atmosphere with averaged rates of 0.8% per year for CH_4 and 0.25% per year for N_2O [*IPCC, 1994*]. Natural emissions of these two gases, which are the focus of this thesis, play important roles in determining their total emissions and feedbacks between their emissions and the natural climate system. Soil N_2O emissions and wetland CH_4 emissions which are addressed specifically in this thesis account for around 65% and 20% of total N_2O and CH_4 emissions (see Table 1.1 and Table 1.2). These natural emissions are closely connected with climate and ecological variables and the interactions among emissions, climate and ecological variables constitute potentially important feedbacks in the global system. For example, climate change directly influences the natural emissions of N_2O and CH_4 and soil organic carbon and nitrogen storage. Perturbations in soil organic carbon and nitrogen storage could then indirectly affect the natural emissions. Furthermore,

Table 1.1: Estimated Emissions (in Tg-N) for N_2O Sources [*IPCC, 1994*]

Source Description	Estimated Emissions	Uncertainties
Natural Soils	6	3.3—9.7
Cultivated Soils	3.5	1.8—5.3
Ocean	3	1—5
Biomass Burning	0.5	0.2—1.0
Industrial Sources	1.3	0.7—1.8
Other Minor Sources	0.4	0.2—0.5
Total	14.7	10-17

N_2O and CH_4 when emitted into the atmosphere could change climate itself through their radiative and chemical effects. These potential roles in the climate system of natural N_2O and CH_4 emissions highlight the importance of scientific understanding of the processes governing their production and accurate prediction of their emissions and the changes in their emissions resulting from climate change. Even though the surface sources and sinks of these gases often have large uncertainties (see Table 1.1 and Table 1.2 for N_2O and CH_4 emission estimates), better understanding of their natural emissions and how these emissions may change can help us better determine the impacts of these two trace gases and help policy-makers make better decisions when they are debating regulations on anthropogenic sources of N_2O and CH_4.

Numerous researchers have been working on the trace gases N_2O and CH_4 with a significant fraction of the work focusing on long-term global measurements [*Steele et al., 1987; Blake and Rowland 1988; Weiss 1981; Prinn et al., 1990; Prinn et al., 1995*] and measurements of emissions at specific locations [*Bartlett and Harriss, 1993; Keller and Matson, 1994*]. To date, we have as a result a lot of data available for N_2O and CH_4 atmospheric concentrations and site-specific emissions and based on these data, a lot of work has been done to estimate the regional and global sources of N_2O and CH_4.

The approaches in determining trace gas sources can be classified into three broad categories. One of these is the flux extrapolation method. Emission flux measurements made at individual sites are extrapolated to larger scales using mapping pro-

Table 1.2: Estimated Emissions (in Tg CH_4) for CH_4 Sources [*IPCC, 1994*]

Source Description	Estimated Emissions	Uncertainties
Wetlands	115	55—150
Termites	20	10—50
Oceans	10	5—50
Other Natural Sources	15	10—40
Fossil Fuel Related	100	70—120
Enteric Fermentation	85	65—100
Rice Paddies	60	20—100
Biomass Burning	40	20—80
Landfills	40	20—80
Animal Waste	25	20—30
Domestic Sewage	25	20—30
Total	535	410-660

cedures to obtain the regional or global emissions. Because available *in situ* flux measurements are geographically very sparse given the scope of the globe, large uncertainties must be involved in the estimates obtained using this flux extrapolation method.

Another approach is the inverse method. The inverse method involves the use of an atmospheric chemical transport model. The model-predicted concentrations are compared with the observed concentrations of trace gases to determine by optimal estimation procedures what distribution of the sources best simulates the observations. Inverse method studies using 2-D [*Cunnold et al., 1983, 1986; Prinn et al., 1990*] and 3-D CTMs(chemical transport model) [*Hartley and Prinn, 1993*] have shown the great potential of this approach for determining the global surface sources of trace gases. However, the imperfect atmospheric circulation in current CTMs places limititations on the current use of the inverse method; specifically when used for estimating regional emissions, the inverse method involves large uncertainties [*Hartley, 1993; Mahowald, 1996*].

Both the extrapolation method and inverse method do not give us insight about what processes are primarily responsible for the trace gas emissions. They enable quantification of the current state but are not capable of addressing issues such as

the emission-related feedbacks we have described.

A third approach involves process-oriented models. If such models are good at simulating trace gas emissions at individual sites, they may be a powerful tool for estimating regional and global emissions of the trace gases. For the latter estimations we need to know the global distribution of the controlling parameters and, for assessing the feedbacks, we need to connect the emission processes with climate processes. The use of process-oriented models without considering horizontal interactions (e.g. horizontal heat and moisture flows in a soil model) could be categorized as an extrapolation method. However, a process-oriented model does not use a simple extrapolation of the relevant variables (e.g. the flux). It is therefore useful to distinguish this method from the extrapolation method. Because a process-oriented model is based on an understanding of the biogeochemistry of trace gas production, the approach using a process-oriented model to estimate the global emissions does not omit explicit connections to the flux-driving varialbes which is unavoidable in simply extrapolating the measured flux to the whole globe.

Global models exist which attempt to simulate the global emissions of N_2O and CH_4 by considering a variety of complex regulating parameters or by synthesizing the available flux measurements and known sources [*Bouwman et al., 1993; Fung et al., 1991*]. However, the main regulating factors of nitrous oxide emissions were treated by an arbitrarily assumed function in Bouwman *et al.* [*1993*] and inadequate OH simulation [*Hartley and Prinn, 1991; Cunnold and Prinn, 1991; Prinn et al., 1995*] and an arbitrary assumption about methane emission by season were used in Fung *et al.* [*1991*] to deduce the methane budget. Nevison *et al.* [*1996*] has done a detailed synthesis for N_2O emission sources with a Nitrogen Biosphere Model (NBM) for soil N_2O emissions. The NBM is based on an existing carbon cycle biosphere model designed for modeling net primary productivity and it does not incorporate those dynamic processes which are vitally important for soil N_2O production. Bartlett and Harriss [*1993*] have done an excellent review on wetland CH_4 emissions but have given an estimate of global wetland CH_4 emissions using an arbitrary assumption about methane emission by season similar to that used in Fung *et al.* [*1991*].

One of the common shortcomings of these various global emission models is that they do not connect emissions with climate parameters and are not therefore capable of addressing the changes in emissions corresponding to climate change and the emission-related feedbacks in the climate system.

This thesis work had the objective to set up accurate emission models for N_2O and CH_4 which have detailed biogeochemical processes and are capable of coupling with climate and chemistry models and thus addressing the natural feedback issue. To meet this objective, a process-oriented global N_2O emission model and a more empirically based global CH_4 emission model have been developed. The biogeochemical climate-driven global emission model for N_2O is designed to model N_2O emissions from soils, which is the major N_2O source connected directly with climate. It includes all those soil C and N dynamic processes for decomposition, nitrification, and denitrification in Li *et al.*'s [*1992a,b*] site model. The model has a soil hydrology component model which dynamically simulates soil temperature and moisture profiles and shifts of aerobic-anaerobic conditions and creates an interface for coupling with a climate model. The global emission model for CH_4 is specifically designed for modeling wetland CH_4 emissions, which is the major CH_4 source connected with climate parameters. Because the nutrients used in CH_4 production processes are currently not fully understood, setting up a process-oriented global model for CH_4 turns out to be unrealistic at the present time. The global wetland CH_4 emission model has therefore been designed in a more empirical way, but still with the flux-controlling parameters tied with climate parameters, which again provides the link for coupling with climate model.

Chapter 2 describes the elements of the global N_2O emission model and presents results for current N_2O emissions and sensitivity experiments. Similarly, Chapter 3 is devoted to the description of the CH_4 model and results for current CH_4 emissions. Because soil N_2O emissions account for a large portion of total N_2O emissions and predicted current soil N_2O emissions have distinct patterns, it is possible to test the emission model by comparing the results of simulations using a chemical transport model (with modeled emissions as input) with observations. The model testing results

are described in Chapter 4. To test how sensitive the response of emission change is to climate change, the emission models developed for N_2O and CH_4 are applied to two extreme climatic cases: that associated with doubling current CO_2 levels and that during the last ice age. These two applications are described in Chapter 5 and Chapter 6. Chapter 7 addresses the work done to couple the emission models to climate and chemistry models and to quantify the emission feedbacks. Finally, the summary and overall conclusions of the thesis are given in Chapter 8.

Chapter 2

Development of Global N_2O Emission Model

2.1 Introduction

The global biogeochemical emission model for N_2O is based on a site emission model developed by Li *et al.* [*1992a, b*] which incorporates the important microbiological and physical processes for soil N_2O production and emission. Because microbiolgists are concerned with biochemical processes and production mechanisms, such site models are usually used to model the behavior of bacteria in a small area which they usually assume to be horizontally homogeneous. In this sense, a site model is really a one-dimensional (or sometimes 0-dimensional) "point source" model.

Li *et al*'s site model is a rainfall-driven, temperature-regulated process model for decomposition, nitrification and denitrification. This site model focuses on the nitrogen and carbon biogeochemistry for agricultural soils and can predict N_2O, CO_2, and N_2 emissions and CH_4 uptake. Nitrification-based N_2O production is calculated in Li *et al*'s model from a submodel for soil organic matter decomposition while N_2O production through denitrification is calculated from another separate submodel which includes calculations for the growth and maintenance of denitrifying bacteria. The model also allows for consumption of N_2O. Model inputs include climate variables (precipitation and surface temperature), soil physical and chemical properties, and

soil organic carbon and nitrogen contents. Agricultural practices (e.g. fertilizer application) and other anthropogenic activities (e.g. deforestation) which would change the soil C and N contents and/or organic matter decomposition rate are considered in the model by treating them as exogenous variables.

The global emission model for N_2O generally adopts the basic biogeochemical processes for decompostion, nitrification and denitrification in Li *et al*'s site model but extends by hypothesis the dynamic processes to other ecosystems besides the agricultural soils. The extension is done by taking into account the global spatial variability of driving variables, which include ecosystem type, soil texture, soil organic carbon and nitrogen, and climate parameters. Ideally, soil biogeochemical processes should be incorporated into a terrestrial ecosystem model to dynamically model the evolution of soil C and N pools and thus the emissions of various trace gases. However, such a complex task is beyond the scope of this thesis. The global N_2O emission model designed here simply parameterizes the interactions between soil biogeochemical processes and other ecological processes (e.g. photosynthesis, plant growth) by using an exogenous variable—soil organic carbon.

2.2 Main Processes Relevant to N_2O Emission

The biological nitrogen cycle of the Earth begins by fixation of atmospheric nitrogen (N_2) to ammonium (NH_4^+) ions. Biogenic N_2 and nitrous oxide (N_2O) are produced in the soils of terrestrial ecosystems by a wide range of processes involved in the mineral nitrogen cycle. The formed N_2 and N_2O then diffuses into the atmosphere thus completing a loop begun by the above nitrogen fixation.

The major biochemical processes regulating N_2O formation in the soils include decomposition, mineralization, nitrification, denitrification, the dissimilatory reduction of nitrate to ammonium, and the assimilatory reduction of nitrate to ammonium wherein N is incorporated in the cell biomass. Of these processes, nitrification and denitrification are the most important with respect to N_2O production. Even though the decomposition process does not directly produce N_2O, it provides substrates for

nitrification and denitrification. Therefore, the decomposition process is also vital in determining N_2O emissions. In order to predict N_2O emission from soils, it is necessary to separately treat each of these processes.

Denitrification

Denitrification is the reduction process of nitrate to form nitrous oxide and molecular nitrogen. Production of N_2O and N_2 by microbial denitrification occurs when bacteria capable of denitrification colonize a location where oxygen is essentially absent and water, nitrate and decomposed organic compounds (or inorganic compounds capable of providing energy) are present. Microbial denitrification is the process in which nitrate (NO_3^-), nitrite (NO_2^-) and nitrous oxide (N_2O) serve as alternative electron acceptors to O_2 for anaerobic bacteria at low O_2 concentrations, with the result that molecular N_2 can be produced ultimately. The reaction sequence for denitrification can be described as follows:

$$NO_3^- \longrightarrow NO_2^- \longrightarrow [NO] \longrightarrow N_2O \longrightarrow N_2$$

In this reductive pathway nitric oxide [NO] may occur as an intermediate between NO_2^- and N_2O but it's existence has not been assessed unambiguously. Munch [*1991*] showed that the formation of NO_x in soil is related directly to the composition of the denitrifier population, and only indirectly to physiochemical soil properties.

While the processes differ slightly among different studies, it is apparent that soluble carbon and nitrate from the decomposition of organic matter are primarily utilized by denitrifiers as electron donor and acceptor respectively. It is also generally agreed that the principal factors controlling biological denitrification and associated N_2O flux from soils are [*Williams et al., 1992*]: 1) Oxygen status (controlled by soil moisture)—if the soil solution in the vicinity of potential denitrifiers is sufficiently aerobic then denitrification would not occur; 2) Organic carbon substrate—an energy source for denitrifier metabolism; 3) nitrate (also nitrite and nitrous oxide)—electron acceptors; 4) denitrifing bacteria. Unless these four factors are present, significant

biological denitrification does not occur. In addition, soil temperature, texture, pH and land use/land cover affect the activities of denitrifiers and then the N_2O flux from soils, although they are of secondary importance in controlling the occurrence of denitrification.

Nitrification

Nitrification is the process of biological oxidation of NH_4^+ to NO_2^- and NO_3^-, or biologically induced increase in the oxidation state of N. This process plays a significant role in the N cycle because it provides N nutrients for denitrifiing bacteria and affects the overall reduction rate of nitrate in the denitrification process.

The process of nitrification is associated with the metabolism of chemoautotrophic bacteria as well as several species of heterotrophic microorganisms. It is widely accepted that most of the nitrification in soil is accomplished by a few genera of chemoautotrophic bacteria.

The biochemical pathway of chemoautotrophic nitrification remains a subject of much debate. There is good evidence that NH_2OH is the first intermediate product of NH_4^+ oxidation [*Dua et al., 1979*], but subsequent intermediates with N oxidation states +1 and +2 are not known with certainty [*Hooper, 1984*]. The oxidation of NO_2^- to NO_3^- is a simple two-electron shift in N oxidation state from +3 to +5 and involves no intermediates [*Schmidt, 1982*].

There is abundant evidence that N_2O is usually included among the products of chemoautotrophic nitrification [*Aulakh et al., 1984; Hynes and Knowles, 1984*]. Recent evidence suggests that production of N_2O by autotrophic NH_4^+ oxidizers in soil results from a reductive process in which the organisms use NO_2^- as an electron acceptor, especially when O_2 is limiting [*Poth and Focht, 1985*]. Because N_2O results from a reductive process, its importance as a product of nitrification should increase as O_2 availability decreases, but whether that increased importance translates into higher total N_2O production depends on how much the overall process rate is reduced by the limited availability of O_2.

The N_2O yield of nitrification is normally relatively small. Of importance is that

nitrification along with ammonia volatilization, adsorption, and plant uptake interact to control the substrate pools for microbial activities and gaseous emissions of N_2O, N_2, and CO_2.

Decomposition

Decomposition is the process of organic matter breakdown and formation of nutrient substrates [*Swift, 1979*]. It has a "cascade" structure in terms of its substrates and organisms. Complex organic molecules are first broken down to simpler organic molecules. These products have a number of possible fates: 1) they may form the building blocks for the synthesis of the molecular components of decomposer tissues; 2) they may act as the respiratory substrates that fuel the decomposition process; 3) they may be finally transformed to inorganic molecules. Many of the newly synthesised organic molecules in the decomposer tissues or in the soil become the substrates for succeeding cascades of the decomposition processes. In this way, organic matter is recycled through succeeding generations of decomposer organisms, with components of the output molecules of one level of decomposition becoming the inputs to the next level. Because of the "cascade" structure of the decomposition process, it can be conceptually divided into various levels and components. This is what has been done in the decomposition modeling by Li *et al.* and in this thesis.

The decomposition process plays a significant role in N_2O emissions through its control on the cycling of soil C and N pools. Organic carbon is either oxidized to CO_2 through the microbe's respiration or transferred to soluble carbon or other carbon substrates. The soluble carbon is the energy source for the denitrification. Organic N is mineralized to ammonium (NH_4^+) which is then nitrified to nitrate. Nitrate is an important nutrient for the denitrifiers.

2.3 Model Conceptualization

Since denitrification is a key process in controlling N_2O emissions to the atmosphere, the N_2O emission model therefore has to focus on modeling the soil denitrification

rate. This can be done by the quantification of substrate pools (most importantly C and N pools) and their evolution which is controlled by soil temperature and moisture.

Soil Climate Parameters

Many processes that occur in soils, including the microbially mediated cycling of carbon and nitrogen and the trace gas generation discussed above, depend upon the soil climate (soil temperature and soil moisture content). Therefore it is necessary to model soil temperature and moisture profiles. Assuming there are no significant horizontal heat and moisture transports in soils, we can achieve this by using a one-dimensional gradient-driven heat and moisture diffusion model.

The one-dimensional diffusion model for soil climate needs boundary conditions to derive the soil temperature and moisture. The global N_2O emission model requires these boundary conditions to be available in a global scale. Observed surface air temperature and precipitation available at weather stations and extrapolated to fine grids, or outputs from climate models, can fulfil the requirement.

Soil physical properties (e.g. thermal and hydraulic conductivities) which are also required in the one-dimensional diffusion model and hence in the global emission model can be obtained by using available global soil texture data sets.

Oxygen Availability

On the basis of field monitoring and experimentation, emissions of nitrous oxide from soils have episodic peaks, generally associated with soil wetting [*Brumme and Beese,(1992);Mosier et al.(1991)*]. Therefore, it is important to quantify oxygen availability in terms of soil moisture.

The enzymes responsible for the dinitrification reduction sequence seem to become active only when they are in anaerobic conditions [*Firestone, 1982*]. However, it is difficult to quantify this anaerobic condition even in the spatial scale of a microsite. Considering denitrifier activity to be regulated by soil water-filled pore space, Li *et al.* [*1992a*] assume that oxygen availability decreases linearly as water-filled pore

space increases. This approach is much simpler than those considering O_2 diffusion, consumption and production [*McConnaughey and Bouldin (1985); Grant (1991)*]. If we are only interested in trace gas flux emitted to the atmosphere, this simplified approach is probably good enough to capture the episodic nature of denitrification.

Li *et al.* assume that soil moisture or oxygen status is not the limiting factor once the denitrification process has begun. The actively denitrifying soil is considered completely anaerobic if the water-filled pore space reaches above 40%. These same assumptions are used in our global emission model for N_2O.

Nitrogen Substrate

Basically two approaches have been used in modeling N-substrate availability for denitrification. The simple one is supplying nitrate concentration as an input parameter (e.g. *McConnaughey and Bouldin, 1985*). The other one is coupling to a model of aerobic soil decomposition and nitrification processes to generate inorganic N pools (e.g. *Li et al., 1992a*). Both of these approaches will be used in the global emission model. Since soil solution concentrations are relatively easy to measure [*Keeney and Nelson, 1986*] and the resultant end products (NO_3^- and NH_4^+) from nitrification and mineralization are fairly uniform across ecosystems [*Firestone and Davidson, 1989*], typical uniform values can be used as initial values for NO_3^- and NH_4^+. The evolution of NO_3^- and NH_4^+ can be calculated using the decomposition and nitrification component model.

Carbon Substrate

Denitrification as a microbially mediated process needs energy for the denitrifier's metabolism. This is supplied by dissolved organic carbon compounds. The soil soluble carbon substrates are considered to be a byproduct of decomposition and they are used as an explicit substrate for denitrifier activitivities. This approach which is used in Li *et al.* [*1992a*] links denitrification to C mineralizable under aerobic conditions without considering the detailed molecular structure of the C substrate compounds.

The global emission model will also use this simplified approach.

2.4 Model Equations

2.4.1 Soil Hydrology

Soil hydrology is modeled as 1-dimensional heat and moisture diffusion process.

Hydrological Model Equations

Soil water flow (Q) and heat flux (q) equations can be written as follows:

$$Q = -K\frac{dh}{dz} \tag{2.1}$$

$$q = -k\frac{dT}{dz} \tag{2.2}$$

where z is soil depth, K and k are hydraulic conductivity and thermal conductivity, h is hydraulic head and T is temperature.

Water and energy balance equations are constructed by using the above fluxes:

$$\frac{dW}{dt} = \frac{1}{n}\frac{dQ}{dz} \tag{2.3}$$

$$\frac{dT}{dt} = \frac{1}{C}\frac{dq}{dz} \tag{2.4}$$

where W is soil water content which is measured by a fraction of soil pore space ($0 \leq W \leq 1$), n is the soil porosity, and C is the net volumetric heat capacity.

Hydraulic conductivity and hydraulic head depend on soil water parameters and soil water content itself. They are described as follows [*Clapp and Hornberger, 1978*].

$$K = K_{\text{sat}}W^{(2\beta+3)} \tag{2.5}$$

$$h = \begin{cases} \phi_{\text{sat}} W^{-\beta} & \text{if } W < W_* \\ \phi_{\text{sat}} W_*^{-\beta} \times f_1 (W_* - f_2)(1 - W_*) & \text{if } W \geq W_* \end{cases} \tag{2.6}$$

where

$$f_1 = \frac{1}{(1 - W_*)^2} - \frac{\beta}{W_*(1 - W_*)}$$

$$f_2 = 2W_* - 1 - \frac{\beta}{f_1 W_*}$$

and β is a soil water parameter, K_{sat} is the saturated hydraulic conductivity, ϕ_{sat} is the water tension parameter, and W_* (a value of 0.92 is used) is the soil water content where the retention curve has an inflection.

Thermal conductivity and heat capacity also depend on soil porosity and soil water content:

$$k = (1 - n) k_{\text{dry}} + nW k_{\text{water}} \tag{2.7}$$

$$C = \rho_{\text{soil}} c_{\text{soil}} + nW \rho_{\text{water}} c_{\text{water}} \tag{2.8}$$

where k_{dry} is the thermal conductivity of mineral soil, k_{water} is the water thermal conductivity, and ρ and c are density and specific heat respectively.

Soils are categorized into 12 different types in the global N_2O emission model. Some of the physical properties are listed in Table 2.1.

Boundary Conditions

Boundary conditions for the hydrological model are imposed by fluxes at the model domain boundaries.

The heat flux at the soil surface (upper boundary) is simplified to be a gradient-driven flux between the soil surface, which is assigned a temperature equal to the mean daily surface air temperature, and the top soil layer temperature at a depth typically of several centimeters. i.e.

Table 2.1: Soil Type and Properties used in the Hydrological Model [*DeVries, 1975; Clapp and Hornberger, 1978*]

Soil Type	n	K_{sat}	β	ϕ_{sat}	c_{soil}	W_{wp}	W_{fc}	$Clay$
Sand	0.395	1.056	4.05	3.50	2000.0	0.10	0.15	0.03
Loamy Sand	0.410	0.938	4.38	1.78	2000.0	0.13	0.25	0.06
Sandy Loam	0.435	0.208	4.90	7.18	2000.0	0.32	0.32	0.09
Silty Loam	0.485	0.043	5.30	56.60	2000.0	0.20	0.40	0.14
Loam	0.451	0.042	5.39	14.60	2000.0	0.22	0.49	0.19
Sandy Clay Loam	0.420	0.038	7.12	8.63	2000.0	0.24	0.52	0.27
Silty Clay Loam	0.477	0.010	7.75	14.60	2000.0	0.26	0.55	0.34
Clay Loam	0.476	0.015	8.52	36.20	2000.0	0.27	0.57	0.40
Sandy Clay	0.426	0.013	10.40	6.16	2000.0	0.28	0.60	0.43
Silty Clay	0.492	0.006	10.40	17.40	2000.0	0.30	0.63	0.49
Clay	0.482	0.008	11.40	18.60	2000.0	0.35	0.73	0.63
Organic	0.700	0.020	7.75	14.60	2500.0	0.26	0.55	0.06

$$q_s = -k_t \frac{T_t - T_{air}}{z_t} \tag{2.9}$$

where k_t, T_t and z_t are thermal conductivity, temperature and depth for the top soil layer (z_t = 5 cm has been used in the model).

The heat flux at the lower boundary is determined by the gradient between the temperature of the model bottom layer and the annual mean air temperature imposed at a suitably deep level below. i.e.

$$q_b = -k_{bl} \frac{T_{bl} - T_{ama}}{z_{bl} - z_{deep}} \tag{2.10}$$

where k_{bl}, T_{bl} and z_{bl} (=50 cm) are thermal conductivity, temperature and depth for the bottom layer; T_{ama} is the annual mean air temperature; and z_{deep} (=500 cm) is the soil depth at which seasonal temperature variation is assumed to be negligible.

The moisture lower boundary condition is very simple. Water flow at the lower boundary is assumed to be driven by gravity drainage only which is given as

$$Q_b = f\, K_{bl} \tag{2.11}$$

where f is a factor to simulate the relative permeability of the underlying soil layer (f is presently fixed at 1.0 in the model) and K_{bl} is the hydraulic conductivity for the bottom layer.

The moisture boundary condition at the soil surface is a little more complicated, because both precipitation and evapotranspiration can affect the soil moisture. Rainfall and evapotranspiration are assumed to directly add/remove water to/from soil without considering the "interception effect" of the overlying vegetation or other "bypass effects". The water addition/removal process is done from the top layer to the botton layer in the model domain. It moves to a deeper layer whenever that layer's soil pore space is completely full/out of water. Water surplus in the whole domain is accumulated to simulate flood.

Water loss by evapotranspiration is calculated using Thornthwaite's formula [*Thornthwaite, 1948*]. First, the potential evapotranspiration (PET) is determined as follows.

$$PET = 1.6(\frac{10\,T(i)}{I})^m \tag{2.12}$$

where

$$I = \sum_{i=1}^{12}(\frac{T(i)}{5})^{1.514}$$

$$m = (6.75 \times 10^{-7})\,I^3 - (7.71 \times 10^{-5})\,I^2 + (7.9 \times 10^{-2})\,I + 0.492$$

and I is an annual heat index, PET is monthly potential evapotranspiration (cm/month), $T(i)$ is monthly mean temperature (°C), and i is the month index.

Then actual evapotranspiration (AET) is calculated assuming that it decreases linearly from PET to zero as soil moisture (W) drops from field capacity (W_{fc}) to wilting point (W_{wp}). The actual water withdrawal from soil due to evapotranspiration therefore depends on soil water content itself.

$$AET = \begin{cases} 0 & \text{if } T < 0°\text{C or } W \le W_{wp} \\ \frac{W - W_{wp}}{W_{fc} - W_{wp}} PET & \text{if } W_{wp} \le W \le W_{fc} \\ PET & \text{if } W \ge W_{fc} \end{cases} \tag{2.13}$$

In the coupled climate-natural emission models which will be discussed in Chapter 7, the heat flux at the lower boundary is calculated using the temperature of the climate model's second soil layer instead of using a fixed temperature at the depth of 500 cm. The actual evapotranspiration is replaced by evaporation calculated in the climate model. As shown in Chapter 7, the changes in boundary conditions do not make a big difference in the emission results.

2.4.2 Decomposition and Nitrification

Nitrogen and carbon substrates, which are the two important nutrients for the denitrifiers, changes continuously as the decomposition process progresses. The evolution of these two pools are estimated by the decomposition and nitrification component model.

Soil Carbon Pools

Soil carbon is categorized using four broad classes of pools in the decomposition model. They are residue, microbial biomass, humads and humus. Each of the first three broad classes has two to three different subclasses. Humus is the final product of the decomposition process and is assumed inactive in the model.

The decomposition of the carbon pools depends on the soil temperature, moisture, and decomposition rate and on the carbon pools themselves. For the residue pool, its decompositon also depends on soil nitrogen availability.

Let $\mathcal{D}_B$, $\mathcal{D}_{HD}$, and $\mathcal{D}_{HU}$ ($\mathcal{D}_x$ where $x = B, HD, HU$) represent the decomposition rates (Kg C/m^3/day) of microbial biomass, humads and humus and let $\mathcal{D}_{R\rightarrow CO_2}$, and $\mathcal{D}_{R\rightarrow B}$ represent the decomposition rates of residue to CO_2 and microbial biomass. These decomposition rates of carbon pools can be calculated using first-order kinetics as follows:

$$\mathcal{D}_x = f_{\mathrm{T}} \cdot f_{\mathrm{W}} \cdot SDR_x \cdot DRF \cdot \mathcal{C}_x \tag{2.14}$$

$$\mathcal{D}_{R\rightarrow CO_2} = f_{\mathrm{T}} \cdot f_{\mathrm{W}} \cdot f_{\mathrm{CN}} \cdot SDR_R \cdot DRF \cdot \mathcal{C}_R \tag{2.15}$$

Carbon Pool	Component	R_{CNX}	SDR (1/day)
Residue	Very Labile	2.35	0.074
	Labile	20.00	0.074
	Resistant	20.00	0.020
Biomass	Labile	8.00	0.330
	Resistant	8.00	0.040
Humads	Labile	8.00	0.160
	Resistant	8.00	0.040
Humus	Inactive		

Table 2.2: Parameters for Soil Carbon Pools (R_{CNX}: C/N ratio in the carbon pools, SDR: Specific Decomposition Rate).

$$\mathcal{D}_{R\to B} = f_{\mathrm{T}} \cdot f_{\mathrm{W}} \cdot f_{\mathrm{CN}} \cdot SDR_R \cdot DRF \cdot f_{\mathrm{B/CO_2}} \cdot \mathcal{C}_R \tag{2.16}$$

where f_{T} and f_{W} are temperature and moisture reduction factors [*Nyhan, 1976; Clay et al., 1985; Li et al. 1992a*], f_{CN} is N availability reduction factor [*Molina et al., 1983*], $f_{\mathrm{B/CO_2}}$ is the ratio between formed biomass and produced CO_2 in residue decomposition (a value of 0.67 is used which implies a microbial efficiency of 40% which is in the middle of the range cited in *Li et al.* [*1992a*]), SDR_i is the specific decomposition rate for carbon pool i [*Gilmour et al., 1985; Molina et al., 1983*], DRF is the decomposition rate factor (this is a correction factor for laboratory results of SDR_i which takes into account natural soil disturbance, a fixed number of 0.025 is used here and in *Li et al.* [*1992a*]), $\mathcal{C}_x$ is the carbon pool (Kg C/m^3) for x, and

$$f_{\mathrm{T}} = \begin{cases} 0 & \text{if } T < 0°\mathrm{C} \\ 0.06T & \text{if } 0 \le T < 30°\mathrm{C} \\ 1.8 & \text{if } 30 \le T \le 40°\mathrm{C} \\ 1.8 - 0.04\ (\mathrm{T} - 40) & \text{if } T > 40°\mathrm{C} \end{cases}$$

$$f_{\mathrm{W}} = \begin{cases} 0.1\ \mathrm{W} & \text{if } W < 0.1 \\ 0.02 + 1.96(\mathrm{W}-0.1) & \text{if } 0.1 \le W \le 0.6 \\ 1 - 2.5(\mathrm{W}-0.6) & \text{if } 0.6 < W \le 0.8 \\ 0.5-0.5(\mathrm{W}-0.8) & \text{if } W > 0.8 \end{cases}$$

$$DRF = \begin{cases} 0.02 & \text{if } z < 10 \text{ cm} \\ 0.01 & \text{if } 10 \leq z < 20\text{cm} \\ 0.005 & \text{if } z \geq 20 \text{ cm} \end{cases}$$

$$f_{\text{CN}} = 0.2 + 7.2 \times \frac{NP}{CP}$$

$$f_{\text{B/CO}_2} = 0.67$$

The carbon balance equations for different pools as functions of time t can then be described in terms of the above carbon changes.

■ Carbon Balance Equation for Residue

$$\frac{d\mathcal{C}_R}{dt} = S_R - (\mathcal{D}_{R\to CO_2} + \mathcal{D}_{R\to B}) \tag{2.17}$$

where S_R is residue source which represents the soil carbon source added in the form of vegetation litter or other organic matter.

■ Carbon Balance Equation for Microbial Biomass

$$\frac{d\mathcal{C}_B}{dt} = \mathcal{D}_{R\to B} - \mathcal{D}_B + \underbrace{\mathcal{D}_B \cdot R_{B\to B} + \mathcal{D}_{HD} \cdot R_{HD\to B}}_{S_{SC}} \tag{2.18}$$

where the source term S_{SC} is the recycled carbon (called soluble carbon) from decomposed microbial biomass and humads. Soluble carbon is therefore a part of biomass carbon. It accumulates in the decomposition process and is then consumed in the denitrification process.

■ Carbon Balance Equation for Humads

$$\frac{d\mathcal{C}_{HD}}{dt} = \mathcal{D}_B \cdot R_{B\to HD} - \mathcal{D}_{HD} \tag{2.19}$$

■ Carbon Balance Equation for Humus

$$\frac{d\mathcal{C}_{HU}}{dt} = \mathcal{D}_{HD} \cdot R_{HD\to HU} \tag{2.20}$$

■ CO_2 Released in Decomposition

$$\frac{d[CO_2]_{DC}}{dt} = \mathcal{D}_{R\to CO_2} + \mathcal{D}_B \cdot R_{B\to CO_2} + \mathcal{D}_{HD} \cdot R_{HD\to CO_2} \tag{2.21}$$

$R_{x\to y}$ in the above equations represents the proportion of the decomposed carbon pool x which goes into pool y. These proportions data are listed in Table 2.3.

Microbial Biomass Decomposition			
Product	New Biomass	Humads	CO_2
Proportion	$R_{B\to B}$	$R_{B\to HD}$	$R_{B\to CO_2}$
Value used	20%	20%	60%
Humads Decomposition			
Product	New Biomass	Humus	CO_2
Proportion	$R_{HD\to B}$	$R_{HD\to HU}$	$R_{HD\to CO_2}$
Value used	20%	40%	40%

Table 2.3: Products of Microbial Biomass and Humads Decomposition and Their Proportions.

Summing up the above five equations, we get the carbon balance equation for all the relevant soil carbon pools in the decomposition process.

$$\frac{d\mathcal{C}_R}{dt} + \frac{d\mathcal{C}_B}{dt} + \frac{d\mathcal{C}_{HD}}{dt} + \frac{d\mathcal{C}_{HU}}{dt} + \frac{d[CO_2]_{DC}}{dt} = S_R \tag{2.22}$$

Since vegetation growth is not included in the global N_2O emission model, addition of soil organic carbon in the form of vegetation litter and other organic matter is not calculated in the emission model. Instead, an observational data set for soil organic carbon [*CDIAC, 1986*], which implicitly includes the soil organic carbon from these sources, is used as initial condition for all the carbon pools in the current climate. Soil organic carbon estimated by the Terrestrial Ecosystem Model [TEM, *Melillo et al., 1993*] are used to represent the percentage changes in soil organic carbon under other different climates.

Soil Nitrogen Pools

Equations for N pools ($[i]$ in Kg N/m^3 where $i = NH_4^+, NO_3^-, N_2O, N_2$) are delineated by quantifying mineralization and other N processes. The mineralization is expressed in terms of carbon pool changes in the decomposition process and some constant C/N ratios (R_{CNx}) for carbon pools.

■ N Balance Equation for NH_4^+

$$\begin{aligned}\frac{d[NH_4^+]}{dt} = & \frac{\mathcal{D}_{R\to CO_2}}{R_{CNR}} + \frac{\mathcal{D}_B \cdot R_{B\to CO_2}}{R_{CNB}} + \frac{\mathcal{D}_{HD} \cdot R_{HD\to CO_2}}{R_{CNH}} \\ & + \frac{\mathcal{D}_{R\to B}}{R_{CNR}} - \frac{[NH_4^+]}{[NH_4^+] + [NO_3^-]} \cdot \frac{\mathcal{D}_{R\to B}}{R_{CNB}} \\ & - F_{\text{ads}} \cdot [NH_4^+] - E_{NH_3-vol} - S_{NO_3^-{}_N} - E_{N_2O_N} \end{aligned} \tag{2.23}$$

where the first three terms on the right side of above equation represent the mineralization of soil organic nitrogen, the next two terms represent the organic nitrogen surplus or deficit when carbon is transferred from one pool to another pool, the other (negative) terms represent various sinks (sources) from other N processes (adsorption, volatilization and nitrification producing NO_3^- and N_2O).

■ N Balance Equation for NO_3^-

$$\frac{d[NO_3^-]}{dt} = -\frac{[NO_3^-]}{[NH_4^+] + [NO_3^-]} \cdot \frac{\mathcal{D}_{R\to B}}{R_{CNB}} + S_{NO_3^-{}_N} \tag{2.24}$$

where the first term on the right side is a fraction of nitrogen deficit resulting from carbon transfer (the other part shared by NH_4^+), and the second term is the NO_3^- source from nitrification.

Various sink (source) terms in above two equations are described as follows.

NH_4^+ Adsorption

NH_4^+ adsorption fraction F_{ads} (range 0.0–0.413) is calculated as a function of NH_4^+ concentration and soil clay index ($\frac{clay}{clay_{max}}$ with a range of 0.0–1.0) [*Nommik, 1965; Li*

et al., 1992a]. The soil clay index is used to represent adsorption sites:

$$F_{\text{ads}} = \left\{0.413 - 0.466 \times \frac{\log[NH_4^+]}{\ln 10}\right\} \times \frac{clay}{clay_{max}} \tag{2.25}$$

Volatilization of NH_3

Ammonia volatilization to the atmosphere during a time interval Δt is represented by a diffusion process. It is calculated as a function of aqueous ammonia concentration and a diffusion coefficient [*Gardner, 1965*]:

$$E_{NH_3-vol}(\Delta t) = 2 \times [NH_3]_{Aq} \times \left(\frac{D \cdot \Delta t}{3.1416}\right)^{0.5} \tag{2.26}$$

where $[NH_3]_{Aq}$ is the liquid phase NH_3 concentration which is represented in terms of NH_4^+ concentration according to NH_4^+–NH_3 and H^+–OH^- equilibria [*Freney et al., 1981*]:

$$[NH_3]_{Aq} = [NH_4^+] \times 10^{pH} \times \frac{K_{H_2O}}{K_{NH_4^+}} \times \frac{clay}{clay_{max}} \tag{2.27}$$

D is the diffusion coefficient (0.025 cm^2/day) used to represent the exchange of ammonia between soil solution and the atmosphere, and $E_{NH_3-vol}(\Delta t)$ is the NH_3 volatilized in the time interval of Δt.

Nitrification

The nitrification of ammonium is computed according to first order kinetics [*Watts and Hanks, 1978*]. Let $[NH_4^+]_N$ be the actual amount of ammonium for nitrification which is equal to $f_M \cdot [NH_4^+]$ where f_M is the moisture reduction factor. The nitrification process can be then represented as:

$$\frac{d[NH_4^+]_N}{dt} = -K_A \cdot [NH_4^+]_N \tag{2.28}$$

i.e., the source of NO_3^- from nitrification is

$$S_{NO_3^-{}_N} = K_A \cdot f_M \cdot [NH_4^+] \tag{2.29}$$

where

$$f_M = \begin{cases} 1.111\ \text{W} & \text{if } 0 \leq W \leq 0.9 \\ 10(1\text{-W}) & \text{if } 0.9 < W \leq 1 \end{cases} \tag{2.30}$$

$$K_A = \begin{cases} (0.0105T + 0.00095T^2) \times K_{35} & \text{if } 0 \leq T < 10°\text{C} \\ (0.032T - 0.12) \times K_{35} & \text{if } 10 \leq T < 35°\text{C} \\ (-0.1T + 4.5) \times K_{35} & \text{if } 35 \leq T \leq 45°\text{C} \end{cases} \tag{2.31}$$

N_2O Formed in Nitrification

N_2O emission to the atmosphere in the nitrification process is calculated using an empirical formula [*Li et al., 1992a*] according to the data in *Bremner and Blackmer [1981]*.

$$E_{N_2O_N} = F_N \cdot f_{TN} \cdot [NH_4^+]_{column} \tag{2.32}$$

where $F_N \left(= \frac{0.0014}{30}\right)$ is the fraction of NH_4^+ which is converted to N_2O in 1 day, $f_{TN} = \frac{0.54+0.51T}{15.84}$ is the temperature reduction factor and $[NH_4^+]_{column}$ is the column soil NH_4^+ in Kg-N/ha.

2.4.3 Denitrification

Criterion for Denitrification

The denitrification process is regulated by soil oxygen status which is modeled in terms of soil water content (W). It is assumed that the threshold for the denitrification process is $W = 40\%$ and the following criterion is therefore used to trigger this important process in the N_2O emission model:

$$W \geq 0.4 \tag{2.33}$$

Nitrogen Pools

- Dynamic Equations for N Species

$$\frac{d[NO_3^-]}{dt} = -CON_{NO_3^-} - SYN_{NO_3^-} \tag{2.34}$$

$$\frac{d[NO_2^-]}{dt} = CON_{NO_3^-} - CON_{NO_2^-} - SYN_{NO_2^-} \quad (2.35)$$

$$\frac{d[N_2O]}{dt} = CON_{NO_2^-} - CON_{N_2O} - SYN_{N_2O} - E_{N_2O} \quad (2.36)$$

$$\frac{d[N_2]}{dt} = CON_{N_2O} - E_{N_2} \quad (2.37)$$

where CON_i is the conversion of NO_3^- to NO_2^-, NO_2^- to N_2O and N_2O to N_2 by their corresponding denitrifiers, SYN_i is the synthesis of NO_3^-, NO_2^- and N_2O by the denitrifiers, E_{N_2O} and E_{N_2} are the gas emissions to the atmosphere (described in a later section "Gas Diffusive Emission"), and

$$CON_i = \left(\frac{G_i}{Y_i} + \frac{M_i \cdot [i]}{\Sigma_{i=1}^{3}[i]}\right) \cdot f_{pH} \cdot f_T \cdot \mathcal{C}_{DN} \quad (2.38)$$

$$SYN_i = \frac{\mathcal{P}_{DN-New}}{R_{CN}} \cdot \frac{[i]}{\Sigma_{i=1}^{3}[i]} \quad (2.39)$$

where $i = NO_3^-, NO_2^-$, or N_2O, $\mathcal{C}_{DN}$ is the carbon pool of all denitrifiers, f_T is the temperature reduction factor for denitrification, f_{pH} is the pH reduction factor, G_i is the relative growth rate of denitrifier i, M_i is the maintenance coefficient of i, Y_i is the maximum growth yield of i, $\mathcal{P}_{DN-New}$ is the carbon production rate of new-formed denitrifiers, and R_{CN} is the C/N ratio for denitrifiers.

An exponential formula with a value of unity at 22.5 °C is used for the temperature reduction factor [*Focht, 1974; Knowles, 1981; Keeney et al., 1979*]:

$$f_T = \begin{cases} 2^{\frac{T-22.5}{10}} & \text{if } T < 75°\text{C} \\ 0 & \text{if } T \geq 75°\text{C} \end{cases} \quad (2.40)$$

The pH reduction factor is presented in Table 2.4 for different denitrifiers.

The N balance equation for all the nitrogen pools in the denitrification process is obtained by summing Equations 2.34-2.37.

$$\frac{d[NO_3^-]}{dt} + \frac{d[NO_2^-]}{dt} + \frac{d[N_2O]}{dt} + \frac{d[N_2]}{dt} = \Sigma_{i=1}^{3} SYN_i - E_{N_2O} - E_{N_2} \quad (2.41)$$

This means that all the inorganic N produced in decomposition (or added at the

Table 2.4: pH reduction factor for different denitrifiers

Denitrifier	pH reduction factor f_{pH} [*Focht,1974; Leffelaar & Wessel, 1988*]
$[NO_3^-]$	$7.14 \times \left(\frac{pH-3.8}{22.8}\right)$
$[NO_2^-]$	1
$[N_2O]$	$7.22 \times \left(\frac{pH-4.4}{18.8}\right)$

beginning) is either absorbed by microbial biomass in the soil or released to the atmosphere as N_2O and N_2.

Carbon Pools

The denitrifier carbon pools (total carbon $\mathcal{C}_{DN}$ and new-formed carbon $\mathcal{P}_{DN-New} \cdot \Delta t$) and soluble carbon pool ($\mathcal{C}_{sc}$) are two important parameters in regulating denitrification. They are also dynamically modeled in the emission model.

- Carbon Balance Equation for Denitrifiers

$$\frac{d\mathcal{C}_{DN}}{dt} = \mathcal{P}_{DN-New} - \frac{\mathcal{C}_{DN}}{\tau} \tag{2.42}$$

where

$$\begin{aligned} \mathcal{P}_{DN-New} &= G_{DN} \cdot \mathcal{C}_{DN} \\ G_{DN} &= \Sigma_{i=1}^{3} G_i \\ G_i &= \left(G_{i,M} \cdot \frac{\mathcal{C}_{sc}}{\mathcal{C}_{sc,\frac{1}{2}} + \mathcal{C}_{sc}} \cdot \frac{[i]}{[i]_{\frac{1}{2}} + [i]} \right) \\ \tau &= \frac{1}{M_{sc} Y_{sc}} \end{aligned}$$

τ is the lifetime of denitrifiers. Other symbols in above four equations have the same meaning as they appeared before except subscripts DN, sc, and $\frac{1}{2}$ refer to denitrifier, soluble carbon, and the half-saturation value respectively. The values of the various constants are listed in Table 2.5.

Table 2.5: Constants used in Denitrification Model

	$G_{i,M}$	$X_{\frac{1}{2}}$	M_i	Y_i
$[NO_3^-]$	0.67	0.083	0.09	0.401
$[NO_2^-]$	0.67	0.083	0.035	0.428
$[N_2O]$	0.34	0.083	0.079	0.151
Soluble Carbon		0.017	0.0076	0.503

Constant	Value
R_{CN}	3.45
R_{BO}	0.02
R_{DB}	0.05

■ Soluble Carbon Balance Equation

$$\frac{d\mathcal{C}_{sc}}{dt} = -\left(\frac{G_{DN}}{Y_{sc}} + M_{sc}\right) \cdot \mathcal{C}_{DN} \tag{2.43}$$

The right hand side is the consumption rate of soluble carbon in the denitrification process. Soluble carbon accumulates in the decomposition process.

The carbon pools are balanced in the denitrification process with some of the consumed soluble carbon released as CO_2.

■ CO_2 Released in Denitrification

$$\frac{d[CO_2]_{DN}}{dt} = \left(\frac{G_{DN}}{Y_{sc}} + M_{sc}\right) \cdot \mathcal{C}_{DN} - \mathcal{P}_{DN-New} \tag{2.44}$$

The carbon balance equation for all carbon pools in the denitrification process is described as follows by summing equations 2.42-2.44.

$$\frac{d\mathcal{C}_{DN}}{dt} + \frac{d\mathcal{C}_{sc}}{dt} + \frac{d[CO_2]_{DN}}{dt} = -\frac{\mathcal{C}_{DN}}{\tau} \tag{2.45}$$

The right side of the above equation is the permanent carbon sink due to the death of denitrifiers which goes to carbon pool humus and no longer participates in the dynamic processes in the emission model.

Gas Diffusive Emission

N_2O Emission to the Atmosphere

The N_2O emitted to the atmosphere is the fraction of the produced N_2O which successfully diffuses to open air from the soil core. This diffusion process is simplified by *Li et al.* [*1992a*] as a function of the absorption coefficient and air-filled porosity according to the data in *Letey et al.* [*1980*].

The "fraction" of the produced N_2O which diffuses from the soil core in 1 day is described as follows:

$$F_{E_{N_2O}} = \left(0.0006 + 0.0013 \cdot 2 \cdot \frac{clay}{0.63}\right) + \left(0.013 + 0.005 \cdot 2 \cdot \frac{clay}{0.63}\right) \cdot (1 - W) \quad (2.46)$$

The N_2O Emission to the Atmosphere is then expressed as:

$$E_{N_2O} = F_{E_{N_2O}} \cdot [N_2O]_{column} \quad (2.47)$$

where $[N_2O]_{column}$ is the column soil N_2O in Kg-N/ha.

N_2 Emission to the Atmosphere

N_2 emission to the atmosphere is calculated the same way as the N_2O emission.

$$E_{N_2} = F_{E_{N_2}} \cdot [N_2]_{column} \quad (2.48)$$

where

$$F_{E_{N_2}} = 0.017 + \left(0.025 - 0.0013 \cdot 2 \cdot \frac{clay}{0.63}\right) \cdot (1 - W) \quad (2.49)$$

and $[N_2]_{column}$ is the column soil N_2 in Kg-N/ha.

2.5 Principal Controls on Global N_2O Emission

Denitrification activities and trace gas fluxes vary substantially across different sites [*Groffman, 1991*]. This variability occurs on large scales due to broad variations in soils, climate, vegetation, land use and other factors [*Ehleringer and Field, 1993*].

All of the currently available models for denitrification are essentially point source models. Macro-scale variability of the modeled trace gas flux thus depends upon the degree of spatial variability of the driving variables. The use of various global data sets for the dominant controlling factors which allow the denitrification component model to be applied to different sites and circumstances is a new and unique aspect of the global N_2O emission model developed for this thesis.

2.5.1 Soil Texture

Soil texture reflects the relative proportion of clay. Clay content directly affects the decomposition rate of organic matter and the adsorption rate of inorganic compounds. Soil physical and chemical properties which strongly affect the soil moisture and temperature profiles also vary with different soil textures.

Soil texture data used in the Terrestrial Ecosystem Model (TEM) [*Melillo et al., 1993*] and described in Raich *et al.* [*1991*] are used in the global N_2O emission model. The soil texture data set contains digital numbers for clay, silt and sand proportions. Clay content is used directly in calculating its effects on the decomposition rate of organic matter and the adsorption rate of inorganic compounds. Global clay data and the clay contents for the 12 typical soil types (Table 2.1) are used to derive the global soil type distribution, which determines the global soil physical and chemical properties (e.g. porosity, field capacity, wilting point, and other parameters listed in Table 2.1).

2.5.2 Vegetation and Soil Organic Carbon

Vegetation has two direct effects on global N_2O emissions through soil organic carbon: 1) Soil organic matter content—different ecosystems have different amount of organic matter in their soils; 2) Soil organic matter profile—different ecosystems have different vertical distributions of soil organic matter (e.g. agricultural tillage can change the distribution of organic matter in the soil profile by physically mixing the soil).

A data set containing worldwide organic carbon measurements from the Carbon

Dioxide Information Analysis Center (CDIAC) of the Oak Ridge National Laboratory [*CDIAC, 1986*] and a global data set for potential ecosystem types (TEM vegetation type) [*Melillo et al., 1993*] are used together to take into account the spatial variability of soil organic carbon.

The observed worldwide organic carbon data are relatively sparse in terms of global coverage. These data are aggregated and averaged according to the ecosystem types (the data for which are available at $0.5° \times 0.5°$ resolution). The global distribution of soil organic carbon is derived by extrapolating globally the mean value for each ecosystem type.

The global distribution of soil carbon content is presented in Figure 2-2. One of the striking features of this map is that high latitudes have fairly high soil carbon content. This can be seen more clearly in Figure 2-3 where the latitudinal profile of soil carbon content is shown. The maximum soil carbon content is located around the 60°N latitude circle with the magnitude being twice that in the tropics. The reason for this is that low temperatures in high latitudes make soil organic matter decompose slowly and accumulate over a long period of time [*Xiao et al., 1996*]. Even though net primary productivity in the moist tropics is very high, most of the carbon is stored in vegetation. Soil carbon storage is small in tropics due to rapid respiration and decomposition induced by high temperatures.

The vertical distribution of soil organic carbon is different across different ecosystems. Figure 2-4 gives typical soil organic carbon profiles for grassland and woody vegetation land. Areas with woody vegetation tend to have a large proportion of carbon storage in the upper layers of the soil, while in grassland areas, there is a more uniform distribution of carbon through the soil profile. The vertical profile of soil organic carbon determines the availability of nutrients and hence the emissions of nitrous oxide.

Soil carbon content is also expected to change for different CO_2 levels and/or different climates. Two approaches can be used estimate the global distribution of soil organic carbon under different climate conditions. The first one utilizes the mean-carbon-content derived today for each ecosystem type. This approach can only

be used when we know the global distributions of ecosystems under the perturbed climate conditions. The ice-age case for N_2O emissions which will be discussed in Chapter 6 uses this approach. The second one is to use predicted soil carbon content from an ecosystem model (e.g. TEM). This approach is used in Chapter 5 for the "$2xCO_2$" N_2O emission case and in Chapter 7 for the coupled emission-climate-chemistry model.

2.5.3 Climate Data

Climate, as one of the driving variables, plays an important role in the global emission model. It controls soil temperature and moisture which regulate bacterial activity and thus N_2O emissions. The global N_2O emission model uses surface air temperature and precipitation only.

Two data sets of long-term averaged monthly surface air temperature and precipitation [*Cramer and Leemans, personal communication; Shea, 1986*] are used as the driving climate. Shea's data have $2.5° \times 2.5°$ resolution while Cramer and Leemans' data have $0.5° \times 0.5°$ resolution. The Cramer and Leemans climate database is an update of the Leemans and Cramer [*1991*], and has been developed using more weather stations and a new algorithm for spatial interpolation. Because of the computational burden of using very fine resolution, the global N_2O emission model is set up at $2.5° \times 2.5°$ resolution. Cramer and Leemans' data are aggregated and averaged (area-weighted scheme for both precipitation and T^4 where T is the surface air temperature) to produce the needed resolution of $2.5° \times 2.5°$.

The global distribution of annual mean surface air temperature and precipitation (aggregated Cramer and Leemans' data) is shown in Figure 2-5. The obvious (and well known) pattern that shows up on the map is that tropics have the highest temperatures and precipitation rates.

Monthly precipitation is converted into rainfall events using a rainfall statistical model developed by Li and Frolking [*1992*]. The rainfall model is based on the statistical results on the correlation of monthly precipitation with frequency of heavy, intermediate and small rainfall events. About 3,000 groups of climate data (monthly

precipitation and rainfall events) were used in the statistics.

2.6 Model Initial Conditions

Soil Hydrological Model

The two prognostic variables in the soil hydrological model are soil temperature (T) and moisture content (W). The initial conditions for these two variables in the global emission model are obtained by running the soil hydrological model for two years using current climate data. Surface air temperature from climate data and an arbitrary moisture content of 0.5 are used as the initial soil temperature and moisture content for this 2-year run. Soil temperature and moisture content at the end of the 2-year integration are then used as the initial conditions for T and W in the global emission model.

Emissions are also calculated in the 2-year initialization run. The monthly and annual global emission results for a 4-year run (two more years are added to the 2-year initialization run) are presented in Table 2.6. As we can see, the global emission is not very sensitive to the initial soil temperature and moisture conditions. After year 2, the monthly emissions for different years are very close. The emission model effectively "remembers" the initial soil temperature and moisture content only for a few months.

Decomposition and Nitrification Model

Carbon Pools

The observed soil organic carbon contents (assumed to define the total carbon for all the relevant pools), which were discussed early, are used as the initial carbon contents. Partitioning of the total carbon into specific carbon pools is done according to the typical proportions of the pools. These typical proportion data are presented in Table 2.7 [*Gilmour et al., 1985; Molina et al., 1983*].

For a situation where soil organic carbon may be different from the observed data

Month	Year 1	Year 2	Year 3	Year 4
1	0.7857	0.6639	0.6659	0.6657
2	0.7227	0.7053	0.7022	0.7022
3	0.8314	0.8222	0.8186	0.8186
4	0.9139	0.9373	0.9351	0.9351
5	0.9864	0.9962	0.9953	0.9953
6	1.0020	1.0149	1.0142	1.0141
7	1.2886	1.2895	1.2891	1.2899
8	1.2753	1.2622	1.2624	1.2624
9	0.9948	0.9895	0.9897	0.9897
10	0.9064	0.9026	0.9027	0.9027
11	0.8791	0.8774	0.8774	0.8774
12	0.8706	0.8731	0.8724	0.8724
Annual Total	11.4568	11.3341	11.3250	11.3254

Table 2.6: N_2O emissions (in Tg-N/month) for different integration times.

Carbon Pool	Component	Initial Content		
Residue	Very Labile	40%		8%
	Labile			32%
	Resistant			60%
Biomass	Labile	40%	2%	90%
	Resistant			10%
Humads	Labile		98%	16%
	Resistant			84%
Humus		20%		

Table 2.7: Initial Content of Various Soil Carbon Pools (in terms of their carbon percentage of total soil organic matter).

Dynamic Variable	Initial Condition
$\mathcal{C}_x$	Observated or Modeled Carbon
$[NO_3^-]$	100 mg N/Kg soil
$[NH_4^+]$	5 mg N/Kg soil

Table 2.8: Initial Conditions for Decomposition and Nitrification Model

(e.g. "2xCO_2", ice age, or predicted future climate), model results (TEM) are used to define the initial carbon contents. The same partitioning scheme is used in these cases.

Nitrogen Pools

Since the C/N ratio is fairly fixed with a specific carbon pool, there is no independent soil organic nitrogen pool. The important nitrogen pools are the inorganic ions $[NH_4^+]$ and $[NO_3^-]$. These two compounds are fairly constant across ecosystems [*Firestone and Davidson, 1989*] and their typical concentrations are used as their conditions in the N_2O emission model. These values are presented in Table 2.8.

Denitrification Model

Carbon Pools

The important carbon pools in the denitrification process are the soluble carbon pool and the denitrifier carbon pool. These carbon pools are not independent of other carbon pools in the decomposition process, because they are a part of other pools. Also, in the denitrification process, some of denitrifiers die and part of soluble carbon is released to the atmosphere as CO_2, which makes them important in the soil carbon cycle dynamics.

Since the dynamic equations in the denitrification model are solved independently, the soluble carbon and denitrifier carbon pool sizes predicted by the decomposition and nitrification model are used for the initial conditions of these two pools. The initial conditions for these two carbon pools for the very first iteration of the denitrification model are described in following two equations.

Soluble Carbon:

$$C_{SC0} = \int S_{SC} dt \tag{2.50}$$

where S_{SC} is the source of soluble carbon described in equation 2.18, which is a part of the other pools in the decomposition process.

Denitrifier Carbon:

Dynamic Variable	Initial Condition
$[NO_3^-]$	100 mg N/Kg soil + $\Delta[NO_3^-]$
$[NO_2^-]$	0
$[N_2O]$	0
$[N_2]$	0

Table 2.9: Initial Conditions for N Species in Denitrification Model

$$C_{DN0} = (C_B + C_{HD}) \cdot R_{BO} \cdot R_{DB} \tag{2.51}$$

where R_{BO} is the ratio of microbial biomass carbon to total carbon in microbial biomass and humads, and R_{DB} is the carbon ratio between denitrifiers and microbial biomass. The values of these two parameters were presented earlier in Table 2.5 [*Woldendorp, 1981; Anderson and Domsch, 1989; Focht and Verstraete, 1977*].

Nitrogen Pools

The dynamic equations for N species are also invoked discontinously. The initial conditions for the N species depends on their concentrations predicted by the the decomposition and nitrification model. Initial conditions for the very first denitrification model iteration can be described in Table 2.9, where $\Delta[NO_3^-]$ is the change in nitrate concentration before the first denitrification segment.

2.7 Model Structure

The structure of the global N_2O emission model is described in Figure 2-1. The flow chart shows how the model proceeds to predict the emissions of various gases.

Data sets of controlling variables are first read in by the model. Climate data, which are typically available on a monthly basis, are processed in the statistical rainfall model to give daily outputs of surface temperature and precipitation. These daily climate data combined with global data for soil texture drive the 1-dimensional soil hydrology model, producing soil temperature and moisture profiles. The soil hydrology model has a vertical domain size of 50 cm and vertical resolution of 5 cm.

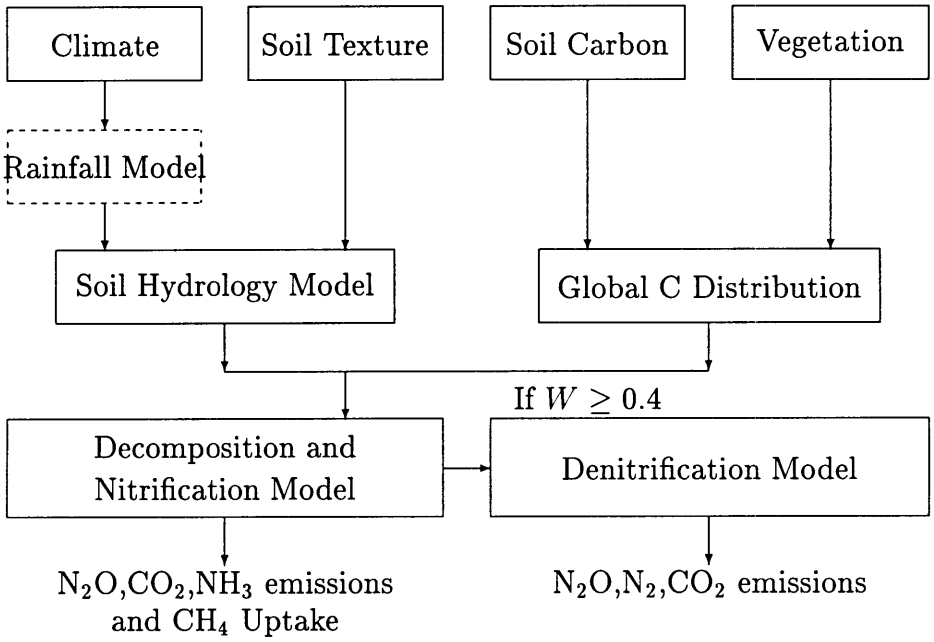

Figure 2-1: Model Structure for N_2O Emission Model.

Model equations are solved using an explicit finite difference scheme with a time step of 15 minutes. Hourly and daily soil temperature and moisture data are saved for use in the nitrification and denitrification models.

Global vegetation data are used together with the observed soil carbon data to obtain the global soil carbon distribution which is then used to define the initial carbon contents for different carbon pools. Partitioning of the soil carbon to specific pools is done at the first iterations of the decomposition and nitrification algorithm.

Given the initial carbon content for all the carbon pools, the decomposition and nitrification algorithms solve all their equations as an initial value problem. An explicit finite difference scheme is also used to predict instantaneous carbon and nitrogen pools. The decomposition and nitrification model has a vertical resolution of around 2 cm (it actually varies with soil porosity) and a time step of 1 day. Daily data of soluble carbon, denitrifier carbon and nitrate are saved for the use in the

denitrification model. Daily N_2O, CO_2, and NH_3 emissions and CH_4 uptake are also predicted in this model.

The denitrification model is invoked only when soil moisture is greater than 40% of soil porosity. Model equations for denitrification are also solved (using an explicit finite difference scheme) as an initial value problem. The denitrification model has the same spatial resolution as the decomposition and nitrification model (i.e. a vertical-layer-thickness of around 2 cm) but with a time step of 1 hour. Daily emissions of N_2O, N_2, and CO_2 are predicted in the denitrification model.

2.8 Model Results and Sensitivities

2.8.1 N_2O Emission Time Series

An example of a one-year N_2O emission time series is given in Figure 2-6. This is a typical emission series for high latitude boreal soils. As we can see from the figure, N_2O emissions are not continuous (panel 4 from top to bottom) but show episodic pulses. These pulses are generally associated with high soil moisture (panel 3) and this is what we would expect from the site emission model. Monthly precipitation is split into discrete rainfall events at regular intervals but with distinct rainfall intensities (panel 2). Soil moisture fluctuates with precipitating water added into and evaporating water subtracted from the soil hydrology model domain. There are sudden jumps in soil moisture immediately following rainfall events (panels 2 and 3). The emission pulse starts with a rainfall event or a snowmelt event. Whenever temperature is below zero, precipitation is added to the soil model domain as snowfall and it accumulates until thaw season comes. There are no N_2O emissions when the temperature is below the freezing point. The first pulse in panel 4 corresponds to the melting of accumulated snow. Note that for each pulse, the emission intensity decreases with time. This is due to the consumption of nutrients which are mostly produced in the decomposition and nitrification processes. As the denitrification process progresses, the available nutrients decrease with time. The "envelope" of the

individual emission pulses has a similar shape as the monthly mean surface air temperature (panel 1). This shows the dependence of bacterial activity on temperature. Emissions of CO_2 are closely connected with the soil microbe's respiration and are therefore highly correlated with temperature. This can be seen by comparing panel 1 and panel 5. Sensitivity experiments including assuming (unrealistically) even rainfall through the month have been conducted to assess the effects of changes in rainfall frequency and intensity on the emission results. It turns out that annual global N_2O emission is not sensitive to these changes (the difference is within 5%) even though the time series and emissions at specific sites may be different (e.g. at some sites emissions for the "even" rainfall case do differ by as large as 14% from the more realistic "pulsed" rainfall case). Overall, the annual emission is more closely related to the annual total precipitation rate.

2.8.2 Current Gloal N_2O Emission Results

The global model for soil biogenic N_2O emission is as noted earlier set up at $2.5° \times 2.5°$ spatial resolution. The model can predict daily emissions for N_2O, N_2, NH_3 and CO_2 and daily soil uptake for CH_4.

As also mentioned earlier, the global model has been run for 4 years using the same current climatology for each year but with year-end soil moisture and temperature of previous year as the initial soil moisture and temperature for this year. Because the predicted precipitation over land is generally larger than the predicted evaporation, this is not an equilibrium problem even if we are running the model using the same climate for every year. We would specifically expect emissions to increase as integration time becomes longer.

The monthly and annual global emission results for the 4-year run have already been shown in Table 2.6. As we can see from the table, the global total emissions decrease for the first three years, and then after year 3 the global total emissions start to increase. The decrease for first 3 years is due largely to a poor guess of the initial soil moisture and temperature conditions for the very first year. After year 3, the emissions start to behave as we would expect. Notice that the year to year

differences in the emissions are nevertheless very small. We select the results for year 3 as the best to represent "current" emission patterns, because the combined effect of a poor guess in initial soil moisture and temperature conditions and the above nonequilibrium effects should be minimal at year 3.

The results for cell-by-cell N_2O emissions are analysed here in order to give us some insight into how soils emit N_2O globally and seasonally.

Figure 2-7 gives the global annual N_2O emission distribution. The results imply that there is a high N_2O emission belt in the wet tropics and and subtropics with maxima occurring in the African forest, south America, southeast U.S.A. and Southeast Asia. Deserts and some of the boreal regions have no or very low emissions. Most of the temperate regions have medium emissions. The spatial distributions of the N_2O emission show similar patterns as the climate, especially the precipitation. This feature leads us to conclude not surprisingly that climate (specially precipitation and the accompanying ecosystem state) is a major control on N_2O emission. The sensitivity experiments which will be discussed later on also support this point. Notice also that the maximum emissions occur in the regions where precipitation level is high and soil texture is fine. This is not surpising, because both precipitation and soil texture are important parameters in determining soil moisture. With higher moisture, the denitrification is more likely to occur and more N_2O thus emitted to the atmosphere. There are some spots at high latitudes which also have very high emissions. This is due to high soil organic carbon content (Figure 2-2) and concomitant optimal climate conditions in these regions.

There are distinct seasonal cycles for the N_2O emissions. The seasonal variation is very strong for temperate and boreal soils, especially in the northern hemisphere. This is due to the strong seasonal effects from temperature and moisture regimes in these regions. Note in Figure 2-8 that in January N_2O emissions from the northern extratropical regions almost vanish while in July the emissions are even larger in North America, Mediterranean regions, and southeast Asia than in the tropics. Seasonal cycles in the southern hemisphere are relatively weak (Figure 2-9). There is a narrow belt in the equatorial region which does not show much seasonal variation. Tropical

soils are active nitrous oxide sources throughout most of the year. That is why a large part of the global emission amount is concentrated in the tropical regions, especially near the equator. Seasonal variations in predicted global N_2O emission amounts have a large amplitude. As we can see from Figure 2-10, the total emission in June is almost twice that in December.

The global N_2O emission amount is estimated at 11.33 Tg-N/yr. For comparison, Nevison *et al* [*1996*] obtain a value of 9.5 Tg-N/yr from natural and managed soils using their Nitrogen Biosphere Model (which does not include detailed nitrogen processes). As we see from Figure 2-11, a large part of the emission is from equatorial regions. The tropics between 30°S and 30°N contribute 7.75 Tg-N/yr while the emission from extra-tropical regions (poleward of 30°) is only 3.58 Tg-N/yr. The northern hemisphere emission is slightly larger than the southern hemisphere emission (6.60 and 4.72 Tg-N/yr, respectively). The large magnitude of soil N_2O emissions relative to the total N_2O source and the above asymmetric features of the soil emissions make it possible to test the above predicted emission patterns with observed N_2O mixing ratios. This will be discussed in Chapter 4.

Generally, the model results show that the spatial and seasonal distributions of N_2O emissions are basically similar to climate patterns (mainly the precipitation pattern and accompanying ecosystem states) with some influence from the soil organic carbon content. Precipitation and soil texture play a dominant role in controlling soil moisture which is vital to denitrification and N_2O emissions. Short emission seasons due to below-zero temperatures in temperate and boreal regions are offset by high emissions in the summer seasons induced by high soil organic carbon content in these regions. In the tropics where temperature is not a limiting factor, wet regions have the highest emissions.

2.8.3 Sensitivity Experiments

Sensitivity experiments have been performed by running the global emission model several times for different input parameters. A "standard case" is defined as the run using the soil input parameters in Table 2.10 and the current-day climate variables.

For each of several other sensitivity runs, the value of a single input parameter is changed relative to its standard value, with all other parameters held fixed. The global total N_2O emission amounts resulting from each run are then compared with the result from the standard run. The results of the sensitivity experiments are summarized in Table 2.11.

Input Parameters for the Standard Case	
Total organic Carbon	0.01 Kg-C/Kg soil
Nitrate(NO_3^-) Content	100 mg-N/Kg soil
Ammonium(NH_4^+) Content	5 mg-N/Kg soil

Table 2.10: "Standard case" input parameters (based on values for agricultural soil)

Sensitivity Experiments					
	Standard Case	2×Soil C	2×NO_3^-	$\overline{P}+\Delta P$	$\overline{T}+\Delta T$
Global Emission (Tg-N)	13.6	26.5	13.3	15.6	14.4
Deviation From (Tg-N) Standard Case	0 (0%)	12.9 (95%)	-0.3 (-2%)	2.0 (15%)	0.8 (6%)

Table 2.11: The annual global N_2O emission amounts for different sensitivity experiments and the deviation relative to the standard case (Table 2.10).

As we can see from Table 2.11, a change in soil organic carbon has a significant effect on global N_2O emissions, with the total emissions being doubled for doubling soil organic carbon. This prominent sensitivity of N_2O emissions to soil organic carbon can be explained by the increase of the soluble carbon content. The soil organic carbon directly affects the soluble carbon content in the soil which in turn controls the growth of denitrifiers. With more organic carbon in soil, it is expected that more soluble carbon and then more denitrifiers would appear in the soil.

Soil NO_3^- has little effect on N_2O emission. It is interesting to note that increasing nitrate causes a decline in N_2O emission. This result is counter-intuitive. The reason for this effect is that with higher nitrate concentrations rapid denitrifier growth

consumes a large fraction of the soluble carbon very quickly, sequesting much of the biomass growth. If more soluble C is available as well as nitrate, the result is completely different. Experiments not presented here show that increasing soil organic C and soil nitrate simultaneously causes very large increases in N_2O emissions.

The sensitivity experiments for climate variables are performed by adding the standard deviations to the mean values (climatologies). The precipitation variation (with a range of 7–879 mm/year for different geographical locations) has a large effect on N_2O emission, with the emissions increasing by about 15% when the precipitation is increased by one standard deviation. Surface temperature seems to have relatively weak influence on N_2O emission. Adding one standard deviation (with a range of 0.13–1.77°C) causes about 6% increase in N_2O emission.

The sensitivity experiments suggest that the soil organic carbon content and precipitation are the dominant factors in controlling the global N_2O emissions. Temperature could introduce spatial variablity but its inter-annual variations do not seem to produce major impacts on the level of global N_2O emission.

2.9 Discussion

The global N_2O emission estimated using the emission model developed here refers only to the soil biogenic sources. The total predicted soil emission amount of 11.33 Tg-N per year is slightly toward the high end of the IPCC [*1994*] estimate for the range for total N_2O emissions from natural and cultivated soils of 5.1-15 Tg-N per year. Therefore, the model results support the conclusion of the IPCC that soil biogenic emissions (including natural and agricultural soils) are a major and perhaps dominant source of atmospheric N_2O. As opposed to our model results, published extrapolation methods tend to underestimate this source which is probably due to these methods neglecting the peaks of N_2O emission fluxes immediately following rainfall events. After Muzio and Kramlich [*1988*] ruled out combustion as a large source for atmospheric N_2O, people have had to rely on other industrial emissions in order to balance the N_2O budget [*Khalil and Rasmussen, 1992*]. A 'missing' N_2O source has

even been proposed [*Cofer et al., 1991*]. The results from this global emission model suggest that soil biogenic emissions of N_2O might have been underestimated. The 'missing' source probably can be explained by this underestimation. Industrial emissions such as nylon production, contaminated aquifers and automobiles are apparently not important compared to soils in contributing to atmospheric N_2O loading. On the other hand the soil source may be overestimated in our model because we use a model developed for managed ecosystems which may not be applicable to unmanaged ones.

The application of fertilizers to soils was considered by the IPCC as a non-negligible source for atmospheric N_2O. However, the model results presented here show that adding nitrate and ammonium by themselves has little effect on N_2O emissions. Adding nitrate even lowers the calculated N_2O emission. Therefore, our model results imply that fertilizer application does not have a substantial influence on global atmospheric N_2O levels.

Soil organic carbon content turns out from our model studies to be the most important soil factor in controlling N_2O emission to the atmosphere. There have been few if any studies of the effect of this factor on N_2O fluxes. Our results suggest that through changing soil organic carbon levels many human land use activities can influence the emissions of N_2O to the atmosphere. For example, agricultural tillage physically changes the soil profiles of organic matter, and residue left in the field increases the soil organic matter content. Also, deforestation substantially changes the soil carbon and rooting environments, which would also have a significant effect on global N_2O emissions based on our model results.

The above discussion suggests that if we can quantitatively relate human actitvities with changes in soil organic carbon, an examination of the effects of anthropogenic land use activities on atmospheric N_2O should be possible using our global emission model. This is a interesting undertaking for the future but beyond the scope of this thesis. It is interesting to note that better relevant data on historical land use should become available as the International Land Use and Land Cover Change (LUCC) project progresses.

The model results also suggest some strategies for field experiments. Since soil

organic carbon and precipitation are the two most important controlling factors on N_2O emissions, measurements capable of capturing the N_2O flux peaks immediately following rain events, or measurements in regions where soil organic carbon contents are very high and/or changing are needed for further testing of our conclusions.

2.10 Conclusions

A process-oriented global biogeochemical model for soil N_2O emissions has been developed. The emission model directly connects soil C and N dynamic processes with climate variables, which makes it possible to assess emission changes resulting from climate changes. The emission-climate connection also makes it sensible to couple the emission model with a climate model.

The N_2O emission model predicts a current annual flux of 11.325 Tg-N per year (17.8 Tg N_2O per year), which is slightly toward the high end of the IPCC [*1994*] estimate for the range for total N_2O emissions from natural and cultivated soils of 5.1-15 Tg-N (8-23.6 Tg N_2O). This source may have been overestimated by our model because we use a site model developed for managed ecosystems which may not be applicable to unmanaged ones. Alternatively, this source could have been underestimated in the past because field experiments often neglect the peaks of N_2O emissions immediately following rainfall events. Emission results strongly support the notion that soil biogenic emission is the major global source for atmospheric N_2O.

The spatial and seasonal variations of modeled N_2O emissions are similar to climate patterns, especially to the precipitation pattern. The predicted large emissions from tropical soils are qualitatively consistent with the observed N_2O latitudinal gradient [*Prinn et al., 1990*] and *in situ* flux measurements [*Keller and Matson, 1994*].

Current CO_2 emissions from soils and CH_4 absorption by soils are predicted by the N_2O emission model to be 14.0 Pg-C and 11.0 Tg-C per year respectively. Sensitivity experiments suggest that soil carbon, precipitation and to a lesser extent temperature are the dominant factors in controlling global N_2O emissions.

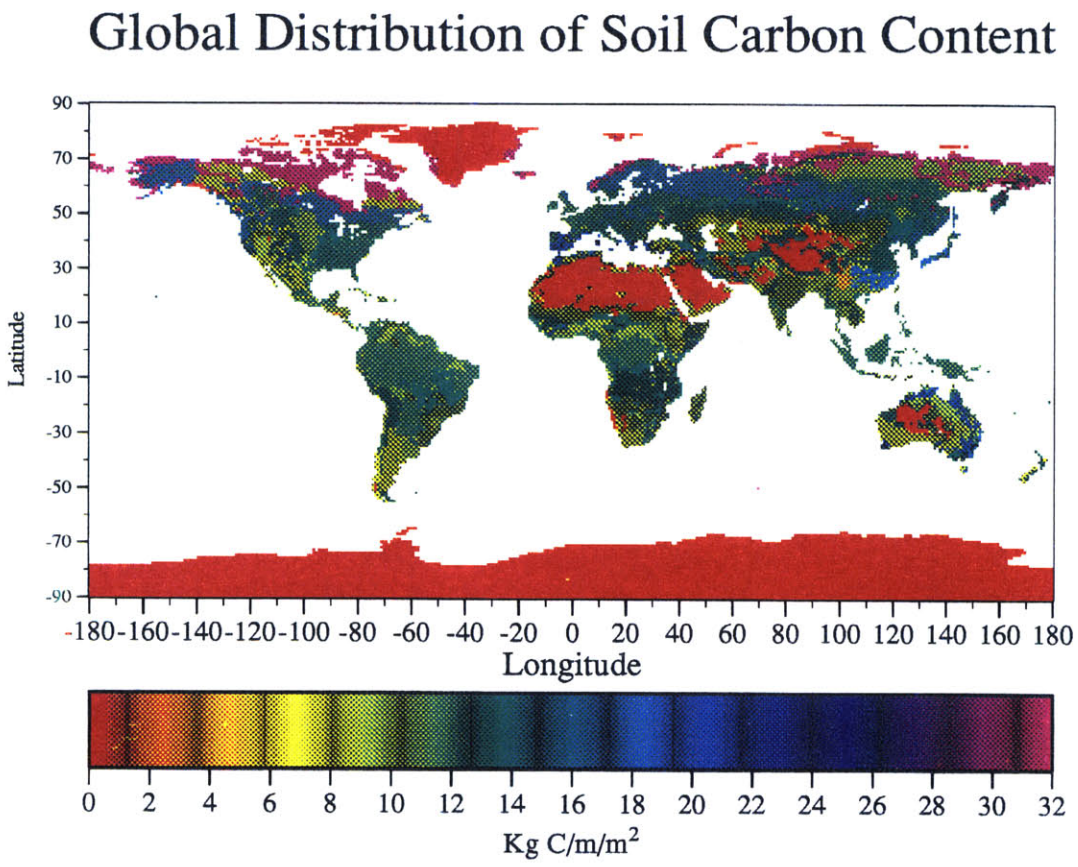

Figure 2-2: Global distribution of soil organic carbon content (in Kg C per meter depth per square meter area).

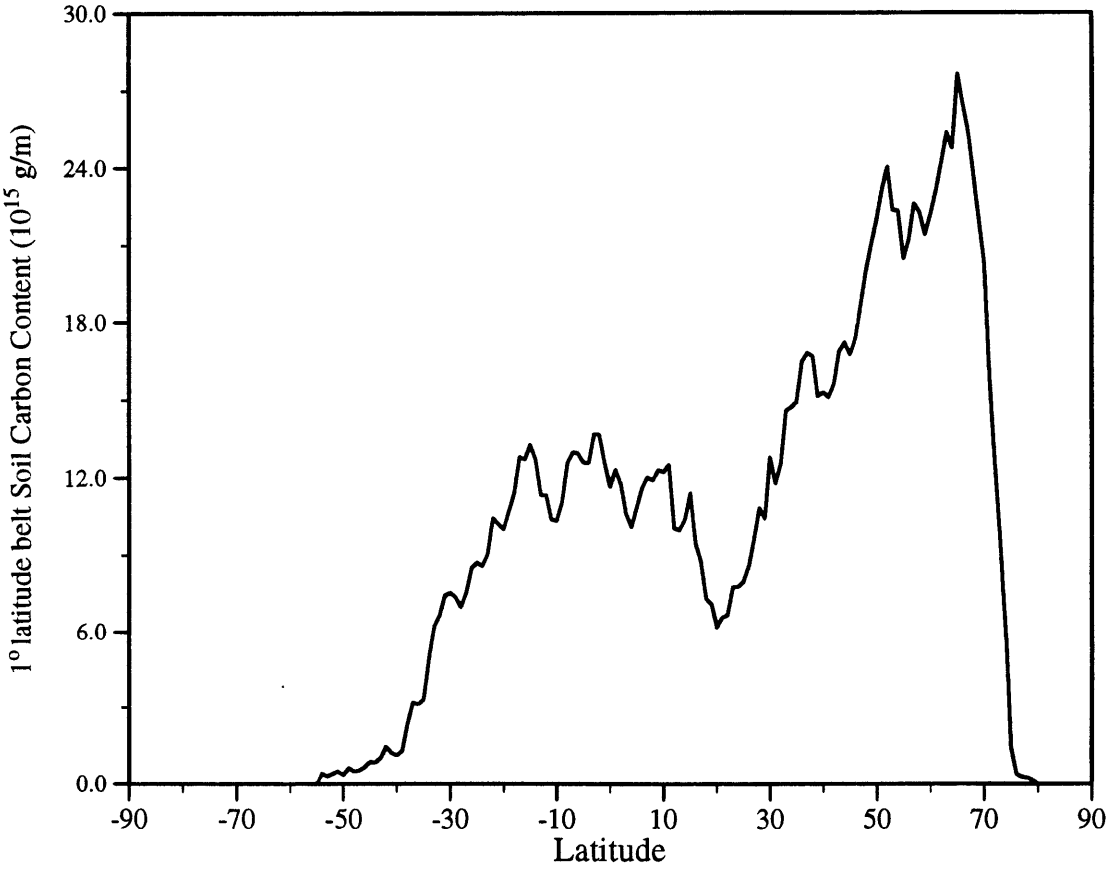

Figure 2-3: Latitudinal profile of meter depth soil organic carbon content (Latitude in degrees, with positive values denoting the Northern Hemisphere).

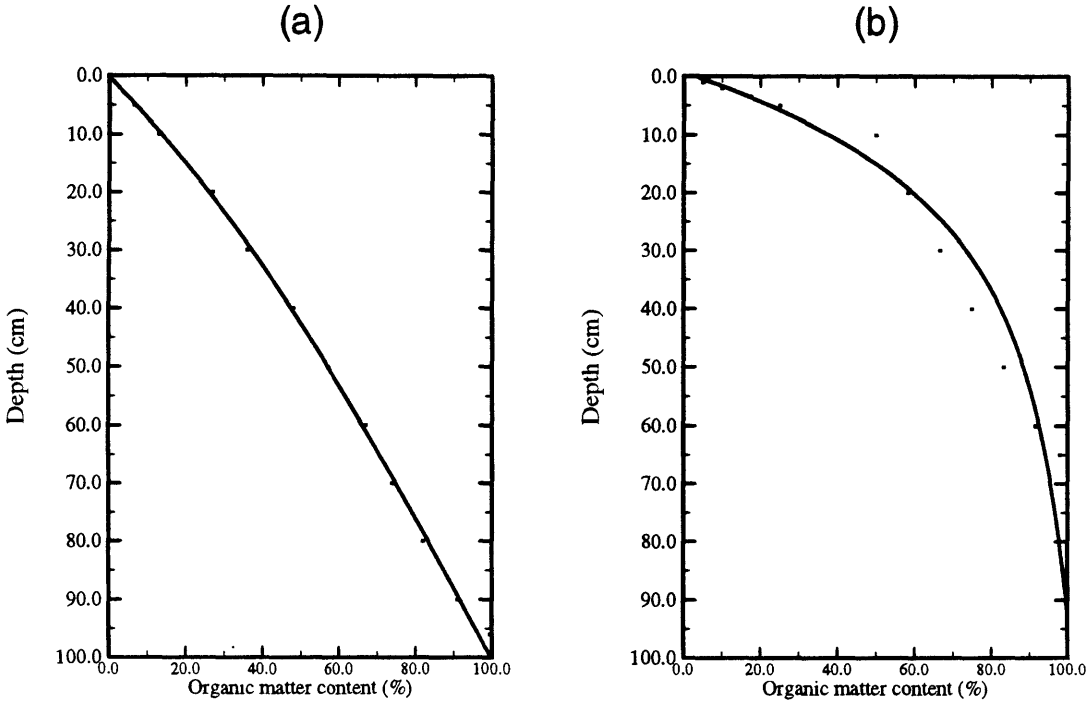

Figure 2-4: Typical organic matter profiles for soils. (a) Grassland. (b) Woody Vegetation.

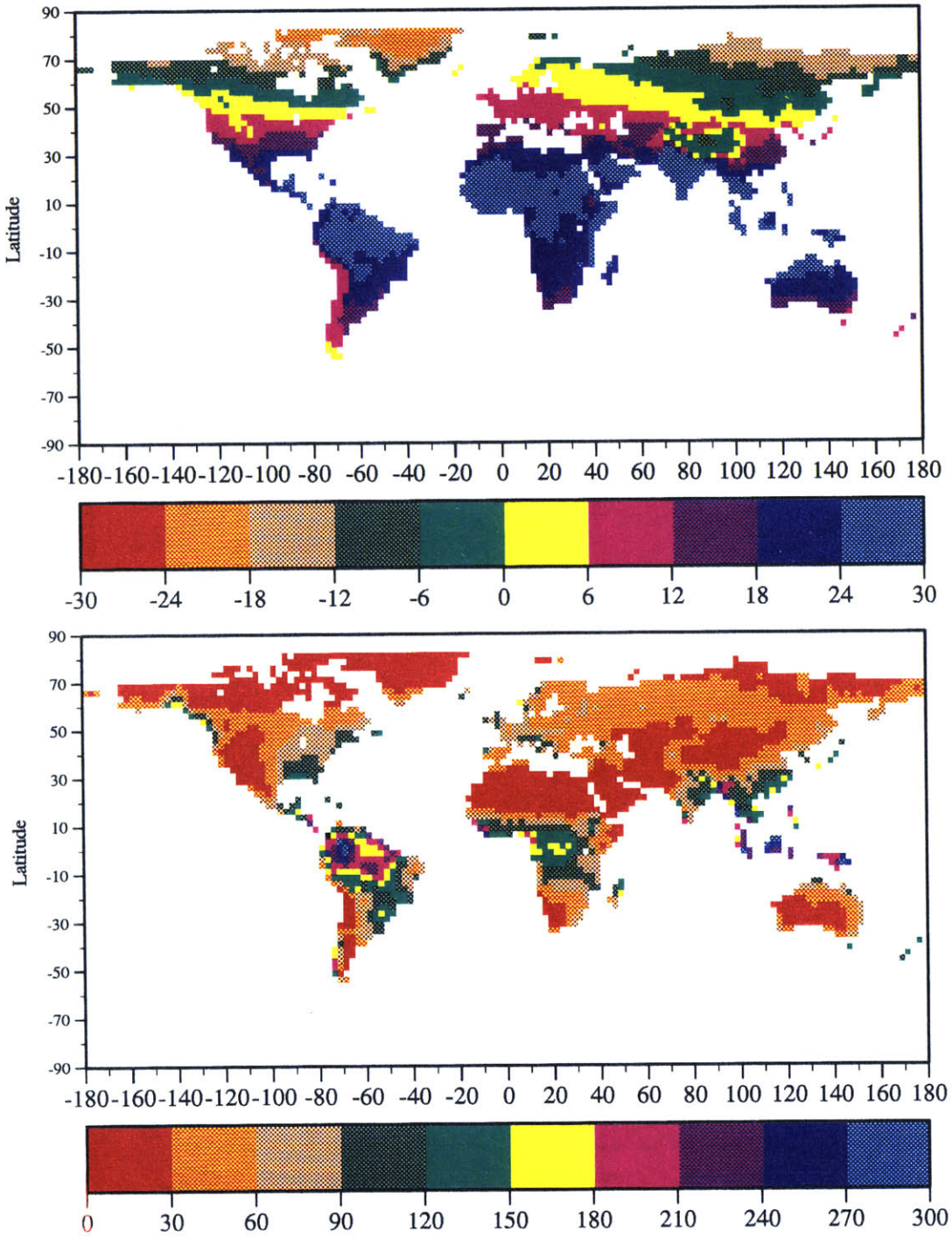

Figure 2-5: Cramer and Leemans' climatology for surface temperature (upper panel, in °C) and precipitation (lower panel, in mm/month) at 2.5°×2.5° resolution.

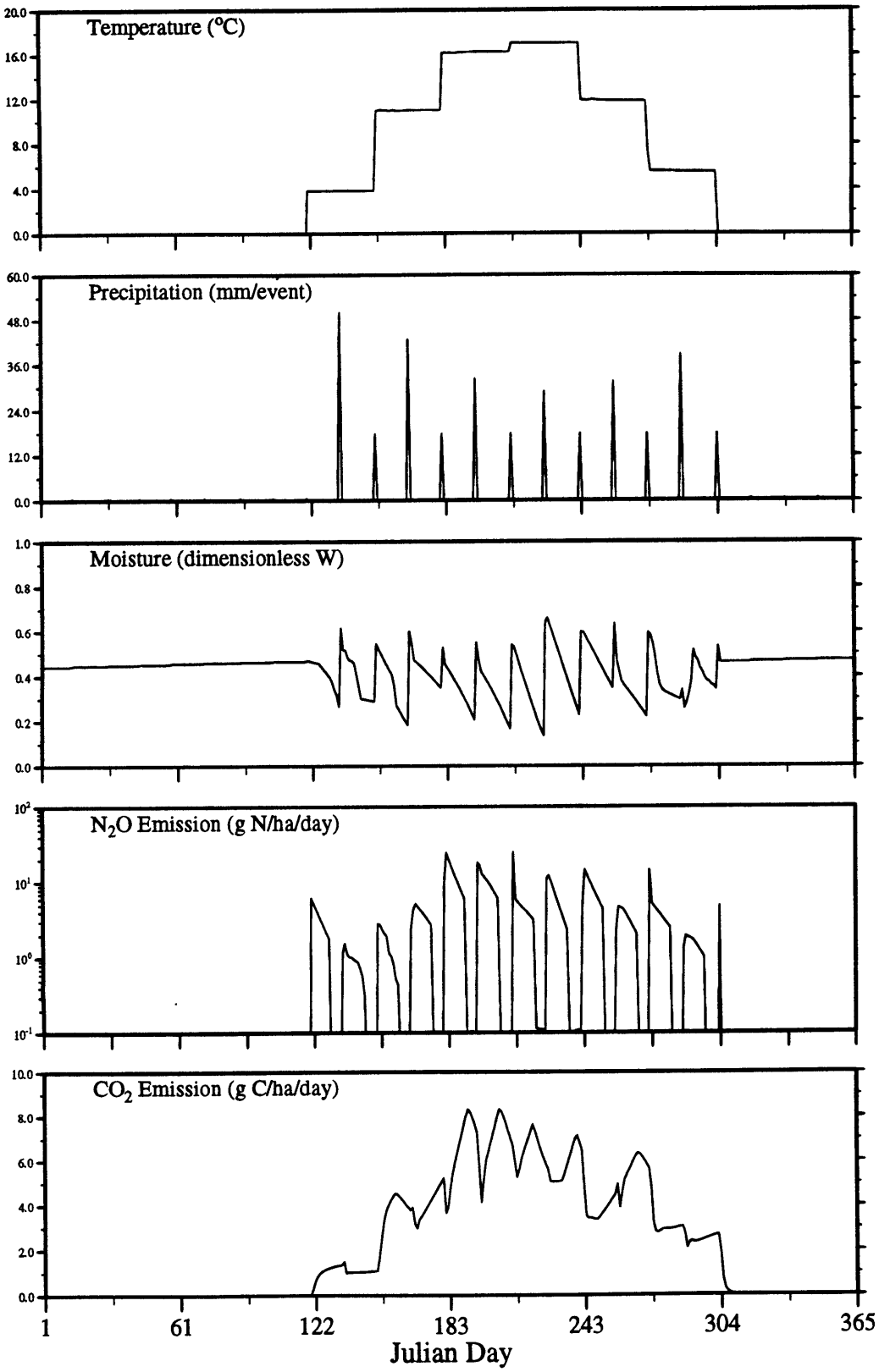

Figure 2-6: Examples of one-year climatology and modeled N_2O and CO_2 emission time series for typical boreal forest soils (The location for the time series: 92.5°W, 52.5°N).

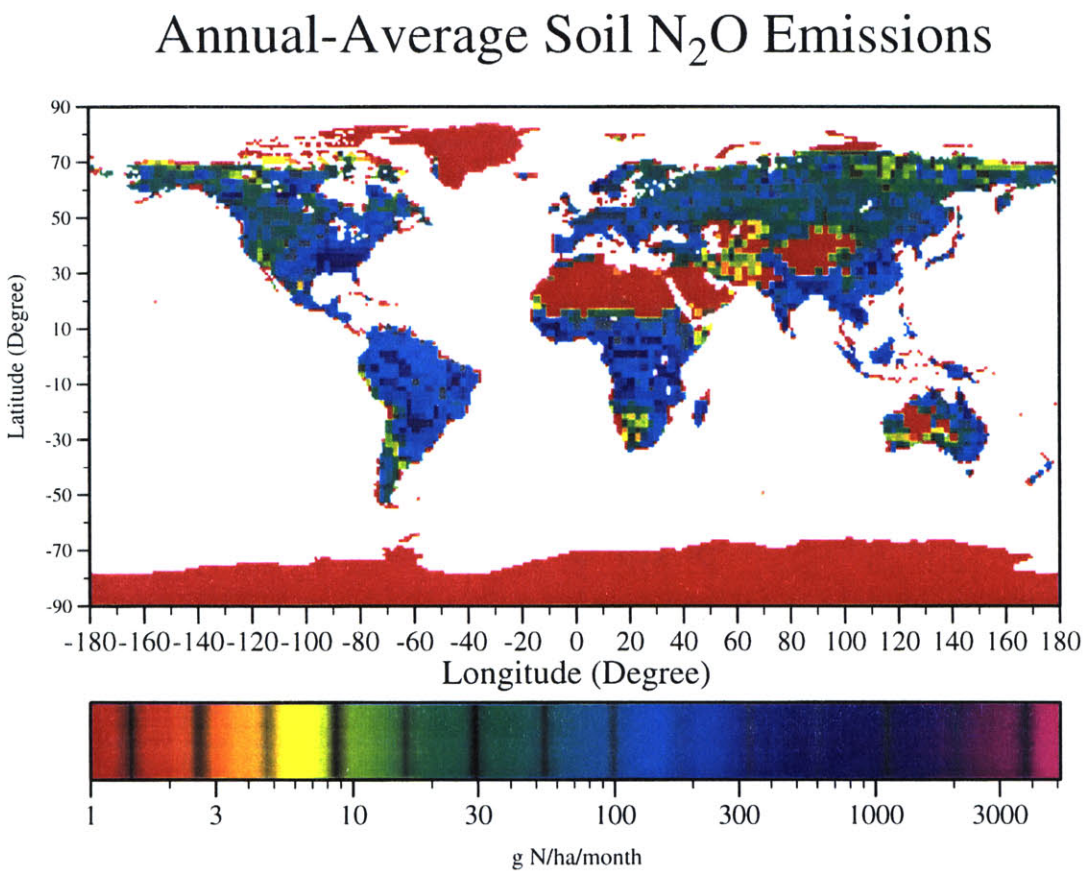

Figure 2-7: Model predicted global distribution of annual-average monthly soil N_2O emissions at $2.5° \times 2.5°$ resolution.

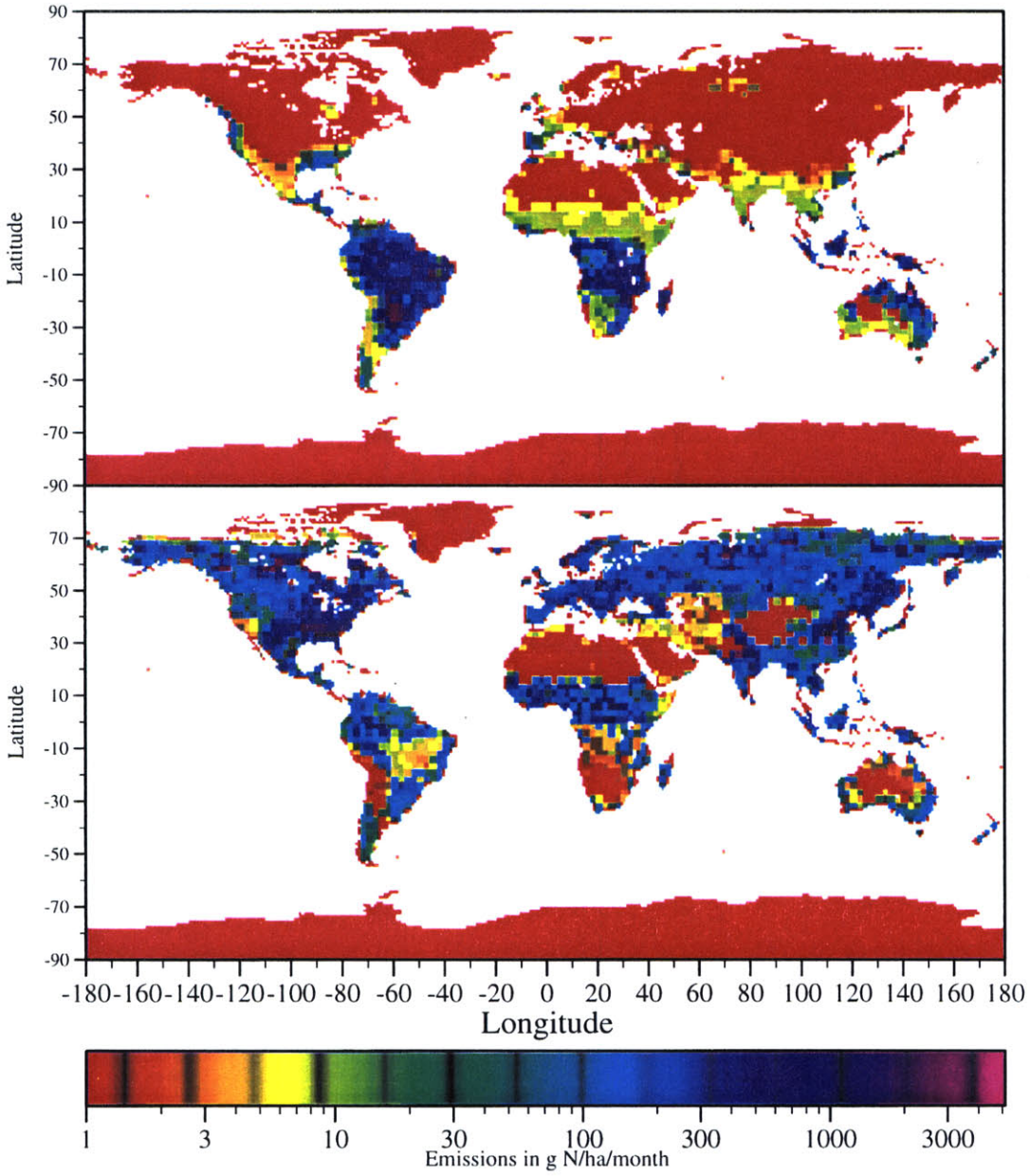

Figure 2-8: Model predicted monthly soil N_2O emissions for January and July at $2.5° \times 2.5°$ resolution.

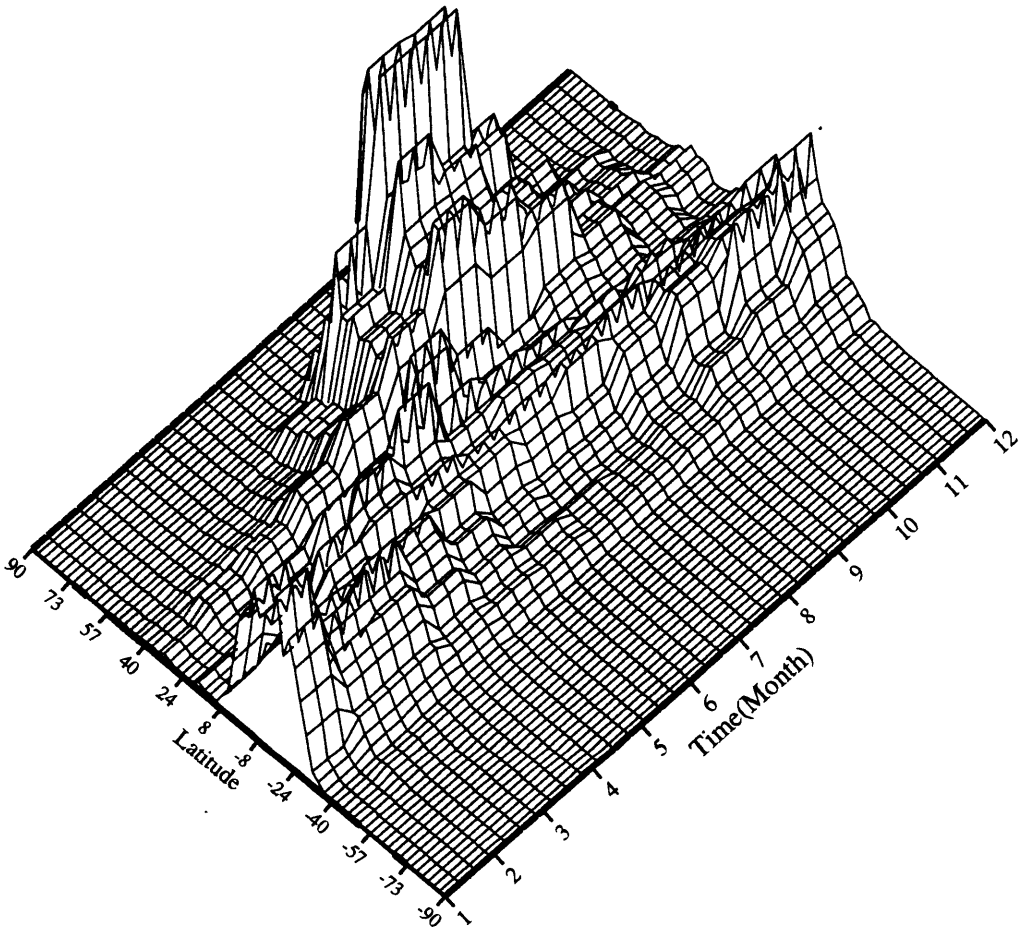

Figure 2-9: Model predicted latitudinal and seasonal variations of soil N_2O emissions (Latitude in degrees, with positive values denoting the Northern Hemisphere).

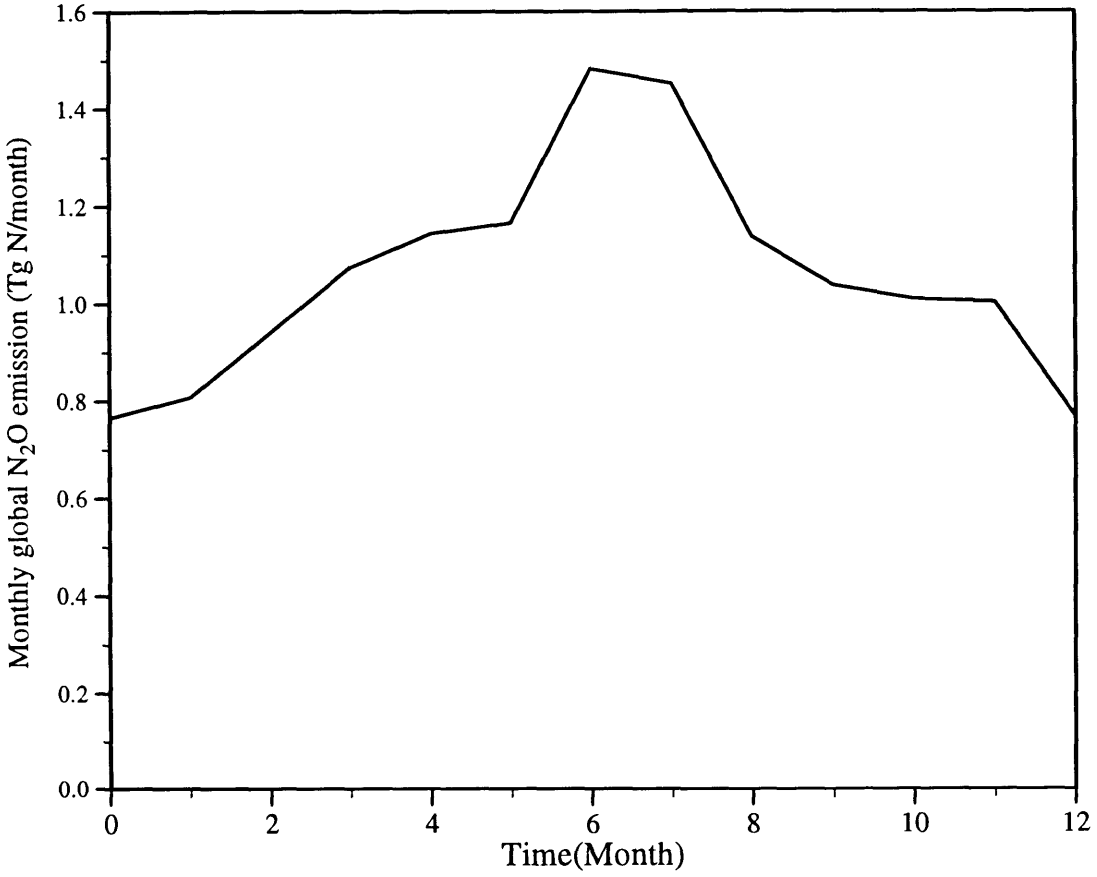

Figure 2-10: Model predicted seasonal variation of total soil N_2O emission.

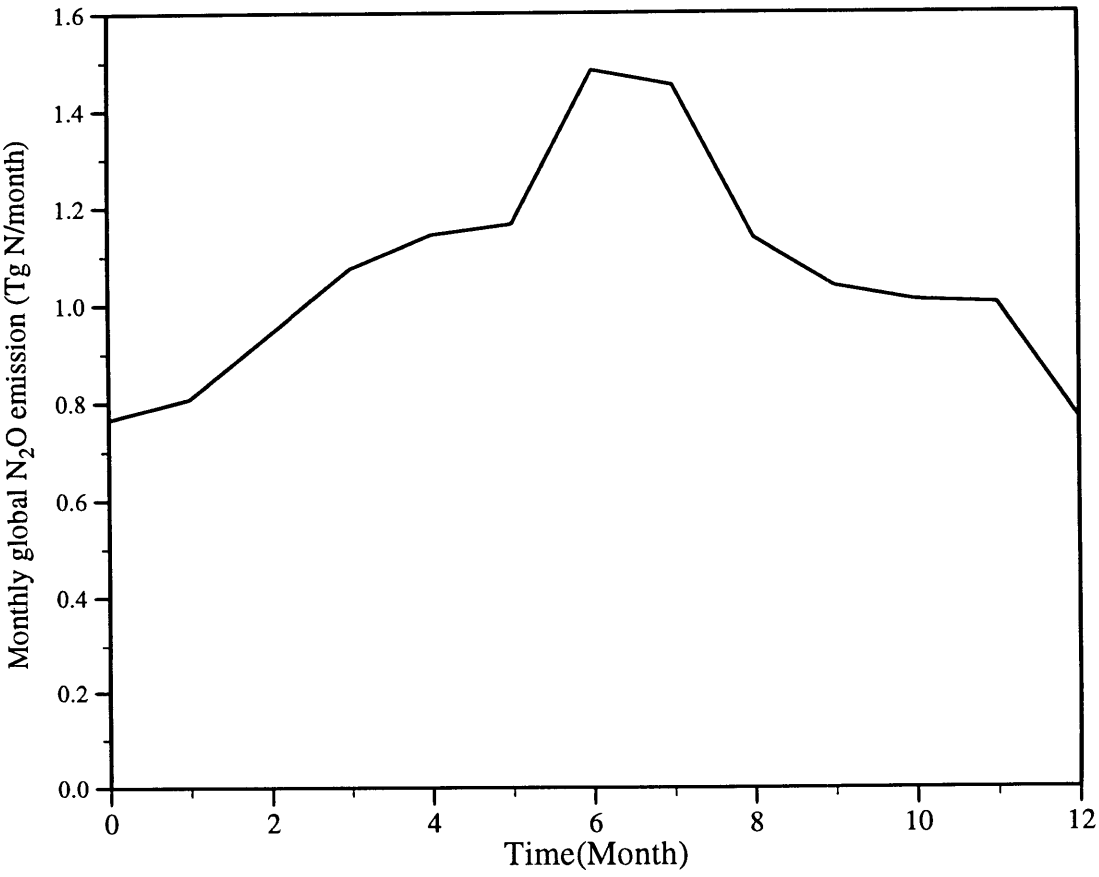

Figure 2-10: Model predicted seasonal variation of total soil N_2O emission.

Chapter 3

Development of Global CH_4 Emission Model

3.1 Introduction

The methane emission model has been developed specifically for global wetlands. Methane emission from high latitude bogs is modeled based on a bog hydrological model and some empirical relations between the methane flux and regulating parameters. Methane emission from tropical wetlands is modeled by connecting the emission flux directly with climate variables. For this purpose, some assumptions have been made regarding the relation between the tropical flux and the climate variables. Methane emission from tundra is modeled by using a constant methane flux and a hypothetical duration for its emission season.

There is a general agreement among the current generation of general circulation climate models (GCMs) that high latitudes should experience the greatest climate change when global climate changes [*Mitchell, 1989*]. Assessments of the global area of natural wetlands by Matthews and Fung [*1987*] and Aselmann and Crutzen [*1989*] show that large wetland areas are concentrated in the boreal/subarctic zone (45°-73°; about 3×10^6 km^2) and the tropics (20°N-20°S; about $1.5\text{–}2\times10^6$ km^2), while temperate wetlands occupy only about 0.8×10^6 km^2. Measurements also show that methane fluxes in northern high latitude wetlands have a strong seasonal variation

[*Crill et al., 1988; Dise et al., 1993; Bartlett et al., 1992; Whalen and Reeburgh, 1988,1992; Moore et al., 1990*]. However, in the tropics, there are very little data on seasonal variations of the methane flux for wetlands. Based on current knowledge, the high latitude bogs would play an important role in the response of natural CH_4 emissions to climatic change particularly if drastic climate change occurs (e.g. the last ice age or potential future warming).

Boreal and sub-arctic bogs have a soil carbon pool of about 450,000 Tg C and the estimated accumulation rate is about 75 TgC/yr [*Gorham, 1991*]. A drastic climate change in high latitudes could result in a significant change in the methane flux and then in the atmospheric methane budget.

Although current understanding of methane microbiological processes is not sufficient for quantification of detailed processes, it is clear from field studies [*Williams and Crawford, 1984; Moore and Knowles, 1989; and those mentioned above*] that soil climate has a stong impact on the methane flux in high latitude wetlands. Also, both temperature and moisture are likely to play a role, although the relation between the methane flux and soil temperature/moisture is presently not well defined. A model of methane flux from high latitude bogs should certainly model the bog climate as a basis for predicting flux.

The methane emission model developed here uses the hydrological model developed at the University of New Hamsphire [*Frolking, 1993*] to predict the high latitude bog soil climate from surface air temperature and precipitation. The relation between the methane flux and soil climate variables is determined by using some existing empirical regression equations and available observational data for methane fluxes.

Detailed process-related simulations for methane fluxes from natural wetlands should be seen as a more distant goal. Proposals for developing process-related site models for methane emissions by high latitude wetlands and rice paddies are only now being initiated (Li, University of New Hampshire, pers. comm.). However, the model developed here is structured so it can be easily adapted to incorporate new microbiological site models as they evolve.

3.2 Main Processes and The Role of Soil Climate

Methane emission from a particular ecosystem is basically controlled by two different microbial processes: CH_4 production and CH_4 oxidation [*Rudd and Taylor , 1980*]. Only that part of CH_4 which is not oxidized will enter the atmosphere. Whereas CH_4-producing bacteria (the methanogens) require strictly anoxic conditions, the CH_4-oxidizing bacteria (the methanotrophs) require oxygen for metabolism. The balance between the microbial processes of methanogenesis and methane consumption controls the methane emissions to the atmosphere.

3.2.1 Methanogenesis

Methanogenesis, the biological formation of methane , is a geochemically important process that occurs in all anaerobic (or anoxic) environments in which organic matter undergoes decomposition: specifically wetlands, paddy rice fields, and the digestive tracts of ruminants and termites. The biogenic CH_4 results from the metabolic activity of a small and highly specific bacterial group, which are terminal members of the food train in their environment. These strictly anaerobic bacteria convert fermentation products formed by other microorganisms, notably CO_2, H_2 and esters and salts of methanoic acid (HCOOH) into CH_4, but other substrates may be used as well [*Cicerone & Oremland, 1988*].

Schutz *et al.* [*1989*] found methane was mainly produced from H_2-CO_2 (30-50%) and from acetate in their radiotracer studies, while Takai and Wada [*1990*] discovered the decarboxylation of ethanoic acid (CH_3COOH) as the most important biochemical pathway of methane formation in waterlogged paddy soils. Yavitt et al. [*1987*] observed that methane production proceeded primarily through the CO_2-reduction pathway in deep peat (30-45cm) and that the rate was controlled in part by the availability of H_2. Williams and Crawford [*1984*] found that adding glucose and H_2-CO_2 to peat stimulated methanogenesis while adding acetate inhibited methanogenesis. The different conclusions of these studies highlight the lack of full understanding of methane formation processes and substrates.

3.2.2 Methanotrophy

A considerable part of the newly generated methane is oxidized microbiologically and does not go into the atmosphere. For example, Oremland and Culbertson [*1992*] found that more than 90% of the methane potentially available was consumed by methanotrophic bacteria. The microorganisms that are responsible for the oxidation of methane can use methane and other C_1-compounds such as methanol as substrates for their metabolism.

Some ammonium oxidizers can also use methane as their substrate. Conrad and Rothfuss [*1991*] found that the oxidation of methane was inhibited by the addition of ammonium. Possibly, the supplied ammonium stimulated nitrification as opposed to CH_4 oxidation and/or it may have constrained the availability of oxygen. Since the methane oxidation process could also occur in anaerobic condition and sulphate is the only apparent oxidant present in sufficient quantity to cause a significant removal of methane under this condition, it is possible that sulphate reducers consume methane under anaerobic conditions [*Yavitt et al., 1987*].

The work reviewed above on processes for methane production and consumption demonstrates that the mechanisms regulating methane flux are very complicated and are not fully understood. This lack of full understanding of the governing precesses and also required substrates make it difficult to quantify accurately the methane fluxes. We must instead resort to some empirical approaches to model methane emissions from wetlands using available observational data. However, if we can link empirically the methane fluxes to some well defined controlling parameters, we can still quantatively capture the characteristics of methane flux change associated with climate change even without fully understanding the processes involved.

3.2.3 Soil Climate Controlling Variables

Soil climate (soil temperature and soil moisture status), which is driven by the surface climate, is known to play a strong role in the emissions of methane from northern high latitude wetlands. It is clear that metabolic activity of soil microbes in wet-

lands is strongly temperature dependent. This holds for methane producing bacteria (methanogens) as well as for methane consuming bacteria (methanotrophs) and also the microbes in the decomposition chain that produce substrates for the methanogens from soil organic matter [*Kelly and Chynoweth,1981; Willians and Crawford, 1984*]. Although the direct relation between the methane flux and temperature derived from the experiments varies, it is generally accepted that increasing temperature induces higher methane production for a rough temperature range of 4°C to 30 °C.

Soil moisture status controls the oxygen availability for methanotrophic bacteria which consume methane under aerobic conditions. This consumption of methane can occur in the surface layer of wetlands above the water table or in the vicinity of roots of plants that can pump oxygen below the water table. The surface layer of wetlands usually has very high porosity and hydraulic conductivity. It is either very wet or very dry if it is below or above the water table. Water table depth therefore becomes an important parameter in describing the oxygen status in wetlands.

Water table depth influences methane flux to the atmosphere in a variety of ways. First, it directly controls the length and diffusivity of the pathway from the zone of methane production to the atmosphere. As this path diffusivity and/or length increases, the opportunity for methane oxidation increases. Second, in some wetlands, the surface layer has the richest organic substrate pools and the highest temperature in summer. A higher water table will therefore allow methane production to occur in the most favorable region, which should enhance production rates. There are still other factors relevant to water table which control methane flux. For example, methanotrophs which prefer certain nutrients seem to exist predominantly at the interface between the zone of production and the zone of potential oxidation [*Fechner and Hemond, 1992*]. Hence, if the water table changes, the population of methanotrophs and the oxidation rate of produced methane change as well.

The empirically derived relation between observed average methane flux and observed average water table depth is generally consistent with this notion that decreasing water table depth induces higher methane flux. However, some field experiments have shown that there is no significant correlation between instantaneous flux rate and

water table depth [*Roulet et al., 1992; Sebacher et al., 1986; Whalen and Reeburgh, 1990*]. This may be caused by increased gas diffusivity and thus release of CH_4 trapped in pore water [*Moore and Roulet, 1993*] after a lowering of the water table (i.e. after an increase in water table depth). The temporal patterns between methane flux and water table position are very complicated and difficult to establish. It seems that there is a strong "hysteresis" between methane flux and the change of water table position (falling and rising) [*Moore and Roulet, 1993*]. However, when expressed as seasonally averaged values, generally there is a strong relationship between methane flux and water table position.

Since soil climate, through its influence on microbial activityy, controls the methane flux from northern high latitude bogs, accurate modeling of the soil hydrology is vital for accurate prediction of the methane flux.

3.3 Bog Soil Hydrology Model

Our soil hydrology model for high latitude bogs uses the two-layer peat hydrological model developed by Frolking [*1993*] at the University of New Hamsphire.

One of the characteristics of northern high latitude bogs is that they have two distinct layers. The surface layer consists of uncollapsed and relatively undecomposed sphagnum moss characterized by very high porosity and hydraulic conductivity and periodic aerobic conditions. The submerged layer below consists of collapsed and decomposed peat which is usually water saturated. The submerged layer has lower porosity and much lower hydraulic conductivity than the surface layer. Our bog soil hydrology model adopts this basic two-layer structure.

3.3.1 Heat Transfer Model

As for our treatment of heat transfer in upland soils in the nitrogen model, the heat flux in bogs is modeled by gradient-driven diffusion:

$$c\frac{\partial T}{\partial t} = \frac{\partial}{\partial z}(k\frac{\partial T}{\partial z}) \tag{3.1}$$

where T is the soil temperature (°C), z is the depth, c is the soil volumetric heat capacity (J·cm^{-3}· °C^{-1}), k is the soil thermal conductivity (W·m^{-1}·°C^{-1}), and t is time (sec).

Since the model has a freeze/thaw component to tract frost penetration in the winter months, substantial attention is devoted to parameterizing c and k in the above equation.

If there is no ice phase appearing in the bogs, c and k can be expressed with linear formuli as follows.

$$c = (1-n)\,c_{org} + n\,c_{liq}\,W \tag{3.2}$$

$$k = (1-n)\,k_{org} + n\,k_{liq}\,W \tag{3.3}$$

where n is the soil porosity, W is the fractional water filled pore space, and the subscripts refer to organic matter and liquid soil components. It is assumed that there is no mineral soil component in the model profile, which is realistic for bog soils.

The soil water is assumed to freeze continuously over a finite temperature range of -1°C–0°C. Above 0°C, the soil water is definitely in the liquid phase. Below -1°C all the soil water is assumed to be in the ice phase. In the defined freeze/thaw range, the fraction of the water that is frozen is parameterized linearly as follows.

$$F_{ice} = \frac{T - T_{sol}}{T_{liq} - T_{sol}} \tag{3.4}$$

where F_{ice} is the fraciton of the soil water that is frozen, T_{sol} is the temperature at which all soil water is frozen (-1°C), and T_{liq} is the temperature at which all soil water is melted (0°C).

While the soil temperature is in this freeze/thaw range the soil contains of course a mixture of ice and water. Hence, the soil heat capacity and thermal conductivity

are given by linear formuli:

$$c = (1-n)\,c_{org} + n\,W\,[(1-F_{ice})\,c_{wat} + F_{ice}\,c_{ice}] + \frac{L_f}{T_{liq}-T_{sol}} \tag{3.5}$$

$$k = (1-n)\,k_{org} + n\,W\,[(1-F_{ice})\,k_{wat} + F_{ice}\,k_{ice}] \tag{3.6}$$

where L_f is the latent heat for ice fusion.

The upper ice/water boundary is considered to be at the depth where the soil temperature is equal to T_{freeze}.

$$T_{freeze} = 0.5\,(T_{sol} + T_{liq}) \tag{3.7}$$

The boundary conditions for the heat transfer model are the same as those for upland soils which were addressed in Chapter 2.

3.3.2 Soil Moisture and Water Table Model

Because the surface layer of the bog behaves differently from regular mineral upland soil, the gradient-driven water flow equations do not apply for the case of bog. A water balance model is instead used for modeling water table fluctuation and soil moisture. The water balance model distributes the water in the vertical profile with the addition of water by rainfall and snowmelt and the removal of water by evaporation and drainage. The water balance equation can be written as follows.

$$Q_{input} = Q_{output} + Q_t \tag{3.8}$$

where Q_{input} is the water added from rainfall and snowmelt, Q_{output} is the water lost by evaporation and drainage, and Q_t is the rate of change of total water content in the profile.

The rainfall is added directly to the bog water budget. The evaporation is calculated using Thornthwaite's formula [*Thornthwaite, 1948*] (see equations in Chapter 2). The snowmelt and drainage are parameterized as equations (3.9) and (3.10):

$$Q_{melt} = 0.5\,T_{air}\,[(MF_{max} + MF_{min})(1 + sin(2\,\pi(day + 81)/365))] \qquad (3.9)$$

where Q_{melt} is snowmelt per hour [*Bras, 1990*], MF_{max} and MF_{min} are snowmelt parameters (0.025 and 0.0125 cm·water·h^{-1}·°C $^{-1}$ respectively from *Bras*), and *day* is the Julian day (for the northern hemisphere). No snowmelt occurs if T_{air} is less than 0°C. Once there is snow at the surface, both the heat transfer model and the soil moisture model have an additional layer above the bog surface with the snow surface temperature taken equal to the surface air temperature. For drainage we have:

$$Q_{dr} = Q_{dr,max}(\frac{z_w - z_{crit}}{z_{pool} - z_{crit}})^2 \qquad (3.10)$$

where Q_{dr} is the drainage rate (cm·water·h^{-1}, $Q_{dr,max}$ is the maximum drainage rate, z_{crit} is the depth at which drainage stops, z_{pool} is the depth at which water is allowed to pool over the peat and thus has its maximum drainage rate, and z_w is the water table depth.

There are two assumptions in distributing water in the bog soil profile. The first one is that the water content drops from a water-filled porosity space equal to 100% to some lower value immediately at the water table depth (i.e. there is a discontinuity of soil moisture at the water table depth), which reflects the weak suction of bog peat. The second one is that the water content falls off linearly with height above the water table in both the surface bog layer and the submerged bog layer (there is also a discontinuity of soil moisture at the interface between the two bog layers). The second assumption allows for a weak capillary effect in the peat [*Boelter, 1969*].

The internal parameters required in the model are surface layer depth (z_a), surface layer and submerged layer porosities (n_a and n_c), surface layer and submerged layer water-filled-porosity-space immediately above the water table (W_a and W_c), gradient of water content above the water table for each layer (α and β), and maximum water table depth (the depth to which evaporation can lower the water table, z_b).

The soil moisture and water table model is schematically described in Figure 3-1.

It is clear from the figure that the change rate of total water content (Q_t) in the profile is as follows.

$$Q_t = \frac{d\left(\int_0^{z_w} n(z,t)\,W(z,t)\,dz + \int_{z_w}^{z_b} n(z,t)\,dz\right)}{dt} \tag{3.11}$$

Since Q_t can be derived from water balance equation, the above equation can be used to invert the water table depth (z_w) and to determine profile distribution of water content.

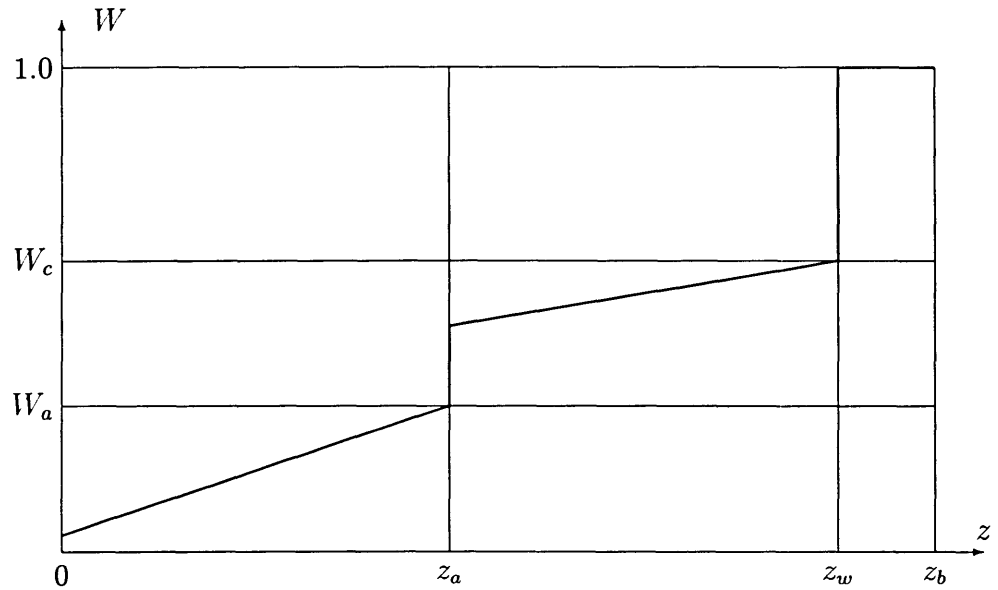

Figure 3-1: The two-layer model for bog soil moisture and water table. Here z is the depth, W is the water filled pore space (WFPS), z_a is the depth for the surface layer, z_b is the maximum water table depth, W_a and W_c are the WFPS just above the water table for the surface layer and the submerged layer, and z_w is the water table depth. The thick line is the distribution of soil moisture: below the water table depth (z_w), W is equal to 1, while above that it increases with depth linearly in both layers. Moisture discontinity occurs at z_a and z_c.

3.4 Bog's Methane Flux Model

The empirically derived flux–temperature and flux–water table depth relations vary widely for different site measurements. While some studies (e.g. Crill *et al.*, [*1988*])

have shown strong correlations between flux and either temperature or water table depth, some simply do not (e.g. Moore *et al.*, [*1990*]; Whalen and Reeburgh, [*1992*]). This inconsistency could be explained by several possibilities. First, because of the high spatial and temporal variability of the methane flux, the available low frequency and spatially sparse measurements could lead to imprecise estimates of the real methane flux. Second, the temperature dependences of rates of microbial CH_4 consumption and production are different: the former have Q_{10} values ranging from 1.2 to 2.1, while the latter fall in the range 2.1 to 6.8 [*Moore and Roulet, 1993*]. Thirdly, the temperature and the water table level are interdependent resulting in confounding influences on the methane flux.

To describe the influence of climate on the methane flux, a relation between this flux and the combined effects of temperature and water table depth is synthesized here based on widely used single relations between methane flux and temperature or water table depth.

Specifically, the relationship between the methane flux and water table depth derived by Moore and Roulet, [*1993*] is adopted to quantify the effect of soil moisture on methane flux:

$$E(z_w) \propto 10^{-0.026\, z_w} \tag{3.12}$$

where E is methane flux in $\mathrm{mg\,CH_4\,m^{-2}\,d^{-1}}$, and z_w is the water table depth in cm.

Several quantitative linear regressions of the logarithm of the methane flux with temperature have been reported (as reviewed by Bartlett and Harriss, [*1993*]). These regressions clearly demonstrate a striking similarity in slopes for their relationships. This similarity exists for a variety of high latitude environments, which implies that a single functional relationship between temperature and methane flux could be used to model large scale methane emissions.

The average slope in Bartlett and Harriss [*1993*] gives following functional relationship:

$$E(T) \propto e^{0.121T} \tag{3.13}$$

where $E(T)$ is methane flux in $\mathrm{mg\,CH_4\,m^{-2}\,d^{-1}}$, and T is temperature in $^\circ C$.

In order to get a functional relation between flux and a combination of temperature and water table depth, it is assumed that the relation has the following exponential form:

$$E = A \cdot e^{bT_{z_w} + cz_w} \tag{3.14}$$

Because methanogenesis occurs below the water table (z_w) and methanotrophs prefer to exist predominantly at the interface between the zone of production and the zone of potential oxidation (which is definitely close to water table), soil temperature at the water table depth is used in above equation. It is further assumed that the above equation keeps the same relationships of emissions to temperature and water table depth as in equation (3.12) and (3.13), which would give us two constants.

$$b = 0.121 \tag{3.15}$$

$$c = -0.0599 \tag{3.16}$$

The coefficient A varies widely for different measurements (with a range of e^1—$e^{4.5}$ in [*Moore and Roulet, 1993*]). The observed methane flux is used to obtain the value for coefficient A as follows. The methane flux model is rewritten as

$$E = F_{obs} \cdot e^{0.121(T_{z_w} - \overline{T_{z_w}})} \cdot e^{-0.0599(z_w - \overline{z_w})} \tag{3.17}$$

where F_{obs} is the mean observed flux (averaged over a specific region and for a specific emission season) and

$$\overline{T_{z_w}} = \frac{\ln \overline{e^{0.121T_{z_w}}}}{0.121}$$

$$\overline{z_w} = -\frac{\ln \overline{e^{-0.0599z_w}}}{0.121}$$

The overbar here represents the mean defined for the same regions and time periods used to define the mean observed flux. Given this definition of the mean, Equation 3.17 ensures that the mean of the modeled flux is exactly the same as the

Regions	Observed Mean Flux (F_{obs})	$\overline{T_{z_w}}$ (°C)	$\overline{z_w}$ cm
60°-90°	96.0 mg $CH_4/m^2/day$	5.20038	9.53192
45°-60°	87.0 mg $CH_4/m^2/day$	10.60985	9.52648
0°-45°	135.0 mg $CH_4/m^2/day$	24.01706	8.60748

Table 3.1: Observed mean methane flux and flux model constants

observed one. This is equivalent to using observed flux as a constraint to obtain the value for A in equation 3.14. Based on available methane flux data [*Moore and Roulet, 1993*], global bogs are divided into three regions in calculating the mean values of the temperature and water table depth. The calculated values and the observed mean methane flux are presented in Table 3.1.

When the soil temperature at the water table depth is below -1°C (at which all the soil water is frozen to ice), the methane flux is assumed to be zero.

3.5 Emission Model for Tropical Wetlands

Methane emissions from tropical wetlands are modeled using a two-factor empirical model. The two factors are temperature and water availability.

The temperature factor is used to model the change in methanogenic activity with temperature. Experiments have shown that the optimal temperature for the majority of methanogens ranges from 30°C to 40°C [*Yamane and Sato, 1961; Neue and Scharpenseel, 1984; Conrad et al., 1987; Schutz et al., 1989; Parashor et al., 1993*]. A temperature factor similar to that used in Cao *et al.* [*1995*] has been used to take into acccount the effect of temperature on methane production.

Soil water creates a low redox potential and an anaerobic soil environment for methanogens, which directly affect methane production. This effect is represented simply by a water availability factor. It is assumed that the methane flux is proportional to the precipitation/evaporation ratio when precipitation is less than evaporation.

Methane emission from tropical wetlands is described by following equation:

Wetlands	Flux
Forested Swamp	100 mg $CH_4/m^2/day$
Nonforest Swamp	202 mg $CH_4/m^2/day$
Alluvial Wetlands	182 mg $CH_4/m^2/day$

Table 3.2: Methane Flux for Tropical Wetlands

$$E_{CH_4} = E_{obs} \cdot f_T \cdot f_W \tag{3.18}$$

where E_{obs} is the observed methane flux from tropical wetlands, and f_T and f_W are the temperature and water availability factors. The mean observed values [*Bartlett and Harriss, 1993*] have been used for E_{obs} in the above formula, which are presented in Table 3.2. The two factors are defined as follows:

$$f_T = \frac{F(T_s)}{\overline{F(T_s)}} \tag{3.19}$$

where

$$F(T_s) = \frac{e^{0.334(T_s-23)}}{1+e^{0.334(T_s-23)}}$$

and T_s is temperature in °C and $\overline{F(T_s)}$ is the mean of $F(T_s)$ over tropical wetlands for the time period when all the measurements used in Table 3.2 are conducted. $\overline{F(T_s)}$ is calculated to be 0.6272 which is equivalent to $\overline{T_s} = 24.5$ °C. The other factor is defined by:

$$f_W = \begin{cases} \frac{P}{E} & \text{if } P \leq E \\ 1 & \text{if } P > E \end{cases} \tag{3.20}$$

3.6 Methane Emissions from Wet Tundra

Methane emissions from wet tundra are calculated by assuming a constant methane flux of 8.5 mg $CH_4/m^2/day$ [*Bartlett and Harriss, 1993*] and an assumed emission season. Note that this flux is much smaller than those in the other wetland types

(Table 3.1 and Table 3.2). The emission season is simply assumed to be the time period when the surface temperature is above freezing point.

3.7 Model Structure

Data sets of driving variables are read in first by the global wetland emission model. These data include the global distribution of wetlands and inundated areal fraction [*Matthews and Fung, 1987*], TEM ecosystem types [*Melillo et al., 1993*] and climate [*Cramer and Leemans, personal communication*].

Matthews and Fung divided the wetlands into five major ecosystems: namely, forested bogs, nonforested bogs, forested swamps, nonforested swamps, and alluvial formations. The bogs are concentrated in high latitudes while the swamps and alluvial formations are in the tropics. The two-layer soil hydrology model described before is used to simulate methane emissions from the bogs. Methane emissions from swamps and alluvial formations (tropical wetlands) are modeled using the two-factor model. The geographical distribution of wet tundra, which is one of the TEM ecosystem types, and the surface temperature are used to calculate methane emissions from wet tundra.

While monthly climate data are directly used in the two-factor model for tropical methane emissions, they are processed by the statistical rainfall model described in Chapter 2 before being used in the two-layer bog hydrology model. The daily outputs of surface temperature and precipitation are then used in the bog hydrology model to give daily mean water table depth and soil temperature at the water table depth. The empirical flux model finally uses these controlling parameters to predict daily methane emissions from bogs. The bog soil hydrology model has 10 layers in the vertical with a maximum water table depth of 30 cm and a domain depth of 100 cm. Bog model equations are solved using the Crank-Nicholson numerical scheme [*Press et al., 1992*] with a time step of 15 minutes.

3.8 Model Results for Methane Emissions

3.8.1 Methane Emission Time Series

An example of a predicted one-year CH_4 emission time series is given in Figure 3-2. This is a typical emission series for high latitude bogs. As we can from the lowest panel (panel 5) in Figure 3-2, CH_4 emissions occur in the nonfreezing season with the emissions regulated strongly by temperature and water table depth. This is what we expect from the empirical flux model. Because soil temperature is modeled by the heat diffusion equation, we would expect soil temperature to have a similar variation as surface air temperature. This basically is what the model shows (Figure 3-2, panel 1 and panel 3). However, the temperature at the water table increases at a smaller rate than surface air temperature for the first half of the nonfreezing season. This may be caused by the existence of ice phase in the spring season and/or by the fluctuation of water table level. Monthly precipitation is split into discrete rainfall (and snowfall) events with different rainfall intensities (Figure 3-2, panel 2). The water table fluctuates in the nonfreezing season with precipitating water added into and evaporating water subtracted from the two-layer hydrology model (Figure 3-2, panel 4). The CH_4 emission time series has a combination of those of the features of the temperature and water table depth time series, which shows the controlling role of these two parameters. Sensitivity experiments show that changes in rainfall frequency and intensity have a less effect on annual global total CH_4 emission than on the N_2O emissions discussed earlier. The annual CH_4 emission is closely related to the annual total precipitation rate.

3.8.2 Current Global Methane Emission Results

The global emission model for methane has a spatial resolution of $1° \times 1°$, and predicts daily methane emissions. Model predictions for present-day climate and wetland conditions do capture some basic features of global methane emissions. The annual-average monthly CH_4 emission is shown in Figure 3-3. The results suggest that

global methane emissions have two strong latitudinal belts. One is concentrated in the boreal/subarctic zone. The other is in the tropics. The global spatial distribution of methane emissions is of course similar to the distribution of wetlands.

There are strong seasonal cycles in the high latitude emissions and hence in the global total emission amount (Figure 3-4 and Figure 3-5). While southern hemisphere wetlands have much weaker seasonal cycles, wetlands in the equatorial regions do not have seasonal variations. The strong seasonal variation at high latitudes is due to the shifts between freezing and nonfreezing seasons and the strong seasonal effect of temperature and moisture regimes in these regions. As we can see from Figure 3-4, in the winter season (especially in January and Feburary), there is no emission from the 30°N–90°N region, while in summer season this region has the strongest emissions. As a result of the seasonal variations at high latitudes, the seasonal variation in the global total emission amount has a large amplitude. Note from Figure 3-5, in February the total emission amount reaches its minimum of 6 Tg CH_4 per month while in August the emission is almost double this value.

The global CH_4 emission amount is 126.8 Tg CH_4 per year, which is in the middle of the range of recent estimates (e.g. IPCC, [*1994*]) for natural wetland emissions. The tropical swamps and alluvial formations between 40°S and 20°N contribute 74.3 Tg CH_4 per year, which constitutes one of the two important latitudinal emission belts. Northern high latitudes between 40°N and 80°N contribute 46.8 Tg CH_4 per year. This is the other important latitudinal belt and this belt is the one which could experience drastic change in methane emissions when climate change occurs. The temperate wetlands emit a relatively small amount of CH_4 to the atmosphere: The latitudes between 20°N and 40°N only contribute 5.7 Tg CH_4 per year. Figure 3-6 shows the latitudinal profile of global CH_4 emissions. The above two emission belts are very obvious in the figure. Note that the high latitude belt covers the region where the bog soil hydrology model is used. Because significant regional climate change is expected to happen at high latitudes when global climate change occurs, we would expect the bog soil hydrology model, which is capable of simulating the strong seasonal variations of high latitude CH_4 emissions, would be also able to capture CH_4 emission

changes corresponding to climate changes.

3.9 Conclusions

A global model for wetland methane emissions has been developed. It has a spatial resolution of $1° \times 1°$. There are three components in this emission model: high latitude wetlands, tropical wetlands and wet tundra. For high latitude wetlands (i.e. northern bogs), the emission model uses a two-layer hydrological model to predict the water table level and the bog soil temperature, which are then used in an empirical formula to predict methane emissions. For tropical wetlands (i.e. swamps and alluvial formations), a two-factor model (temperature and water availability) is used to model the methane flux by taking into account the temperature and moisture dependence of methanogenic activity. Methane emissions from wet tundra are calculated by assuming a constant small methane flux and a prescribed emission season. The latter emission season is assumed to be the time period when surface temperature is above the freezing point. The hydrological model and the two-factor model are driven by surface temperature and precipitation. The emission season for wet tundra is controlled by surface temperature only. All these link methane emissions with climate. This linkage forms the basis for the predicted interactions between methane emissions and climate in the coupled emission-climate model described later.

The global CH_4 emission model predicts an annual flux of 127 Tg CH_4 for present-day climate and wetland conditions, which is in the middle of the range of recent estimates for natural wetland emissions [*Bartlett and Harriss, 1993; Reeburgh et al., 1993; IPCC, 1994*]. Global methane emissions are predicted to have two strong latitudinal bands with one in the tropics and the other in the northern high latitudes. There are strong seasonal cycles for the high latitude CH_4 emissions and hence for the global total emission amount.

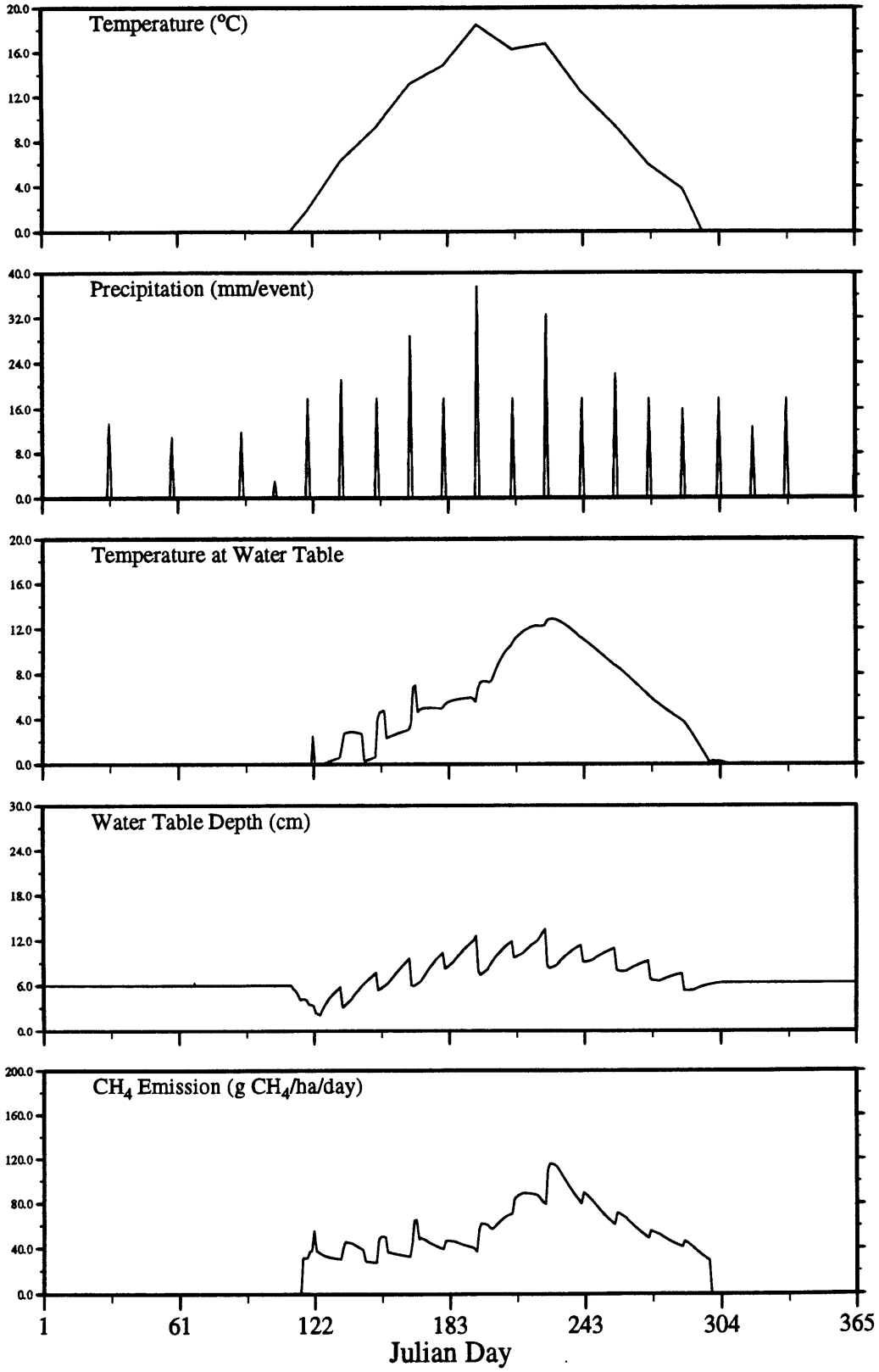

Figure 3-2: An example of predicted one-year CH_4 emission time series and related soil and climate variables for typical northern hemisphere bog (The location for the time series: 95°W, 51°N).

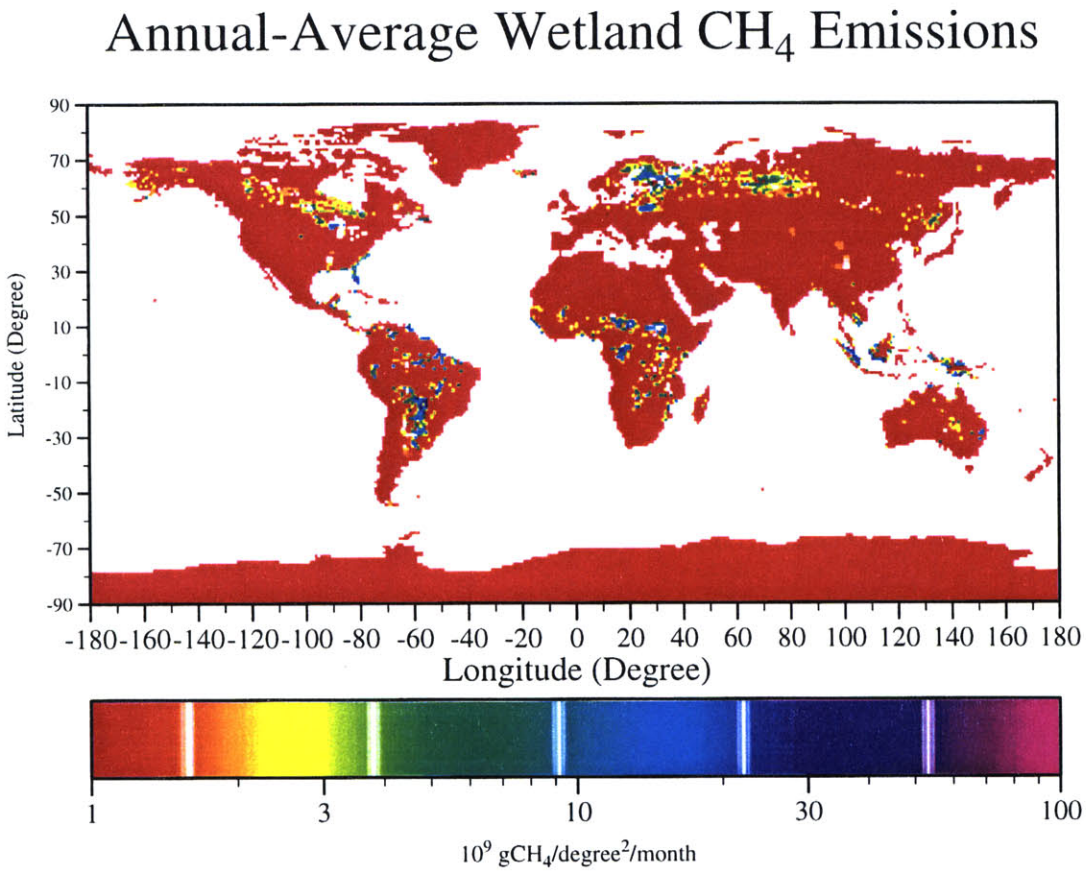

Figure 3-3: Global distribution of predicted annual-average monthly wetland CH_4 emissions at $1^\circ \times 1^\circ$ resolution.

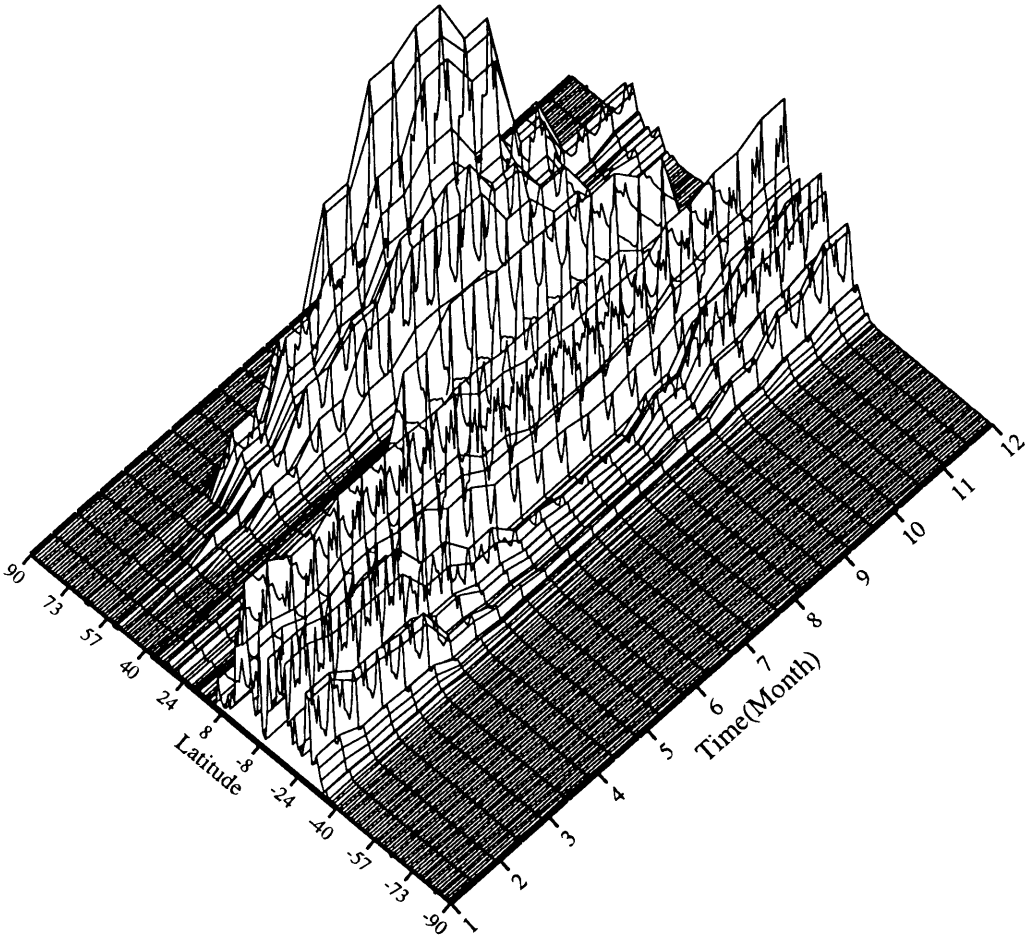

Figure 3-4: Predicted latitudinal and seasonal variations of wetland CH_4 emissions (Latitude in degrees, with positive values denoting the Northern Hemisphere).

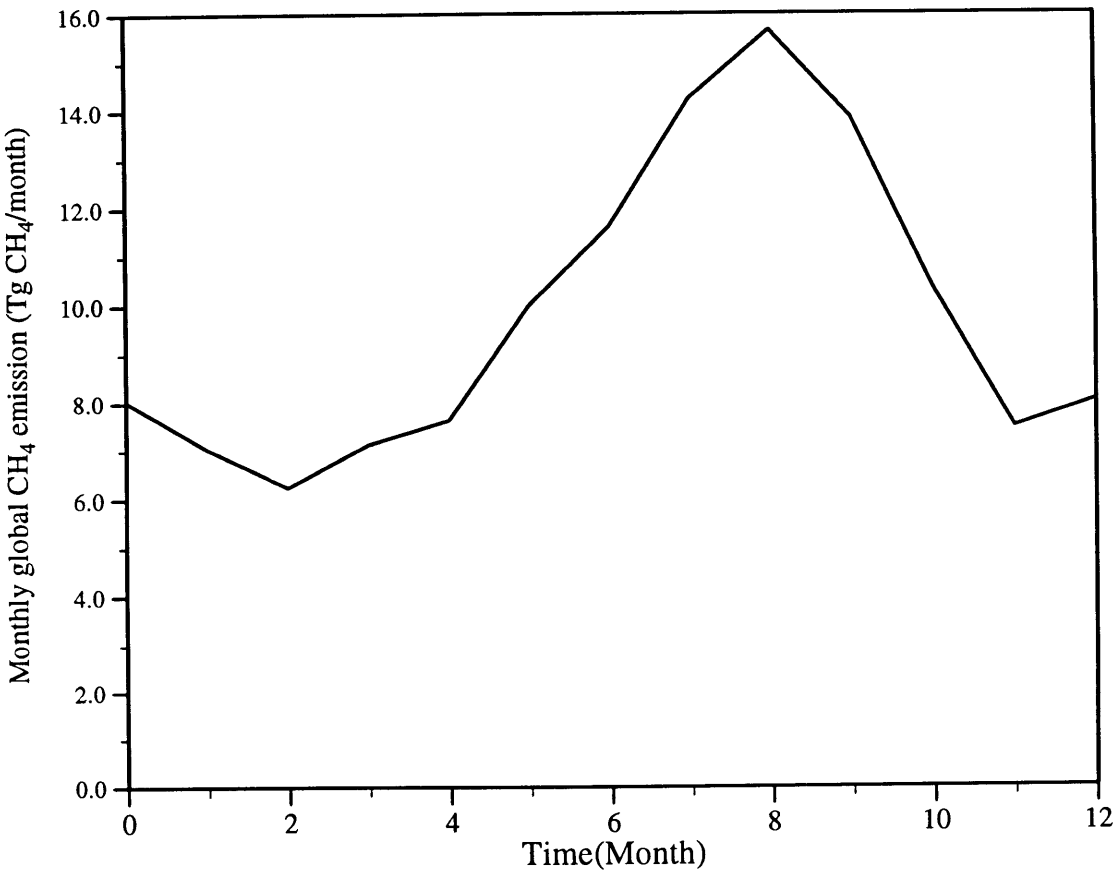

Figure 3-5: Predicted seasonal variation of total wetland CH_4 emission.

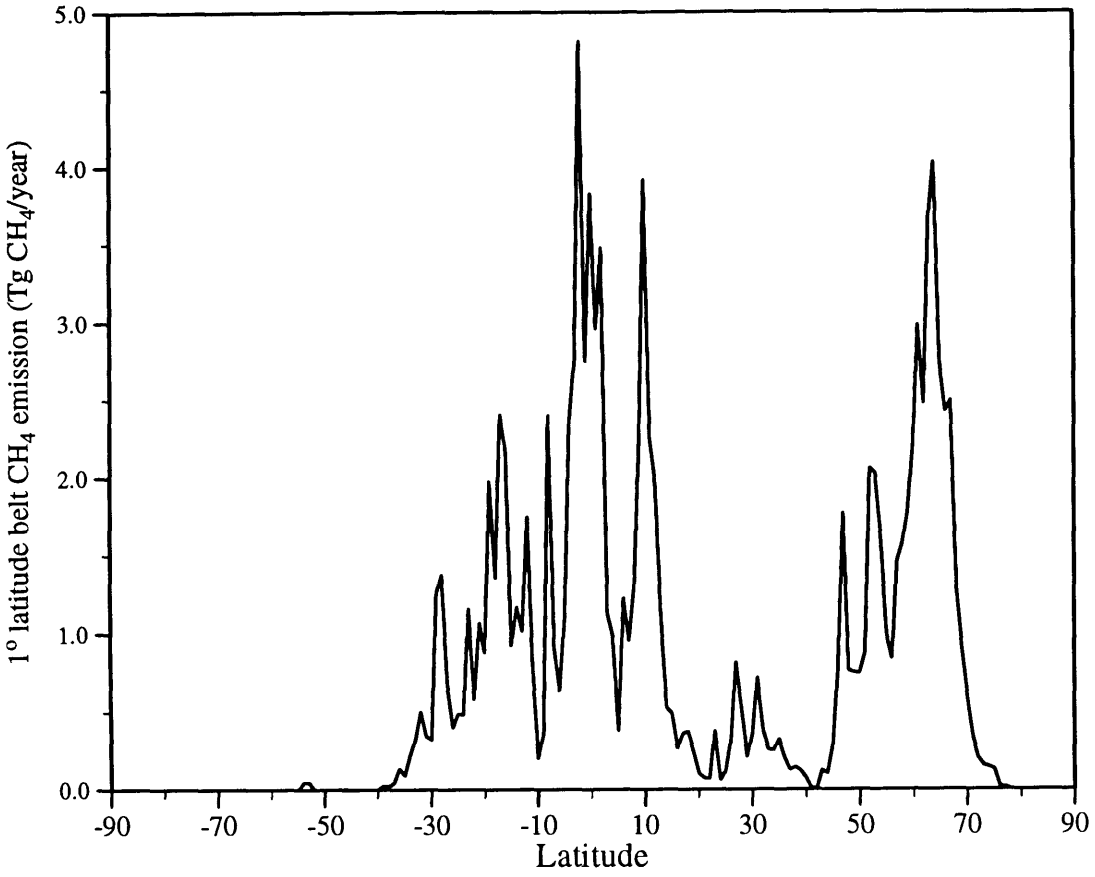

Global total emission calculated is 126.8 Tg CH_4 yr^{-1}
The tropics between 40°S and 20°N contribute 74.328 Tg CH_4 yr^{-1}
The emission from poleward of 40° is 46.789 Tg CH_4 yr^{-1}
The Northern Hemisphere emission is 79.284 Tg CH_4 yr^{-1} while
the Southern Hemisphere emission is 47.516 Tg CH_4 yr^{-1}

Figure 3-6: Predicted latitudinal distribution of annual CH_4 emissions (Latitude in degrees, with positive values denoting the Northern Hemisphere).

Chapter 4

Emission Model Testing

4.1 Introduction

Because of both the spatial and temporal variabilities of the controlling parameters and the resultant observed fluxes and the uncertainties in the N_2O and CH_4 budgets, the testing of the emission models for N_2O and CH_4 is quite challenging. As far as current availability of observational data is concerned, the emission models can be tested in two methods. The first method compares the model-predicted flux directly with the measured flux. The dynamics of the N_2O site emission model used in our global model has been tested using this method by Li *et al.* [*1992b*], and reproduced observed fluxes quite successfully. Our wetland CH_4 emission model is actually based on field flux measurements so this type of test is not possible. The second method of testing involves the use of a chemical transport model (CTM). The output surface mixing ratios from CTMs are compared to observations in order to test the spatial/seasonal distribution and temporal trend of the emission sources.

Since modeled wetland methane emissions account for only about 20% of total CH_4 emissions [*IPCC, 1994*] and CH_4 budget involves large uncertainties (other sources are not well known), testing our modeled natural CH_4 emissions using observed concentrations is unrealistic at this stage. For N_2O, however, the large magnitude of the soil emissions and their distinct emission patterns makes it possible to test if the modeled emissions are consistent with observed surface mixing ratios.

There have been some transport model studies using prescribed N_2O emissions. For example, Levy *et al.* [*1982*] examined the influence of an assumed uniform emission source for N_2O on predicted surface mixing ratios using the GFDL Eulerian GCM. The GFDL model predicted generally well-mixed tropospheric N_2O and about a 3 ppb excess in the southern hemisphere, which is not consistent with the observed 0.8 ppb higher mixing ratios in the northern hemisphere. Golombek and Prinn [*1986*] examined the case of uniform emissions outside of polar regions producing a very uniform global N_2O distribution. Taylor [*1992*] used a 3-D Lagrangian tracer model and a NPP-based (Net Primary Productivity) soil source plus other sources in his N_2O transport study. The mean predicted mixing ratio was 0.4 ppb higher in the northern hemisphere. The interhemispheric gradient is qualitatively consistent with observations. The model also predicted higher N_2O surface mixing ratios over continental source regions than over oceans by up to 8 ppb.

In this Chapter, we give the results of a transport model study using the modeled soil N_2O emissions plus other minor sources and the 3-D spectral transport model with detailed stratospheric chemistry of Golombek and Prinn [*1986*]. This study is conducted to test if the patterns of the modeled soil N_2O emissions are consistent with those of observed N_2O surface mixing ratios.

Our calculations of other (minor) sources of N_2O are documented in the first half of this chapter. The second half is devoted to comparisons of the 3-D model outputs with observations.

4.2 Other Sources for N_2O

Three other (minor) sources could be important for atmospheric N_2O. They are fossil fuel burning, biomass burning and oceans. These three sources are discussed below and are input into the CTM along with the modeled soil N_2O emissions.

4.2.1 N_2O Emission from Fossil Fuel Burning

Fossil fuel burning was once considered to be a major anthropogenic source of atmospheric N_2O. Muzio and Kramlich's [*1988*] discovery of a subtle artifact in sampling ruled out this as a big source. The mechanism responsible for the artifact N_2O is believed to be following heterogeneous reaction:

$$2\,HNO_2\,(l) + 2\,H_2SO_3\,(l) \longrightarrow N_2O\,(g) + 2\,H_2SO_4\,(l) + H_2O\,(l) \tag{4.1}$$

where $HNO_2\,(l)$ and $H_2SO_3\,(l)$ originate from SO_x and NO_x generated during combustion.

Measurements of new flask samples, from which SO_2 has been removed, have led to drastically reduced estimates of direct N_2O emission from fossil fuel burning [*Linak et al., 1990; Sloan and Laird, 1990; Yokoyama et al., 1991*].

There are two major mechanisms for N_2O emission from fossil fuel burning: stationary combustion and mobile combustion. N_2O production by stationary combustion (mostly conventional energy use) is believed to result from the following reaction [*Elkins, 1989*]:

$$NO + NCO \longrightarrow N_2O + CO \tag{4.2}$$

where NO and NCO originate from nitrogen compounds in fuel.

N_2O production from mobile combustion, in particular by cars equipped with catalytic converters, results from a different mechanism when NO_x is incompletely reduced to N_2:

$$NO + CO \longrightarrow \frac{1}{2}N_2 + CO_2 \tag{4.3}$$

$$2\,NO + CO \longrightarrow N_2O + CO_2 \tag{4.4}$$

$$N_2O + CO \longrightarrow N_2 + CO_2 \tag{4.5}$$

The global distribution of N_2O emission from fossil fuel burning is estimated using the so-called "emission factor" approach. For conventional stationary fossil fuel burning, to first order, the total N_2O emission is directly related to the amount of fossil fuel used. The following formula involving N_2O/CO_2 emission factor is used:

$$E_{N_2O} = E_{CO_2} \times \varepsilon \tag{4.6}$$

where E_{N_2O} and E_{CO_2} are emission rates from fossil fuel burning for N_2O and CO_2, and ε is the emission factor for N_2O which is defined as follows:

$$\varepsilon = \frac{\Delta \chi_{N_2O}}{\Delta \chi_{CO_2}} \tag{4.7}$$

where χ is mixing ratio and the differences (Δ) are with respect to background air concentrations.

The emission factor ε can be measured by sampling experiments. After the discovery of the sampling artifact, this emission factor has been found to be very small. Because of the fact that the formation of N_2O may occur in the plume farther downwind [*Khalil and Rasmussen, 1992*], the maximum values of Yokoyama et al. [*1991*] and Khalil and Rasmussen [*1992*] are chosen and averaged as the typical emission factor for stationary fossil fuel burning.

$$\varepsilon = \frac{60 + \frac{40+110+20}{3}}{2} \times 10^{-7} = 5.833 \times 10^{-6} \tag{4.8}$$

The CO_2 emission rate from fossil fuel burning over the globe has been estimated by Fung and coworkers [*Fung et al., 1987; Houghton et al, 1987; Marland, 1989; Tans et al., 1990*] using country estimates and population density to assign emissions in each $1° \times 1°$ cell over the globe. The global source strength is estimated by then to be 5300 TgC/yr. Assuming this source number is for conventional fossil fuel burning and using the emission factor calculated above, we estimate the conventional stationary fossil fuel N_2O emission to be 0.08 Tg-N/yr, which is even smaller than the uncertainties of mobile combustion N_2O source (the estimation of which is discussed

in the following paragraph).

N_2O emission from mobile combustion can be estimated using the same method discussed above. However, the emission factor ε is different for mobile combustion than for conventional stationary burning. Since it was recognized that N_2O emission is higher from cars equipped with catalytic converters than from other cars, concern has grown that catalyst-equipped cars may represent a significant source of N_2O. Dasch [*1992*] reports that the noncatalyst-bearing cars emit about 8% of the N_2O emission of cars equipped with catalysts. Recent measurements of N_2O and CO_2 emissions of a fleet of about 40,000 cars conducted in roadway tunnels in two different places show that the average emission factor for the catalyst-equipped cars is $\varepsilon = 3.8 \times 10^{-4}$ [*Berges et al.,1993*]. Applying this number and the amount of gasoline sold in the world in 1991, they conclude that the annual N_2O emission is 0.48±0.28 Tg-N if all cars are catalyst-equipped.

Because the N_2O emission from mobile combustion depends on technology change, it's obvious that this portion of N_2O emission changes with time. In 1986, only 36.67% of the cars registered in the world were equipped with catalysts [*Dasch, 1992*]. Using the above numbers we calculate that the N_2O emission from mobile combustion in 1986 was

$$E_{N_2O} = 0.48 \times \frac{36.67}{100} + 0.48 \times \frac{8}{100} \times (1 - \frac{36.67}{100}) \qquad (4.9)$$

i.e. 0.2 Tg-N/yr. The total N_2O emissions from fossil fuels is then estimated to be 0.28 Tg-N/yr.

Since 1986, this number has been increasing because of technology change. If we assume the present fraction of catalyst-equipped cars to be 50%, we calculate a N_2O emission of 0.26 Tg-N/yr from mobile combustion and a total emission of 0.34 Tg-N/yr from fossil fuel burning. This number is very close to the latest estimate of this source by Bouwman et al. [*1995*].

N_2O emissions from fossil fuel in 1986 (0.28 Tg-N/yr) are distributed according to the fossil fuel CO_2 emissions distribution from Fung et al. [*1987*], which are then

Region	Savanna	Fuelwood	Residues	Wild Fires	Prescribed Fires	Total
Australia	300.0	1.2	30.0	20.0	6.0	357.2
Temperate		200.0		110.0	20.0	330.0
Boreal		100.0		140.0		240.0

Table 4.1: Extratropical Biomass Burning (in Tg Dry Matter per year).

Fire Type	N/C Ratio
Forest	0.01
Savanna	0.006
Fuel Wood	0.005
Residue	0.015

Table 4.2: N/C ratio for different forms of biomass burning [*Crutzen and Andreae, 1990*].

used in chemical transport model study. The latitudinal profile of the fossil fuel CO_2 emissions distribution is shown in the top panel of Figure 4-1.

4.2.2 N_2O Emission from Biomass Burning

A thorough study has been conducted regarding trace gas emissions from biomass burning. The basic methodology is similar to the one used above in estimating N_2O emission from fossil fuel burning. The difference is that we have different emission factors for different trace gases corresponding to different types of fire. A data set of global biomass burning with spatial and temporal variations [*Hao and Ward, 1993; Hao and Liu, 1994*] has been used here in calculating the trace gas emissions from biomass burning.

Hao and Liu's [*1994*] biomass burning data only cover the tropics with a seasonal cycle tuned using observed ozone concentrations. Extratropical data, which are only available as approximate numbers [*Hao and Ward, 1993*], have to be used to construct a global data set.

Tropical biomass burning is categorized into four types: forest, savanna, fuelwood

Species	Emission Factors	Units	References
N_2O	0.7%	N/N burned	[*Crutzen and Andreae, 1990*]
NO_x	12.1%	N/N burned	[*Crutzen and Andreae, 1990*]
CO	10.0%	mole CO/mole CO_2	[*Crutzen and Andreae, 1990*]
CH_4 (a)	1.0%	mole CH_4/mole CO_2	[*Crutzen and Andreae, 1990*]
SO_2	0.3%	mole CH_4/mole CO_2	[*Crutzen and Andreae, 1990*]
CH_4 (b)			
Fire Type	Emission Factors	Units	References
Tropical Forest	9.3	g CH_4/Kg dry matter	[*Hao and Ward, 1993*]
Temperate and Boreal Forest	6.1	g CH_4/Kg dry matter	[*Hao and Ward, 1993*]
Savanna	1.5	g CH_4/Kg dry matter	[*Hao and Ward, 1993*]
Fuel Wood	7.6	g CH_4/Kg dry matter	[*Hao and Ward, 1993*]
Residue	2.7	g CH_4/Kg dry matter	[*Hao and Ward, 1993*]

Table 4.3: Trace Gases Emission Factors for Biomass Burning

and residues. Each type has a different N/C ratio. Data for tropical biomass burning are documented at a spatial resolution of $5° \times 5°$. Total dry matter burned in tropics is estimated as 5023.4 Tg/year. The allocation of the burned dry matter to the four categories is as follows: 35.78% from forest, 47.25% from savanna, 12.03% from fuelwood and 4.94% from residues.

The amount of biomass burned annually in the extratropics (including Australia, temperate and boreal regions) is estimated to be 927.2 Tg dry matter per year. The detailed distribution is presented in Table 4.1.

The numbers in Table 4.1 are distributed geographically according to the global vegetation distribution from TEM. For Australia, biomass burned in the form of savanna fires is distributed in savannas only. Biomass burned in other forms is uniformly distributed in all the rest of the vegetation types in the Australia continent. For the temperate and boreal regions, biomass burned in all forms is distributed uniformly in all vegetation types in those regions (35°N-60°N for the temperate and 60°N-90°N for the boreal) except in wetlands and deserts.

Species	Emissions
N_2O	0.26 Tg N/yr
NO_x	4.53 Tg N/yr
CO	241.00 Tg C/yr
SO_2	38.56 Tg SO_2/yr
CH_4 (a)	24.10 Tg C/yr
CH_4 (b)	30.16 Tg CH_4/yr

Table 4.4: Calculated Global Trace Gases Emissions from Biomass Burning

The trace gas emissions from biomass burning are calculated using the above data for burned dry matter and emission factors obtained from the literature. The emission factors and the N/C ratios are listed in Table 4.3 and Table 4.2. The calculated global total emissions of various trace gases from biomass burning are shown in Table 4.4. The calculated latitudinal profile and seasonal cycle of N_2O emission from biomass burning are shown in Figure 4-2. As we can see from the figure, emission is mostly in the tropics where the biomass burning is concentrated. The emission seasonal cycle peaks in Spring and Fall corresponding to the most intensive tropical burning seasons.

4.2.3 N_2O Emission from Oceans

Introduction

Although oceans are considered to be a net source of atmospheric N_2O, little is known about the variations in the strength of this source. It is generally understood that oceans are a significant but not dominant source of N_2O to the atmosphere. A lack of understanding of the processes which regulate N_2O in the natural system and a lack of spatially and seasonally extensive data are the major reasons for uncertainties in the assessment of N_2O emission from oceans.

Early estimates of the oceanic source were as high as 120 Tg N/yr [*Hahn, 1981*]. However, the consumption of dissolved N_2O by ocean microbial respiration in conditions of low oxygen offers an important sink for marine N_2O [*Elkins et al., 1978*] and tends to rule out oceans as a very large source for atmospheric N_2O. Although

a reliable value for the global source strength of N_2O from oceans is not available, it is believed that the marine contribution to atmospheric N_2O should not exceed 10 Tg-N/yr [*Elkin et al., 1978*]. Current estimates tend to converge to the range of 1–6 Tg-N/yr [*Seiler and Conrad, 1987; IPCC, 1992; Watson et al., 1992; Nevison, 1994*].

Because fluxes from water surfaces cannot be measured directly, oceanic gas fluxes are generally modeled from supersaturation measurements in the surface water and the water-air gas transfer coefficient. The spatial and temporal scarcity of N_2O supersaturation measurements and the uncertainty in gas transfer coefficients lead to considerable uncertainty in the oceanic source estimates [*Erickson, 1988; Watson et al., 1992; Nevison, 1994*].

An attempt at reestimating the N_2O oceanic source by using observational oceanic surface wind data and four alternative formulae for calculating the N_2O sea-air gas transfer coefficients has been conducted and is presented here. The resulting seasonal and global N_2O ocean emissions combined with the modeled soil source and our estimates for the other minor sources are used later as inputs to the chemical transport model.

Regulating Processes and Resulting N_2O

Like nitrous oxide produced in soils, oceanic nitrous oxide is produced in deep water by both nitrification and denitrification processes. Although debate still exists as to which process plays a more important role in oceanic N_2O production, most studies seem to conclude that nitrification is the major process. The mechanism of oceanic N_2O production has not been fully understood, but it is believed that while ammonium is oxidized to nitrate or nitrite, a small fraction of ammonium is also oxidized to N_2O in the nitrification process [*Butler et al, 1989; Yoshida et al., 1988, 1989; Kim and Craig, 1990; Najjar, 1992*].

In the oceanic surface layer, little nitrous oxide is produced because of high oxygen levels which inhibit the growth of denitrifiers and the strong photosynthetic activity of phytoplankton and heterotrophic bacteria which easily win the competition for the available substrates. N_2O production often increases with depth and peaks in the

thermocline, which is usually rich in organic matter and poor in oxygen. Beyond the maximum, N_2O production generally decreases with depth, due largely to the decreasing availability of organic matter and possibly to consumption of N_2O by denitrifiers in extremely low oxygen environments.

Similar to the situation for soil N_2O emissions, temperature is an important factor in regulating oceanic N_2O emission. It has been observed that higher temperature results in higher oceanic N_2O production [*Elkins, 1978; Butler et al., 1989*].

The complicated oceanic N_2O production pattern and its dependency on a number of factors result in a spatially and temporally varying surface N_2O supersaturation which is an important variable in flux calculations. Hence, realistic modeling of the oceanic N_2O flux requires the use of an ocean GCM. In the study presented here, the observed supersaturation [*Weiss et al., 1992*], observed surface wind and sea surface temperature [*Oort, 1983*] and observed salinity [*Levitus, 1982*] are used with an extrapolation scheme in the modeling of the oceanic N_2O flux.

Flux Modeling

The flux of a slightly soluble gas across the air-water interface can be expressed as

$$F = k\,(C_w - \alpha\, C_a) \tag{4.10}$$

where k is the gas transfer velocity, C_w is the gas concentration in the bulk of the water near the interface, α is the Ostwald solubility coefficient, and C_a is the concentration of gas in the air phase near the interface.

Gas transfer of CO_2, N_2O and some other gases is often expressed as a gas transfer coefficient K. The flux equals the gas transfer coefficient multiplied by the partial pressure difference between air and water:

$$F = K\,(pN_2O_w - pN_2O_a) \tag{4.11}$$

where $K = kL$ and L is the solubility expressed in units of concentration/pressure and the partial pressure difference is often written as $pN_2O_w - pN_2O_a = \Delta\, pN_2O$.

The conventional units and meanings of the above variables are specifically listed as follows:

Variable	Meaning	Units
F	Flux from ocean to atmosphere	$\text{mole}\,\text{cm}^{-2}\,\text{hr}^{-1}$
K	gas transfer coefficient	$\text{mole}\,\text{atm}^{-1}\,\text{cm}^{-2}\,\text{hr}^{-1}$
pN_2O_w	N_2O partial pressure in surface water	atm
pN_2O_a	N_2O partial pressure in atmosphere	atm
k	gas transfer velocity	$\text{cm}\,\text{hr}^{-1}$
L	solubility	$\text{mole}\,\text{cm}^{-3}\,\text{atm}^{-1}$

N_2O solubility L can be calculated using Weiss and Price's formula [*1980*] which is:

$$L = exp\left[A_1 + A_2\frac{100}{T} + A_3 \ln\frac{T}{100} + S\left(B_1 + B_2\frac{T}{100} + B_3\left(\frac{T}{100}\right)^2\right)\right] \qquad (4.12)$$

where T is temperature in Kelvin, S is salinity in parts per thousand and L is in units of $\text{mole}\,\text{liter}^{-1}\,\text{atm}^{-1}$. The coefficients in the above equation are listed in following table:

A_1	-62.7062	B_1	-0.05842
A_2	97.3066	B_2	0.033193
A_3	24.1406	B_3	-0.0051313

The gas transfer velocity k is a function of the interfacial turbulence, the kinematic viscosity of the water (μ), and the diffusion coefficient of the gas (D). The dependence of k on the last two terms is often expressed as the Schmidt number ($Sc = \frac{\mu}{D}$). For a smooth liquid interface, k is proportional to $Sc^{-\frac{2}{3}}$, while for an interface with waves, most models predict that k is proportional to $Sc^{-\frac{1}{2}}$. Typically, k is calculated by using the following formula with a standard Schmidt number [*Erickson, 1993*]:

$$k_{gas} = k_{std}\left(\frac{Sc_{gas}}{Sc_{std}}\right)^n \qquad (4.13)$$

where

$$n = -\frac{2}{3} \quad for \quad V < 3.6 \quad m/s$$

$$n = -\frac{1}{2} \quad for \quad V > 3.6 \quad m/s$$

and V is the interfacial scalar wind speed.

A few commonly used standard Schmidt numbers and their corresponding transfer velocities are listed in following table:

Schmidt Number	Transfer Velocity	Comments
$Sc = 600$	k_{600}	CO_2 in fresh water at 20 °C
$Sc = 660$	k_{660}	CO_2 in sea water at 20 °C
$Sc = 885$	k_{885}	Radon in fresh water at 20 °C

The Schmidt number for N_2O in sea water can be calculated using the following formula [*Wanninkhof, 1992*]:

$$Sc_{N_2O} = 2301.1 - 151.1T + 4.7364T^2 - 0.059431T^3 \tag{4.14}$$

where T is temperature in °C.

Many observational studies have resulted in the parameterization of the transfer velocity of trace gases as a function of wind speed or some other variables such as sea surface temperature. A number of empirical relationships which are used in the N_2O oceanic flux calculation are presented in the following table:

References	Transfer Velocity Formula
Liss and Merlivat, 1986	$k_{600} = \begin{cases} 0.17V & \text{if } V \leq 3.6 \text{ m/s} \\ 2.85V - 9.65 & \text{if } 3.6 < V \leq 13 \text{ m/s} \\ 5.9V - 49.3 & \text{if } V > 13 \text{ m/s} \end{cases}$
Tans et al., 1990	$k_{600} = \begin{cases} 0 & \text{if } V \leq 3 \text{ m/s} \\ 5.85(V-3) & \text{if } V > 3 \text{ m/s} \end{cases}$
Wanninkhof, 1992	$k_{660} = 0.31V^2$
Erickson, 1993	$k_{885} = k_m(1-W) + k_t W$

For Erickson's formula [*1993*], k_m (9.58 cm/hour) and k_t (475.07 cm/hour) refer respectively to transfer velocities associated with a nonwhitecap area and with a turbulent whitecap vent. W^* is the fraction of the sea surface covered by whitecap. Whitecap coverage (W^*) is known to be a function of wind speed, water temperature and the stability of the air-sea interface. Wu [*1975*] derives the following relation for W^*

$$W^* \propto u_*^3 \tag{4.15}$$

which after calibration becomes

$$W^* = 0.2u_*^3 \tag{4.16}$$

Here u_* is the friction velocity (m/s), which can be calculated as

$$u_* = C_D^{0.5} V \tag{4.17}$$

where C_D is the local drag coefficient (dimensionless) and V is the surface wind speed in m/s.

The local drag coefficient is a function of both wind speed and thermal stability at the air-sea interface. In this study, we simply use the neutral drag coefficient over the ocean from Trenberth *et al.*, [*1989*]:

$$C_N = \begin{cases} (0.62 + \frac{1.56}{V}) \times 10^{-3} & \text{if } V < 3 \text{ m/s} \\ 1.14 \times 10^{-3} & \text{if } 3 \leq V \leq 10 \text{ m/s} \\ (0.49 + 0.065V) \times 10^{-3} & \text{if } V > 10 \text{ m/s} \end{cases} \quad (4.18)$$

ΔpN_2O Data Extrapolation

The observed pN_2O difference (ΔpN_2O) between the surface ocean and the atmosphere represents the thermodynamic driving potential for transfer of N_2O gas across the sea surface and includes implicitly the combined effects of all the processes that influence the N_2O distribution in the oceans and atmosphere. Measurements of pN_2O obtained from Weiss *et al.* [*1992*] have been analyzed and used in our N_2O flux estimates.

Weiss *et al.*'s monthly data for surface water and atmospheric N_2O concentrations are averaged at a spatial resolution of $0.5° \times 0.5°$. Partial pressure differences are therefore calculated at this resolution using all available measurements. Because the available measurements do not cover all the ocean grid cells, an extrapolation scheme is used to fill in the missing data. First, zonal annual means are calculated for all the 0.5° latitude bands. Linear interpolation/extrapolation is used to fill in the missing data if some latitude bands do not have any data at all. The resulted zonal annual means for each of the 360 0.5°-latitude-bands are then used to fill in all the missing oceanic data (including missing grid cells and missing months). The $0.5° \times 0.5°$ partial pressure difference data are finally aggregated and averaged in order to match the $5° \times 4°$ resolution for available sea surface wind and temperature observational data sets [*Oort, 1983*].

Oceanic Emission Results

The oceanic N_2O emission depends on the transfer velocity and sea surface wind. Our study uses the four k's mentioned above and the observational surface wind [*Oort, 1983*]. A uniform wind of 10 m/s is also used to compare the sensitivities of these four different transfer velocity fomulae. The resulting annual N_2O ocean fluxes are

Surface Wind	L & M	Tan	Wanninkhof	Erickson
Monthly Mean (obs)	0.86	2.02	1.60	2.45
10 m/s (constant)	4.34	9.44	7.49	3.69

Table 4.5: Calculated global annual N_2O ocean fluxes (in Tg-N/year using different sea-air transfer coefficient formulae and surface winds.

summarized in Table 4.5.

The global N_2O ocean fluxes reported in the above table range from 0.86 to 2.45 Tg-N/year, which agrees very well with the 1.4–2.6 Tg-N/year range estimated by Elkins [*1989*]. The range of the reported fluxes reflects only the difference associated with the use of the four sea-air transfer coefficient formulae. Including other possible sources of uncertainty definitely would widen this range. For example, uncertainties in observed wind speed, sea surface temperature and our procedure for filling in missing pN_2O-difference data, are not accounted for in the above calculations.

The calculated N_2O flux using Erickson's sea-air transfer formula is used as the ocean N_2O source in the transport model experiment discussed later. The reasons for this choice are that Erickson's formula takes into account the stability at the air-sea interface and, while it yields the largest estimates (Table 4.5), this may be appropriate since the observed wind used in the calculations is monthly averaged wind, which would presumably give a smaller oceanic N_2O flux than the real situation.

Figure 4-3 presents the latitudinal profile and seasonal cycle of oceanic N_2O emission using the Erickson formula. The latitudinal profile (top panel) shows that there are three distinct N_2O emission regions, with the strongest one in the tropics, the weakest one in the northern hemisphere, and a moderate one in the sourthern hemisphere. There are distinct seasonal cycles in the oceanic N_2O emissions, with high values in northern winter and low values in northern spring and fall.

The global seasonal cycle is related to the dominance of emissions from different regions at different times of the year. Warmer ocean surface temperature decreases N_2O solubility, tending to favor N_2O emission. Realizing that the tropics have relatively small seasonal variations in sea surface temperature, we can conclude that the

January peak of oceanic N_2O emissions (bottom panel of Figure 4-3) is due to the dominance of the summertime southern hemisphere oceanic emissions while the small increase between April and September is due to the warmer sea surface temperatures of the northern hemisphere summertime oceans.

4.2.4 Industrial and Other Minor Sources

Industrial processes which involve nitrogen oxidation in overall reducing conditions are potential sources of N_2O. The major industrial process sources for atmospheric N_2O are believed to be from the manufacturing of adipic acid and nitric acid [*Thiemens and Trogler, 1991; Watson et al., 1992*].

Adipic acid is a compound primarily used for the production of nylon. Based on world adipic acid production capacity and locations of the factories, Castellan et al. [*1991*] and Bouwman et al. [*1995*] derived two quite similar inventories for N_2O emission from adipic acid production which had global N_2O emissions of 0.4 and 0.3 Tg-N per year respectively. Bouwman et al. included adipic acid production from the developing countries and used a new N_2O emission rate which takes into account N_2O abatement. For the N_2O transport model study, Bouwman et al.'s emission of 0.3 Tg-N per year is used in our study, and is distributed on to $1^\circ \times 1^\circ$ grid points according to the factory locations assuming no seasonal cycle (the bottom panel of Figure 4-1 shows the resultant latitudinal distribution of the adipic acid source).

Emission of N_2O from nitric acid production is mainly associated with its use in fertilizer production. Bouwman et al. [*1995*] estimated the emission as 0.2 Tg-N per year based on a global nitric acid production of 11 Tg N per year. This number is used later in the chemical transport modeling study. The emission is spread spatially using the same pattern described for N_2O from fossil fuel combustion. No seasonal cycle is assumed in the emissions.

Nitrous oxide is also emitted by a large number of smaller sources, most of which are difficult to evaluate. These include other industrial processes, sewage, farm cattle and cattle feed lots. Khalil and Rasmussen [*1992*] estimate a global sewage N_2O flux of 0.2-2 Tg-N per year and a global cattle and feed lots flux of 0.2-0.5 Tg N per year.

	Sources	Individual Estimates (Tg N_2O-N yr^{-1})	IPCC(*1994*) Uncertainties (Tg N_2O-N yr^{-1})
1	Fossil Fuels	0.28	added to 4
2	Biomass Burning	0.26	0.2—1.0
3	Oceans	2.45	1.0—5.0
4	Industrial Processes	0.5	0.7—1.8
5	Other Minor Sources	0.5	0.2—0.5
	Subtotal	3.99	
6	Soil Sources (modeled)	11.325	5.1—15
	Total	15.315	

Table 4.6: Global N_2O Budget used in the 3D Transport Model Study.

A number of 0.5 Tg-N per year is used later in the chemical transport model study to represent all the minor sources. This flux is distributed using the same pattern for fossil fuel CO_2 emissions.

4.3 N_2O Budget

All the N_2O sources are summarized in Table 4.6. Note that soil biogenic emission, which is modeled by the global N_2O emission model, is the primary atmospheric N_2O source, accounting for about 74% of the total emission. Seasonal and latitudinal profiles of total N_2O emissions are presented in Figure 4-4. In Figure 4-4 the seasonal variations and interhemispheric differences in N_2O emissions result mainly from the soil biogenic emissions. This is a very important point because it provides a distinct emissions pattern which can be used to test the N_2O emission model using the observed N_2O mixing ratios.

4.4 Chemical Transport Model

The 3D spectral chemistry transport model, developed by Golombek and Prinn [*1986*], has been used to simulate chemistry and transport of N_2O. The transport model

has a very high vertical domain and resolution with 26 layers from the surface up to approximately 72 km. Stratospheric chemistry and hence the stratospheric N_2O sink are fully resolved in the model. The model has a low horizontal resolution with a spectral resolution of R6 for the dynamics and a corresponding grid-point resolution of $22.5° \times 12°$ for the chemistry. This spectral chemical transport model is computationally very efficient. It takes about 1 hour of CPU time on NASA's CRAY Y-MP for a 10-year run.

Golombek and Prinn's model uses precalculated 3-dimensional fields of vorticity, vertical velocity, temperature, and ozone concentration from a "balance type" dynamical-chemical model [*Cunnold et al., 1975, 1980*]. Horizontal transport in the model is accomplished by the specified horizontal winds predicted from the "balance type" model. Vertical transport is accomplished both by the predicted vertical wind and by eddy diffusion. The eddy diffusion is intended to represent the vertical transport due to some dynamic features (e.g. tropical convection, midlatitide tropopause folding) which are not resolved in the "balance type" model. The 3D spectral model has been reasonably successful in simulating various long-lived gases with stratospheric sinks and well known emission sources (e.g. $CFCl_3$, CF_2Cl_2).

The N_2O sources summarized in Table 4.6 are used as inputs to the 3D spectral model. Data for the global distribution of these sources are aggregated first to match the resolution of $22.5° \times 12°$. The N_2O chemistry (i.e. photodissociation and photooxidation) is then explicitly calculated at this resolution.

The 3D spectral model is initialized with a realistic N_2O height profile, which is scaled to surface mixing ratios at different latitudinal bands. The surface mixing ratios are obtained by linearly-extrapolating 1978 year-end observations at ALE/GAGE stations [*Prinn et al., 1990*]. The transport model is then run for 15 years using the same N_2O emissions (Table 4.6) and dynamics (precalculated fields) for every year.

4.5 Comparison and Discussion

Model results of N_2O surface mixing ratios are compared to observations at ALE/GAGE stations [*Prinn et al., 1990*]. Figure 4-5 shows the geographical locations of the five ALE/GAGE stations: Ireland, Oregon, Barbados, Samoa and Tasmania. Note that Samoa is the only station in the middle of Pacific ocean while all other stations are in or near coastal regions of large continents.

The modeled and observed trends of N_2O mixing ratios at the five stations are plotted in Figure 4-6. The figure shows that the modeled trends agree reasonably well with the observed ones at all five stations. The increasing trends are caused by the imbalance between sources and sinks, and not by the variation in source strength (a fixed total emission is used for all the years). Fitting the observed trends requires the emission source to exceed stratospheric loss by about 28%. The good fit here may be fortuitous because the expected uncertainty in the global annual emissions predicted by our model could be as large as $\pm 28\%$. Nevertheless it demonstrates that this emission model yields emission estimates consistent with (but not necessarily validated by) observations. The largest model uncertainties are in handling of denitrification in the site process model, definition of the global maps of relevant ecosystem properties, and use of a site model for managed ecosystems in unmanaged ones.

There are short term (standard deviations shown by vertical bars) and long term (interannual) variations in the observed mixing ratios. The long term variations may be due to the variations in soil biogenic N_2O emissions caused by climate variations. The short term variations are mainly due to transport. There are seasonal cycles in the modeled concentrations with a maximum amplitude of up to 0.5 ppb for the northern hemisphere. The amplitudes of these seasonal cycles are smaller than the short term variations, so that the predicted small amplitude seasonal cycles are simply "buried' in the "noise". That is why we cannot discern and verify such a cycle clearly in the observed concentrations. However, the predicted seasonal cycles if correct could contribute in part to the short term variations which are evident in the observations.

Figure 4-7 plots the annual zonal mean of the modeled N_2O mixing ratios for the

year 1986 and the 5-year mean (with year 1986 in the middle) of the modeled and observed N_2O mixing ratios at the five ALE/GAGE stations. The model predicted interhemispheric gradient is evidently in good agreement with the observed one (average around 1 ppb in Prinn *et al.* [*1990*]). Note that the observations at Samoa and Tasmania seem systematically lower than the modeled values. The systematically higher modeled values in the southern hemisphere could be caused by too large southern hemispheric emissions or by faster-than-real-case interhemispheric transport in the 3D spectral model. Also note that the modeled mixing ratio at Samoa is lower than the modeled zonal mean by a larger degree than the modeled mixing ratios at other stations. This larger difference for Samoa is due to the fact that this station is far from significant N_2O emission source regions at the same latitude and hence has lower N_2O levels than the zonal mean.

The global distribution of the surface N_2O concentrations is presented in Figure 4-8 through Figure 4-11. The altitude-latitude distribution of the N_2O concentrations is presented in Figure 4-12 through Figure 4-15.

Figure 4-8 through Figure 4-11 reveal that surface N_2O concentrations over tropical Africa and South America, East Asia, North America and Europe are significantly higher than over the adjacent oceans. These enhancements are caused by strong N_2O emission sources in these regions. Over the South American continent, N_2O mixing ratios exceed adjacent oceanic values by as much as 3 ppb. N_2O is generally well-mixed in the air over the oceans. The predicted enhancement agrees with Taylor's results [*1992*], although the magnitude of the enhancement is smaller in this study.

The surface N_2O concentrations also show seasonal cycles, which are caused largely by the seasonal cycles of global N_2O emissions. Note that in the northern hemisphere winter, the global surface concentration maxima occur in the southern hemisphere over tropical Africa and South America, while in the northern hemisphere summer the maxima occur in East Asia, North America and Europe. In spring and fall, these maxima occur in the equatorial and adjacent regions.

Altitude-latitude distributions of N_2O concentrations predicted by the model show that N_2O is quite well mixed in the troposphere. The interhemispheric gradient is

seasonally dependent. Figure 4-13 and Figure 4-15 reveal that while there is only a very small or no interhemispheric gradient in the spring season, the gradient is as high as 1.6 ppb in the fall season. For northern hemisphere summer and winter (Figure 4-12 and Figure 4-13), the interhemispheric gradient falls somewhere in between these two extremes, with the magnitude a little larger for the northern hemisphere summer season. These seasonal variations are caused largely by the seasonality of the northern hemispheric N_2O emissions. The occurrence of a maximum interhemispheric gradient in the northern hemisphere fall and a minimum one in the spring are due to the atmospheric build-up due to emissions occurring substantially during the summer but not the winter in the northern hemisphere.

4.6 Conclusions

The atmospheric N_2O distribution predicted by the 3D spectral transport model, using the predicted soil biogenic emissions from the model discussed in Chapter 2 and the calculated emissions from other minor sources calculated in this chapter, is generally quite consistent with the limited number of available observations.

The observed temporal trends are very well reproduced by the chemistry transport model. The predicted nterhemispheric gradient is seasonally dependent. When averaged over a full year, the gradient agrees very well with the observed $\sim$1 ppb interhemispheric gradient. Model results further suggest that surface N_2O mixing ratios over strong continental source regions may be higher by up to 3 ppb than over adjacent oceans. This result is less easily validated, due to the lack of monitoring sites in continental interiors, although lower observed N_2O mixing ratios at Samoa than the zonal average supports the above predictions. Predicted seasonal cycles have smaller amplitude than the natural variations seen in observations, which makes it hard to validate the predicted seasonality using currently available observations.

The predicted spatial distribution and seasonality of atmospheric N_2O concentrations predicted using the combined soil emission model and 3D spectral transport model can be further checked in the future as more measurements become available.

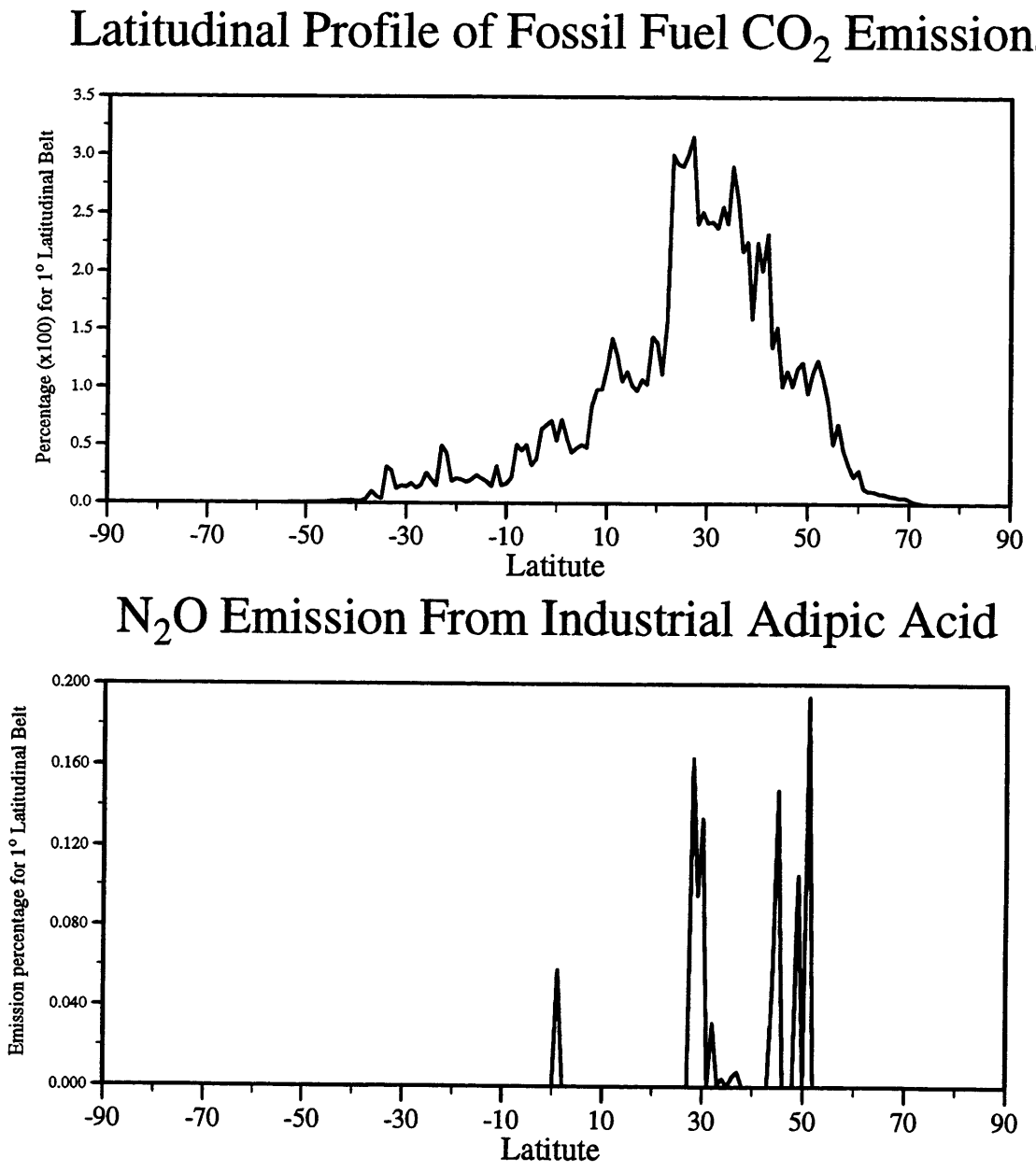

Figure 4-1: Latitudinal profile of fossil fuel CO_2 emissions (top panel) and latitudinal distribution of N_2O emission from industrial adipic acid.

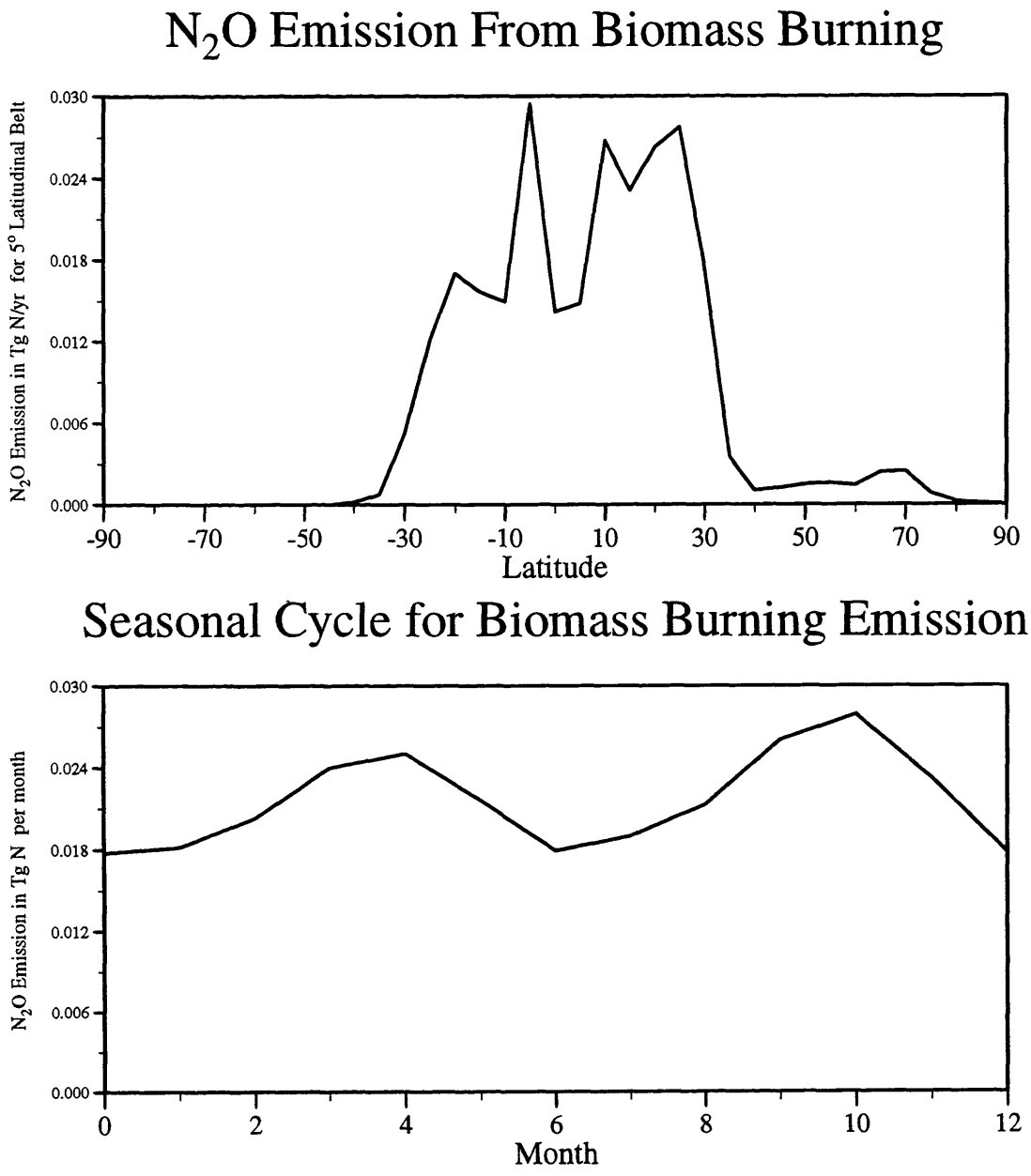

Figure 4-2: Calculated latitudinal profile and seasonal cycle of N_2O emission from biomass burning.

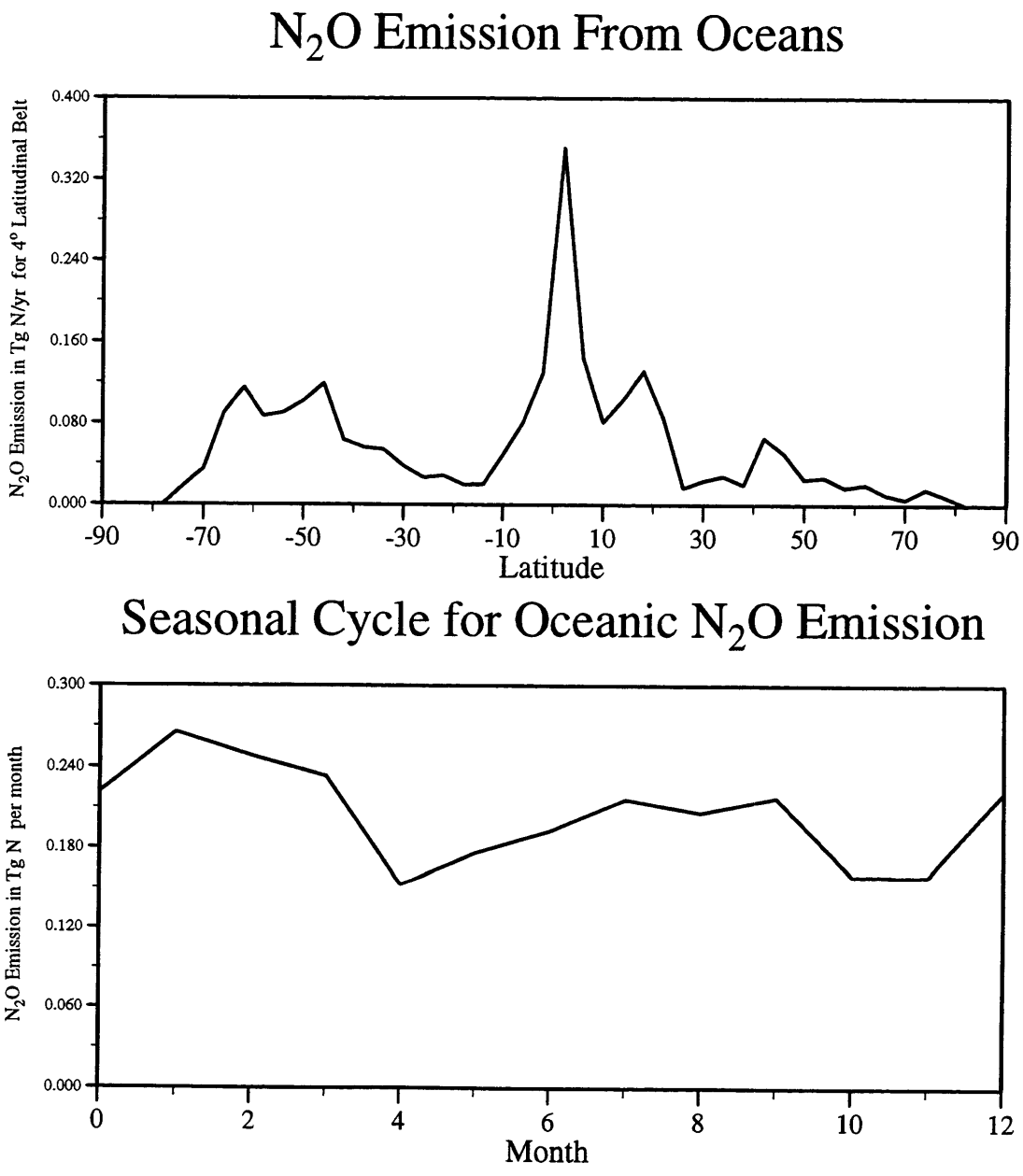

Figure 4-3: Calculated latitudinal distribution and seasonal cycle of oceanic N_2O emissions (Erickson's transfer coefficient has been used).

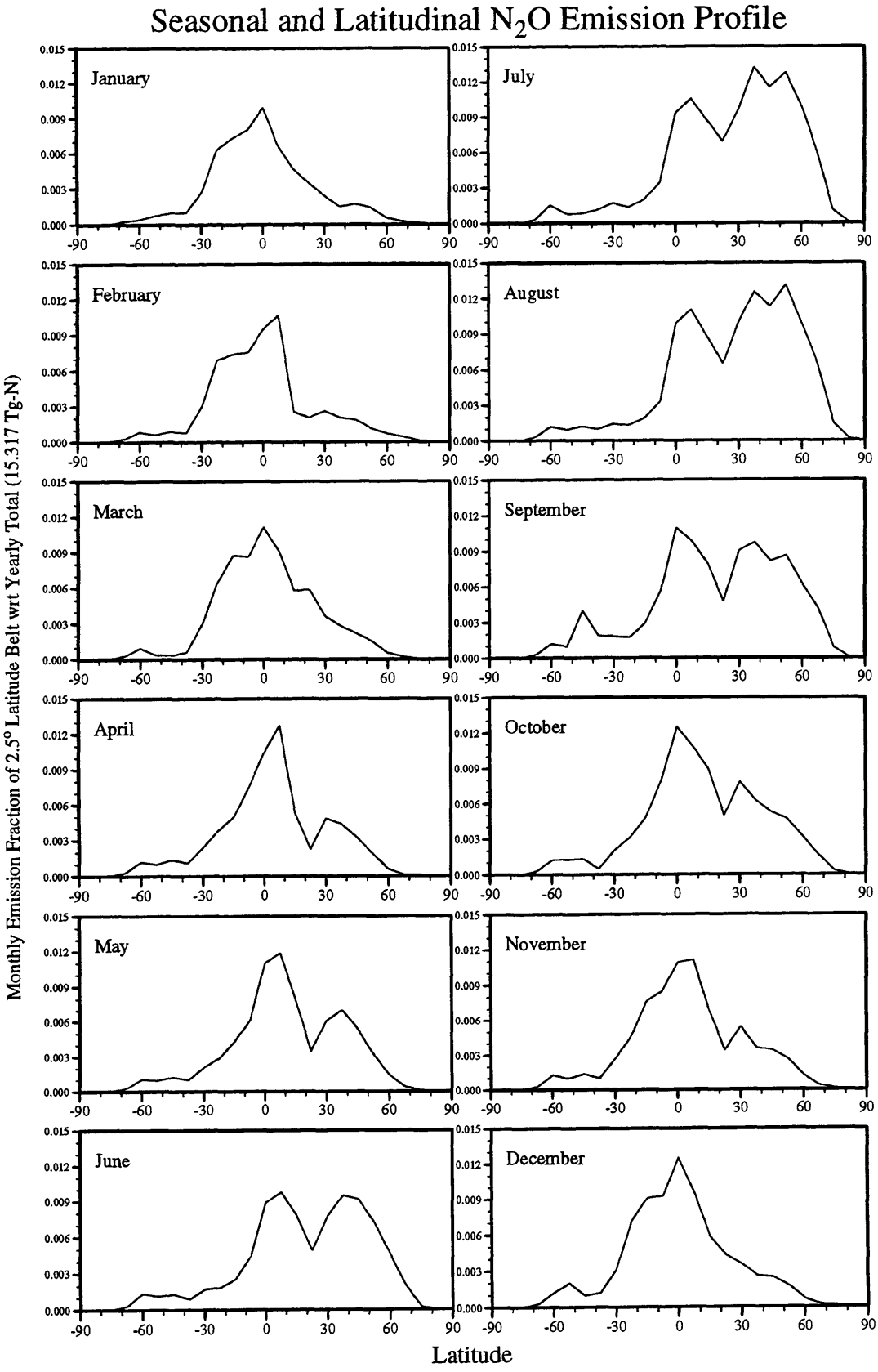

Figure 4-4: Calculated seasonal and latitudinal profiles of total N_2O emissions.

ALE–GAGE Monitoring Stations

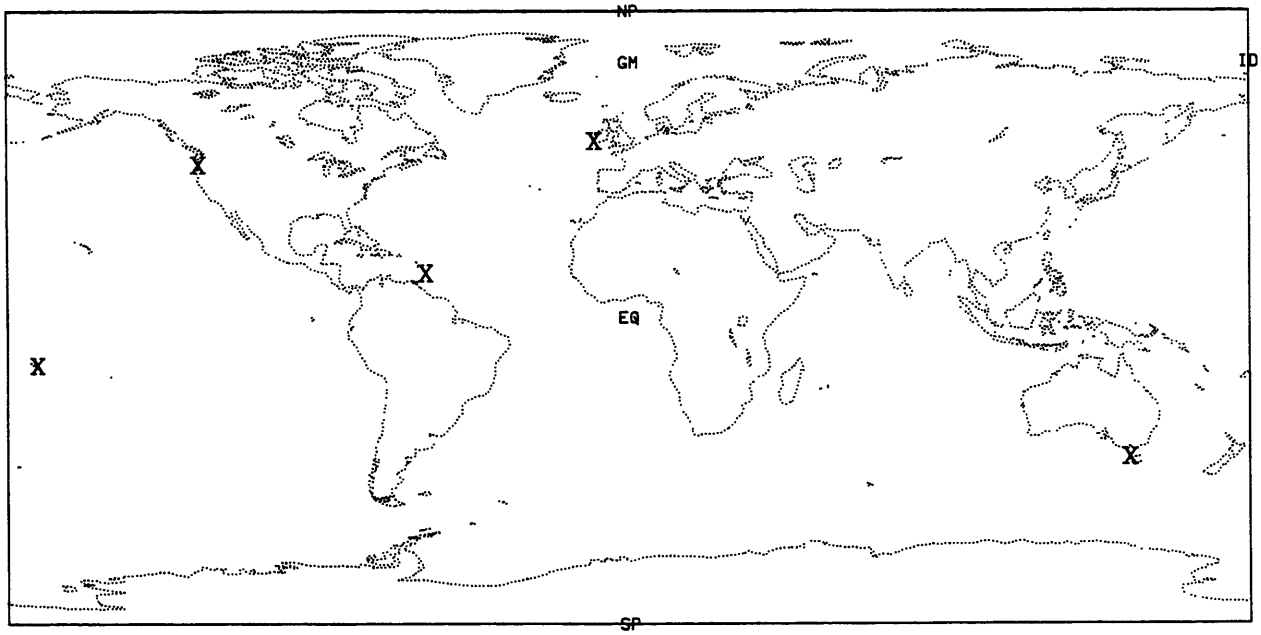

Figure 4-5: Geographical locations of ALE/GAGE stations: Ireland, Oregon, Barbados, Samoa and Tasmania.

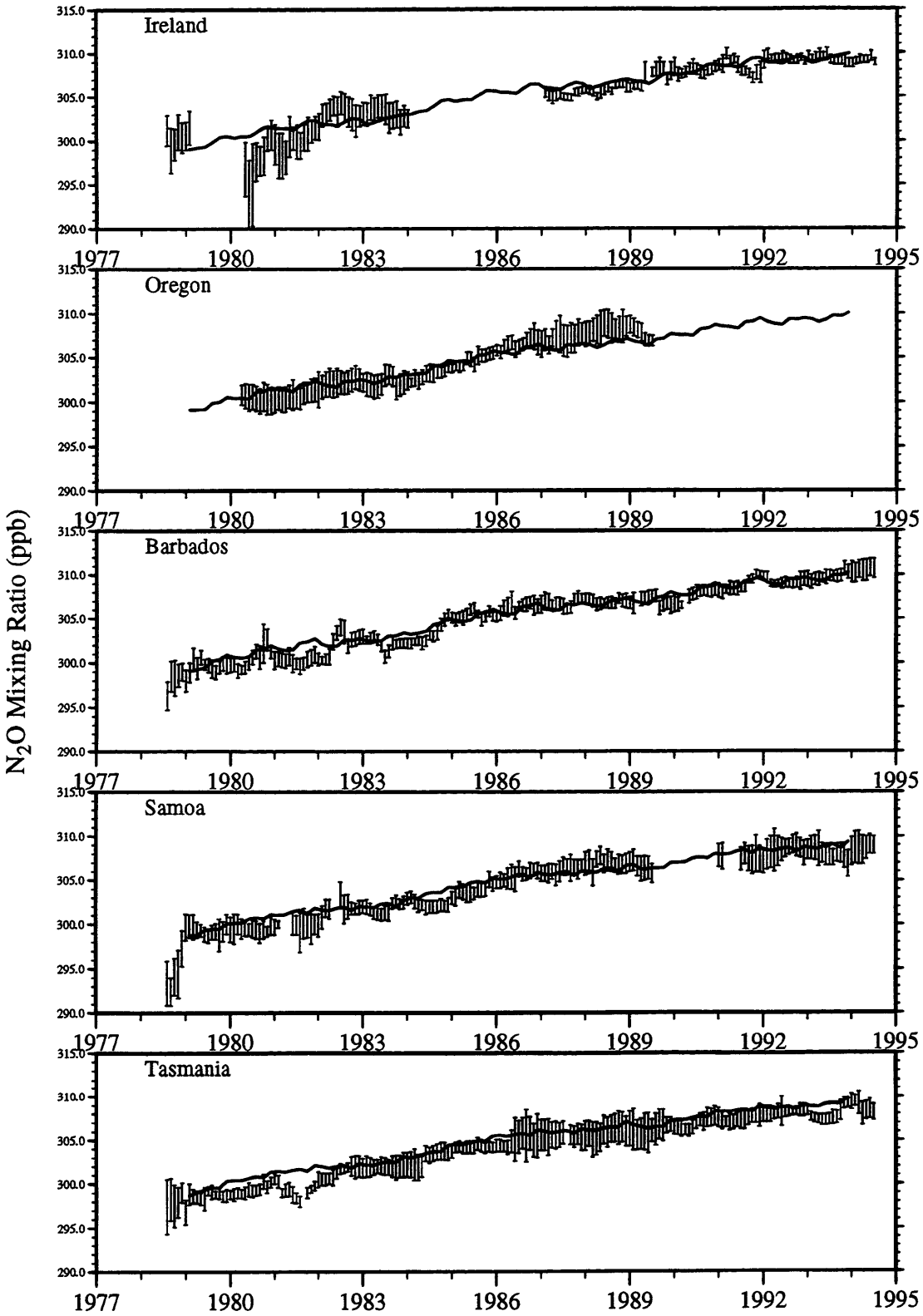

Figure 4-6: The modeled (solid lines) and observed (vertical bars denoting monthly means and standard deviations) trends of N_2O mixing ratios at the five ALE/GAGE stations.

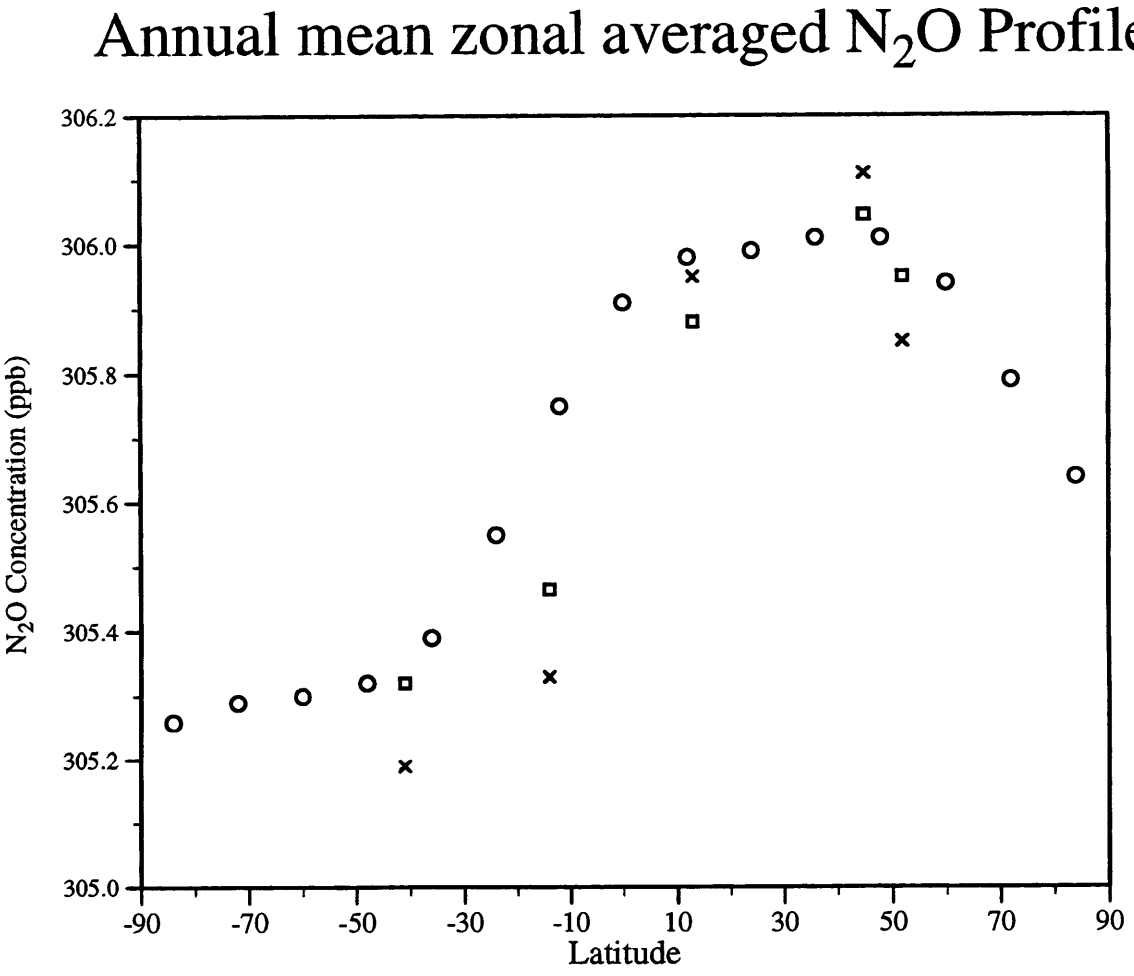

Figure 4-7: Annual zonal mean of the modeled N_2O mixing ratios for year 1986 (circles) and 5-year mean (with year 1986 in the middle) of the modeled (squares) and observed (crosses) N_2O mixing ratios at the five ALE/GAGE stations.

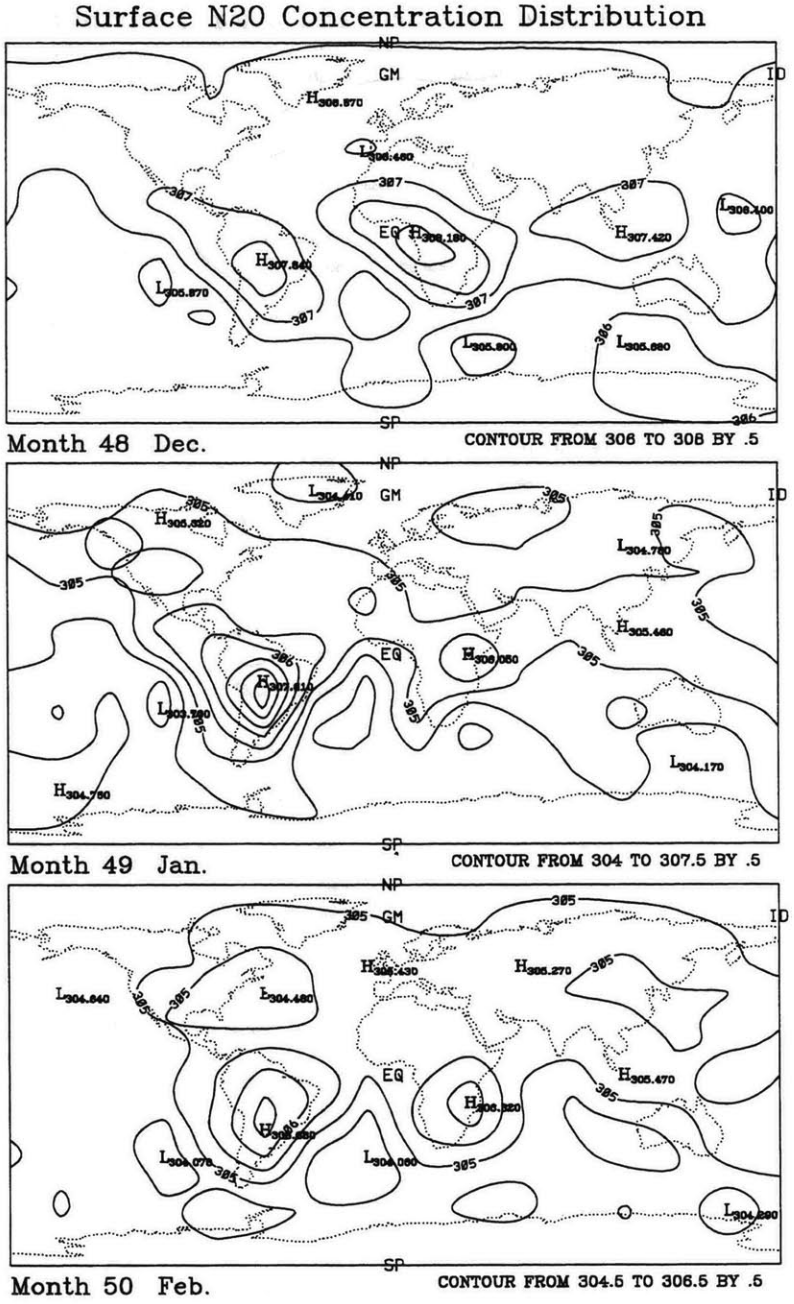

Figure 4-8: Predicted global distribution of surface N_2O concentrations in ppb units (for the northern hemisphere winter).

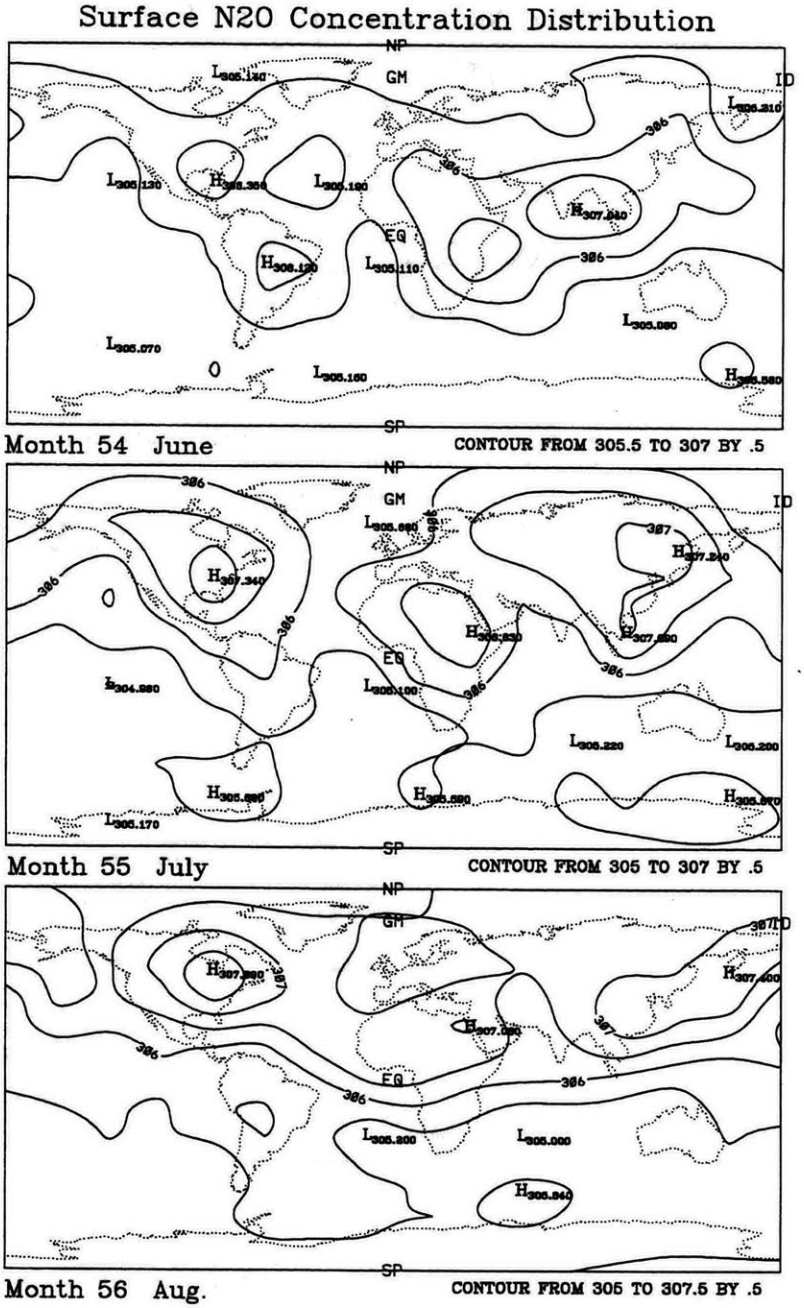

Figure 4-9: Predicted global distribution of surface N_2O concentrations in ppb units (for the northern hemisphere summer).

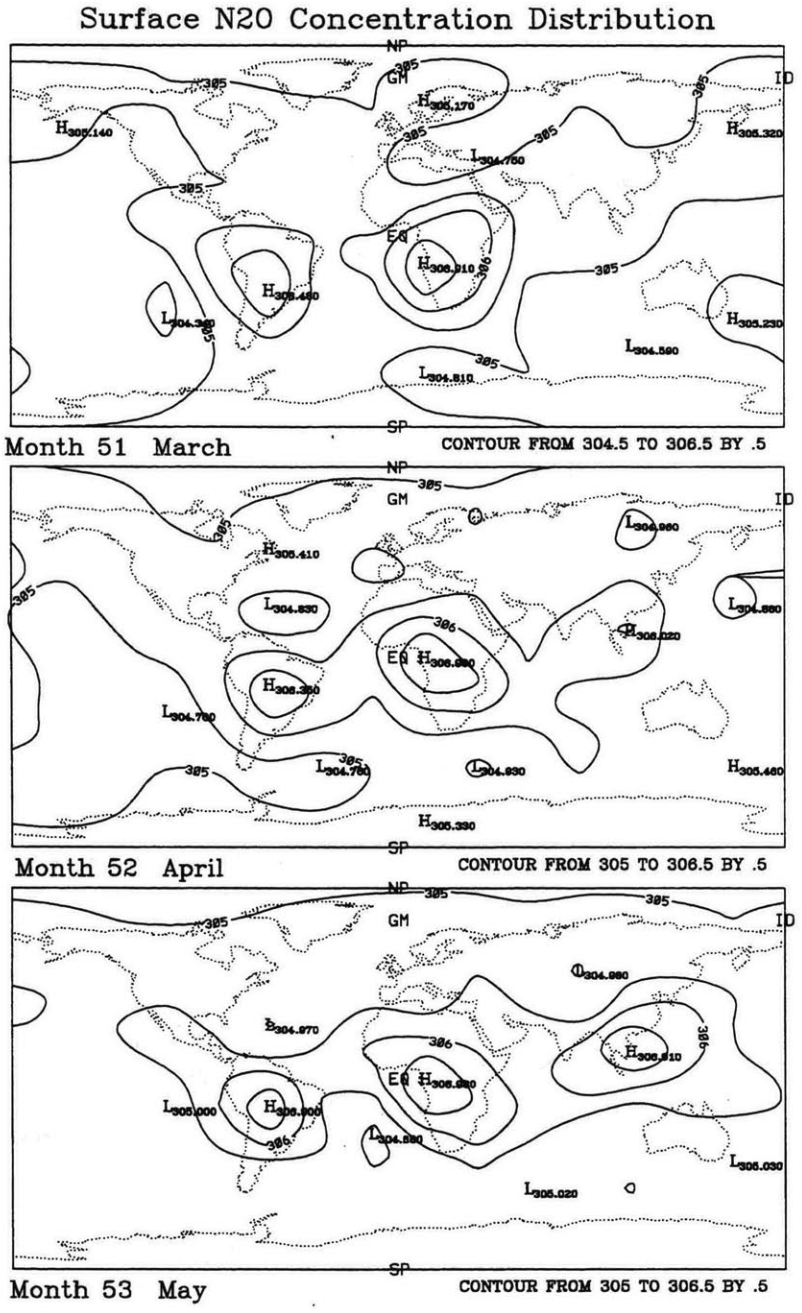

Figure 4-10: Predicted global distribution of surface N_2O concentrations in ppb units (for the northern hemisphere spring).

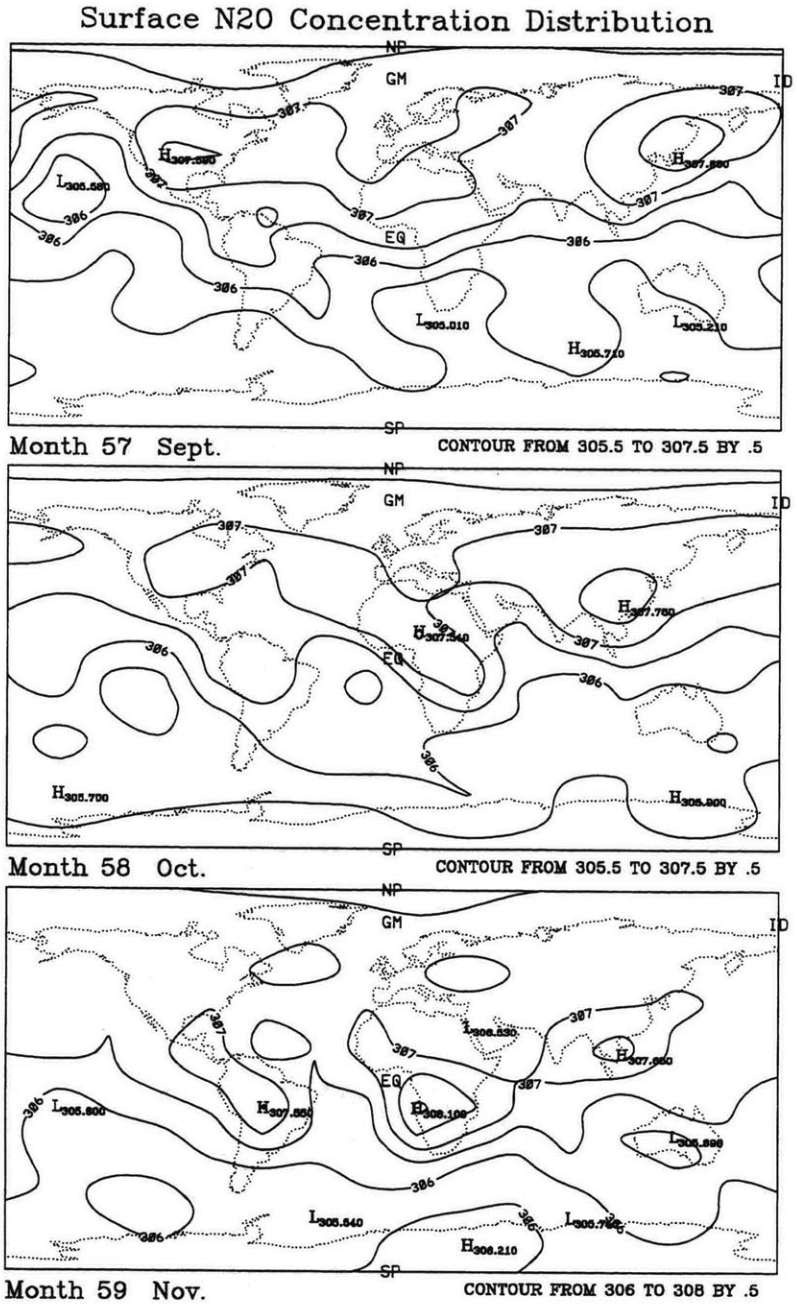

Figure 4-11: Predicted global distribution of surface N_2O concentrations in ppb units (for the northern hemisphere fall).

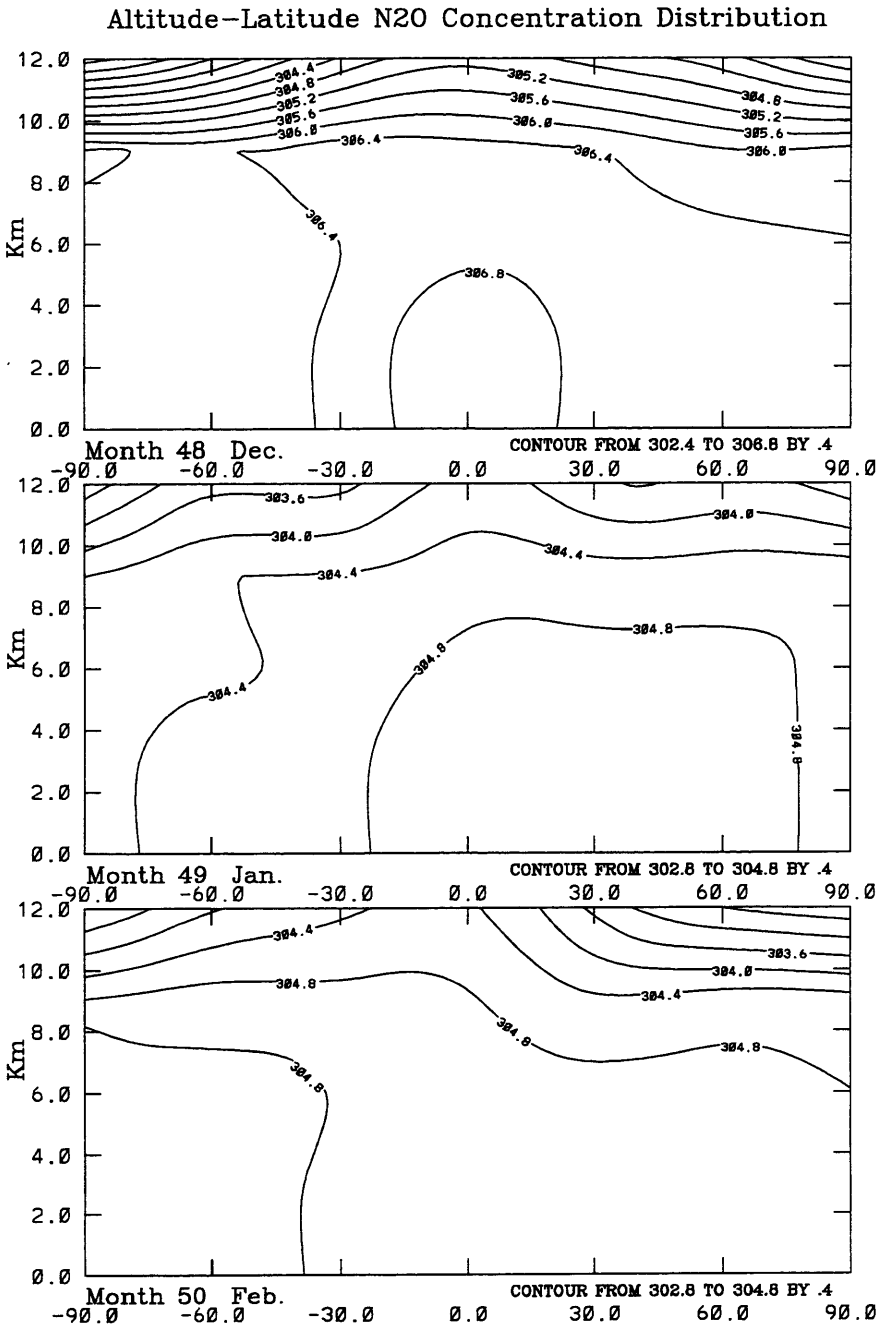

Figure 4-12: Predicted altitude-latitude distribution of N_2O concentrations in ppb units for the northern hemisphere winter(Latitude in degrees, with positive values denoting the Northern Hemisphere).

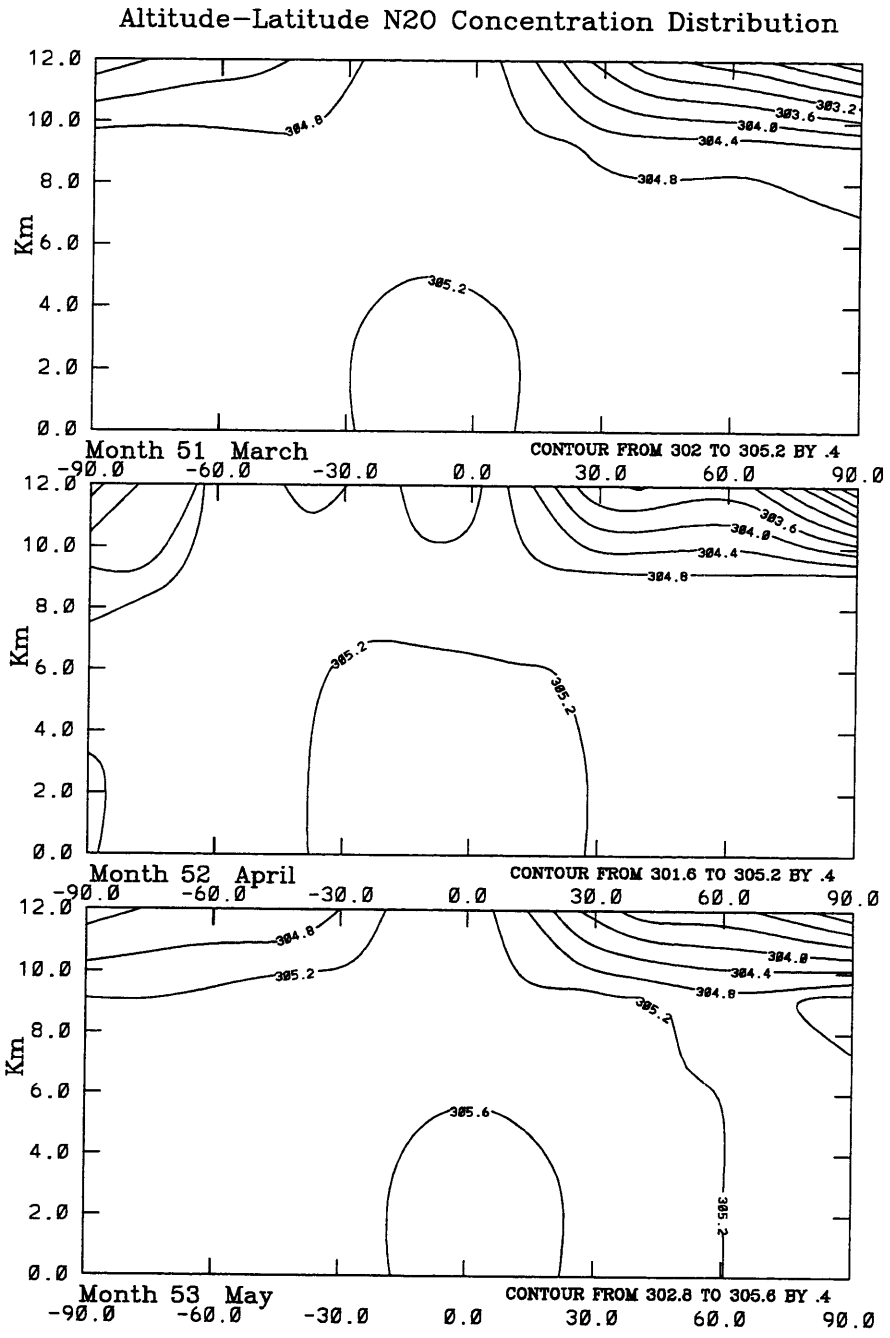

Figure 4-13: Predicted altitude-latitude distribution of N_2O concentrations in ppb units for the northern hemisphere spring (Latitude in degrees, with positive values denoting the Northern Hemisphere).

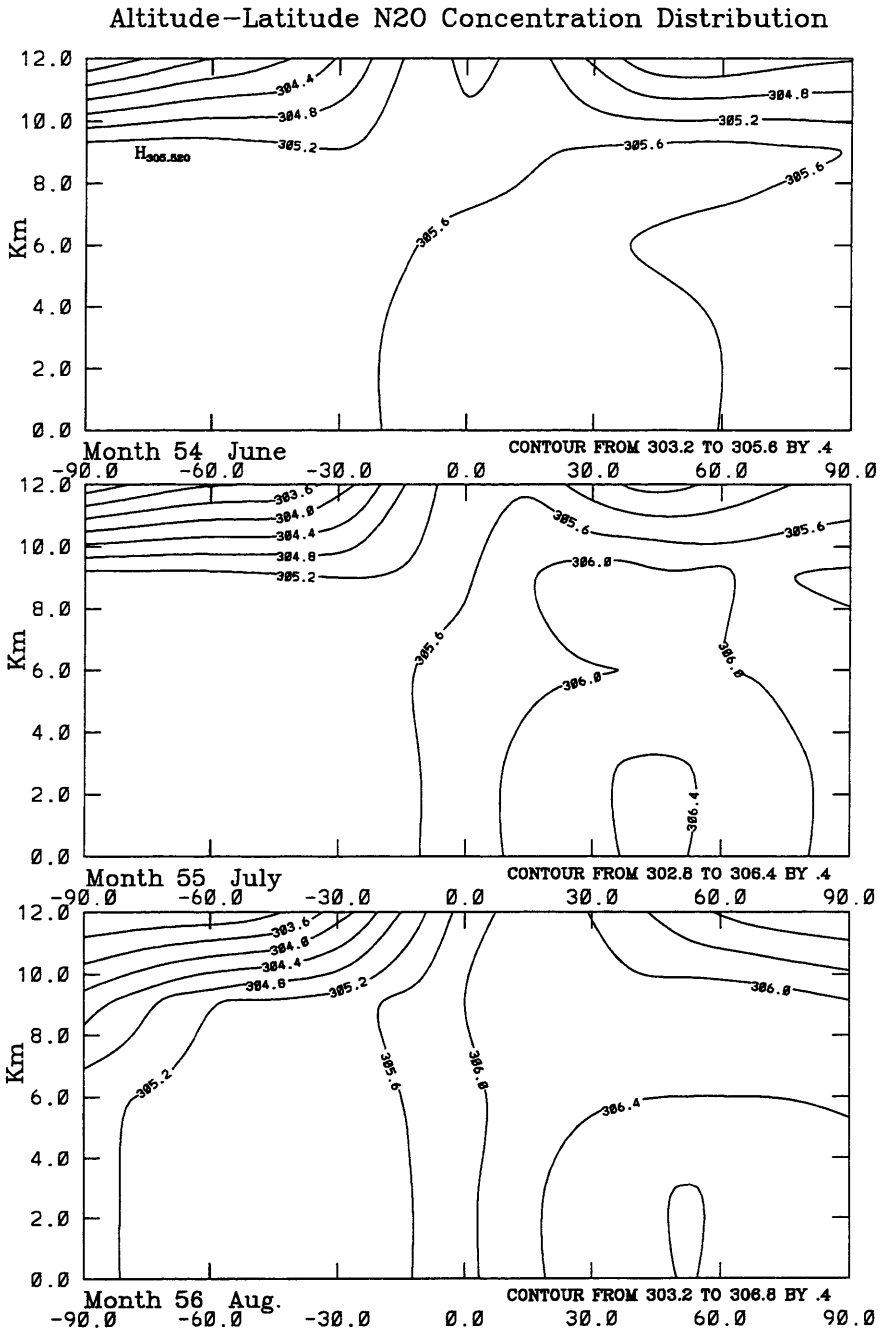

Figure 4-14: Predicted altitude-latitude distribution of N_2O concentrations in ppb units for the northern hemisphere summer (Latitude in degrees, with positive values denoting the Northern Hemisphere).

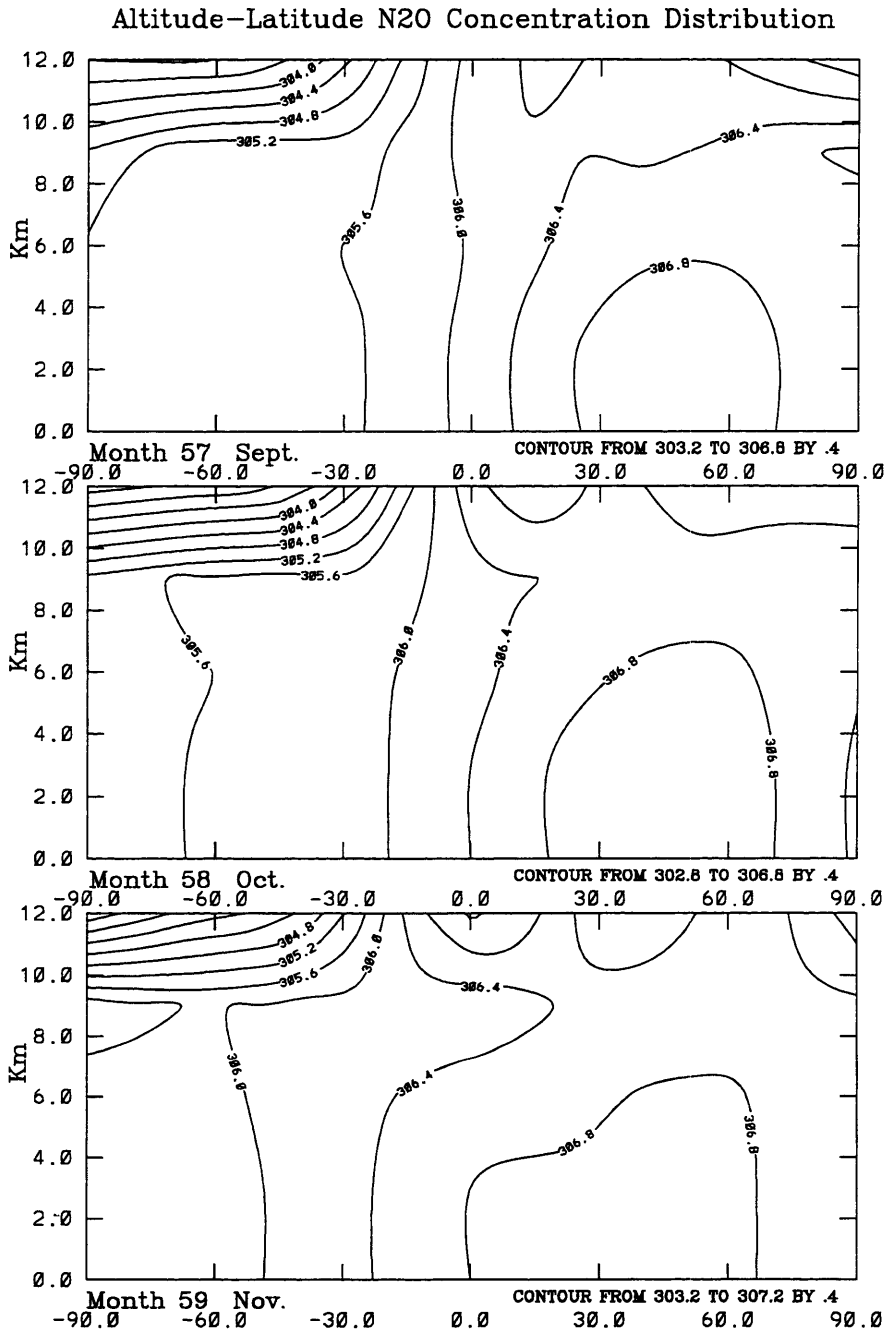

Figure 4-15: Predicted altitude-latitude distribution of N_2O concentrations in ppb units for the northern hemisphere fall (Latitude in degrees, with positive values denoting the Northern Hemisphere).

Chapter 5

Emission Models Application I: Doubling CO_2 Case

5.1 Introduction

The global models for natural N_2O and CH_4 emissions, described in Chapter 2 and Chapter 3, have been used to investigate the responses of these natural emissions to changes in equilibrium climate and soil organic carbon induced by doubling current atmospheric CO_2 concentration. Equilibrium climate outputs from the 2D MIT L-O climate model [*Sokolov and Stone, 1995*] and 3D GISS [*Hansen et al., 1983*] and GFDL-q [*Wetherald and Manabe, 1988*] atmospheric general circulation models (GCMs) and soil organic carbon outputs from MBL terrestrial ecosystem model (TEM, [*Melillo et al., 1993*]) are used to construct climate and soil organic carbon predictions for the artificial "doubling CO_2" case. Global emissions of these two gases are obtained by running the emission models using the predicted driving variables. Sensitivity experiments have also been conducted by using different combinations of driving variables to determine what are the major forces in driving the emission responses.

5.2 Climate Scenarios

Climate outputs for $1\times CO_2$ and $2\times CO_2$ simulations from the two 3D GCMs, i.e., GISS and GFDL-q; and the 2D MIT L-O climate model have been used in constructing climate scenarios for the "doubling CO_2" condition. These climate outputs orginally have the resolutions of the relevant climate models and have been interpolated to $0.5° \times 0.5°$ by Xiao *et al.* [*1996*] using a spherical interpolation scheme. The resulting data are aggregated and averaged to the emission model resolution of $2.5° \times 2.5°$ (for N_2O) or $1° \times 1°$ (for CH_4), which are then used in a conversion scheme to generate the $2\times CO_2$ climate.

The conversion scheme is designed to make use of current observed climate [*Cramer and Leemans, personal communication*] and the modeled climate change. The scheme is described in equations(5.1)—(5.4).

$$\Delta T(i,j) = T_{M2\times CO_2}(i,j) - T_{M1\times CO_2}(i,j) \tag{5.1}$$

$$R(i,j) = \frac{P_{M2\times CO_2}(i,j)}{P_{M1\times CO_2}(i,j)} \tag{5.2}$$

$$T_{2\times CO_2}(i,j) = T_{obs}(i,j) + \Delta T(i,j) \tag{5.3}$$

$$P_{2\times CO_2}(i,j) = P_{obs}(i,j) \times R(i,j) \tag{5.4}$$

where T and P denote surface temperature and precipitation, indices i and j denote longitude and latitude, subscript *obs* denotes observational data, and M denotes the model simulations.

Basically, the absolute difference in surface temperature between $2\times CO_2$ and $1\times CO_2$ model simulations is added to the current observed surface temperature to generate the assumed $2\times CO_2$ surface temperature. The precipitation ratio between $2\times CO_2$ and $1\times CO_2$ model simulations is multiplied by the current observed precipitation to generate the assumed $2\times CO_2$ precipitation.

For the 2D MIT L-O climate model, an additional assumption has been made regarding the climate change: For this 2D model there is no available predicted longitudinal variation in the temperature difference and precipitation ratio defined in (5.1) and (5.2). Therefore, in a given latitudinal band the observed T and P in all the grid cells are adjusted using constant ΔT and R values to give the assumed $2\times CO_2$ climate variables.

To check this procedure, zonal averages of the GISS 3D climate outputs are used to form "GISS 2D" climate outputs, which are then used to construct a $2\times CO_2$ climate in the same way as used for the MIT 2D L-O climate outputs. Emissions predicted with this "GISS 2D" climate are then compared with the emissions predicted using the GISS 3D and MIT 2-D climate models.

Projected changes in global annual mean temperature vary little among the three climate models: 4.2° for the GISS GCM, 4.0° for the GFDL-q GCM, and 4.2° for the MIT 2D L-O model. The predicted change in global annual precipitation is 8.3% for the GFDL-q, 11.0% for the GISS, and 11.5% for the MIT 2D L-O model [*Xiao et al., 1996*].

5.3 Soil Organic Carbon

Soil organic carbon outputs from the TEM model [*Xiao et al., 1996*] are handled in the same way as the precipitation outputs, i.e., the carbon ratio between $2\times CO_2$ and $1\times CO_2$ model simulations is multiplied by the current observed soil organic carbon to generate the assumed $2\times CO_2$ soil organic carbon. The current observed soil organic carbon data from CDIAC [*1986*] are used, which were discussed in detail in Chapter 2.

The outputs in soil organic carbon are obtained by running the equilibrium version of the TEM model using the predicted equilibrium climates discussed in the previous section and of course using doubled CO_2 concentration. These soil carbon data have the resolution of the TEM model, i.e., $0.5° \times 0.5°$. They are aggregated and averaged the same way for precipitation to match the emission model's resolution of $2.5° \times 2.5°$.

The equilibrium run of TEM for the doubled CO_2 conditions predicts a decrease

in total soil carbon storage. The average decrease of soil organic carbon for the different climate model outputs is about 1.3%. The reason for the decrease in total soil carbon storage is the response of heterotrophic respiration to the change in surface temperature. The equilibrium constrainst ensures that net annual average ecosystem production is zero, i.e., the annual net primary production is equal to the annual heterotrophic respiration. For the doubled CO_2 conditions, the predicted increase in surface temperature leads to more heterotrophic respiration, which results in a decrease in soil carbon storage.

5.4 Results for the Doubling CO_2 Case

5.4.1 N_2O Emissions

Four climate and soil organic carbon scenarios from the three different climate models and the TEM model are used in conducting the doubled CO_2 experiments. The results are displayed in Table 5.2 (compare with the results for the current conditions presented in Table 5.1). It is apparent that the four climate models lead to similar results. The difference between "GISS 2D" and "GISS 3D" is very small. This result demonstrates that a 2-D climate model is appropriate for assessing the global impact of climate change on natural emissions. Emissions of N_2O and CO_2 and uptake of CH_4 all increase for the doubled CO_2 situation. All four runs indicate that the equilibrium climate changes due to doubling CO_2 would lead to about a 34% increase in natural N_2O emissions, even though soil organic carbon predicted by TEM is reduced by 1.3% for the same climate and CO_2 changes. This is obviously an important (positive) feedback between climate change and N_2O emissions.

The global distribution of annual-average monthly soil N_2O emissions is plotted in Figure 5-1 (for the outputs of the MIT 2D-LO and TEM models). Comparing this plot with the one for current N_2O emissions (Figure 2-7), we can clearly see that N_2O emissions at high latitudes (especially in the boreal regions where soil organic carbon content is high) are much larger for the doubled CO_2 situation than for current

Climate	Soil C (in 10^{15} g C)	N_2O Emission (in 10^{12} g N)	CO_2 Emission (in 10^{15} g C)	CH_4 Uptake (in 10^{12} g C)
Leamans and Cramer	1821.54	11.325	14.042	11.450

Table 5.1: Emissions with current climate and soil carbon (observed)

Climate	Soil C (in 10^{15} g C)	N_2O Emission (in 10^{12} g N)	CO_2 Emission (in 10^{15} g C)	CH_4 Uptake (in 10^{12} g C)
MIT 2D	1800.00	15.817	16.613	14.061
GISS 2D	1801.87	14.744	16.289	13.423
GISS 3D	1805.82	14.961	16.405	13.395
GFDL	1784.78	15.290	16.459	13.865
Mean	1798.12	15.203	16.442	13.686
Stddev	9.217	0.467	0.135	0.330
Change	-1.3%	34.2%	17.1%	19.5%

Table 5.2: Emissions with doubled CO_2 climates from climate models and soil carbon from TEM model.

climate conditions. They are now comparable to or even larger than the emissions in the tropics. This high latitude enhancement in emissions is caused by the predicted large climate changes at high latitudes.

Experiments have also been conducted to determine what roles the driving variables (soil organic carbon, temperature and precipitation) play in contributing to the increase in N_2O emissions for the doubled CO_2 situation. These experiments have been performed by using different combinations of these driving variables.

Table 5.3 presents the results for doubled CO_2 climate but without a change in soil carbon. As we would have expected, N_2O emissions are somewhat (9%) higher than the values in Table 5.2. The 1.3% decrease in soil organic carbon corresponding to doubled CO_2 equilibrium climate thus reduces N_2O emission by about 9%.

Table 5.4 and Table 5.5 give the results using the changes in temperature only and the changes in precipitation only. All other driving variables (soil organic carbon, precipitation or temperature) are kept at current levels in these experiments. As we

Climate	Soil C (in 10^{15} g C)	N_2O Emission (in 10^{12} g N)	CO_2 Emission (in 10^{15} g C)	CH_4 Uptake (in 10^{12} g C)
MIT 2D	1821.54	16.881	16.961	14.117
GISS 2D	1821.54	15.566	16.993	14.211
GISS 3D	1821.54	16.000	17.136	14.169
GFDL	1821.54	16.385	17.045	14.437
Mean	1821.54	16.191	17.034	14.234
Stddev	0.000	0.532	0.077	0.141
Change	0%	43.0%	21.3%	24.3%

Table 5.3: Emissions with doubled CO_2 climates from climate models but without change in soil carbon.

Climate	Soil C (in 10^{15} g C)	N_2O Emission (in 10^{12} g N)	CO_2 Emission (in 10^{15} g C)	CH_4 Uptake (in 10^{12} g C)
MIT 2D	1821.54	15.623	16.575	14.199
GISS 2D	1821.54	13.549	16.373	14.252
GISS 3D	1821.54	13.488	16.330	14.218
GFDL	1821.54	15.000	16.718	14.516
Mean	1821.54	14.415	16.499	14.296
Stddev	0.00	1.066	0.181	0.148
Change	0.0%	27.3%	17.5%	24.9%

Table 5.4: Emissions using only temperature changes from the modeled doubled CO_2 climates.

can see, the change in temperature alone has a very large impact on N_2O emissions (27.3% increase from current), while precipitation change alone seems to have a small influence (3% increase in N_2O emission from current) in these experiments.

Figure 5-2 gives the global distributions of annual average monthly N_2O emissions corresponding to using the temperature change only or the precipitation change only (for the outputs of the MIT 2D-LO climate model). These distributions give some hints about why there is a large impact on N_2O emission caused by a surface temperature change but only a small impact caused by a precipitation change.

The striking difference between the top panel (temperature change only) and the bottom panel (precipitation change only) is in the N_2O emissions at high latitudes.

Climate	Soil C (in 10^{15} g C)	N_2O Emission (in 10^{12} g N)	CO_2 Emission (in 10^{15} g C)	CH_4 Uptake (in 10^{12} g C)
MIT 2D	1821.54	11.541	14.268	11.448
GISS 2D	1821.54	11.797	14.042	11.450
GISS 3D	1821.54	11.946	14.625	11.437
GFDL	1821.54	11.398	14.246	11.445
Mean	1821.54	11.670	14.295	11.445
Stddev	0.00	0.247	0.242	0.006
Change	0.0%	3.0%	1.8%	0.0%

Table 5.5: Emissions using only precipitation changes from the modeled doubled CO_2 climates.

Climate	Swamps	Tundra	Bogs	Total
Cramer and Leemans	69.979	4.237	52.585	126.801

Table 5.6: CH_4 emissions with current observed climate (in Tg CH_4 per year)

The large N_2O emissions in these areas induced by temperature change could be due to the lengthened emission season caused by the higher temperatures or to there being more precipitation in the form of rainfall instead of snowfall. These issues will be discussed in more detail later.

5.4.2 CH_4 Emissions

Climate	Swamps	Tundra	Bogs	Total
MIT 2D	79.998	5.743	121.159	206.900
GISS 2D	81.851	5.353	97.460	184.664
GISS 3D	83.753	5.500	97.906	187.159
GFDL-q	77.627	6.064	118.526	202.218
Mean	80.807	5.665	108.763	195.235
Stddev	2.616	0.311	12.840	10.982
Change	15.5%	33.7%	106.8%	54.0%

Table 5.7: CH_4 emissions with doubled CO_2 climates (in Tg CH_4 per year)

Since soil organic carbon is not a driving variable in the global model for natural CH_4 emissions, only the four climate scenarios from the three climate models are used in the doubled CO_2 experiments for CH_4 emissions. The results of these experiments are summarized in Table 5.7. For the purpose of comparison, CH_4 emissions for the current conditions are displayed in Table 5.6. Model outputs for the doubling CO_2 climates lead to similar emission results, with some difference existing between two "groups" of models (one consisting of the GISS models and the other consisting of the MIT 2D and GFDL-q models). This difference is due mainly to the difference in simulated climates at high latitudes for the three different climate models. Note that the largest difference happens in the emissions from bogs which are mostly located in the boreal regions. However, the difference between "GISS 2D" and "GISS 3D" is negligibly small, which again demonstrates that a 2-D climate model is appropriate for first order analysis of the effects of climate change on natural emissions. The average of the four runs indicates that the changes in equilibrium climate due to doubling CO_2 would lead to about a 54% increase in natural CH_4 emissions. This increase in CH_4 emissions is largely due to emissions from high latitude bogs. The emissions from these bogs are more than double the current ones (i.e. increase by 107%). Tropical wetlands (swamps) experience a relatively small change (increase by about 16%). Tundra emits a small amount of CH_4 in all cases, but it experiences about a 34% increase due to climate change associated with doubling CO_2.

5.5 Discussion

An analysis of the driving climate has been conducted to determine why there is a big impact on N_2O emissions by surface temperature change, why there is a distinct difference in emissions (more obvious in CH_4 emissions) between the two "groups" of models (one consisting of the GISS models, and the other consisting of the MIT 2D and GFDL-q models). This analysis has been done by plotting the change in the zonal and nonfreezing-seasonal mean of surface temperaure and the change in zonal and annual mean of rainfall (i.e. total precipitation minus snowfall). The zonal mean

in both these cases is defined as the average over emitting land areas only (soils for N_2O, wetlands for CH_4).

Figure 5-3 plots the changes in the defined mean surface temperature (top panel) and annual rainfall (bottom) for the combination of doubled CO_2 temperature and doubled CO_2 precipitation with the means done with respect to N_2O emitting regions. While the change in rainfall is similar among the four models, the change in temperature clearly has two distinct groups. The GISS models (2D and 3D) predict higher temperature in the tropics and lower temperature at northern high latitudes than the MIT 2D and GFDL-q models. Since northern high latitudes have higher soil organic carbon content (Chapter 2), we would expect the MIT 2D and GFDL-q models to predict larger changes in soil N_2O emissions, which is the case (Table 5.2).

Figure 5-4 is similar to Figure 5-3 but plots the changes with the means done with respect to CH_4 emittng wetland regions. Again, the difference is in the surface temperature between the two groups of models, with higher temperature at northern high latitudes and lower temperature in the tropics predicted by the MIT 2D and GFDL-q models. Since bogs are mostly located in the high latitude regions, the MIT 2D and GFDL-q models predict higher emissions from this source (Table 5.7). Tropical emissions are not very sensitive to the temperature changes. That is why the difference in swamp emissions is relatively small.

In summary both for N_2O and CH_4 emissions, the climate changes at high latitudes play a significant role in contributing to the predicted emission changes.

Figure 5-5 plots the changes in the defined zonal mean annual rainfall for two combinations of temperature and precipitation designed for the sensitivity experiments discussed in Section 5.4.1. The top panel is for the combination of doubled CO_2 precipitation and current surface temperature. The bottom panel is for the combination of doubled CO_2 surface temperature and current precipitation.

Compared with the bottom panel in Figure 5-3, the top panel in Figure 5-5 shows small changes in rainfall at all latitudes, although the doubled CO_2 precipitation is used in this case. Because current temperature is used in this combination, most of the increased precipitation reaches the ground in the form of snow, which does

not effectively increase soil N_2O emissions. In the tropics, soil organic carbon is not as high as in high latitudes, and already it is almost all in active pools. Hence an increase in precipitation here does not have a big effect on N_2O emissions. All these arguments demonstrate why precipitation change alone does not have a big impact on N_2O emissions. The bottom panel in Figure 5-5 tells a different story. Even though precipitation is not changed in this case, rainfall actually increases because some of the snowfall becomes rainfall due to the warmer temperatures. Warmer temperature also effectively increases the soil N_2O emission season. Note that increased rainfall happens at northern high latitudes. These are the regions with rich soil organic carbon. The result of these combined effects is the substantial increase in N_2O emissions at the northern high latitudes, which are very clear in the top panel of Figure 5-2. Therefore, increasing temperature alone at high latitudes is equivalent to increasing both temperature emitting season and rainfall. This explains why temperature alone has such a big impact on N_2O emissions.

5.6 Conclusions

The emission models developed in Chapter 2 and Chapter 3 are capable of addressing the issue of emission changes corresponding to climate changes using climate and soil organic carbon predictions done offline. Experiments discussed here show that doubling CO_2 leads to a 34.2% increase in N_2O emissions, even though soil organic carbon is reduced by 1.3%, and a 54% increase in CH_4 emissions. Potentially, these are important (positive) feedbacks between climate change and trace gas emissions.

The comparison between the hypothetical "GISS 2D" model and the GISS 3D GCM demonstrates that a 2-D climate model is appropriate for first order analysis of the effect of climate change on natural emissions. Four different models produce similar results with some difference existing due to differences in predicted climate, especially in high latitude regions.

While changes in soil organic carbon corresponding to equilibrium climate change associated with doubling CO_2 reduces soil N_2O emissions by about 10%, changes in

surface temperature and precipitation increase N_2O emissions. However, temperature and precipitation play different roles in contributing to the emission increase. The temperature increase seems to dominate the the two by also lengthening the emission season and increasing the effective rainfall in carbon-rich high latitude regions. Precipitation change alone does not have a big impact on emissions, because most precipitation still reaches the ground in the form of snowfall and tropical emissions are not sensitive to precipitation change. Geographical coherence of predicted changes in surface temperature and precipitation in climate models is significant in determining the predicted change in global emissions.

For both N_2O and CH_4 emissions, climate changes at high latitudes play a significant role in contributing to the emission changes.

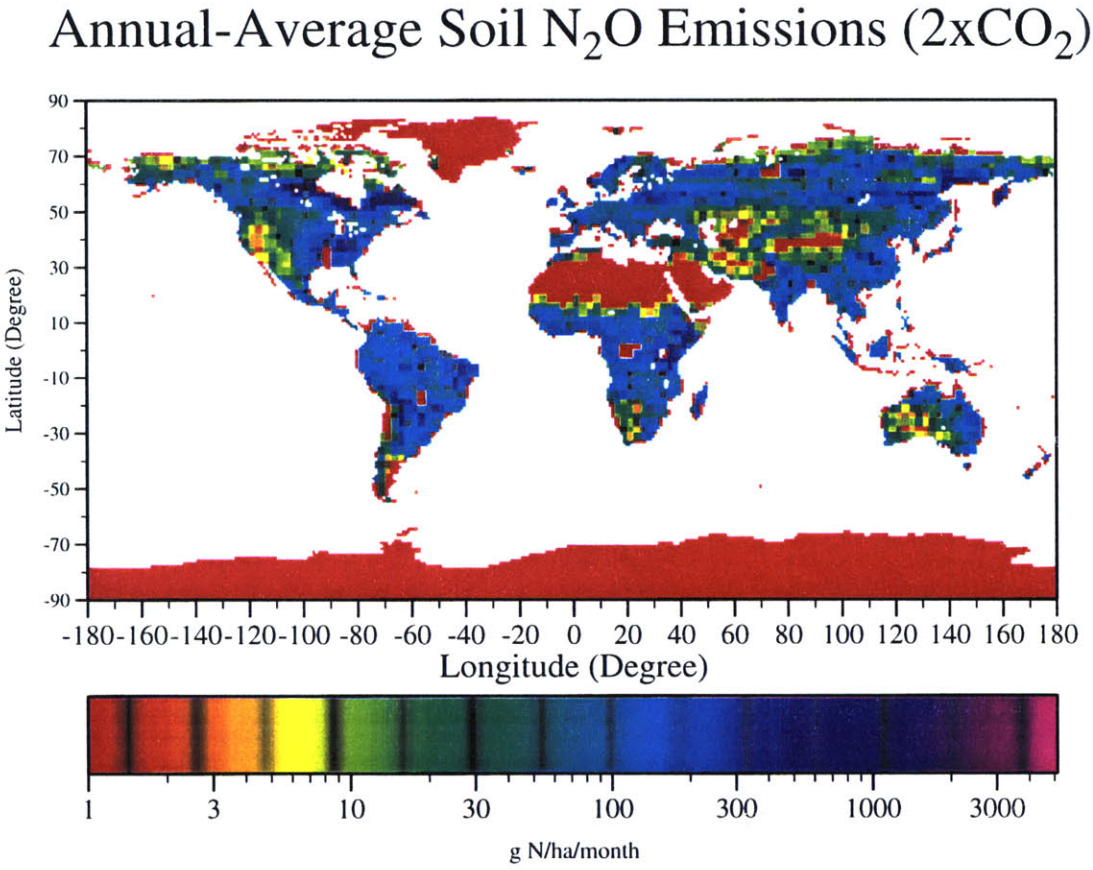

Figure 5-1: Predicted global distribution of annual-average monthly soil N_2O emissions at $2.5° \times 2.5°$ resolution for the predicted climate and soil organic carbon conditions associated with doubling CO_2 (for the MIT 2D-LO climate and TEM models).

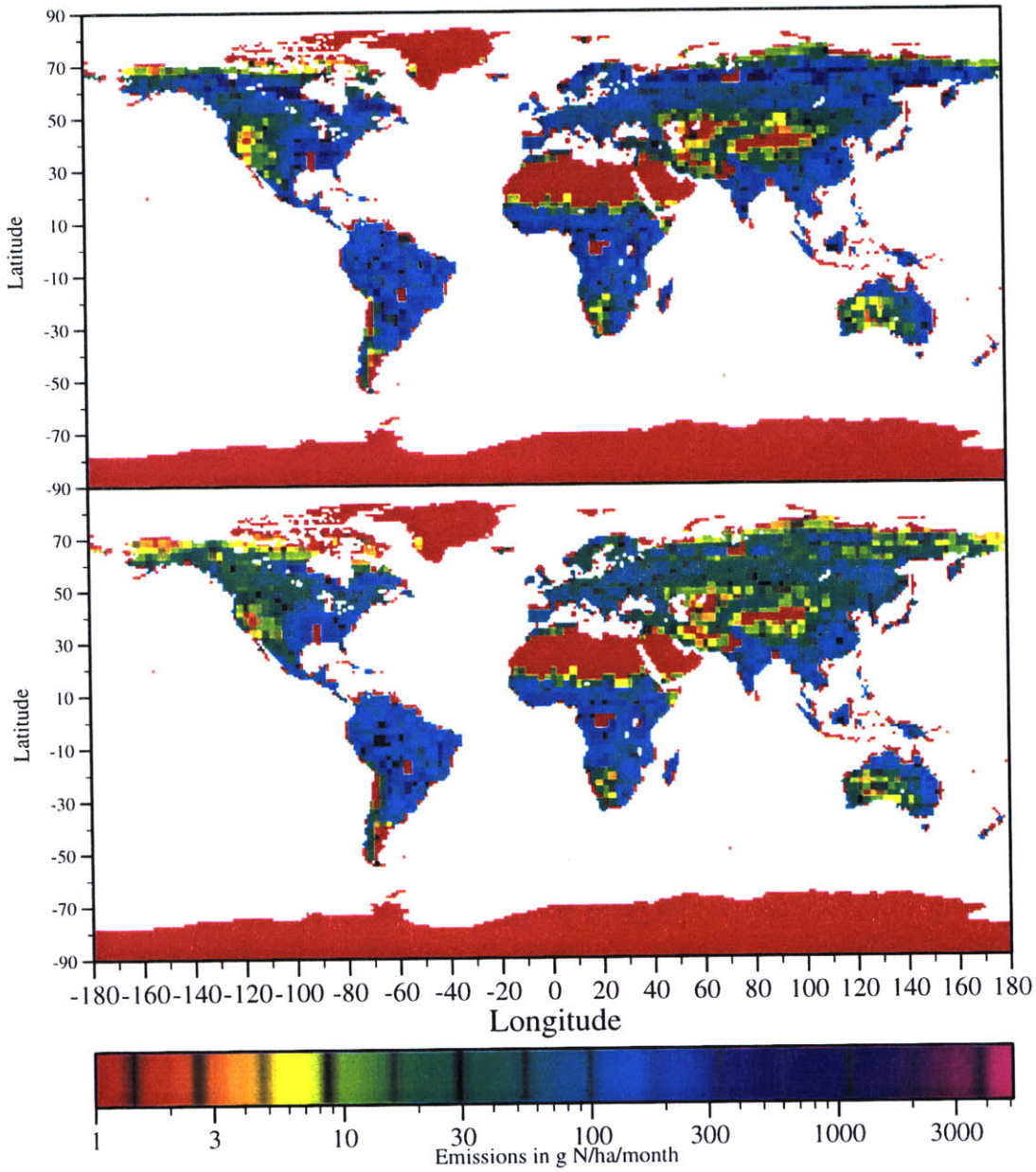

Figure 5-2: Predicted global distributions of annual-average monthly soil N_2O emissions at $2.5° \times 2.5°$ resolution for temperature change only (top panel) and precipitation change only (bottom panel) (for the MIT 2D-LO climate model).

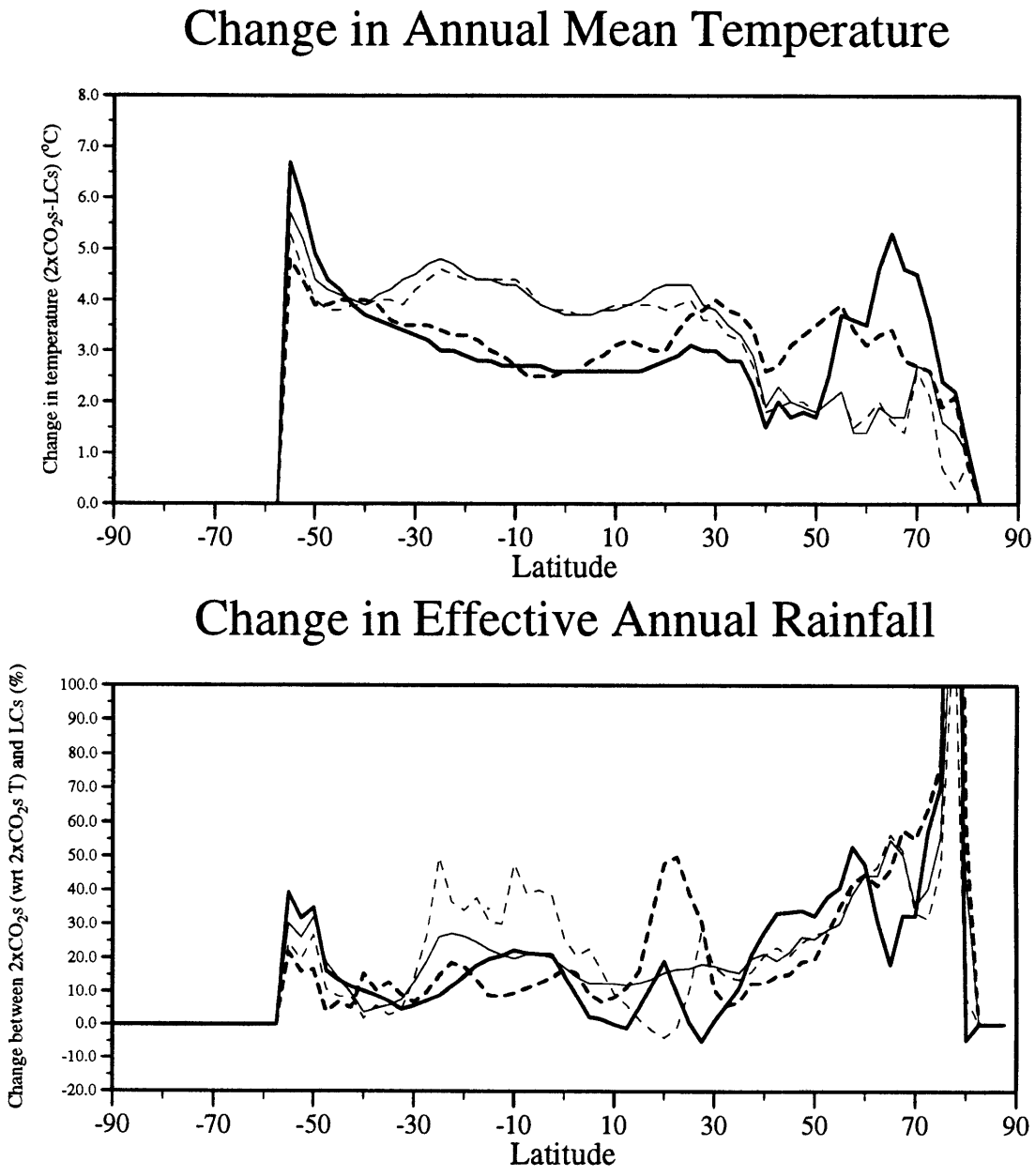

Figure 5-3: Changes in zonal and nonfreezing-seasonal mean of surface temperature (top panel) and zonal and annual mean rainfall (bottom panel) for the combination of doubled CO_2 temperature and doubled CO_2 precipitation with means being defined with respect to N_2O emitting regions.

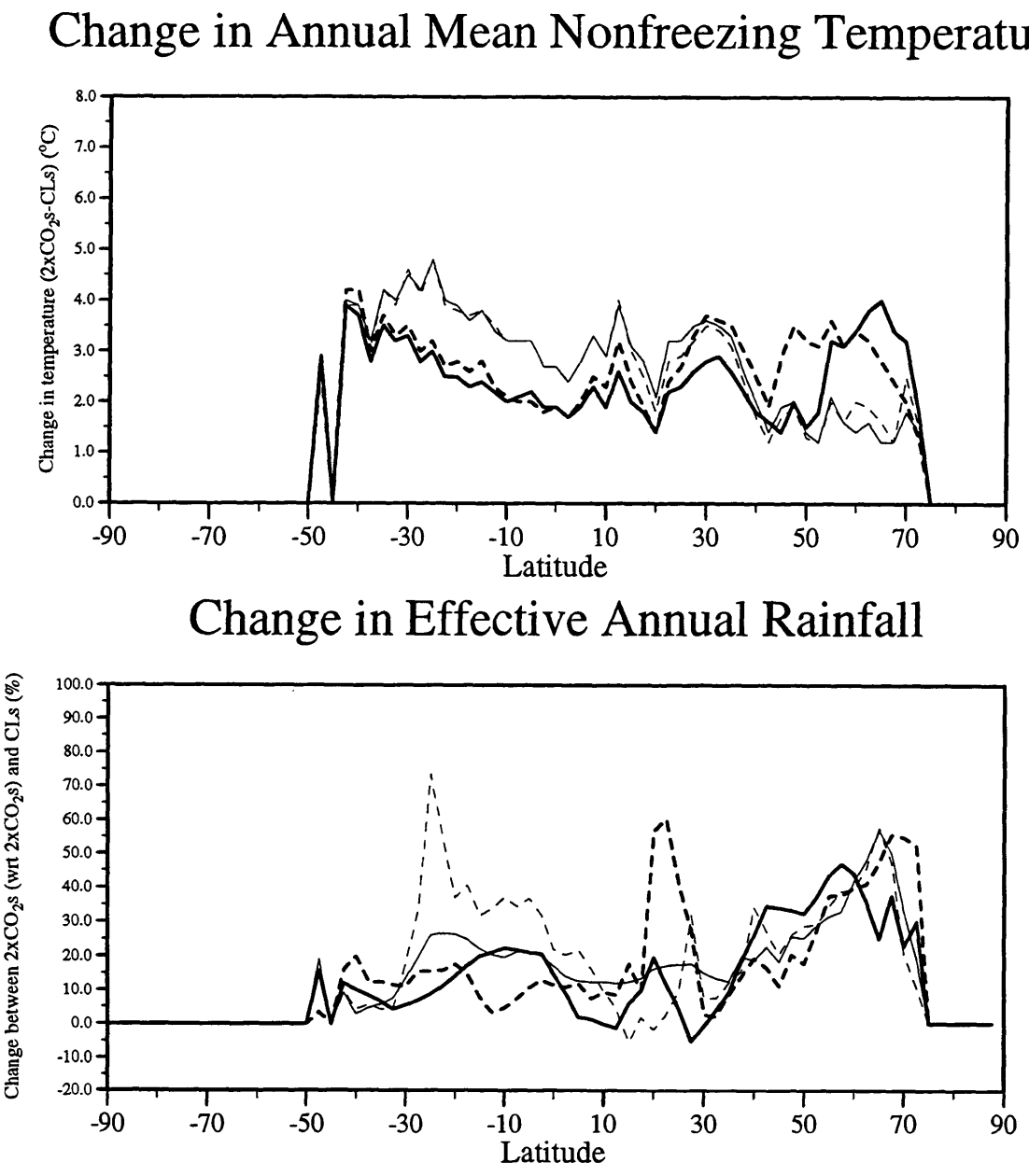

Figure 5-4: Changes in zonal and nonfreezing-seasonal mean of surface temperature (top panel) and zonal and annual mean rainfall (bottom panel) for the combination of doubled CO_2 temperature and doubled CO_2 precipitation with means being defined with respect to CH_4 emitting regions.

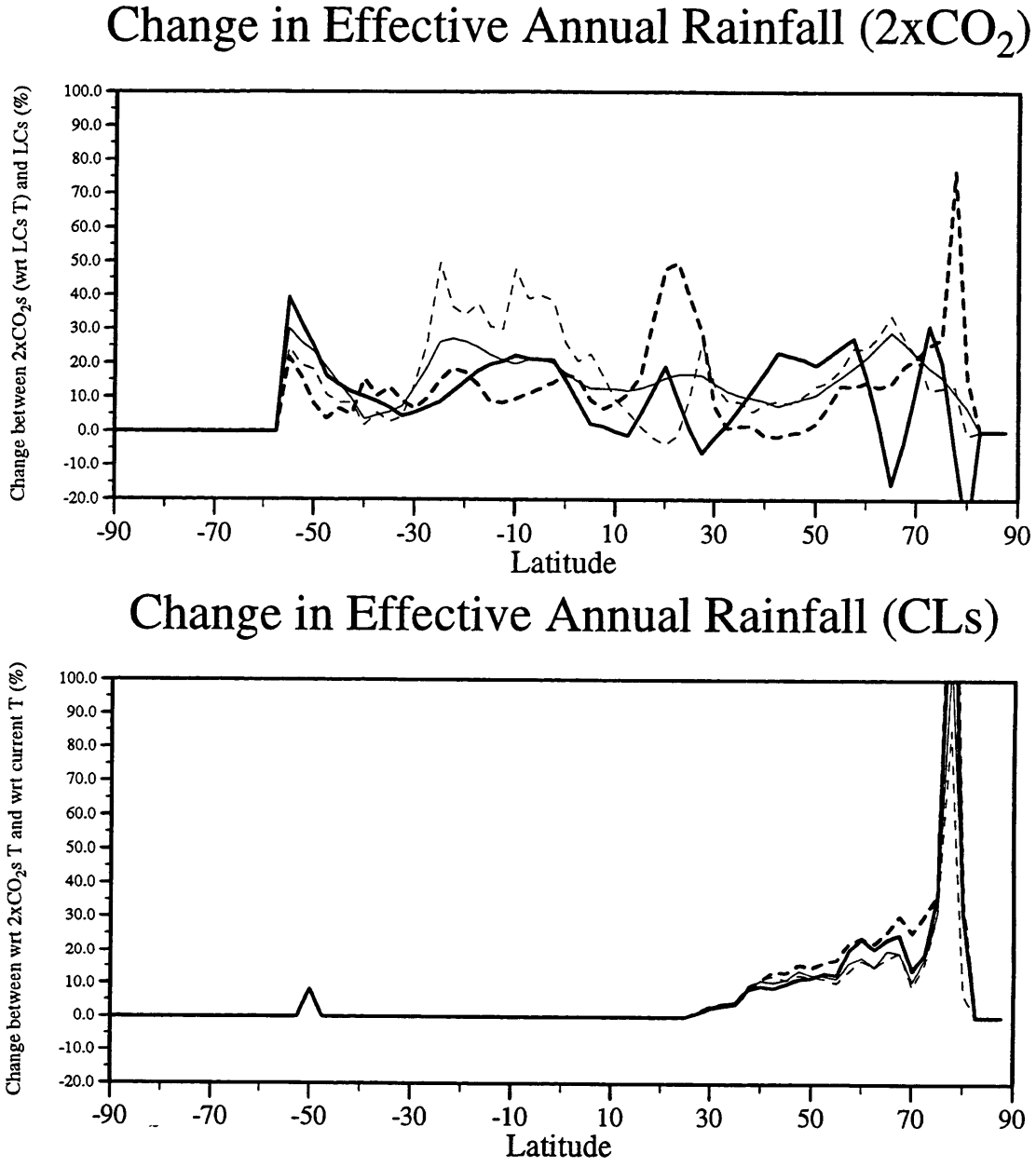

Figure 5-5: Changes in zonal and annual mean rainfall for the combination of doubled CO_2 precipitation and current temperature (top panel) and the combination of doubled CO_2 temperature and current precipitation (bottom panel) with means being defined with respect to N_2O emitting regions.

Chapter 6

Emission Models Application II: Ice Age Case

6.1 Introduction

The models developed for N_2O and CH_4 natural emissions have also been applied to determining the emissions of N_2O and CH_4 for ice age conditions (specifically the Last Glacial Maximum (LGM), 18,000 years Before Present). The assessment was done by using as inputs to N_2O and CH_4 emission models a combination of CLIMAP data [*CLIMAP, 1981*] and GISS 3D GCM ice-age-run climate outputs [*Hansen et al., 1984*]. The results of the runs of the emission models show that the natural soil source of N_2O for the LGM is around 6 Tg N/year and the natural wetland source of CH_4 is around 60 Tg CH_4/year. Although the accuracy of these estimates depends considerably on the data used in representing the conditions during the LGM as well as the uncertainties in models themselves, the results do shed some light on how a dramatic climate change could influence natural emissions both spatially and temporally.

6.2 Paleo N_2O Emission Model

As discussed in Chapter 2, the principal controlling parameters for global N_2O emissions include vegetation and soil organic carbon, which control the supply of nutrients for N_2O-producing bacteria, and soil texture and climate data which regulate bacterial activity. The development of the paleo N_2O emission model required estimation of various input parameters corresponding to the LGM conditions.

6.2.1 Paleo Soil Organic Carbon

The global distribution of soil organic carbon for paleo conditions is obtained by using a combination of the CLIMAP current and LGM vegetation distributions and current observational soil organic carbon data. Specifically, we calculate soil organic carbon for every CLIMAP vegetation type using current soil carbon and vegetation data and apply these soil organic carbon values to the vegetation distribution under LGM conditions. CLIMAP data for current and LGM vegetation distributions [*CLIMAP, 1981*] and current soil organic carbon data from Carbon Dioxide Information and Analysis Center of the Oak Ridge National Laboratory [*CDIAC, 1986*] have been used in this scheme. The basic assumption underlying the scheme is that the soil organic carbon for a particular ecosystem type does not change substantially when climate changes but the distribution of these ecosystems does change.

The CLIMAP vegetation has 9 broad classes. Each of the first 8 classes has 4 subclasses. Adding class 9 for lichen and rice paddies, these constitute 34 different vegetation types. Although the definition of these vegetation classes and subclasses may be different from others (e.g. the TEM vegetation types), consistency is maintained as long as current and paleo vegetation are defined using the same definitions of classes and subclasses.

6.2.2 Paleo Soil Texture

CLIMAP does not provide any data for soil texture under ice age conditions. However, it does have a data set for soil types. A scheme similar to the one used to derive the

paleo soil organic carbon has been used here to infer the soil texture (basically the clay content of soil) for the LGM. First, the clay content for each soil type is calculated using current CLIMAP soil type and clay content distributions. These clay contents are then applied to paleo CLIMAP soil type distributions to produce the paleo soil texture values. Again, the assumption is that the clay content for each CLIMAP soil type does not change when climate changes although the distribution of each soil type does change.

There are 5 broad classes and each class has 4 subclasses, thus yielding 20 different soil types. For some of the soil type subclasses, there are no data available in the CLIMAP soil type data base. The mean value of that particular soil type class to which the subclass belongs is used to fill the "missing" data in these cases.

6.2.3 Climate Data for the Ice Age

The LGM CLIMAP data sets unfortunately do not include surface temperature and precipitation over land, which is what is needed in the N_2O emission model. This necessitated the use of modeled climate data. Hansen et al. [*1984*] conducted a 3-D GCM equilibrium run for the LGM using CLIMAP data as surface boundary conditions. The use of the climate outputs from this run (which is called RUN 903) is consistent with the use of the other CLIMAP data in this analysis.

GISS 3-D GCM has a resolution of 7.83°×10° (i.e. 24×36 surface grid points). The modeled climate outputs are linearly interpolated to fit a resolution of 2°×2° which is the resolution for CLIMAP data and the paleo versions of the N_2O and CH_4 emission models. After the interpolation, the 'difference' and 'ratio' schemes used in Chapter 5 are used to obtain the LGM climate data by adding (or multiplying) the difference (or ratio) with current climate data [*Leemans and Cramer, 1990*].

Annual mean surface temperature and annual mean monthly precipitation are presented in Figure 6-1 with the resolution of 2°×2°. These are the data directly used in the emission models. Values for grid points over oceans, ice sheets and deserts, which do not have any vegetation at all, are not shown on the graphs.

The modeled global average surface temperature for the LGM is about 4°C cooler

than that for current conditions. Much greater cooling than the average occurs in the northern high latitudes, especially in southern Canada and northern Europe. Some high latitude regions, including Alaska, are at about the same temperature in the ice age as today. There is no universal high latitude enhancement of climate change. Temperature changes over the tropical and subtropical regions are generally of the order of 1°C. Numerous low latitude areas also experience substantial cooling of the order of 5°C.

6.2.4 N_2O Emission Results for the Ice Age

The paleo N_2O emission model is run for four years using the same climate data. The initial condition for the soil temperature profile was obtained by setting temperatures at all depths equal to the surface air temperature. For soil moisture, the initial condition was somewhat arbitrary, and was obtained in the same way as we did for the current-day N_2O emission model as discussed in Chapter 2. Again, because the emission results are not sensitive to these initial conditions after the first year of integration, it does not pose a problem for the paleo N_2O emission model.

As we discussed earlier, because precipitation over land is generally larger than evaporation, the multi-year run with the same climate is not an equilibrium problem. Rather, once free of the initial conditions we would expect emissions to increase very slowly as the integration time goes longer due to accumulation of moisture in the soil. Actually, this is indeed what happens with the multi-year run. The relation between global total N_2O emission and integration time is described in Table 6.1. As we can see from Table 6.1, the global total N_2O emission starts to increase after year 3. This trend continues after year 4 (data are not presented in the table). The first 2 years appear to be sensitive to the initial conditions with the emissions for years 1 and 2 being bigger than that for year 3. Taking into consideration the damping out of the effects of the initial conditions and the phasing in of the nonequilibrium effect in multi-year integration, we have selected the results for year 3 as the most appropriate to represent the paleo N_2O emissions. These results are shown graphically in Figure 6-2 through Figure 6-5.

Integration Time (Year)	1	2	3	4
N_2O Emissions (Tg-N)	6.1838	6.0432	6.0415	6.0417

Table 6.1: The relation between the global total emission of N_2O and integration time for the ice age case.

Figure 6-2 shows the global distribution of annual-averaged monthly N_2O emissions at the model resolution of $2° \times 2°$. Basically, the spatial pattern of N_2O emissions is quite similar to that for the current N_2O emissions. For example, there is a strong emission band in the tropical and subtropical regions. This high emission band is caused by the highest surface temperature and the largest precipitation being in these regions. Extratropical regions have no or very low emissions. The striking difference between the spatial patterns for the LGM emissions and the current emissions is that there is no LGM emission at all poleward of the high latitude line defined by the ice sheet boundary in the northern hemisphere summer. As we have discussed in Chapter 2, high latitudes are actually the regions with the richest soil organic carbon. Therefore, we would expect dramatically smaller N_2O emissions under the ice age conditions and this is indeed the case.

The global total N_2O emission is estimated at 6.04 Tg N per year, which is only slightly more than half of the current emission from the same natural source. The tropical regions between 30°S and 30°N contribute 4.62 Tg N per year, which is about 75% of the total and is close to the percentage contribution from these regions for the current N_2O emissions. Although the hemispheric difference in N_2O emissions is quite large (the difference is around 18% with the northern hemispheric emission being 3.55 Tg N/yr and the southern hemispheric emission being 2.49 Tg N/yr), the latitudinal profile of the emissions is quite symmetric. This can be seen in Figure 6-3 which shows the latitudinal distribution of the predicted paleo N_2O emissions. The latitudinal profile has a peak in the equatorial region and gradually decreases as one moves to high latitudes. This profile is quite different from that for the current N_2O emissions which has a 'double-peak' shape. One of the peaks is due to the almost continuous N_2O emissions during the year in the tropics. The other is due to the

strong summer emissions from the extensive northern middle and high latitude areas.

Seasonal cycles for the paleo N_2O emissions are smaller compared with those for the current emissions, but they are still significant. These cycles are very clear in Figure 6-4 and Figure 6-5. For example in Figure 6-4, in January there is little emission from northern extratropical regions while in July emission is significant from these regions. The tropics by comparison barely have any seasonal variations (Figure 6-5 shows the seasonal variations for all latitudes). The seasonal variation of total paleo N_2O emission is therefore almost entirely caused by these seasonal cycles in the high latitude northern hemisphere.

6.2.5 Discussion

The simulated paleo N_2O emissions presented here are strongly dependent on the input data sets used in the emission model, and thus their accuracy is dependent significantly on the reliability of these data sets. An attempt has been made to try to test the emission predictions using observations. However, because there is a lack of information about the atmospheric lifetime and concentration of N_2O at the ice age, such tests are difficult. The test presented here is therefore very tentative and simple.

Past N_2O variations are much less well documented in the geologic record than those of CO_2 and CH_4. Data from ice core measurements concern mainly the last 3,000 years [*Khalil and Rasmussen, 1988; Etheridge et al., 1988*]. The pre-industrial level was reported to be 285 ppb. The ice core measurement with the earliest date (around 13,600 years BP) was reported by Zardini et al. [*1989*] indicating a N_2O level of 244 ppb. With only this information in hand, we can only see whether the LGM estimate here fits extrapolations back to the LGM (18,000 BP).

Assuming the atmosphere is a single box, we have following one-box model for a specific chemical species.

$$\frac{dM}{dt} = E - \frac{M}{\tau} \tag{6.1}$$

where M is the global total mass of the species in the atmosphere, E is the emission and τ is the lifetime of the species.

If we further assume that there is an equilibrium existing for this species, the model equation is simplified as follows.

$$E = \frac{M}{\tau} \tag{6.2}$$

If $\overline{\chi}$ is the global average mixing ratio for this species and m stands for molecular weight, we then have

$$\overline{\chi} = \frac{\frac{M}{m}}{\frac{M_{air}}{m_{air}}} \tag{6.3}$$

Combining the above two equations gives

$$\overline{\chi} = \frac{m_{air}}{m} \cdot \frac{E \cdot \tau}{M_{air}} \tag{6.4}$$

Since ice core data contain the surface atmospheric concentrations of a chemical species, it is necessary to relate the global average mixing ratio with the surface mixing ratio. A simple formula has been used to accomplish this:

$$\overline{\chi} = \frac{\int_0^\infty \chi_z \cdot [M_{air}]_z dz}{\int_0^\infty [M_{air}]_z dz} \tag{6.5}$$

where χ_z is the mixing ratio at the height of z, and $[M_{air}]_z$ is the air density at at the height of z.

The above equation can be simplified as follows based on the notion that N_2O is well mixed in the troposphere and mainly destructed in the stratosphere:

$$\overline{\chi} = \overline{\chi}_t \left(f_t + \frac{\overline{\chi}_s}{\overline{\chi}_t}(1 - f_t) \right) \tag{6.6}$$

where $\overline{\chi}_t$ and $\overline{\chi}_s$ are the average tropospheric and stratospheric N_2O mixing ratios, and f_t is the fraction of the tropospheric air mass to the global total air mass.

In order to calculate the N_2O surface mixing ratio (i.e. the tropospheric average N_2O mixing ratio due to the well-mixing), we must have an estimate of M_{air} and f_t.

Here is a simple way of doing this. If P_s is the average surface pressure and P_t is the tropopause pressure, then we have

$$M_{air} = \frac{4\pi R^2 \times P_s}{g} \tag{6.7}$$

$$M_{air-s} = \frac{4\pi R^2 \times P_t}{g} \tag{6.8}$$

$$f_t = \frac{M_{air} - M_{air-s}}{M_{air}} \tag{6.9}$$

where M_{air-s} is the mass of the air above the tropopause, R is the mean radius of the earth, and g is the gravity at sea level.

Using $P_s = 1013.25$ mb and $P_t = 100$ mb, we get

$$M_{air} = 5.26667 \times 10^{21} \text{ grams}$$

$$f_t = 0.90131$$

The ratio between the average stratospheric and tropospheric N_2O mixing ratios is calculated according to satellite data [*Jones and Pyle, 1984*]. The LGM value of this ratio is assumed to be the same as the current one.

$$\frac{\overline{\chi_s}}{\overline{\chi_t}} = 0.1986$$

If the natural soil source (11.325 Tg N) for N_2O is the only source for pre-industrial N_2O (285 ppb), we can get an estimate of pre-industrial N_2O lifetime using equation (6.4).

$$\tau = 117.86 \text{ years}$$

If we assume that the LGM N_2O lifetime is the same as the pre-industrial N_2O lifetime, we then get the LGM N_2O mixing ratio using the emission we got for the ice age.

$$\chi_{N_2O} = 152.1 \text{ ppb}$$

References	IPCC [1994]	Estimated by this thesis	Wang *et al.* [1996]	Implied		Prinn *et al.* [1990]
				Polynomial	Linear	
Lifetime (years)	110.0	117.9	128.0	144.1	183.4	166.0
Paleo χ_{N_2O} (ppb)	142.0	152.1	165.2	185.9	236.5	214.2

Table 6.2: The inferred ice age N_2O mixing ratios using the estimated emission in this thesis and various values of lifetime, and the implied lifetimes for ice age N_2O using projected mixing ratios from ice core data.

Obviously, using a different lifetime will give us a different predicted N_2O mixing ratio for the ice age. A number of calculated values for the N_2O lifetime obtained from the literature [*IPCC, 1994; Prinn et al, 1990; Wang et al., 1996*] have been used to give an idea of the possible range of estimates for the ice age N_2O mixing ratio. These are presented in Table 6.2.

Polynomial and linear fitting is performed by using the available ice core N_2O mixing ratio data (back only to 13,600 years BP) [*Zardini et al., 1989*]. The fitted curves are plotted in Figure 6-6 together with the calculated N_2O mixing ratios in Table 6.2. Using the fitted polynomial and linear curves to extrapolate back in time gives inferred N_2O mixing ratios for the LGM of 185.9 ppb and 236.5ppb respectively. The estimate (152.1 ppb) we got using the assumed pre-industrial N_2O lifetime (117.85 years) is close to the mixing ratio projected by the polynomial curve (185.9ppb) but is far off the one projected by the linear curve (236.5ppb). If we make an analogy to CH_4, the polynomial curve seems better in reflecting the ice age conditions, because the ice age (LGM), which is about 5,000 years before the earliest N_2O data point, has much lower temperature. CH_4 ice core data, which are available back to 20,000 BP, would support a polynomial curve for CH_4 (Figure 6-11). The polynomial-projected mixing ratio of 185.9 ppb implies that the N_2O lifetime at the LGM is 144.1 years while the linearly-projected mixing ratio of 236.5ppb would imply a lifetime of 183.4 years.

Although there are a number of assumptions involved in calculating the ice age

(LGM) N_2O mixing ratios from our emission estimates, the values we get are below 244 ppb which is the measured value for 13,600 years BP. This is in the right direction if N_2O behaves similar to CH_4. Also, the ice age N_2O mixing ratio estimate of 185.9 ppb obtained by the polynomial-extrapolation of the ice core data falls in the calculated range using the paleo model estimated N_2O emission and a feasible range of its lifetime (110-166 years) based on current photochemical models.

6.3 Paleo CH_4 Emission Model

The most difficult problem in estimating wetland CH_4 emission for a dramatically different climate is obtaining reliable estimates for the global wetland distribution. Besides climate, this is the only other input which distinguishes the paleo CH_4 emission model from the current CH_4 emission model. What we do here is to make an assumption about the wetland distribution: namely that all current wetlands also existed in the ice age except for those wetlands which would have been covered by the ice sheet. Numerical experiments have also been performed with an adjustment to this assumed ice age wetland distribution consisting of the addition of ice-age specific wetlands created by melting of the huge ice sheet during summer season. The emission model using the above assumption without the adjustment is called Version 1 with the wetland adjustment is called Version 2. The driving climate used in these two versions is the GISS 3-D GCM modeled climate for the LGM, which was discussed in the section on the paleo N_2O model. The results of these two different versions are presented in the following two sections.

6.3.1 CH_4 Emission Results of Model Version 1

As before, in order to assess the effect of the initial conditions, we ran the CH_4 emission model for four years with the same LGM climate data. As we can see from Table 6.3 for monthly CH_4 emissions, the emission results are not as sensitive as N_2O to initial conditions. The results of year 3 are again selected as the best to represent paleo CH_4 emissions. Again, this is not an equilibrium run, because the

Month	Year 1	Year 2	Year 3	Year 4
1	4.70	5.02	5.02	5.02
2	4.61	4.73	4.73	4.73
3	5.60	5.70	5.71	5.70
4	5.12	5.20	5.21	5.21
5	4.91	4.84	4.85	4.85
6	4.86	4.80	4.79	4.79
7	5.39	5.08	5.09	5.09
8	5.56	5.44	5.45	5.46
9	5.15	5.21	5.23	5.20
10	4.57	4.56	4.56	4.57
11	4.17	4.18	4.18	4.19
12	4.42	4.43	4.44	4.45
Annual Total	59.08	59.18	59.27	59.29

Table 6.3: Monthly CH_4 emissions (in Tg CH_4/month) for different integration times.

model predicted precipitation and evaporation are not balanced over land.

Results for this version are shown in Figure 6-8 and in the top panels of Figure 6-7 and Figure 6-10. The global distribution of annual-averaged monthly CH_4 emissions (top panel of Figure 6-7) has a similar pattern to the one for current CH_4 emissions: namely, there are two latitudinal CH_4 emission bands. One is concentrated in the northern areas around 60° latitude and the other is in the tropics. The magnitude of the emissions are much larger in the tropics than in the extratropical regions. As for N_2O, the big difference between paleo (LGM) and current CH_4 emissions is that there is no emission during the LGM beyond the high latitude line defined by the ice sheet boundary for the LGM northern hemisphere summer. Because this ice-covered region is where we have a huge wetland area under current conditions, we expect significantly smaller CH_4 emission for the ice age.

The predicted global CH_4 emission amount is 59.27 Tg CH_4 per year with a large fraction from the tropical emission band. The tropics between 30°S and 30°N contribute 51.92 Tg CH_4/yr, which is almost 90% of the total emission. This fraction is much larger that the current-day one. Also, the latitudinal profile of the paleo CH_4 emissions is quite different from that of the current CH_4 emissions (Figure 6-8). The

northern and the southern hemispheres contribute almost equally to the global total emission amount. The profile is quite symmetric about the equator with only a small portion (about 7 Tg CH_4/yr which is a little more than 10% of the total) from the northern extratropical regions (30°N—90°N).

There is almost no seasonal cycle for the ice age CH_4 emissions (top panel of Figure 6-10). This is not surprising, because the seasonal cycle in current times stems from the wetlands in northern high latitudes and this region, being largely ice-covered during the LGM, is only a very small source for LGM CH_4 (Figure 6-8).

6.3.2 CH_4 Emission Results of Model Version 2

One of the potential effects of the appearance of large scale ice sheets at high latitudes is the possible formation of new wetlands in the ice sheet boundary areas caused by the melting of these ice sheets in the summer season. To investigate the impact of the appearance of new wetlands on CH_4 emissions, the wetland area between 30°N and 70°N has been tripled in Version 2 numerical experiments. The results are shown in Figure 6-9 and in the bottom panels of Figure 6-7 and Figure 6-10. The spatial pattern of CH_4 emissions is similar for Version 2 and Version 1. For example, there are two distinct emission bands, with one in the tropics and the other in the northern high latitude regions. However, the magnitude of the emissions is comparable in Version 2 for these two bands, in contrast with Version 1 where tropical emissions are much larger than the high latitude emissions.

The predicted Version 2 global CH_4 emission amount is 71.83 Tg CH_4 per year, with the tropical emissions between 30°S and 30°N being the same as in Version 1. The emissions from extra-tropical regions (poleward of 30°) are as expected almost tripled (there are some emissions from 30°S and 90°S, see Figure 6-9). The emission from the northern hemisphere is now about 55% larger than that from the southern hemisphere.

Unlike in Version 1, there are significant seasonal cycles for CH_4 emissions in Version 2. The bottom panel of Figure 6-10 plots the seasonal cycle for the global CH_4 emission amount. CH_4 emission peaks in August with the magnitude about 60%

larger than that in the winter season. Obviously, these seasonal cycles are caused by larger emissions from the hypothesized ice-sheet fed wetlands in northern high latitudes.

6.3.3 Discussion

Even though both versions of the paleo CH_4 emission model have a significant number of assumptions underlying their estimates, the results do give us some insights into what CH_4 emissions would look like in an extremely cool climate like the last ice age. Testing the emissions, however, is extremely difficult, because there is a lack of understanding of paleo OH field needed to determine the CH_4 atmospheric lifetime and there are also other natural sources beyond wetlands involved in the atmospheric CH_4 budget (e.g. termites, wild ruminants). An analysis has been done to determine what the range of total paleo CH_4 emissions would have been and how well the estimate presented here would fit into that range.

We use the same one-box model used for N_2O discussion. Unlike N_2O, CH_4 is largely destroyed in the troposphere. Thus equation (6.4) is directly used in calculating paleo CH_4 mixing ratio or emission, with M_{air} replaced by the mass of the tropospheric air only. Paleo CH_4 concentrations are very well documented. Ice core data show that the LGM CH_4 concentration is around 350 ppb [*Chappellaz et al., 1990*]. Assuming this concentration and a range of 6—12 years for the paleo CH_4 lifetime, we come up with a range of 76.5—153.0 Tg CH_4 per year for the total CH_4 emission for the LGM. Adding other natural sources (totally 45 Tg CH_4 per year) estimated by Chappellaz and Fung [*1993*] (Table 6.4), our estimate of 60 Tg CH_4/year (total of 105 Tg CH_4/year) is in the middle of the estimated range from the ice core data.

Alternatively, using the estimated total emission of 105 Tg CH_4/year for the LGM and a range of 6—12 years for ice age CH_4 lifetime, we estimate that the range for LGM CH_4 concentrations is 276—549 ppb (Table 6.5). These values are plotted in Figure 6-11 along with ice core data. As we can see, the documented ice age CH_4 concentration is within the estimated range.

Sources	Annual Emission
	(Tg CH_4/year)
Wetlands	75
Wild Animals	20
Termites	20
Wildfires	5
Ocean/freshwater	10
Soil Sink	10

Table 6.4: CH_4 Natural Budget for the LGM [*Chappellaz and Fung, 1993*]

Lifetime (years)	6.0	7.65	12.0
Mixing ratio (ppb)	276.0	350.0	549.0

Table 6.5: CH_4 lifetime and mixing ratio corresponding to Ice Age methane emissions

Chappellaz and Fung [*1993*] estimated ice age wetland CH_4 emission at 75 Tg CH_4/year, which is close to our result for Version 2. If their estimate is correct and we assume that no more new wetlands appeared in other regions for the ice age, then wetland areas between 30°N and 70°N in the ice age would need to be three times as large as in current climate conditions.

Our estimate of the LGM CH_4 mixing ratios fall within the reasonable range suggested from ice core data, but this does not necessarily say our estimate here is accurate. It does show that our model results are plausible for paleo wetland CH_4 emissions.

6.4 Conclusions

The paleo natural emission models, CLIMAP soil and vegetation data, and a GISS 3D GCM ice-age equilibrium climate run are used to estimate soil N_2O emissions and wetland CH_4 emissions for the Last Glacial Maximum. Model results indicate that N_2O and CH_4 emissions for the LGM are about half of those for the current climate conditions (53% for N_2O and 47% for CH_4). This again, as in the $2\times CO_2$ case,

indicates that there are important feedbacks in the natural system between climate change and changes in natural N_2O and CH_4 emissions.

The spatial pattern of ice age N_2O emissions is quite similar to the one for the current emissions with high emissions in both cases in the tropics. Seasonal cycles for ice age N_2O emissions are smaller than today's but still significant. Polynomial-extrapolation of ice core data suggests a N_2O mixing ratio of 185.9 ppb for the LGM, which falls in the calculated range using our model estimated N_2O emissions and different assumptions about its lifetime (110—166 years).

Ice age CH_4 emission also shows a similar pattern to today's, with two emission bands in both cases. There is however no significant seasonal cycle in the global LGM emissions. Numerical experiments indicate that CH_4 emission could be significantly underestimated using the assumption that only current wetlands not covered by ice age glaciers existed in the ice age. Our estimate for the LGM wetland emissions when added to other expected LGM CH_4 sources falls into the range calculated using the well documented ice age CH_4 mixing ratio of 350 ppb. However, emission between 30°N and 70°N has to be tripled to be consistent with the Chappellaz and Fung [*1993*] estimate for the LGM emissions.

For both N_2O and CH_4, there is of course no emission for land covered by the ice sheet in summer. This is one of the reasons why there is a smaller or even no seasonal cycle in N_2O and CH_4 emissions predicted by their paleo emission models. Both N_2O and CH_4 predicted emissions are quite symmetric about the equator in the ice age conditions.

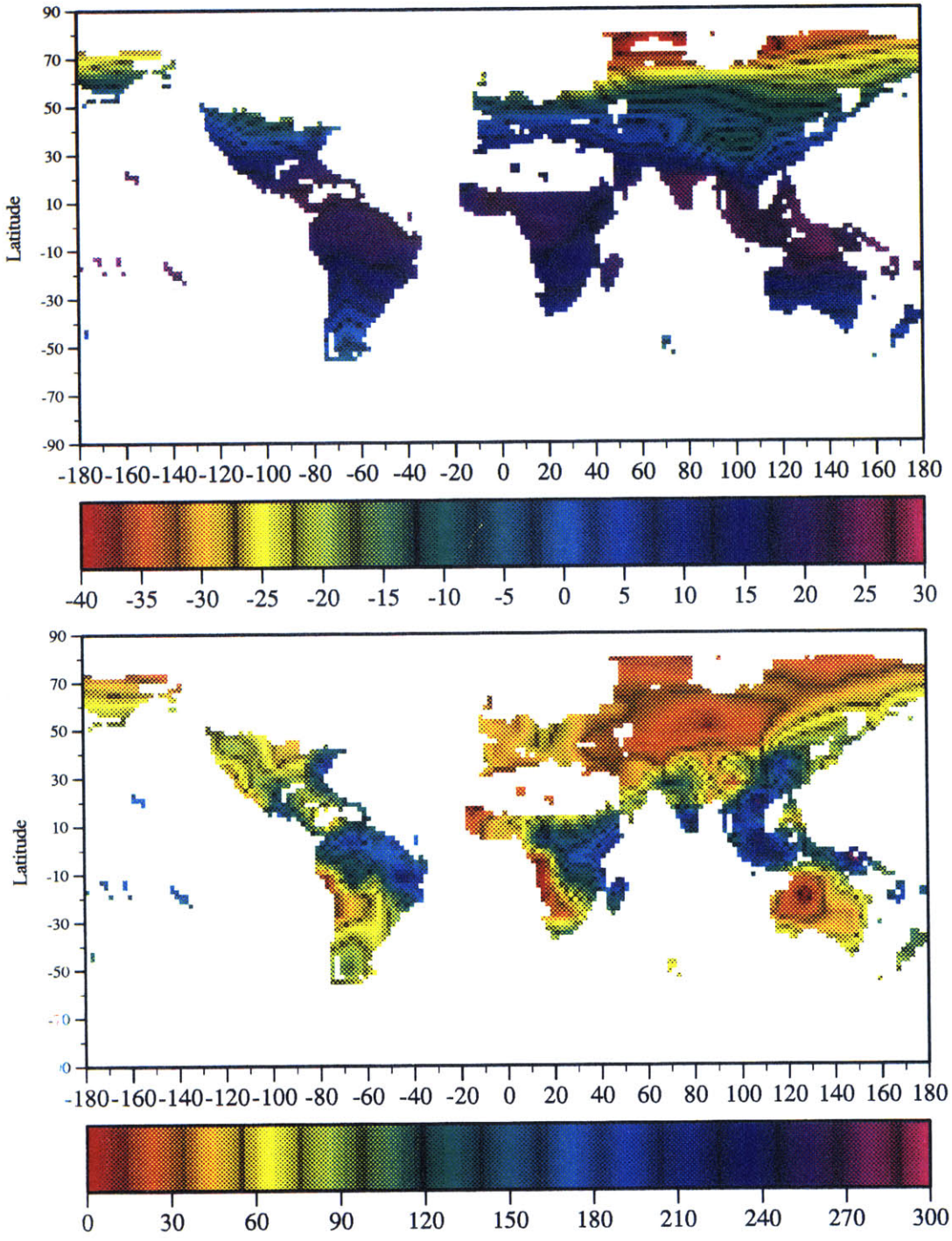

Figure 6-1: GISS 3D model predicted annual mean surface temperature (upper panel, in °C) and annual mean monthly precipitation (lower panel, in mm/month) for the LGM at 2°×2° resolution.

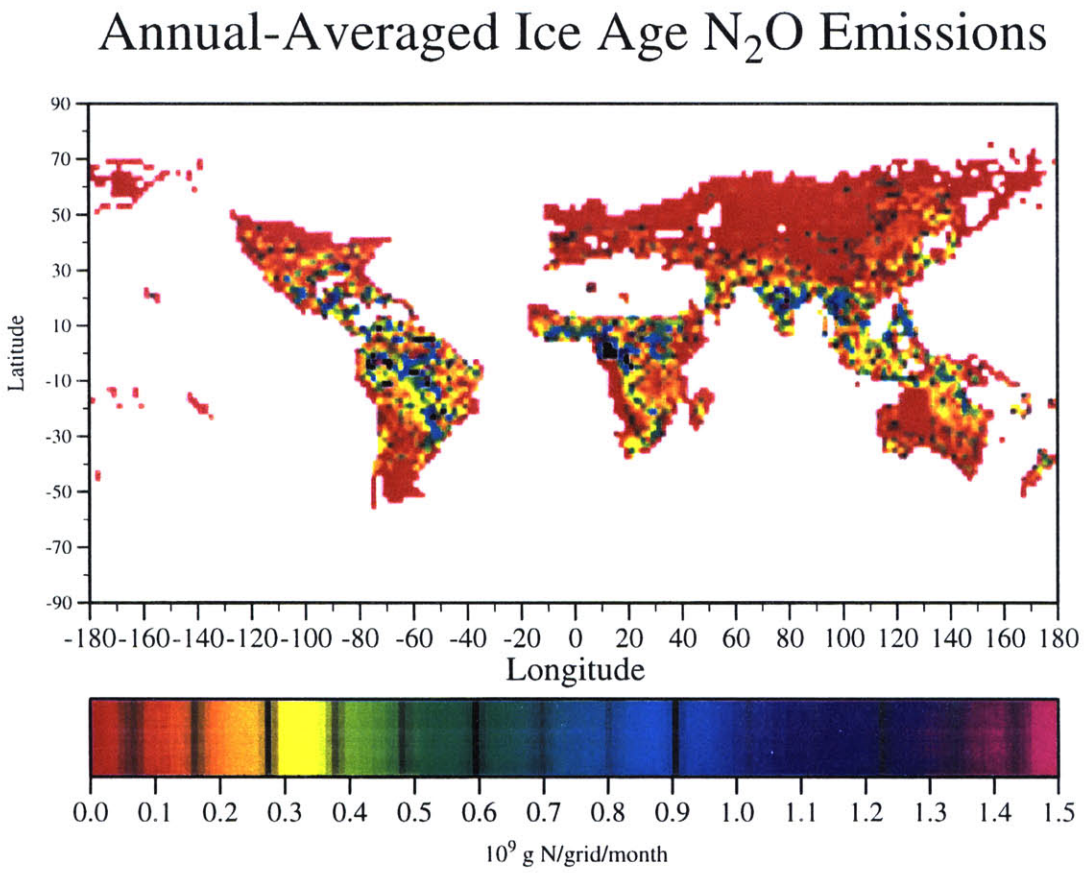

Figure 6-2: Global distribution of paleo annual-average monthly N_2O emissions at $2° \times 2°$ resolution.

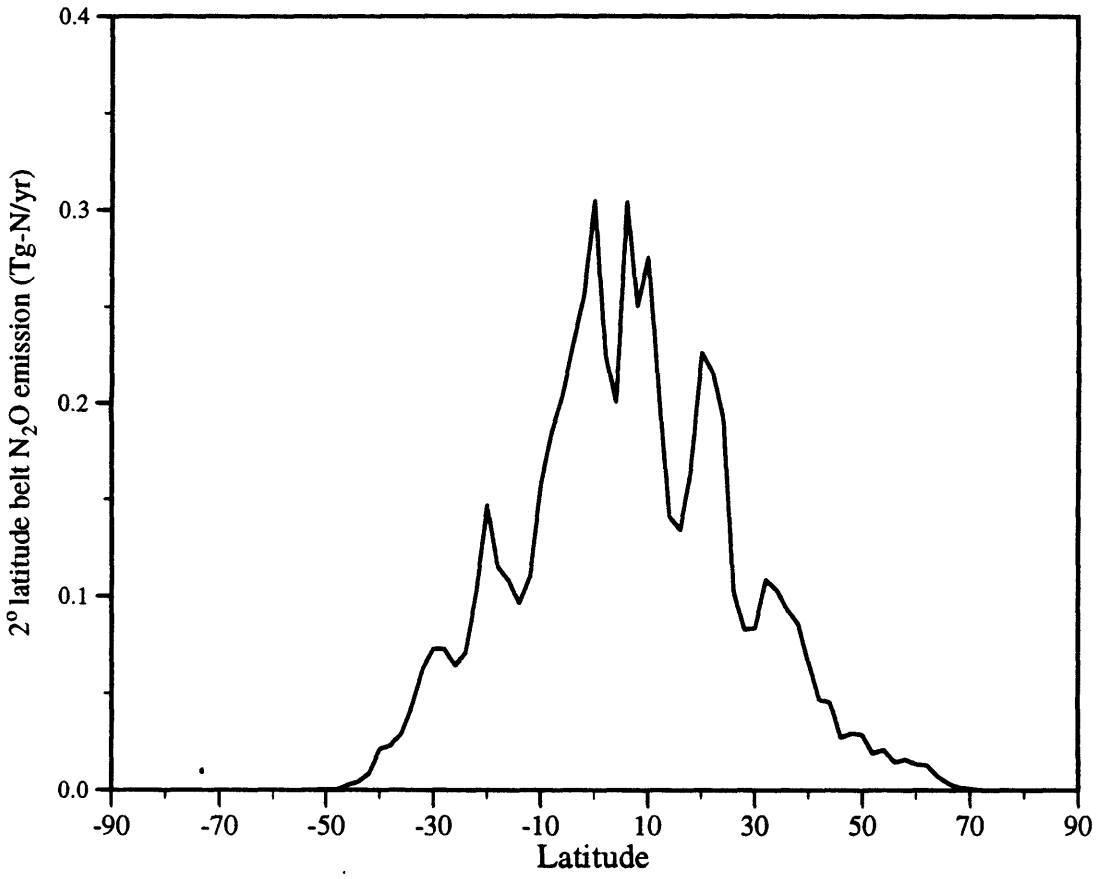

Global total emission calculated is 6.042 Tg-N yr^{-1}
The tropics between 30°S and 30°N contribute 4.618 Tg-N yr^{-1}
The emission from extra-tropical(poleward of 30°) is 1.424 Tg-N yr^{-1}
The Northern Hemisphere emission is 3.549 Tg-N yr^{-1} while
the Southern Hemisphere emission is 2.493 Tg-N yr^{-1}

Figure 6-3: Latitudinal distribution of paleo annual N_2O emissions at 2° resolution (Latitude in degrees, with positive values denoting the Northern Hemisphere).

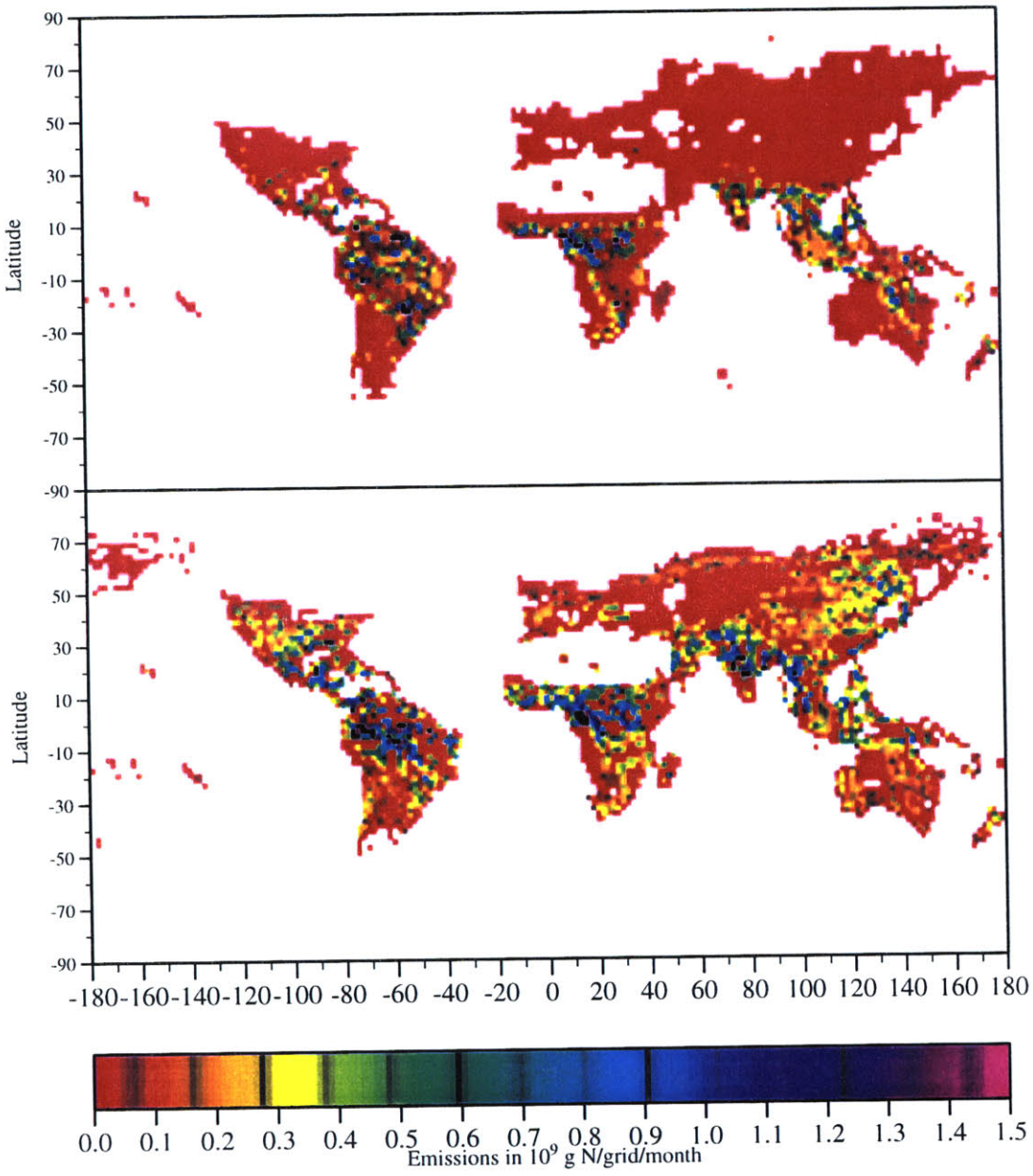

Figure 6-4: Monthly paleo N_2O emissions for January (upper panel) and July (lower panel) at $2° \times 2°$ resolution.

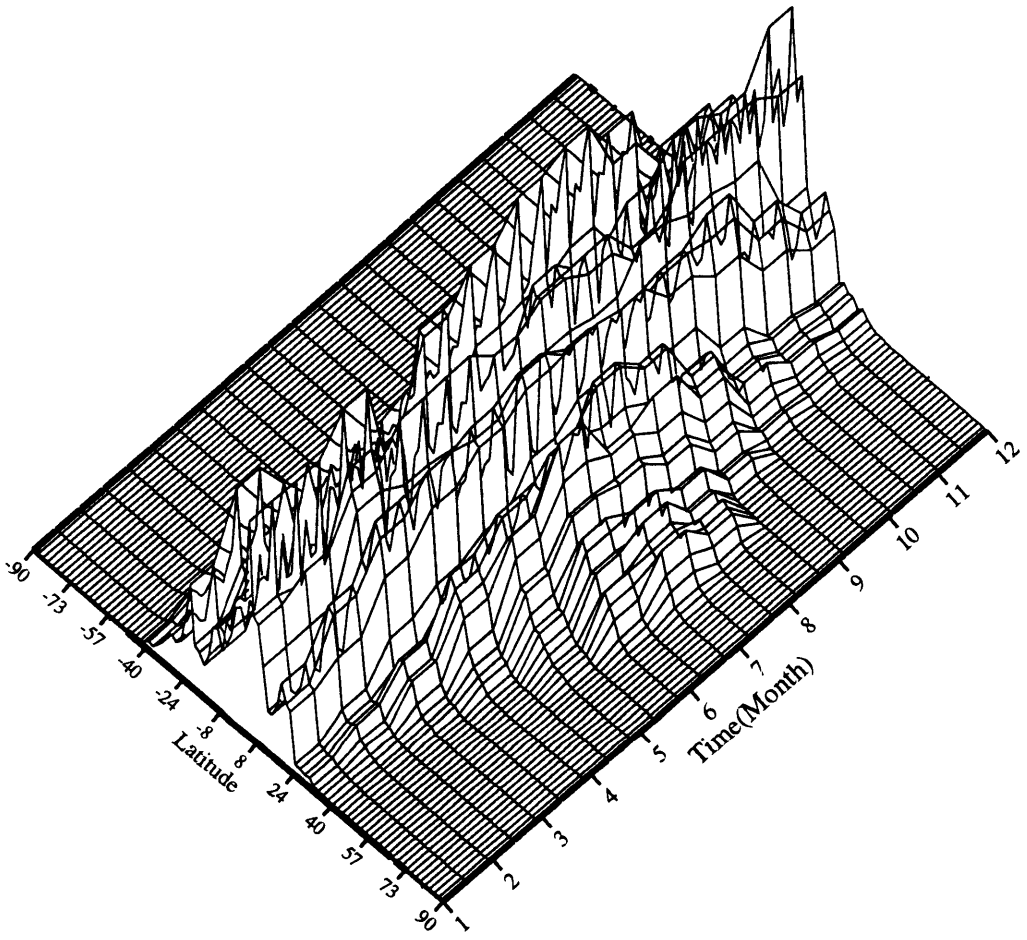

Figure 6-5: Latitudinal-Seasonal variation of paleo N_2O emissions (Latitude in degrees, with positive values denoting the Northern Hemisphere).

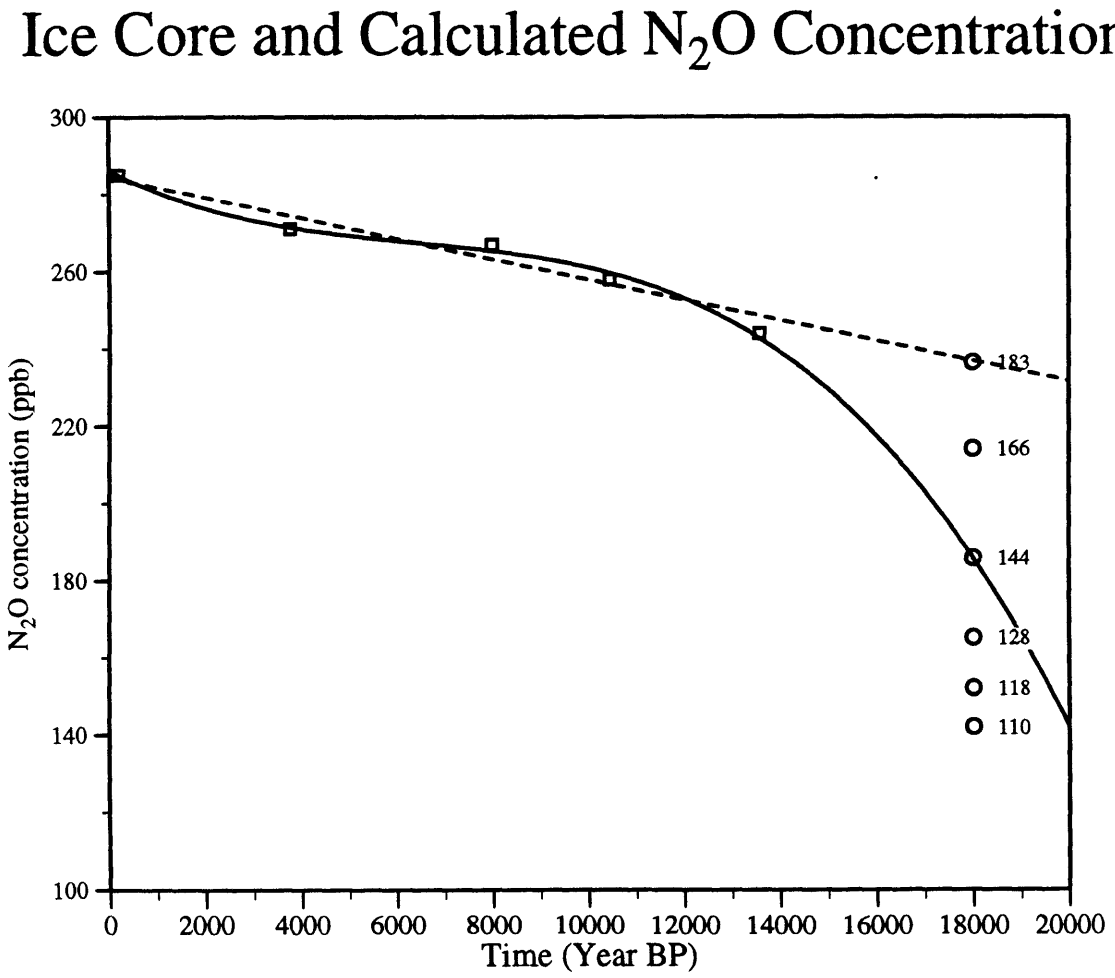

Figure 6-6: Polynomial (solid) and linear (dashed) curves fitted using measured N_2O mixing ratios in ice cores (squares, no data available before 14,000 BP) and calculated N_2O mixing ratios for the LGM (circles) using indicated assumed lifetime (in years) and estimated N_2O emission from paleo model.

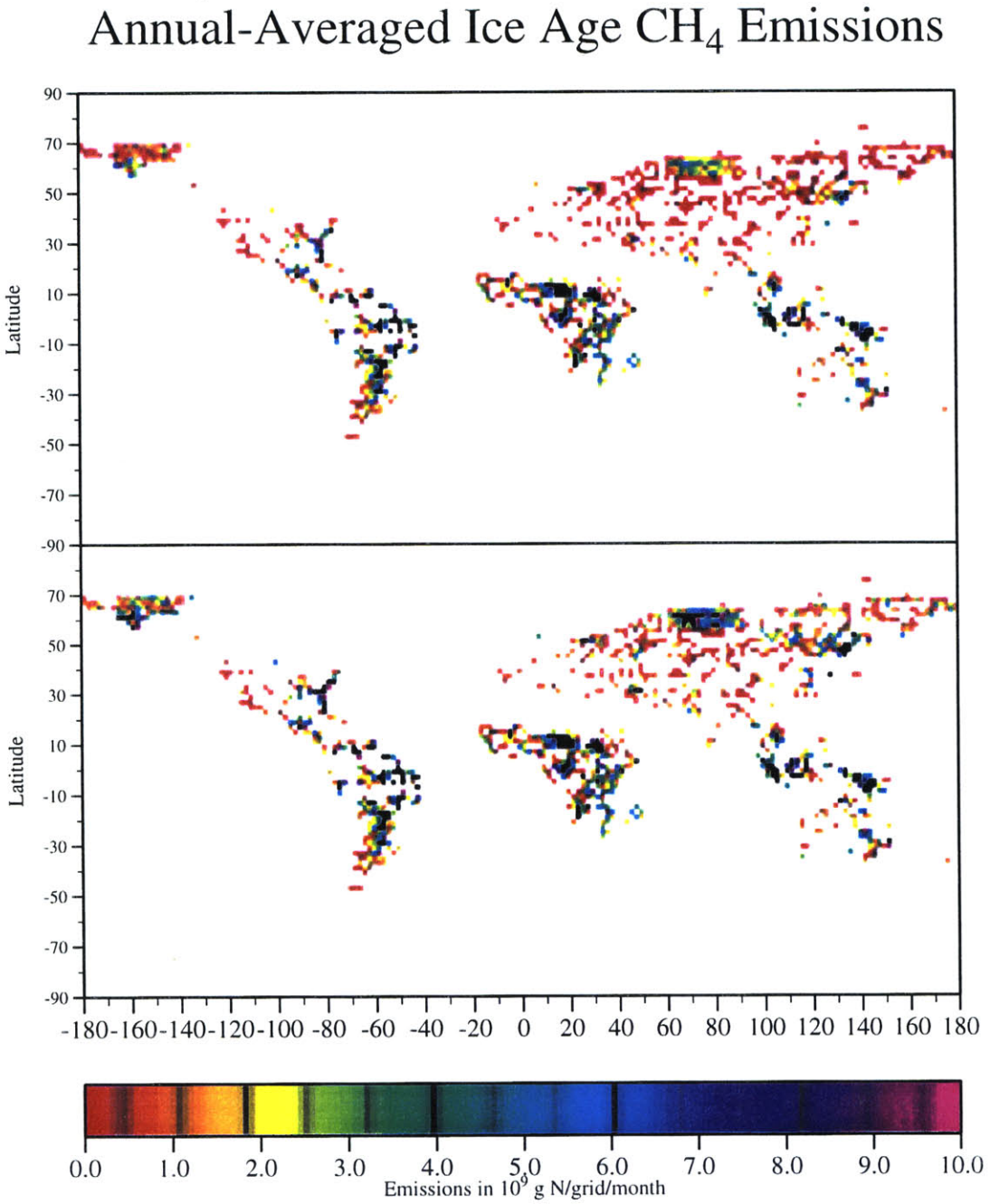

Figure 6-7: Global distribution of paleo annual-average monthly CH_4 emissions at $2^\circ \times 2^\circ$ resolution (top panel for Version 1 and bottom panel for Version 2).

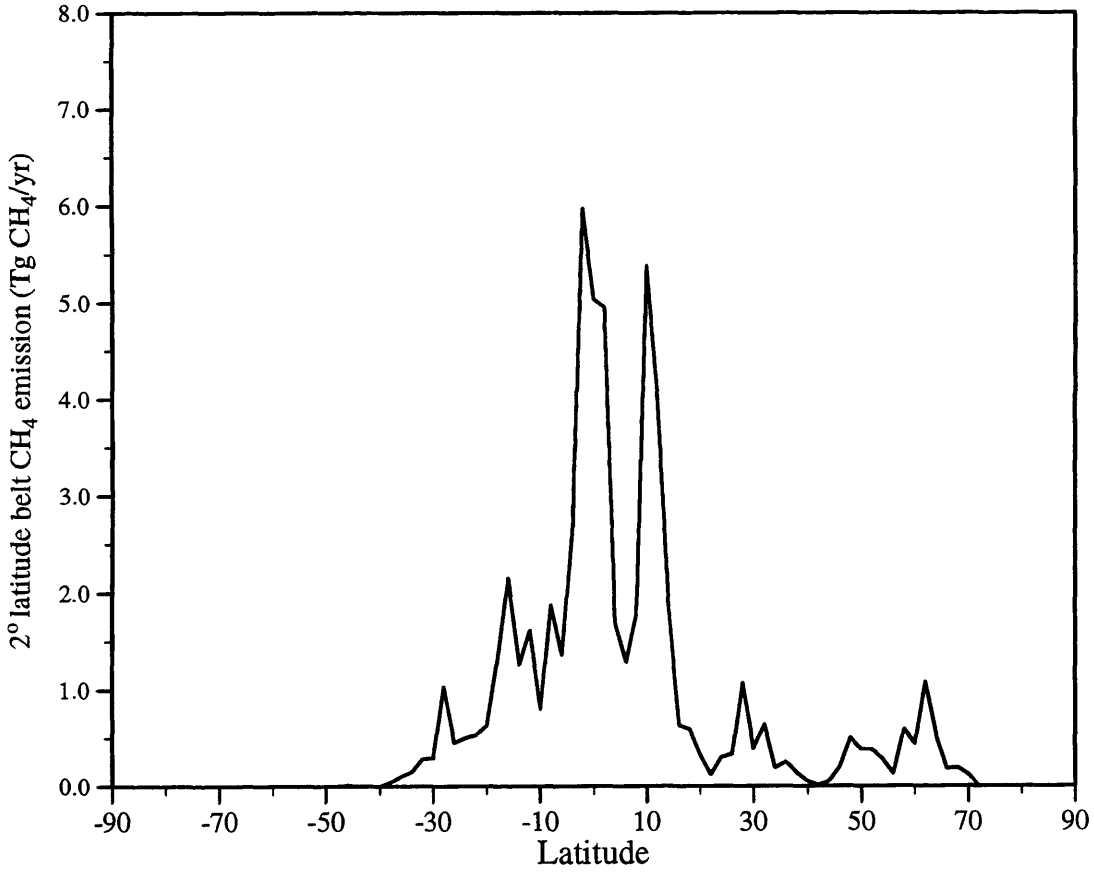

The global emission calculated is 59.120 Tg CH_4 yr^{-1}
The tropics between 30°S and 30°N contribute 51.920 Tg CH_4 yr^{-1}
The emission from extra-tropical(poleward of 30°) is 7.200 Tg CH_4 yr^{-1}
The Northern Hemisphere emission is 31.090 Tg CH_4 yr^{-1} while
the Southern Hemisphere emission is 28.030 Tg CH_4 yr^{-1}

Figure 6-8: Latitudinal distribution of paleo annual CH_4 emissions at 2° resolution (Version 1) (Latitude in degrees, with positive values denoting the Northern Hemisphere).

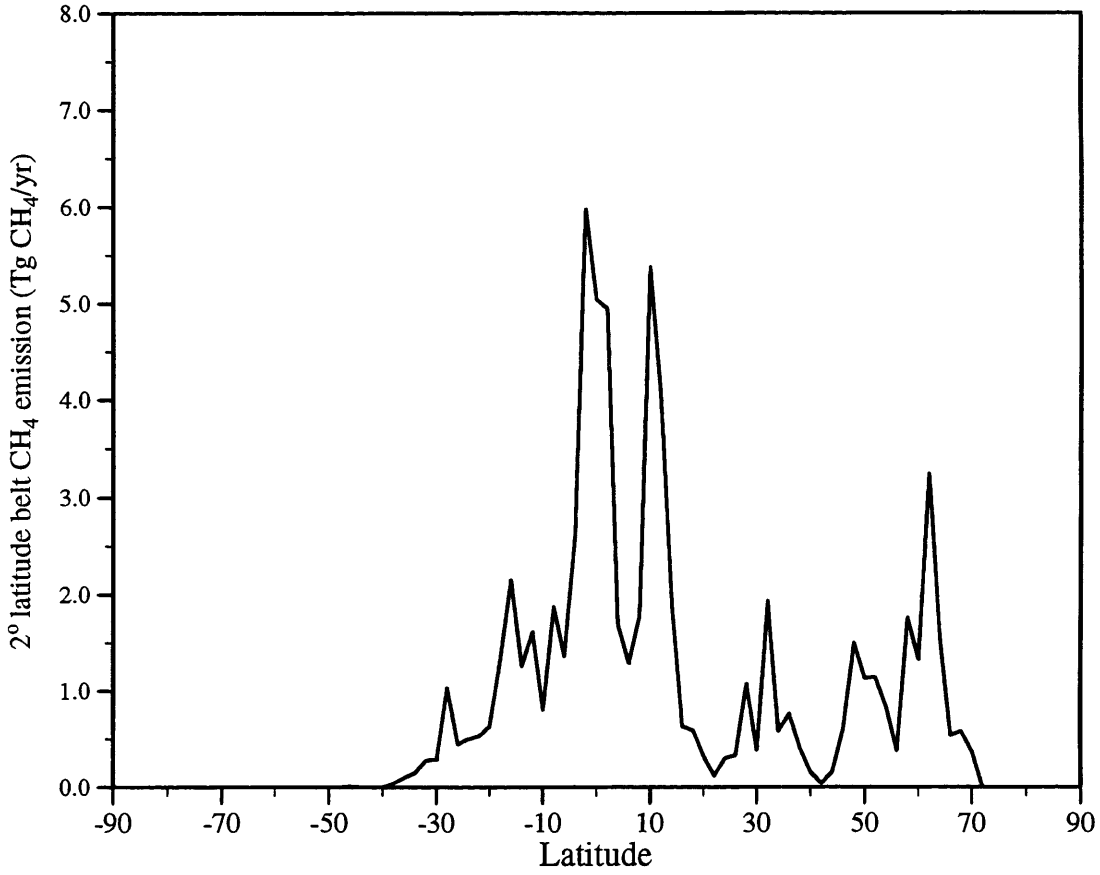

The global emission calculated is 71.829 Tg CH_4 yr^{-1}
The tropics between 30°S and 30°N contribute 51.920 Tg CH_4 yr^{-1}
The emission from extra-tropical(poleward of 30°) is 19.909 Tg CH_4 yr^{-1}
The Northern Hemisphere emission is 43.799 Tg CH_4 yr^{-1} while
the Southern Hemisphere emission is 28.030 Tg CH_4 yr^{-1}

Figure 6-9: Latitudinal distribution of paleo annual CH_4 emissions at 2° resolution (Version 2) (Latitude in degrees, with positive values denoting the Northern Hemisphere).

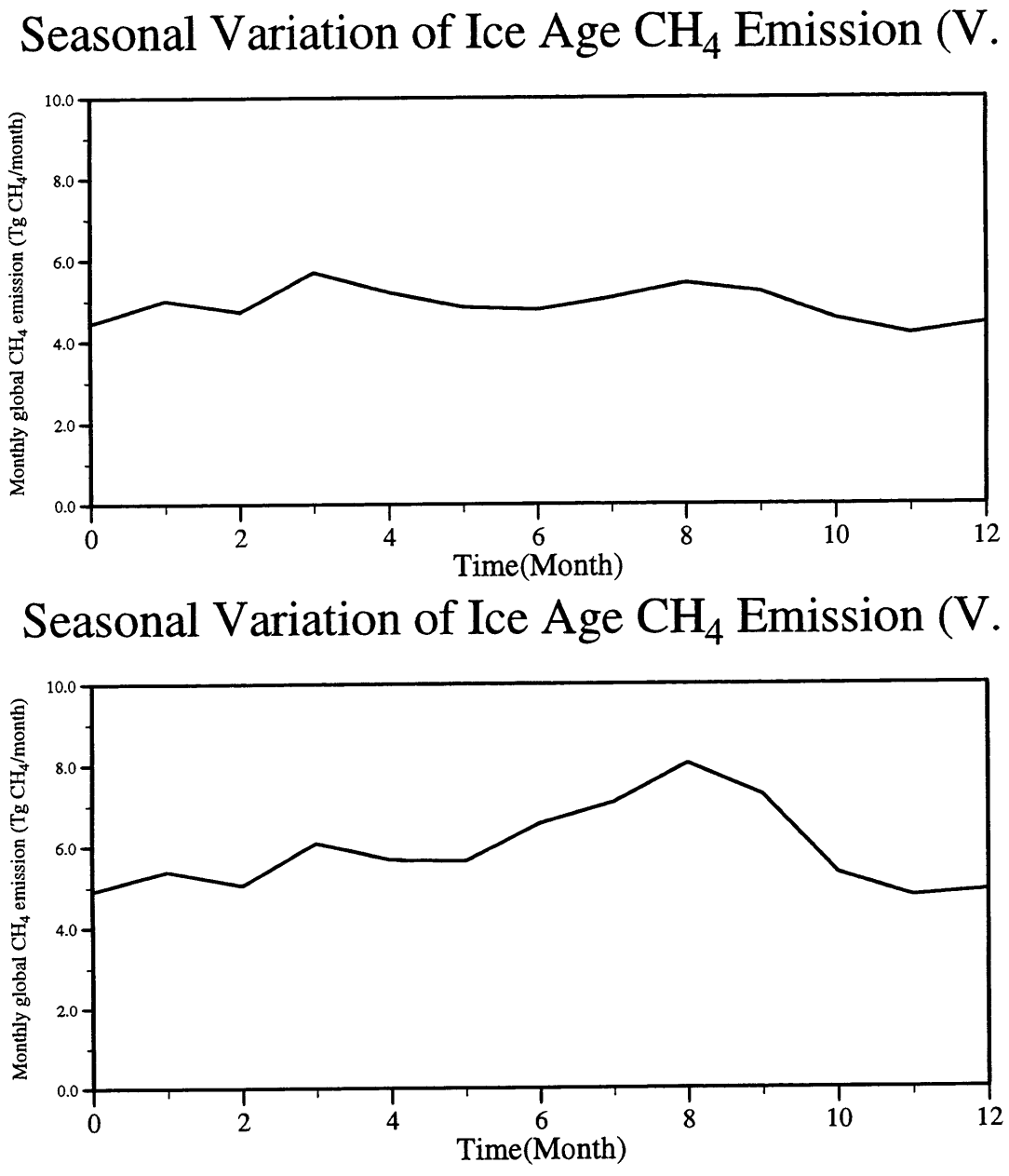

Figure 6-10: Seasonal variation of total paleo CH_4 emissions (top panel for Version 1 and bottom panel for Version 2).

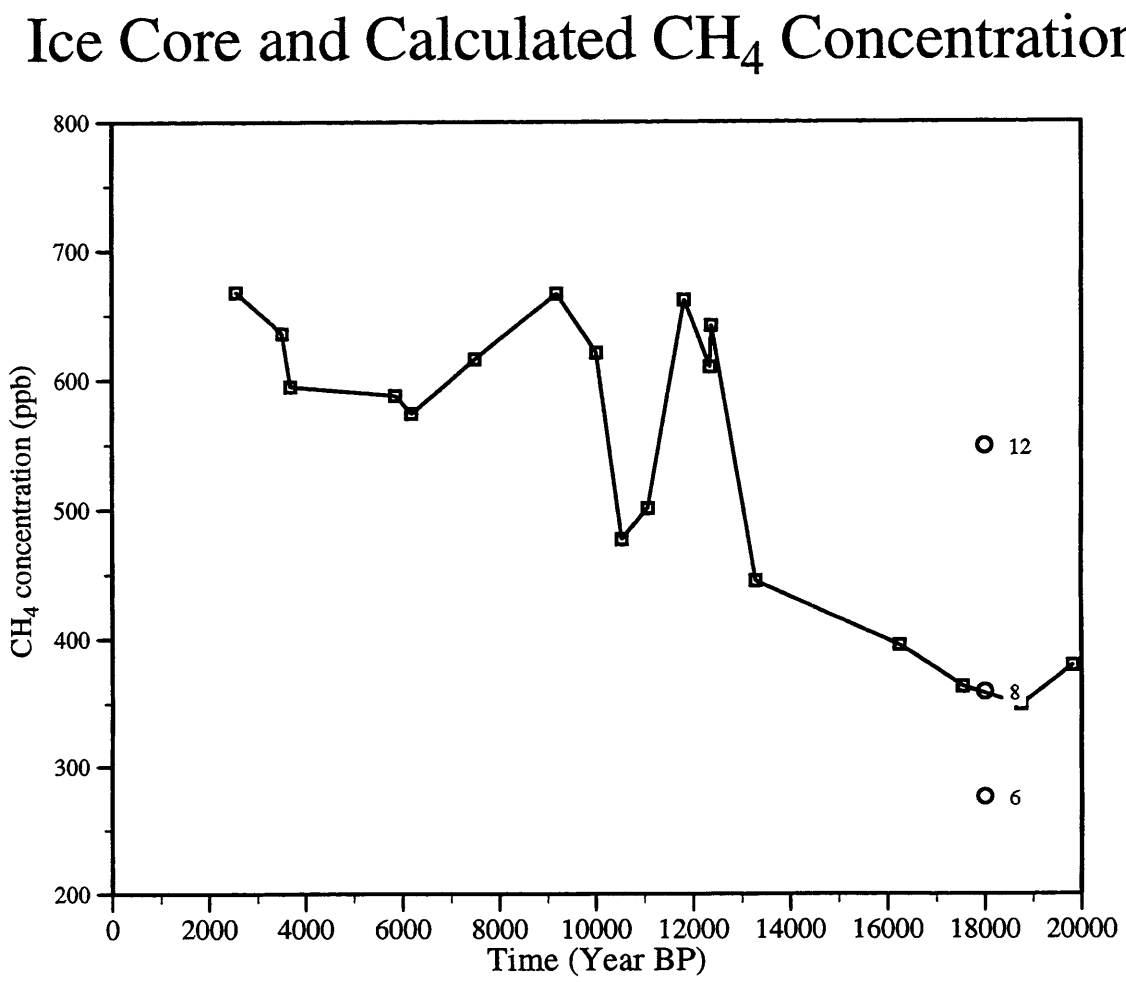

Figure 6-11: Measured CH_4 mixing ratios in ice cores (squares and solid line) and calculated CH_4 mixing ratios for the LGM (denoted by circles) using indicated assumed lifetime (in years) and estimated CH_4 emission from paleo model.

Chapter 7

Coupling of Emission Models with Climate and Chemistry Models

7.1 Introduction

The global emission models for N_2O and CH_4 use climate as one of their input parameters and can in principle be coupled interactively with a climate and chemistry model. This has been done as the final stage of this thesis using the global system model of the MIT Joint Program on Global Change Science and Policy [*Prinn et al., 1996*]. Specifically, the N_2O and CH_4 emission models have been coupled on a monthly basis with the 2D-LO coupled-climate-chemistry model contained in the global system model. First, "off-line" coupling was achieved by using transient climate data saved from the climate-chemistry model. Full-coupling was then realized with the month-by-month emissions serving as input to the chemistry model after the computational efficiency of the emission models was improved. The resultant fully integrated system of models not only can predict changes in trace gas emissions but also can assess emission-radiative forcing feedbacks in the climate system.

The coupled-climate-chemistry model is a 2-dimensional model with only one dimension for the earth surface (latitude). A "mapping" scheme similar to the one used with this 2D-LO model for the "doubling CO_2" case has been used to obtain a 2-dimensional surface climate for the land from the 1-dimensional climate outputs.

Adoption of this mapping procedure, together with the computational efficiency of the 2D-LO climate-chemistry model compared to 3D coupled ocean-atmosphere GCMs, made this exercise possible.

For the emission-climate feedback in the climate system, there is necessarily a time lag of one time step in the full-coupling unless we can solve climate and emission equations simultaneously, which is practically very difficult and we argue is not be necessary. Ideally, if we can choose a small time step (e.g. the climate model time step), we can minimize this "time lag" effect. However, if we have too small a time step, we would have other problems. First there would be a huge computational time problem for long-term integrations. Second, we would have an "every day raining" problem because that is mostly the case at each latitude grid point for the 2D-LO climate model. We have instead chosen a time step of one month for coupling both N_2O and CH_4 models with the 2D-LO coupled-climate-chemistry model. The "every day raining" problem is solved by using the rainfall statistical model discussed in Chapter 2. The problem associated with the one-month "time lag" for both emission models and still significant computational time required for the N_2O emission model had to both be addressed.

Two projection schemes have been created to solve the one-month time lag and computational time problems. For the CH_4 emission model, the computational time demand with a one-month time step is not a problem, so a simple projection scheme was designed to project the emission for the next month using the calculated emissions for previous months. A correction term is then added to constrain the projected annual emission to equal to the calculated annual emission. This proved to be a very effective way of handling the time lag problem. For the N_2O emission model, a scheme was designed to project uncalculated future emissions using extrapolated emissions followed by corrections obtained by interpolation with a demand to minimize errors in total accumulated emissions. This scheme reasonably reproduces calculated emissions and successfully solves both the time lag and the computational time problems.

A significant number of long-term simulations, corresponding to the simulations done to investigate the behavior of the global system model of the MIT Joint Program

on Global Change Science and Policy [*Prinn et al., 1996*], have been carried out using both the "off-line" coupled and the "fully-coupled" emission models. As a whole, the results demonstrate that natural N_2O and CH_4 emissions change significantly with climate and the climate-emission feedback is important, at least for the conditions in some of the simulations.

7.2 The Coupled-Climate-Chemistry Model

The coupled 2D-LO climate and chemistry model contained in the global system model developed in the MIT Joint Program on Science and Policy of Global Change [*Prinn et al., 1996; Sokolov and Stone, 1995; Wang et al., 1996*] has been used to couple with the N_2O and CH_4 emission models. The climate model resolves the land and ocean at each latitude and is capable of reproducing many characteristics of the current zonally-averaged climate. Its dynamics is parallel in most ways to that for the GISS 3D GCM [*Hansen et al., 1983*]. The atmospheric chemistry model includes 25 chemical species with 53 chemical reactions. The transport for the chemical species is driven by the climate model dynamics, and the chemistry, dynamics and radiation are all fully interactive.

7.3 Description of the Coupling

Since one of the goals of the MIT Joint Program is to evaluate uncertainties in global change prediction [*Prinn et al., 1996*], the 2D-LO coupled-climate-chemistry model is designed to conduct numerous long-term experiments covering a wide spectrum of different assumptions. A number of modifications have been made to the original emission models to couple them interactively with the 2D-LO model and to further serve this general goal.

7.3.1 Integration Structure

The global emission models for N_2O and CH_4 were initially designed to be integrated in a sequential fashion for each grid point on a yearly basis. This meant that one full year of integration for a single grid cell was done before the model moved to the next grid cell. This procedure was imposed by the calculation of evaporation using Thornthwaite's formula [*Thornthwaite, 1948*] which requires a full year of monthly data on precipitation and surface temperature in order to calculate the evaporation for a specific month. A computational structure like this is not compatible with coupling to a climate model and has other disadvantages when a significant number of long-term integrations need to be carried out. For example, the structure does not have a flexible time step and is not convenient in communicating data back and forth with a climate model.

Modifications have therefore been made to the structure of the original models to make them compatible with the 2D-LO coupled-climate-chemistry model.

First, Thornthwaite's formula was replaced with a procedure in which evaporation is calculated directly in the climate model (details will be discussed later in the Boundary Conditions Section). This lifts the one-year time step restriction we had before and allows flexibility in choosing the coupling time step. The model structure was then modified to use the chosen one-month time step. The emission models as subroutines are called on a monthly basis in the climate model. Three-way emission data communication between emission models and climate model and between emission models and chemistry model is also done on a monthly basis. Soil temperature and moisture data can be saved at any time during the climate integration in order to carry out a later run.

7.3.2 Time and Space Resolution

The hydrological and biogeochemical cycles within the original emission models have a time step of 15 minutes, a horizontal grid cell size of $2.5° \times 2.5°$ and two vertical mesh sizes of 2 cm and 3 cm for the N_2O and CH_4 emission models. It takes about 4 CPU

Test Number	1	2	Original
Temporal Resolution (hour)	1	2	0.25
Horizontal Resolution	2.5°×2.5°	2.5°×2.5°	2.5°×2.5°
Vertical Resolution (cm)	4	4	2
Total Emission (Tg N/yr)	12.025	22.795	11.325

Table 7.1: Numerical resolution sensitivity test experiments for N_2O emission model.

Test Number	1	2	Original
Temporal Resolution (hour)	1	2	0.25
Horizontal Resolution	2.5°×2.5°	2.5°×2.5°	2.5°×2.5°
Vertical Resolution (cm)	6	6	3
Total Emission (Tg CH_4/yr)	128.61	132.17	126.82

Table 7.2: Numerical resolution sensitivity test experiments for CH_4 emission model.

hours for the original N_2O emission model and about 1 CPU hour for the original CH_4 emission model to do a one-year global integration on a DEC Alpha 3000-400. The above resolutions add enormous computational burden to the 2D-LO coupled-climate-chemistry model in runs needing 100 years or more of integration. Modifications have therefore been made to make the emission models run more efficiently for long-term experiments.

Numerical stability analyses regarding the major time-consuming equations (mainly the thermal and hydraulic diffusion equations) shows that there is room for adjusting resolutions to improve computational efficiency without losing numerical stability. This is true especially for the CH_4 emission model where the Crank-Nicholson scheme used in solving these equations is unconditionally stable. This gives us some potential for improving overall computational efficiency. A number of experiments have been conducted to test sensitivity to resolution. The results are presented in Table 7.1 and Table 7.2.

The results presented demonstrate that quadrupling the original temporal resolution and doubling the vertical spatial resolution (test number 1 in the tables) reproduce the emission results very reasonably.

Regions	$\overline{Z}_w$ (cm)	$\overline{T}_{zw}$ (°C)
60°–90°	7.10796	6.45006
45°–60°	10.15860	14.51815
0°–45°	9.80447	25.36087

Table 7.3: Methane flux coefficients for the coarser resolution CH_4 emission model.

In the CH_4 emission model, the only other data set used besides climate is the wetland distribution at a resolution of 1°×1°. Because of the structural flexibility of the CH_4 emission model and its relative insensitivity to changes in horizontal resolution, a horizontal resolution of 4°×5° has been chosen to further reduce the computational time. The reason why we choose the 4°×5° resolution is that a data set for current climate including surface temperature, precipitation and evaporation [*Leemans and Cramer, 1990*] is available which has that coarse resolution. Current climate is used in the "mapping scheme" to obtain 2-dimensional surface climate for land from 1-dimensional model surface outputs. The "mapping scheme" will be discussed in a later section.

Experiments have been carried out to determine the consistency of the coarser resolution version of CH_4 model with the original version. This also involves resetting the coefficients for the CH_4 flux model. The new coefficients are presented in Table 7.3.

A comparison between the results of the coarser resolution CH_4 emission model and the original model is shown in Table 7.4. The coarser version reasonably reproduces the emissions of the original model with the difference being less than 8% for the global total.

The resolutions for Test 1 in Table 7.1 (temporal resolution of 1 hour, horizontal resolution of 2.5°×2.5° and vertical resolution of 4 cm) have been used in the coupled climate-N_2O emission model; and the resolutions for the coarser version of the CH_4 model in Table 7.4 (temporal resolution of 1 hour, horizontal resolution of 4°×5° and vertical resolution of 6 cm) have been used in the coupled climate-CH_4 emission model. The emission results of the coupled climate-N_2O and climate CH_4 emission models have been multiplied by a correction factor ($\frac{11.325}{12.025}$, i.e. 94% for N_2O and $\frac{126.82}{135.84}$,

	Coarser Version	Original Version
Temporal Resolution (hour)	1	0.25
Horizontal Resolution	4°×5°	2.5°×2.5°
Vertical Resolution (cm)	6	3
Emission (Tg CH_4)	135.84	126.82

Table 7.4: CH_4 emission model comparison between the coarser version and the original version.

i.e. 93% for CH_4) to take into account the small numerical errors introduced by the change in resolution.

7.3.3 Coupling Interface: Climate Variables

The emission models use surface climate (basically surface temperature and precipitation, and also evaporation in the coupled climate-emissions models) as boundary conditions for their soil hydrological component models. Ideally, these hydrological equations should be solved simultaneously with the climate model. However, there are two reasons why this is not practical. First, adding a detailed hydrological model in the climate model would create a computational time problem. Second, the climate model has a very coarse resolution and does not have or need the detailed information about soil properties which are very important for biogeochemical models.

Transient data from the climate model are used as upper boundary conditions for the emission models through monthly data (mean for surface temperature, total for precipitation and evaporation) being output from the climate model and input to the emission models. A statistical rainfall model in the emission models is invoked to disaggregate the monthly precipitation into daily rainfall events. The hydrological models within the emission models use the daily upper boundary conditions to determine soil temperature and moisture profiles using a shorter time step (1 hour in the coupled climate-emissions models).

As mentioned before, in the original emission models the evaporation was calculated using Thornthwaite's formula. In the coupled climate-emission models, the

evaporation calculated directly in the climate model is used to keep the coupling consistent. The evaporation calculation in the climate is done by a surface flux scheme based on the Monin-Obukhov similarity theory [*Sokolov and Stoñe, 1995*]:

$$E = \beta \rho C_n D_m D_e |\vec{V}_s| (q_g - q_s) \tag{7.1}$$

where β is the ratio of available water to field capacity for the top soil layer, ρ is air density, C_n is the transfer coefficient for neutral stratification, D_m and D_e are functions of bulk Richardson number, $\vec{V}_s$ is surface wind, and q is specific humidity. Subscripts g and s refer to ground and top of the first climate model surface atmospheric layer.

Lower boundary conditions for the hydrological models are imposed by specifying heat flux and water drainage. The water drainage is kept the same as in the original models. The heat flux, however, is modified to be consistent with the climate model. The heat flux in the original models is calculated using temperature gradient between the bottom layer of the hydrological model and a fixed deep layer (1.5 m). The temperature for the fixed deep layer is assumed to be constant throughout a whole year and is equal to the annual mean surface temperature. This is not consistent with the climate model's two-layer hydrological cycle model.

In the coupled emission models, the temperature for the second layer of the climate model's hydrological model is used to replace the yearly constant temperature for the fixed deep layer. The second layer has a depth of 2 meters. The same down-gradient diffusion approach is applied to calculate the bottom heat flux.

A number of numerical experiments have been performed to test how sensitive the emission results are to the changes in the boundary conditions. The results are presented in Table 7.5.

Replacement of Thornthwaite's Formula with Equation 7.1 seems to have a relatively large impact. The global total emissions differ by a factor of 5% for both N_2O and CH_4 cases. The change in lower boundary heat flux only has a small effect on global emissions. The difference is only about 1.5% for N_2O and 0.06% for CH_4.

Change in Boundary Conditions	Emissions (Tg N/year)	Difference Compared with Coupled Model
Using Thornthwaite's Formula	12.600	4.8%
$T_{z=2m} = 0°C$ (Fixed Deep Layer)	11.843	-1.5%

Table 7.5: Sensitivity of the N_2O emission model to changes in boundary conditions.

Change in Boundary Conditions	Emissions (Tg CH_4)	Difference Compared with Coupled Model
Using Thornthwaite's Formula	142.53	4.9%
$T_{z=2m} = 0°C$ (Fixed Deep Layer)	135.92	0.06%

Table 7.6: Sensitivity experiments of CH_4 emission model in response to changes in boundary conditions.

Overall, the differences in current N_2O and CH_4 emissions introduced by the changes in boundary conditions are reasonably small. Furthermore, self-consistency is maintained for the fully-coupled models by using the already available variables from the climate model.

7.3.4 Coupling Interface: Soil Organic Carbon

Offline soil organic carbon outputs from TEM are used in the coupled emission models. A transient version of the terrestrial ecosystem model, in which fluxes are no longer constrained to be in balance (the $2\times CO_2$ case), is driven offline by the coupled 2D-LO climate-chemistry model outputs and predicts transient soil organic carbon storage. Unlike the equilibrium case, the soil organic carbon is predicted to increase in various transient simulations [*Prinn et al., 1996*].

7.3.5 "Mapping" Scheme

A "mapping scheme" based on observed current climate is used to obtain 2-dimensional climate for the earth's surface from the modeled 1-dimensional surface outputs. The basic underlying assumption is that zonal variations of climate variables are the same for different climate conditions. Given a 2-dimensional climate model, this is the best we can do.

Taking into account of the nature of the physical variables, we use different definitions for defining zonal variations. For extensive variable like temperature, the zonal deviation (temperature difference) is used to define zonal variations. For intensive variables like precipitation and evaporation, the ratio between zonal deviation and zonal mean is used to define zonal variations.

Based on these assumptions and definitions the temperature difference and precipitation/evaporation ratios are calculated using observed current climate data and the following three equations:

$$DT_{obs}(i,j) = T_{obs}(i,j) - \overline{T}_j \tag{7.2}$$

$$RP_{obs}(i,j) = \frac{P_{obs}(i,j)}{\overline{P}_j} \tag{7.3}$$

$$RE_{obs}(i,j) = \frac{E_{obs}(i,j)}{\overline{E}_j} \tag{7.4}$$

where $\overline{T}_j$, $\overline{P}_j$, and $\overline{E}_j$ are zonal means of observed temperature, precipitation and evaporation, the indices i, j refer to longitude and latitude, and subscript *obs* refers to observational data.

Once these zonal variations are calculated from observations, they can be applied to different climate conditions. Modeled 1D surface climate can then be superimposed (added or multiplied) to the above variations (difference and ratios) to get the global surface climate (2D surface), which is finally used in the emission models. The superimposition is described in following three equations:

$$T(i,j) = DT_{obs}(i,j) + T_j \tag{7.5}$$

$$P(i,j) = RP_{obs}(i,j) \times P_j \tag{7.6}$$

$$E(i,j) = RE_{obs}(i,j) \times E_j \tag{7.7}$$

7.3.6 Projection Scheme

To address the time lag and computational time problems, a numerical scheme was designed to project future emssions using previous calculated emissions. Generally, the following extrapolation function should solve these two problems:

$$E_p^t = \sum_{j=0}^{j=N} a_j P_j(t) + \sum_{k=0}^{j=M} (s_k \sin(\frac{2\pi t}{\tau_k}) + c_k \cos(\frac{2\pi t}{\tau_k})) \tag{7.8}$$

where P_j is the Legendre polynomial with order j.

The extrapolation function E_p^t is obtained by an optimal fit to some or all of the calculated emissions prior to time t. The first set of terms in the function resolve the long-term variations in emissions and the second set of terms resolve diurnal, seasonal or inter-annual cycles.

To ensure that the errors created by this extrapolation function do not accumulate and create errors in the chemistry model, a constraint is imposed resulting in a correction term. Recognizing that the lifetime for both N_2O and CH_4 is very long ($\sim$110 years for N_2O and $\sim$10 years for CH_4), we design the correction term in such a way that total accumulated projected emissions equal total accumulated calculated emissions. This condition is expressed by the following equation:

$$\int_{t_i}^{t_f} (E_p^t - E_c^t) dt = 0 \tag{7.9}$$

where E_c^t is the calculated emission and $t_f - t_i$ is the total integration time.

Since we have selected the time step of one month for coupling the climate and emission models, the data available for defining the function E_p^t are monthly emissions. Given these available monthly emissions, a simplified version of (7.8) and (7.9) is created as follows by using emissions calculated for two adjacent months:

$$
\begin{aligned}
E_p(y,m) &= E_c(y-1,m) && \text{Baseline Term} \\
&\quad + E_c(y,m-1) - E_c(y-1,m-1) && \text{Interannual Term} \\
&\quad + \frac{1}{12}\sum_{n=1}^{12}[E_c(y-1,n) - E_p(y-1,n)] && \text{Correction Term} \qquad (7.10)
\end{aligned}
$$

where indices y and m or n denote year and month, subscripts p and c correspond to projected and calculated emissions.

The baseline term and interannual term can be rearranged to become a baseline term of $E_c(y, m-1)$ and a seasonal term of $E_c(y-1,m) - E_c(y-1,m-1)$. What this scheme does is use calculated emissions for the previous month or the same month of the previous year as a baseline estimate and then adds the seasonal or interannual variations to obtain the emission for next month which is needed in the chemistry model. The correction term is just the difference between the calculated and the projected mean monthly emissions for the previous year.

This scheme works very well for both N_2O and CH_4 emission models. This can be seen in the results presented in Figure 7.1 and Figure 7.2 where the projected emissions (solid line) are very close to the calculated emissions (circles). Note that the "Reference Run" in Figure 7.1 and Figure 7.2 is an offline-coupled emission-climate model run of 120-year integration with a "reference projection" of all other anthropogenic trace gas emissions. For both the first and last 5 years of the 120-year integration, the scheme's projections are in a good agreement with the calculated emissions. There is no error propagating with time. This gives us confidence in using this scheme in the fully-coupled-emission-chemistry-climate model.

The only problem when using this scheme is that the N_2O emission model still takes far two much of the total running time of the coupled climate-chemistry-emissions model. Another scheme is designed to integrate the N_2O emission model only one in every five years. This scheme produces reasonable results but has not been used in the feedback analysis. The feedback analysis will be discussed in the "Results" section.

7.4 Results

Offline coupling experiments are first conducted to investigate how natural emissions of N_2O and CH_4 would respond to different climate change predictions corresponding to different assumptions in the coupled-climate-chemistry model. The offline coupling simply uses the transient climate outputs from the coupled-climate-chemistry model to drive the emission models. The emission-climate feedbacks can then be included approximately in another run of the climate-chemistry model by adding the offline predicted changes in natural N_2O and CH_4 emissions to the chemistry model.

All the offline experiments with the emission models were performed using the outputs of a series of sensitivity runs of the MIT global system model in which key parameters or assumptions in the component models were varied by finite amounts from their "reference" values [*Prinn et al., 1996*]. The key parameters and assumptions are summarized into three categories (emissions, forcing and sensitivity) with "H", "R", "L" denoting high, reference and low values respectively of these parameters. A particular run is labeled by these 3 parameters (e.g. HHH, LLH, etc.). The "reference" values of these parameters are consistent with the estimates reported in IPCC [*1992, 1996*]. Because of computational time restrictions, the feedback experiment (full as oppsed to offline coupling of climate, chemistry, and emissions) is performed with the "Reference Run" only.

7.4.1 Offline Coupling

Figure 7-3 gives the predicted emissions of N_2O and CH_4 from various runs of the emission models using the offline climate (from the 2D-LO coupled climate-chemistry model) and soil organic carbon data (from the TEM model driven by the same climate model). These results indicate significant sensitivity of natural N_2O and CH_4 emissions to outputs from the climate (temperature, precipitation) and TEM (total soil organic carbon, C_T) models. For the reference case, natural soil emissions of N_2O rise about 30% between 1985 and 2100, and wetland CH_4 emissions rise by 35%. For the other sensitivity experiments shown (HHH, HHL, LLH, LLL), the increase rate

of the natural emisisons between 1985 and 2100 varies from 15% to 40% for N_2O, and from 15% to near 70% for CH_4. The predicted changes in climate (surface temperature and precipitation) and soil organic carbon over the 1977–2100 period for various model runs are shown in Figure 7-5 and Figure 7-6 respectively.

Two runs driven by reference climate outputs only (denoted R in the upper panel of Figure 7-3) and by reference climate plus TEM outputs (denoted $R+C_T$ in the same panel) indicate that climate and soil carbon changes contribute about equally to the predicted very significant increase in N_2O emissions. Note that by the end of the year 2100 natural N_2O emissions increase by about 15% without the soil organic carbon feedback. When the soil organic carbon feedback is added in, the emissions increase by about 30%.

The natural emission increases largely result from the sensitivity of wetland CH_4 emissions and soil N_2O emissions to the predicted large high-latitude temperature and precipitation increases, and from the sensitivity of the global soil N_2O emissions to changes in soil organic carbon. This can be seen very clearly in Figure 7-4. For both CH_4 and N_2O, there are two latitudinal bands (30°S–60°S and 60°N–90°N in Figure 7-4) which experience more than 50% increase in predicted emissions. In particular for N_2O, the emissions in the 70°N region increase by more than 100%. As we can see from Figure 7-5, the predicted increases in temperature and precipitation are very large at these two latitudinal bands compared with those at lower latitudes. These increases in temperature and precipitation would effectively lengthen the emission seasons (nonfreezing seasons) for both N_2O and CH_4 and create more favorable environments for anaerobic bacteria, which result in large increases in N_2O and CH_4 emissions. Furthermore, high latitudes are the regions with large soil organic carbon content, which is why the increase of N_2O emission at some high latitudes exceeds 100%.

Overall, the offline experiments indicate that including the feedbacks to climate forcing involving changing natural emissions of N_2O and CH_4 is very important. This is true especially when both climate and soil organic carbon are predicted to change significantly as occurs in the MIT global system model runs.

7.4.2 Full-Coupling and Feedbacks

Figure 7-7 and Figure 7-8 plot the predictions from the fully coupled emission-chemistry-climate model for globally averaged N_2O and CH_4 concentrations. There are three model runs reported in these graphs. Curve "C" is for the reference run without including the emission feedbacks (natural emissions are assumed to be constant (at present-day values) through the integration time). Curve "A" is for the reference run with the climate-emission feedback included but without soil organic carbon-emission feedback (soil organic carbon is assumed to be constant for all the integration years). Curve "B" is for the "realistic" case with all feedbacks included in the reference run.

As we have anticipated from the offline runs, the emission feedbacks are important in contributing to the atmospheric loading of N_2O and CH_4. At year 2100, the feedbacks increase atmospheric N_2O and CH_4 concentrations (curves "B" in Figure 7-7 and Figure 7-8) by about 30 ppb (7.3%), and 0.2 ppm (6.3%) respectively. The extra loading of these two gases in the atmosphere would affect climate through their added radiative and chemical effects. The impact of this extra loading can been seen in Figure 7-9 where the predicted changes in globally averaged temperature are plotted as a function of integration time. Except for the period between 2015 and 2025, the predicted globally averaged temperature is persistently higher by about 0.2 °C for the run including the emission feedbacks than for the run ignoring these feedbacks. By the year 2100, the difference is around 0.25 °C. The crossing of the two curves at year 2015 and 2025 in Figure 7-9 is due to the "natural" variability exhibited by the climate model.

Soil organic carbon change is as important as climate change in contributing to the extra atmospheric N_2O loading (since CH_4 emissions are not related to soil organic carbon, only climate change is responsible for the changes in CH_4 emissions. That is why curve "A" and curve "B" are identical in Figure 7-8). As we can see from Figure 7-7, by the year 2100, soil organic carbon change contributes about 40% of the predicted 30 ppb increase in atmospheric N_2O concentration. The importance of

the soil organic carbon feedback is more evident in the predicted globally averaged temperature change. Figure 7-10 shows a persistent increase in temperature of around 0.1 °C throughout the integration time when adding the soil organic carbon feedback in the coupled reference run.

The above climate changes induced by the emission feedbacks (both climate and soil organic carbon driven) are significant. They are comparable with the predicted climate changes induced by recently proposed policies to lower global anthropogenic emissions [*Jacoby et al, 1996*]. These results demonstrate again that it is important to include the emission feedbacks in order to accurately address global climate change issues.

7.5 Conclusions

When coupled with computationally efficient 2-D climate and chemistry models, the global emission models for N_2O and CH_4 are capable of assessing the feedbacks involving natural emissions in global climate modeling.

Offline runs indicate that changes in natural N_2O and CH_4 emissions corresponding to long term climate change are significant. For the reference case, soil N_2O emissions increase by about 30% and wetland CH_4 emissions increase by 35% between 1977 and 2100. Predicted emissions of N_2O and CH_4 indicate significant sensitivity to the driving parameters of climate and soil organic carbon (the latter for N_2O only). The increased rates of natural emissions from 1977 to 2100 vary from 15% to 40% for N_2O and from 15% to 70% for CH_4 for various runs using different but feasible climate model outputs. These increases in emissions result in a significant part from the predicted large changes in surface temperature and precipitation at high latitudes in the climate model.

Fully interactive runs show that there is a significant positive feedback between natural emissions of N_2O and CH_4 and climate. Globally averaged surface temperature increases by about 0.25°C at year 2100 if this emission-related feedback is included in the global climate system model.

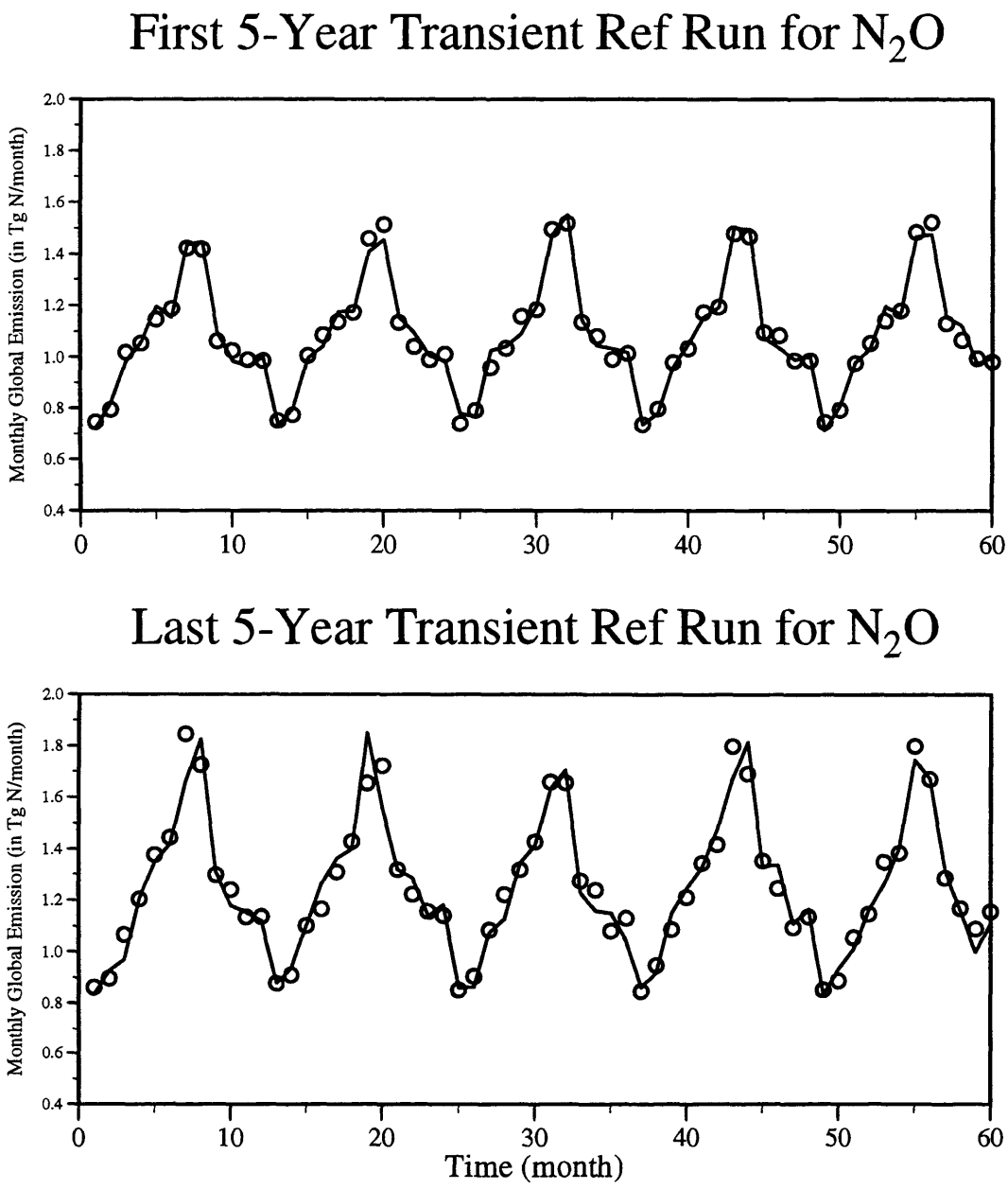

Figure 7-1: Projected (solid line) and model calculated (circles) N_2O emissions for first and last 5 years of the reference run.

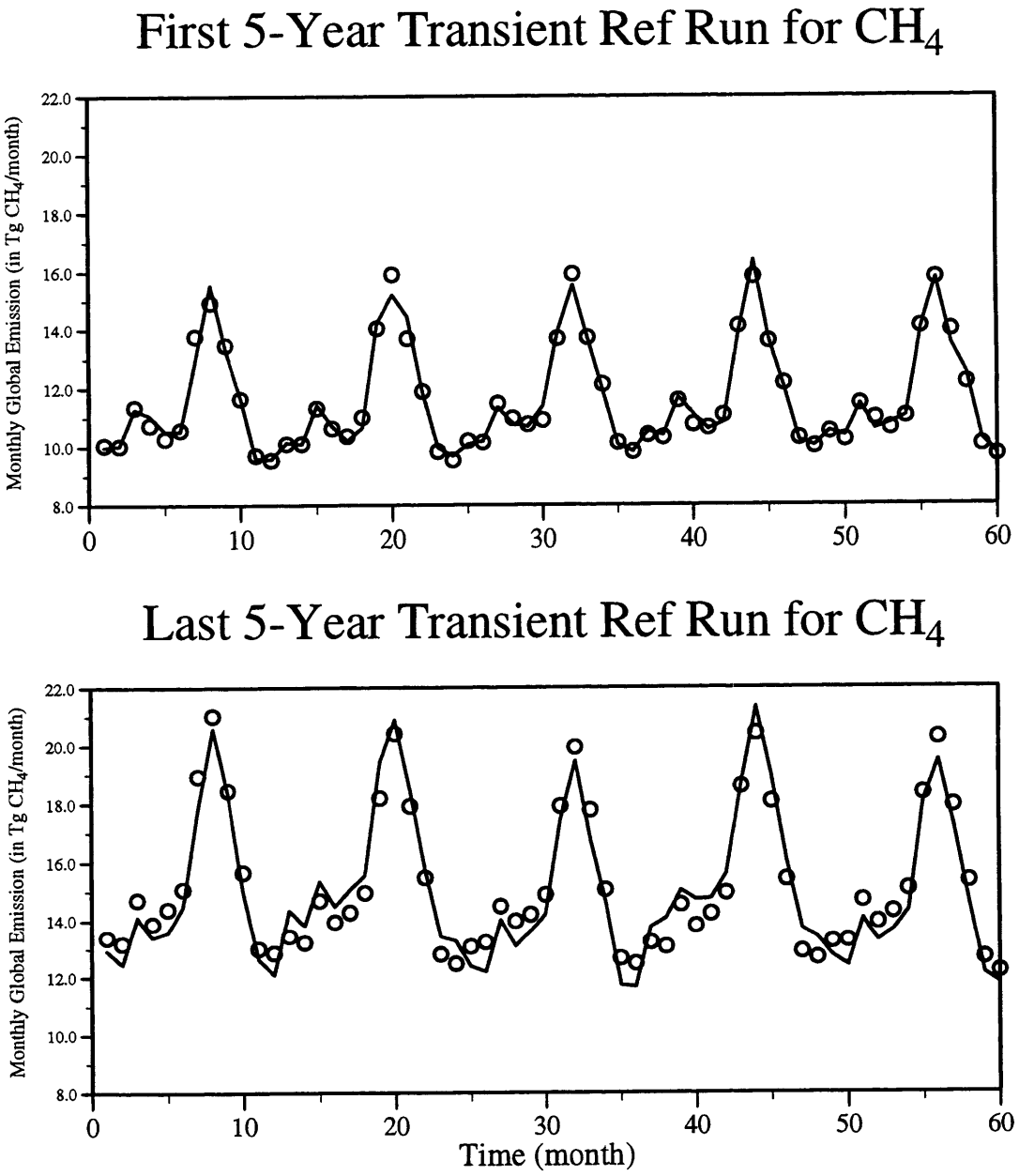

Figure 7-2: Projected (solid line) and model calculated (circles) CH_4 emissions for first and last 5 years of the reference run.

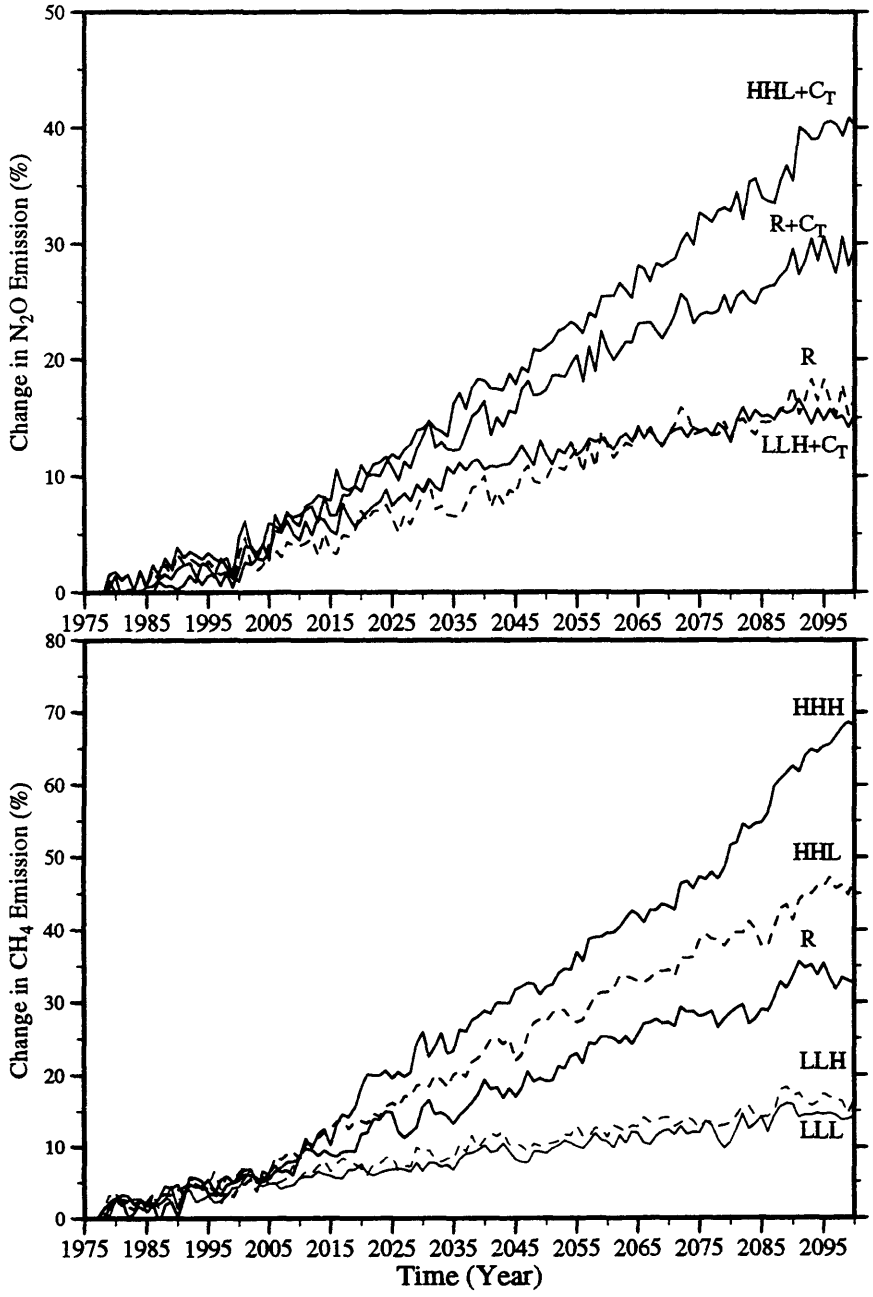

Figure 7-3: Predicted percentage changes in annual natural emissions of N_2O (upper panel) and CH_4 (lower panel) driven offline by the indicated climate model runs and (for N_2O) also by the indicated climate plus TEM model runs (the latter denoted by the addition of C_T to the run designation).

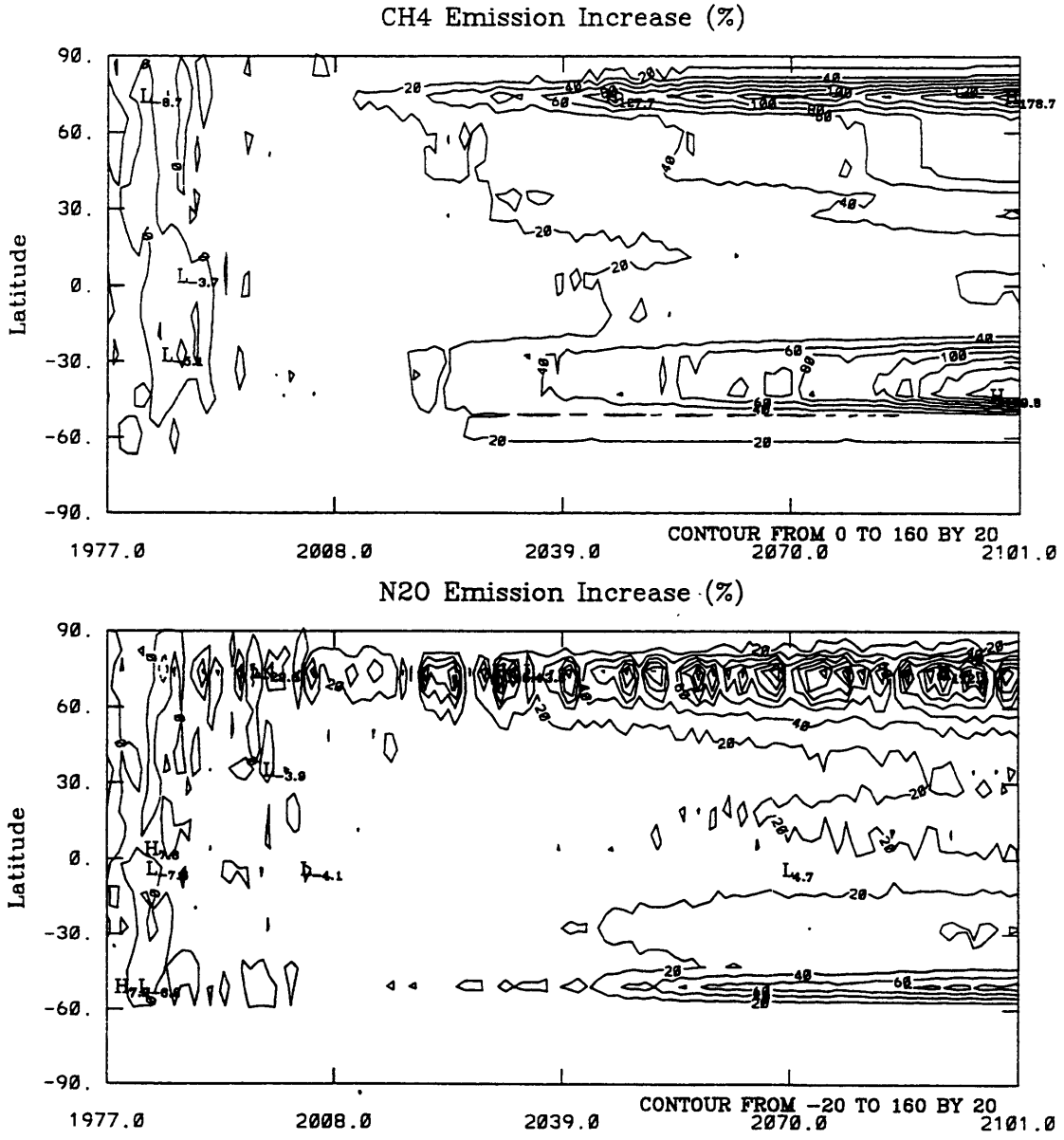

Figure 7-4: Latitude-time distribution of predicted changes in annual natural emissions of N_2O (lower panel, for R+C_T case) and CH_4 (upper panel, for HHH case). Latitude in degrees, with positive values denoting the Northern Hemisphere.

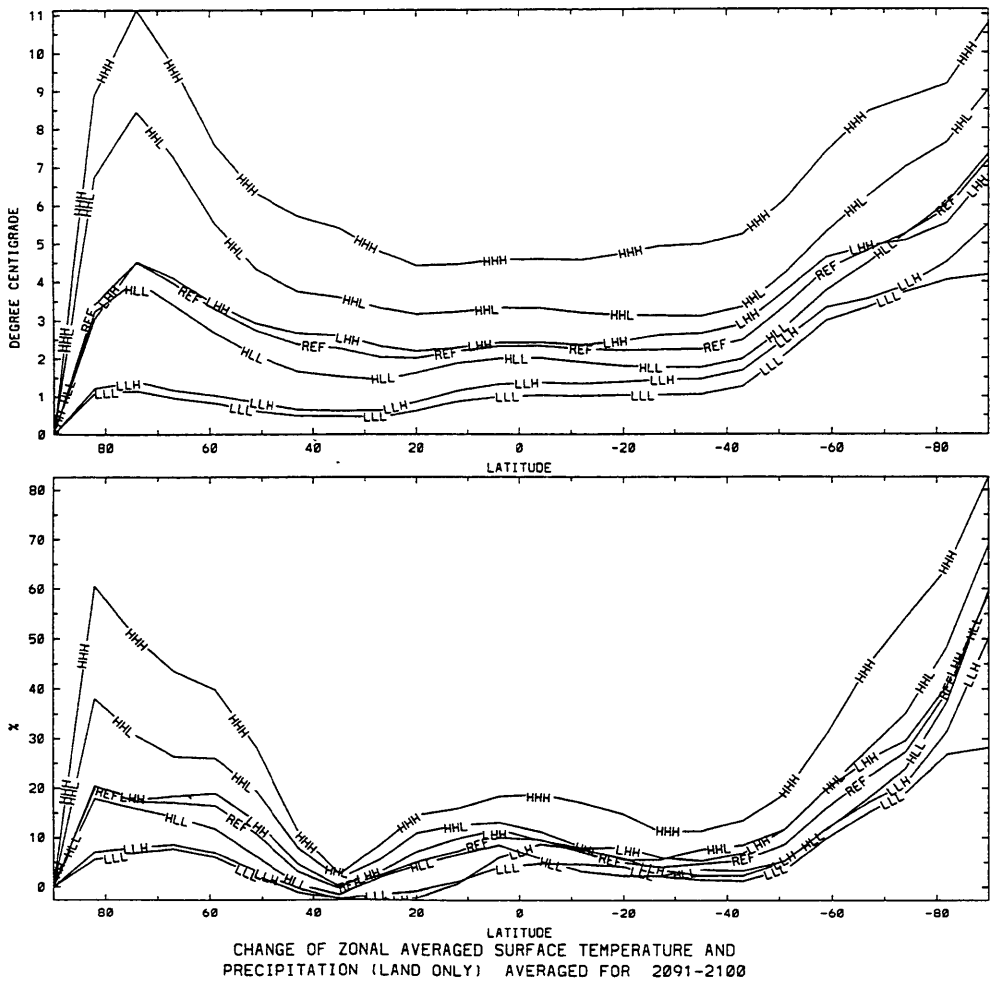

Figure 7-5: Changes (between 1977 and the average for 2090–2100) of longitudinally averaged temperature (°C) (upper panel) and precipitation (%) (lower panel) over land for the seven sensitivity runs. Latitude in degrees, with positive values denoting the Northern hemisphere.

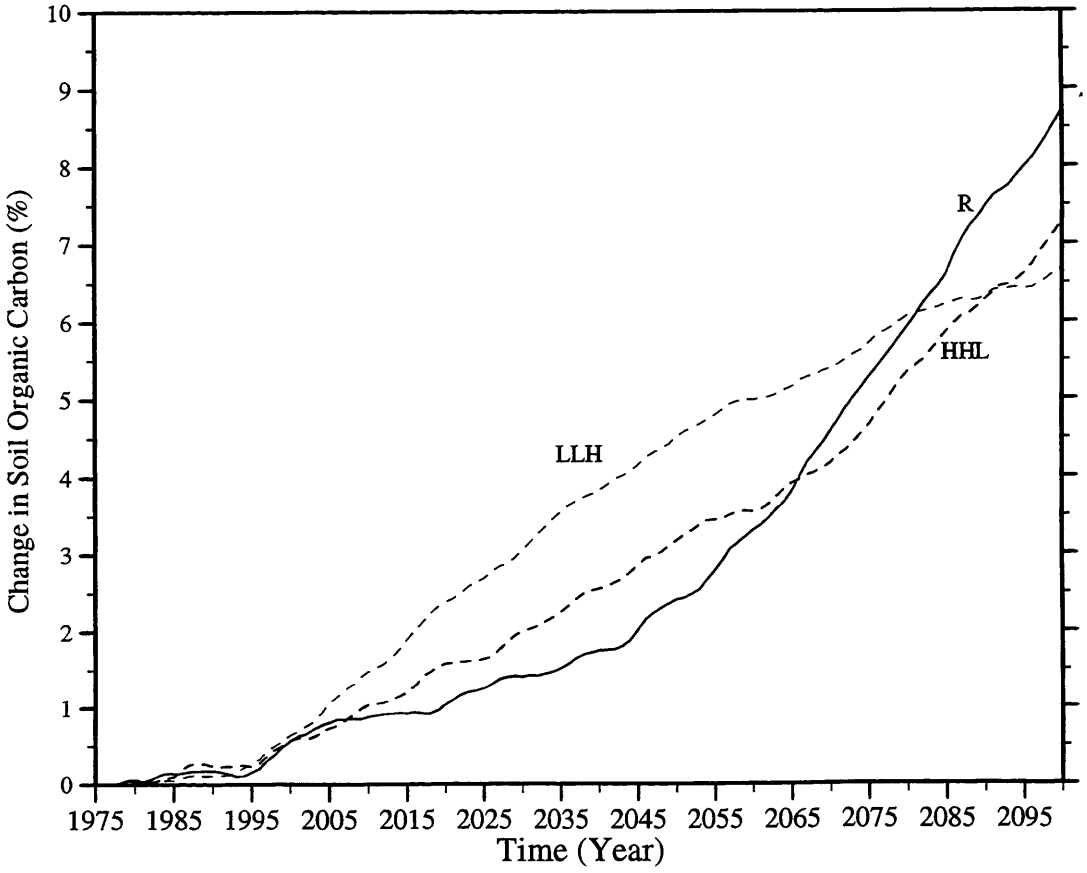

Figure 7-6: Changes in soil organic carbon predicted in transient TEM driven by the CO_2 and climate variables from the reference (R) and two selected sensitivity runs (HHL and LLH).

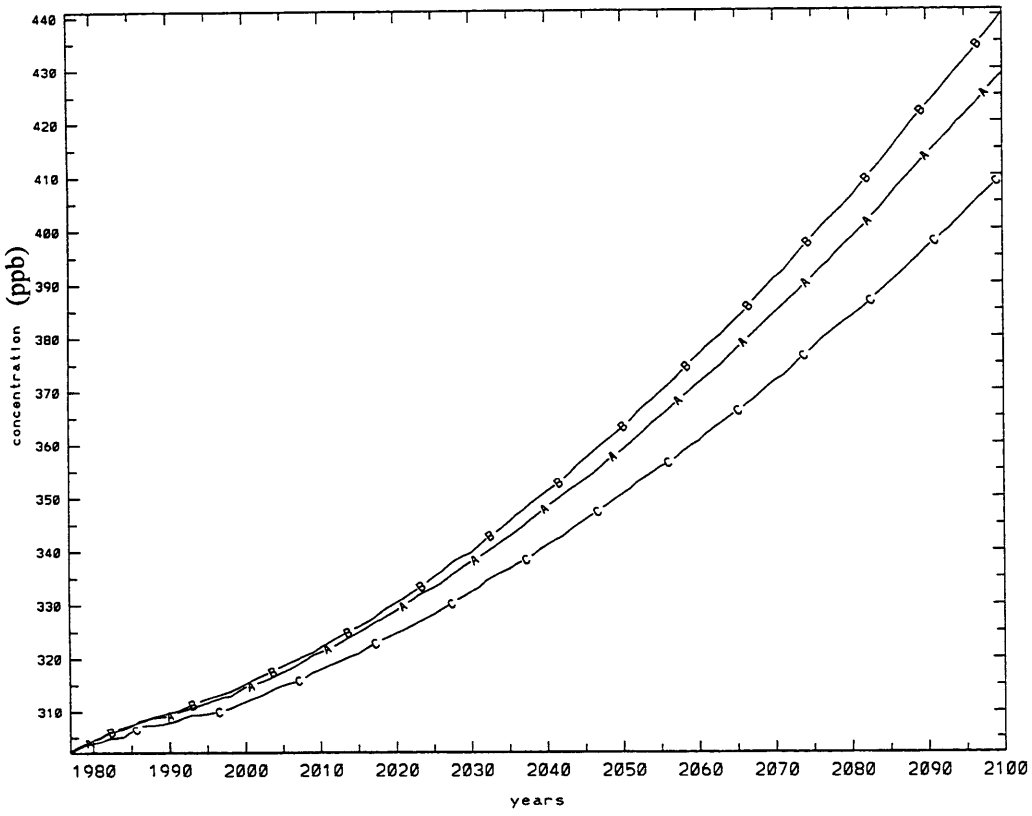

Figure 7-7: Predictions from the fully-coupled-emission-chemistry-climate model for globally averaged N_2O concentration (C: reference case without the emission feedbacks; A: reference case with the climate-emission feedback but without the soil organic carbon-emission feedback; and B: reference case with all the emission feedbacks).

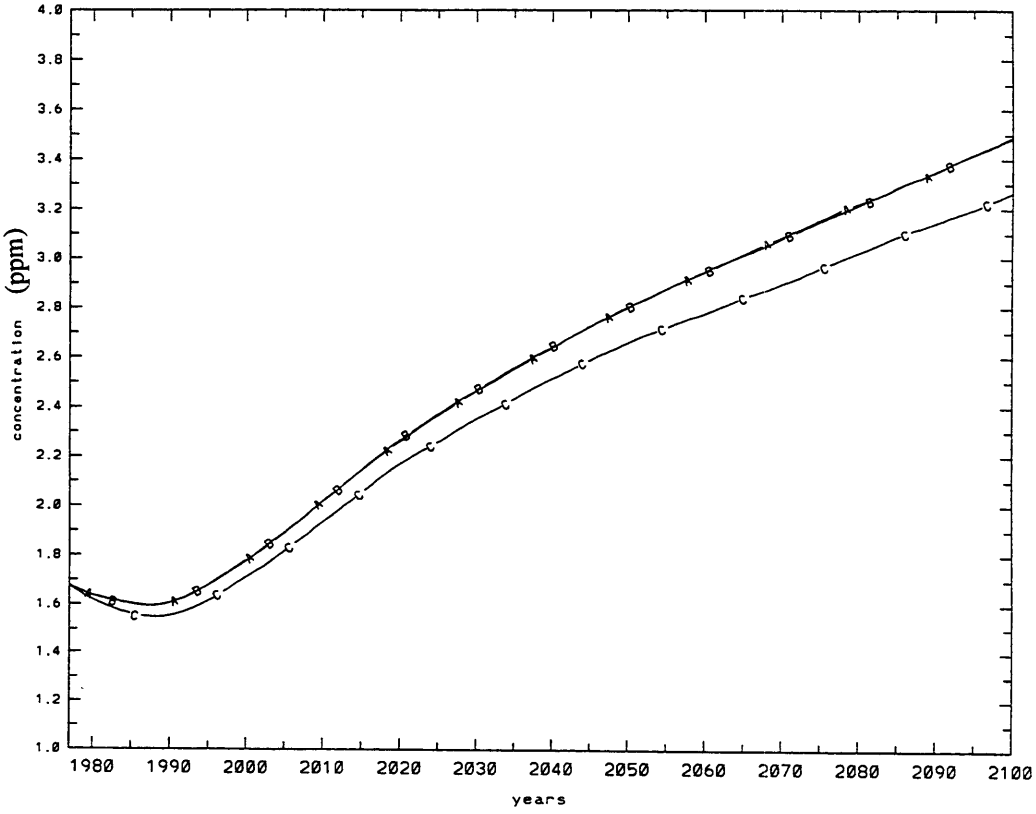

Figure 7-8: Predictions from the fully-coupled-emission-chemistry-climate model for globally averaged CH_4 concentration (C: reference case without the emission feedbacks; A: reference case with the climate-emission feedback but without the soil organic carbon-emission feedback; and B: reference case with all the emission feedbacks. A and B are identical because CH_4 emissions are not related to soil organic carbon).

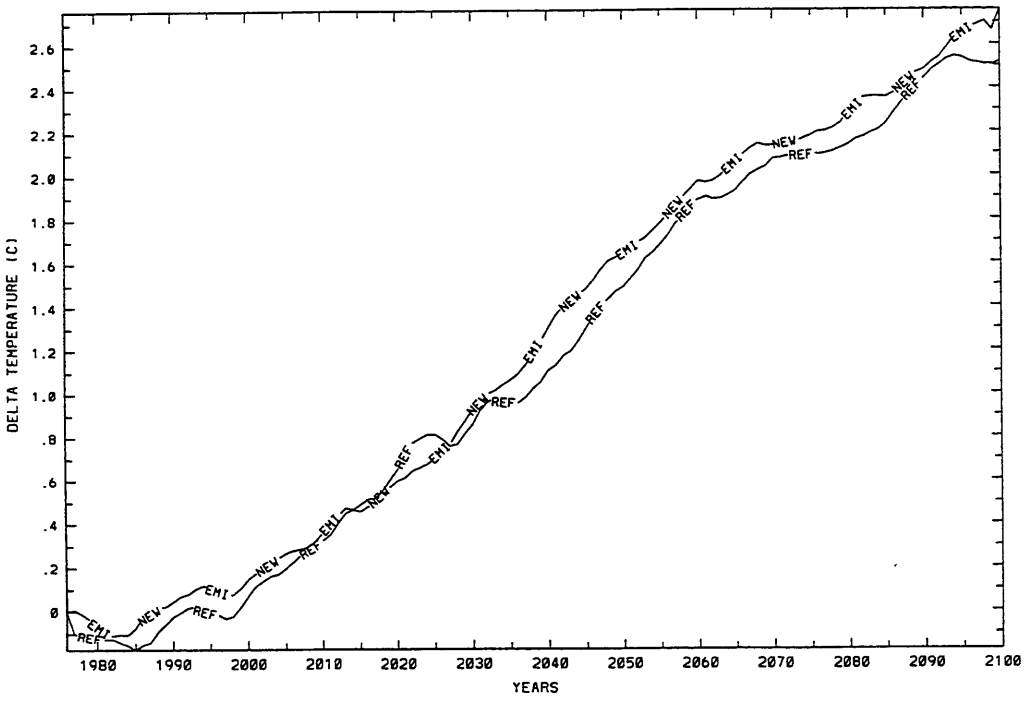

Figure 7-9: Predictions from the fully-coupled-emission-chemistry-climate model for the globally averaged temperature change from 1977 values (REF: reference case without the emission feedbacks; NEW–EMI: reference case with all the emission feedbacks).

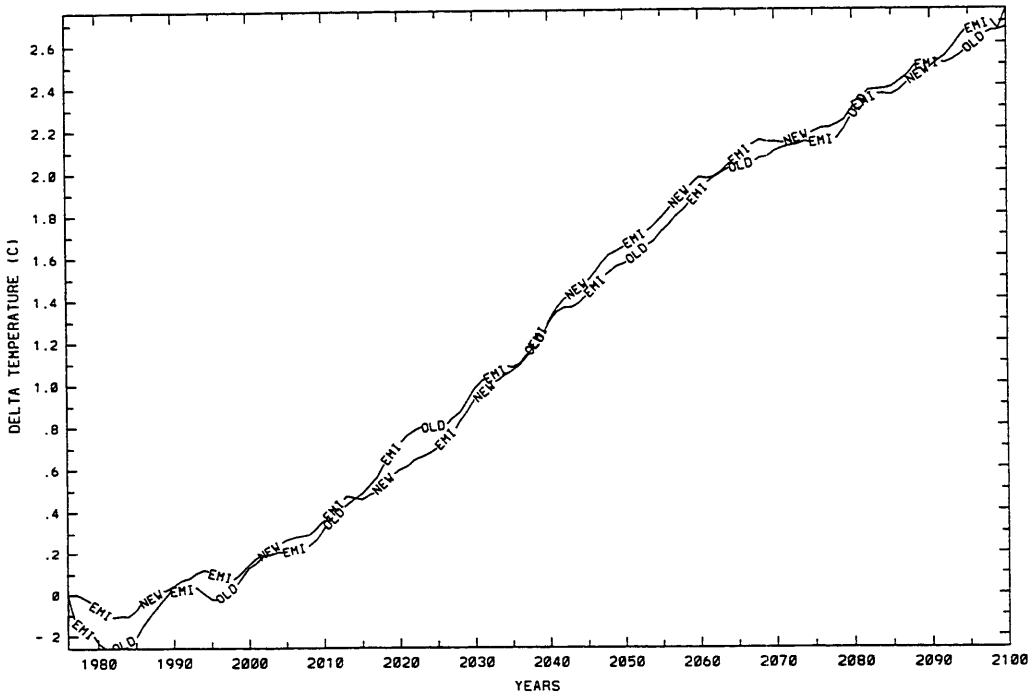

Figure 7-10: Predictions from the fully-coupled-emission-chemistry-climate model for the globally averaged temperature change from 1977 values (OLD–EMI: reference case with climate-emission feedback but without soil organic carbon-emission feedback; NEW–EMI: reference case with all the emission feedbacks as also shown in Figure 7-9).

Chapter 8

Summary and Overall Conclusions

The general goal of this thesis was to study certain aspects of the natural biogeochemical cycles of atmospheric N_2O and CH_4 and their connections with climate. A more specific goal was to identify and quantify feedbacks between natural emissions of these gases and climate. A process-oriented global biogeochemical model for soil N_2O emissions and a more empirically based global model for wetland CH_4 emissions were developed to address this general goal. The models predict the present-day N_2O and CH_4 emissions which are generally consistent with available observations. Application of the models to two extreme climate cases ($2\times CO_2$ and ice age) provided valuable insights into the magnitude and patterns of natural emission changes expected from significant climate change. The more specific goal of this thesis was realized by coupling the natural emissions models with an existing computationally efficient coupled 2-D climate and chemistry model. A summary of and results from the various parts of this thesis work are presented here.

The global emission model for N_2O, which focuses on soil biogenic N_2O emissions, has a spatial resolution of $2.5°\times 2.5°$. The model can predict daily emissions for N_2O, N_2, NH_3 and CO_2 and daily soil uptake of CH_4. It is a process-oriented biogeochemical model including all the major relevant soil C and N dynamic processes including decomposition, mineralization, nitrification, denitrification, volatilization and gas diffusion. The model takes into account the spatial and temporal variability of the driving variables, which include vegetation type, total soil organic carbon, soil

texture, and climate parameters. Climate variables, particularly surface temperature and precipitation, drive a one-dimensional soil hydrology model for determining dynamic soil temperature and moisture profiles and shifts between aerobic and anaerobic conditions. Soil C and N pools are modeled in these two distinct environments by two important N_2O-relevant process model components: the decomposition and nitrification model for the aerobic environment, and the denitrification model for the anaerobic environment.

The methane emission model is developed specifically for wetlands and has a resolution of $1° \times 1°$. There are three components for the global wetland methane emission model: high latitude wetlands (bogs), tropical wetlands (swamps and alluvial formations), and wet tundra. For the high latitude wetlands, the emission model uses a two-layer hydrological model and observationally-based empirical relations between the methane flux and regulating parameters. The hydrological model solves a one-dimensional heat diffusion equation and water balance equation. A synthesized empirical formula which uses the water table level and the bog soil temperature at the water table level is then used to predict methane emissions. For tropical wetlands, a two-factor model (temperature and water availability) is used to model the methane flux by taking into account the temperature and moisture dependence of methanogenic activity. Methane emissions from wet tundra are calculated in the global emission model by assuming a constant methane flux over a prescribed emission season. The emission season is assumed to be the time period when surface temperature is above the freezing point. The hydrological model and the two-factor model are driven by surface temperature and precipitation, thus linking methane emissions with climate.

For present-day climate and soil data sets the N_2O emission model predicts an annual flux of 11.3 Tg-N/yr (17.8 Tg N_2O/yr). This flux is somewhat toward the higher end of the IPCC estimate for the range for total N_2O emissions from natural and cultivated soils of 5.1-15 Tg-N/yr (8-23.6 Tg N_2O/yr). This N_2O global source may have been overestimated in this thesis because we use a model developed for managed ecosystems which may not be applicable to unmanaged ones. Alternatively,

this global source may have been underestimated by others in the past because a lot of field measurements are conducted in fair weather conditions which do not capture the peaks of N_2O emissions immediately following rainfall events. The spatial distribution and seasonal variation of modeled current-day N_2O emissions are similar to the driving climate patterns, especially the precipitation pattern. The predicted large emissions from tropical soils are qualitatively consistent with the observed latitudinal gradient for N_2O and with *in situ* tropical flux measurements. Chemical transport model predictions of atmospheric concentrations using the modeled soil N_2O emissions plus the deduced emissions from other (minor) sources show good agreement with observations of surface N_2O mixing ratio temporal trends and interhemispheric gradient. Sensitivity experiments suggest that soil organic carbon content, precipitation and surface temperature are the dominant factors in controlling global N_2O emissions.

Current-day CO_2 emissions from soil and CH_4 absorption by soils are predicted by the N_2O emission model to be 14 Pg-C per year and 11.5 Tg-C per year respectively.

The global CH_4 emission model predicts an annual flux of 127 Tg CH_4 for present-day climate and wetland conditions, which is in the middle of the range of recent estimates for natural wetland emissions. Modeled global methane emissions indicate two strong latitudinal bands with one in the tropics and the other in the northern high latitudes. There are strong seasonal cycles for the high latitude CH_4 emissions (due in the model to the strong seasonal effect of temperature and moisture regimes in these regions) and hence for the global total emission amount.

The two emission models for N_2O and CH_4 have been applied to two extreme climatic cases: that associated with doubling current CO_2 levels and that during the last glacial maximum (LGM). For the "doubled CO_2" case, the equilibrium ecosystem and climate states for doubled current CO_2 level from ecosystem and climate models are used to drive the emission models. We specifically use predicted soil organic carbon from the Terrestrial Ecosystem Model (TEM) of the Marine Biology Laboratory and four climate scenarios from three climate models (MIT 2D L-O, GISS 3D and GFDL). Results are quite similar for these four different climate scenarios. They

indicate that doubling CO_2 would lead to a 34% increase in N_2O emissions, even though soil organic carbon predicted by TEM is reduced by 1.3% for the predicted climate and CO_2 changes. Natural wetland CH_4 emissions increase by about 54% for the climate change associated with doubled CO_2. Temperature increases seem to be the dominant contributors to the predicted increases in N_2O and CH_4 emissions. Geographical coherence of predicted changes in surface temperature and precipitation is significant in determining the predicted changes in global emissions. The "ice age case" is examined by using a GISS 3D model ice age (LGM) equilibrium run and CLIMAP data. Our emission models predict significantly smaller soil N_2O emissions and wetland CH_4 emissions (about 50% of current emissions) under the ice age (LGM) conditions.

Finally, the emission models were coupled with existing 2D climate and chemistry models developed at MIT. Model results indicate that changes in natural N_2O and CH_4 emissions corresponding to long term climate change are significant. For example, between 1977 and 2100, for the reference case (in which global average temperature increased by about 2.5°C), soil N_2O emissions are predicted to increase by about 30%, and wetland CH_4 emissions increase by about 35%. Various runs of the N_2O and CH_4 emission models indicate significant sensitivity to outputs from the climate (surface temperature and precipitation) and TEM (total soil organic carbon) models. The predicted changes result largely from the the sensitivity of emissions to high-latitude climate change and global soil carbon change (for N_2O). Climate and soil organic carbon changes contribute about equally to the predicted increase in N_2O emissions. The soil organic carbon-emission feedback is almost as important as the climate-emission feedback in contributing to the extra warming induced by the changes in natural N_2O and CH_4 emissions. Fully interactive runs show that there is a significant positive feedback between emissions and climate. Global average surface temperature increases by about 0.25°C at year 2100 in the reference run if the feedback is added in the global climate system model.

We thus conclude that it is important to include these emission-related feedbacks for more accurate predictions of climate. The global system model developed at MIT

now has incorporates the emission models developed in this thesis into its general framework.

This thesis represents the first very detailed study of interactions between natural emissions and climate. However, there is still much more to do in this area and the work done here leads to the following suggestions for future work:

- **Coupling of soil C and N dynamics with an ecosystem model**

  The interactions between soil C and N dynamic processes and ecosystems are simplified in the global N_2O emission model by an exogenous variable—soil organic carbon. Ideally, soil C and N processes should be dynamically modeled together with photosynthesis, plant respiration and growth. The coupling of soil C and N dynamics with an ecosystem model would improve both models in predicting C and N cycles.

- **Improvement in computational efficiency for N_2O emission model**

  Coupling of the current soil N_2O emission model with either a climate model or ecosystem model requires a very large amount of computer time. It is necessary to further change the N_2O model structure and algorithms in order to improve its computational efficiency.

- **Examining the anthropogenic impact on soil C and N cycles**

  One of the important impacts of human activity on the environment is its influence on soil C and N dynamics through changes in soil carbon and nitrogen pools. For example: agricultural tillage changes the vertical profiles of soil organic matter; residues left in the field increase soil organic matter content; and fertilizers directly add inorganic compounds into the soil. All these effects can be examined using the emission models developed here once the relevant data become available for these basic human activities (e.g. historical data on land use).

- **Development of a process-oriented model for CH_4 emissions**

As the understanding of CH_4 production and consumption processes become clearer (e.g. Cao *et al.* [*1995*] has developed a process-oriented methane emission model for agricultural soils), the global model for CH_4 emissions should be updated with more realistic treatment of the governing processes gradually added in.

- **Assessment of the impact on CH_4 emissions by wetland redistribution**

  Assumptions have been made in this thesis for estimating CH_4 emissions under perturbed climate conditions ($2\times CO_2$ and the Ice Age). Further studies are needed to assess the changes in CH_4 emissions corresponding to the redistribution of wetlands. For example, changes in sea level will change wetland areas thus affecting CH_4 emissions.

- **Study on other feedbacks induced by the changes in emissions**

  The predicted substantial change in N_2O emissions due to climate and ecosystem changes has significant impact on stratospheric ozone levels and thus also on radiative forcing by ozone. Such chemical feedbacks need to be studied further.

Bibliography

[1] Anderson, T.H., and K.H. Domsch, Ratios of microbial biomass carbon to total organic carbon in arable soils, *Soil Biol. Biochem., 21, 471-479, 1989*

[2] Aselmann, I., and P. J. Crutzen, Global distribution of natural freshwater wetlands and rice paddies, their net primary productivity and possible methane emissions, *J. Atmos. Chem., 8, 307-358, 1989*

[3] Aulakh, M.S., D.A. Rennie, and E.A. Paul, Acetylene and N-serve effects upon N_2O emissions from NH_4^+ and NO_3^- treated soil under aerobic and anaerobic conditions, *Soil Biol. Biochem., 16, 351-356, 1984*

[4] Bartlett, K. B., P.C. Crill, R. L. Sass, R.C. Harriss and N. G. Dise, Methane emissions from tundra environments in the Yukon Kuskokwim Delta, Alaska, *J. G. R., 97, 16645-16660, 1992*

[5] Bartlett, K. B. and R. C. Harriss, Review and assessment of methane emissions from wetlands, *Chemosphere, 26, 261-320, 1993*

[6] Berges, M.G.M., R.M. Hofmann, D.Scharffe, and P.J. Crutzen, Nitrous oxide emissions from motor vehicles in tunnels and their global extrapolation, *J. G. R., 98, 18,527-18,531, 1993*

[7] Blake, D.R. and F.S. Rowland, Continuing world increase in tropospheric methane, 1978-1987, *Science, 239, 1129-1131, 1988*

[8] Boelter, D., Physical properties of peats related to degree of decomposition, *Soil Sci. Soc. Am. Proc., 33, 606-609, 1969*

[9] Bouwman, A.F., I. Fung, E. Matthews, and J. John, Global Analysis of the Potential For N_2O Production in Natural Soil, to be published. Cited by Williams et al. in NO_x and N_2O emissions from soil, Global Biogeochemical Cycles, 6, 351-388, 1993

[10] Bouwman, A.F., K.W. Van der Hoek, and J.G.J. Olivier, Uncertainties in the global source distribution of nitrous oxide, *J. G. R., 100, 2785-2800, 1995*

[11] Bras, R., Hydrology: An Introduction to Hydrologic Science, *Addison-Wesley, Reading, MA, 1990*

[12] Bremner, J. M., and A. M. Blackmer, Terrestrial nitrification as a source of atmospheric nitrous oxide, in *Denitrification, Nitrification, and Atmospheric Nitrous Oxide*, edited by C. C. Delwiche, John Wiley, New York, 1981

[13] Brumme, R. and F. Beese, Effects liming and nitrogen fertilization on emissions of CO_2 and N_2O from a temperate forest, *J. G. R., 97, 12,851-12,858, 1992*

[14] Butler, J.H., J. W. Elkins and T. M. Thompson, Tropospheric and Dissolved N_2O of the West Pacific and East Indian Oceans During the El Nino Southern Oscillation Event of 1987, *J. G. R., 94, 14,865-14,877, 1989*

[15] Cao, M., J.B. Dent, and O.W. Heal, Modeling methane emissions from rice paddies, *Global Biogeochemical Cycles, 9, 183-195, 1995*

[16] Castellan, A., J.C.J. Bart and S. Cavallaro, Adipic Acid, *Catalysis Today, 9, 1-32, 1991*

[17] CDIAC, *Worldwide Organic Soil Carbon and Nitrogen Data*, NDP-018, Carbon Dioxide Information Analysis Center, Oak Ridge National Laboratory, 1986

[18] Chappellaz, J., J. M. Barnola, D. Raynaud, Y. S. Korotkevich and C. Lorius, Ice-core record of atmospheric methane over the past 160,000 years, *Nature, 345, 127-131, 1990*

[19] Chappellaz, J., I. Fung, The atmospheric CH_4 increase since the Last Glocial Maximum, (I) Source Estimates, *Tellus, 45B, 1993*

[20] Cicerone and Oremland, Biogeochemical aspects of atmospheric methane, *Global Biogeochemical Cycles, 2, 299-328, 1988*

[21] Clapp, R.B., and G.M. Hornberger, Empirical equations for some soil hydraulic properties, *Water Resour. Res., 14, 601-604, 1978*

[22] Clay, D. E., J. A. E. Molina, C. E. Clapp, and D. R. Linden, Nitrogen-tillage-residue management, II, Calibration of potential rate of nitrification by model simulation, *Soil Sci., Soc., Am. J., 49, 322-325, 1985*

[23] CLIMAP, Project Members, A. McIntyre, project leader: Seasonal Reconstruction of the Earth's Surface at the Last Glacial Maximum, *Geol. Soc. Amer., Map and Chart Series, No. 36, 1981*

[24] Cofer III, W. R., J.S. Levine, E. L. Winstead, B. J. Stocks, New estimates of nitrous oxide emissions from biomass burning, *Nature, 349, 689-691, 1991*

[25] Conrad, R., H. Schutz, and M. Barbble, Temperature limitation of hydrogen turnover and methanogenesis in anoxic paddy soil, *FEMS Microbiol. Ecol., 45, 281-289, 1987*

[26] Conrad, R. and F. Rothfuss, Methane oxidation in the soil surface layer of a flooded rice field and the effect of ammonium, *Biol. Fert. Soil, 12, 28-32, 1991*

[27] Crill et al. Methane flux from Minnesota peatlands, *Global Biogeochemical Cycles, 2, 371-384, 1988*

[28] Crutzen, P.J., and M.O. Andreae, Biomass burning in the tropics: Impact on atmospheric chemistry and biogeochemical cycles, *Science, 250, 1669-1678, 1990*

[29] Cunnold, D., F Alyea, N. Phillips, and R. Prinn, A three-dimensional dynamical-chemical model of atmospheric ozone, *J. Atmos. Sci., 32, 170-194, 1975*

[30] Cunnold, D., F. Alyea, and R. Prinn, Prelimniary calculations concerning the maintenance of the zonal mean ozone distribution in the northern hemisphere, *Pure Appl. Geophys., 118, 329-354, 1980*

[31] Cunnold, D., Prinn, R., Rasmussen, R., Smmonds, P., Alyea, F., Cardelino, C., Crawford, A., Fraser, P., and Rosen, R., The atmospheric lifetime experiment 3, Lifetime methodology and application to three years of $CFCl_3$ data, *J. G. R., 88, 8379-8400, 1983*

[32] Cunnold, D., Prinn, R., Rasmussen, R., Smmonds, P., Alyea, F., Cardelino, C., Crawford, A., Fraser, P., and Rosen, R., The atmospheric lifetime and annual release estimates for $CFCl_3$ and CF_2Cl_2 from 5 years of ALE data, *J. G. R., 91, 10797-10817, 1986*

[33] Cunnold, D., and R. G. Prinn, Comment on "Tropospheric OH in a three-demensional chemical tracer model: An assessment based on observations of CH_3CCl_3", by C.M. Spivakovsky et al., *J.G.R., 96, 17391-17393, 1991*

[34] Dasch, J.M., Nitrous oxide emissions from vehicles, *J. Air Waste Manage. Assoc., 42, 63-67, 1992*

[35] DeVries, D.A., Heat transfer in soils, in *Heat and Mass Transfer in the Biosphere, 1*, edited by D.A. DeVries and N.H. Afgan, John Wiley, New York, 1975

[36] Dise, H., E. Gorham, and E. Verry, Environmental factors controlling methane emissions from peatlands in northern Minnesota, *J. G. R., 98, 10583-10594, 1993*

[37] Dua, R. D., B. Bhandari, and D. J. D. Nicholas, Stable isotope studies on the oxidation of ammonia to hydroxylamine by *Nitrosomonas europaea, FEBS Lett., 106, 401-404, 1979*

[38] Ehleringer, J.R. and C.B. Field, Scaling physiological processes: Leaf to globe, *Academic Press, San Diego, 1993*

[39] Elkins, J.W., S.C.Wofsy, M.B. McElroy, C.E. Kolb, and W.A. Kaplan, Aquatic sources and sinks of Nitrous Oxide, *Nature, 275, 602, 606, 1978*

[40] Elkins, J.W., State of the research for atmospheric nitrous oxide (N_2O) in 1989, Contribution for the IPCC, 1989

[41] Erickson, D.J., Simulation of the global air-sea transfer velocity of Helium, *Geophys. Res. Lett., 15, 1495-1498, 1988*

[42] Erickson III, D.J., A stability dependent theory for air-sea gas exchange, *J. G. R., 98, 8471-8488, 1993*

[43] Etheridge, D. M., G. I. Pearman, and F. de Silva, Atmospheric trace-gas variations as revealed by air trapped in an ice core from Law Dome, Antarctica, *Annals of Glaciology, 10, 28-33, 1988*

[44] Fechner, E. and H. Hemond, Methane transport and oxidation in the unsaturated zone of a Sphagnum peatland, *Global Biogeochem. Cys., 6, 33-44, 1992*

[45] Federer, C. A. Brook90: A simulation model for evapotranspiration, soil water, and streamflow, version 2.1 (Computer Freeware and Documentation), *USDA Forest Service, P.O.Box 640, Durham, NH 03824, 1993*

[46] Firestone, M. and E. Davidson, Microbiological basis of NO and N_2O production and consumption in soil, in *M.O. Andreae and D.S. Schimel (eds), Exchange of trace gases between terrestrial ecosystems and the atmosphere, Johy Wiley and Sons, NY, 1989*

[47] Firestone, M.,Biological denitrification, in *F.J. Steveson (ed), Nitrogen in Agricultural Soils, Agronomy Soc. Am., Madison, WI, 1982*

[48] Focht, D. D., The effect of temperature, pH and aeration on the production of nitrous oxide and gaseous nitrogen—A zero order kinetic model, *Soil Sci., 118, 173-179, 1974*

[49] Focht, D. D., and W. Verstraete, Biochemical ecology of nitrification and denitrification, in *Advances in Microbial Ecology*, vol. 1, edited by M. Alexander, pp. 135-214, Plenum, New York, 1977

[50] Freney, J. R., J. R. Simpson, and O. T. Denmead, Ammonia volatilization, *Ecol. Bull., 33, 291-302, 1981*

[51] Frolking, S., Modeling soil climate controls on the exchange of trace gases between the terrestrial biosphere and the atmosphere, Ph.D Thesis, University of New Hampshire, Durham, NH, 1993

[52] Fung, I., C.J. Tucker and K.C. Prentice, Application of AVHRR vegetation index to study atmosphere-biosphere exchange of CO_2, *J. G. R., 92, 2999-3015, 1987*

[53] Fung, I., J. John, J. Lerner, E. Matthews, M. Prather, L. P. Steele, and P. J. Fraser, Three-Dimensional Model Sythesis of the Global Methane Cycle, *J. G. R., 96, 13,033-13,065, 1991*

[54] Gardner, W.R., Movement of nitrogen in soil, *Agronomy, 10, 550-572, 1965*

[55] Gilmour, J.T., M.D. Clark, and G.C. Sigua, Estimating net nitrogen mineralization from carbon dioxide evolution, *Soil Sci. Soc. J., 49, 1398-1402, 1985*

[56] Golombek, A., and R. G. Prinn, A global three-dimensional model of the circulation and chemistry of $CFCl_3$ and CF_2Cl_2, CH_3CCl_3, CCl_4, and N_2O, *J.G.R., 91, 3985-4001, 1986*

[57] Gorham, E., Northern peatlands: role in the carbon cycle and probable responses to climatic warming, *Ecol. Appl., 1, 182-195, 1991*

[58] Grant, R.F., A technique for estimating denitrification rates at different soil temperatures, water contents, and nitrate concentrations, *Soil Sci, 152, 41-52, 1991*

[59] Groffman, P.M., Ecology of nitrification and denitrification in soil evaluated at scales relevant to atmospheric chemistry, in *J. Rogers and W. Whiteman (eds), Microbial production and consumption of greenhouse gases: Methane, Nitrogen Oxides, and Halomethanes, Am. Soc. Microbio., Washington D.C., 1991*

[60] Hahn, J., *Tellus, 26, 160-168, 1974*

[61] Hansen, J. *et al.*, Efficient three-dimensional global models for climate studies: Models I and II, , *Mon. Wea. Rev., 111, 609-662, 1983*

[62] Hansen, J., A. Lacis, D. Rind, G. Russell, P. Stone, I. Fung, R. Ruedy, J. Lerner, Climate Sensitivity: Analysis of Feedback Mechanisms, *Geophys. Monogr. Ser., Vol. 29, edited by J. E. Hansen and T. Takahashi, pp. 130-163, AGU, Washington, D.C., 1984*

[63] Hao, W.M., D.E. Ward, Methane production from global biomass burning, *J. G. R., 98, 20,657-20661, 1993*

[64] Hao, W.M., M.H. Liu, Spatial and temporal distribution of tropical biomass burning, *Global Biogeochemical Cycles, 8, 495-503, 1994*

[65] Hartley, D., and R. G. Prinn, Comment on "Tropospheric OH in a three-demensional chemical tracer model: An assessment based on observations of CH_3CCl_3", by C.M. Spivakovsky et al., *J.G.R., 96, 17383-17387, 1991*

[66] Hartley, D. and R. Prinn, Feasibility of determining surface emissions of trace gases using an inverse method in a three-dimensional chemical transport model, *J. G. R., 98, 5183,-5198, 1993*

[67] Hartley, D., Deducing trace gas emissions using an inverse method in three-dimensional chemical transport models, Ph.D. thesis, MIT, Cambridge, MA, 1993

[68] Hooper, A.B., Ammonia oxidation and energy transduction in the nitrifying bacteria, in *Microbial Chemoautotrophy*, edited by W.R. Strohl and O.H. Tuovinen, pp. 133-167, Ohio State University Press, Columbus, 1984

[69] Houghton, R.A. et al., The flux of carbon from terrestrial ecosystems to the atmosphere in 1980 due to changes in land use: geographic distribution of the global flux, *Tellus, 39B, 122-139, 1987*

[70] Hynes, R.K., and R. Knowles, Production of nitrous oxide by *Nitrosomonas europaea*: Effects of acetylene, pH, and oxygen, *Can. J. Microbiol. 30, 1397-1404, 1984*

[71] IPCC, *Climate Change 1992: The Supplementary Report to the IPCC Scientific Assessment*, Cambridge Univ. Press, Cambridge, UK, 1992

[72] IPCC, *Climate Change 1994: Radiative Forcing of Climate Change and an Evaluation of the IPCC IS92 Emission Scenarios*, Cambridge Univ. Press, Cambridge, UK, 1994

[73] IPCC, *Climate Change 1996: Second Assessment*, Cambridge Univ. Press, Cambridge, UK, in press, 1996

[74] Jacoby, H., R. Prinn, et al., Integrated global system model for climate policy analysis: II, Impact assessment and selected policy studies, manuscript in preparation, 1996

[75] Jones, R.L., and J.A. Pyle, Observation of CH_4 and N_2O by the Nimbus 7 SAMS: A comparison with *in situ* data and two-dimensional numerical model calculations, *J. Geophys. Res., 89, 5263-5279, 1984*

[76] Keeney, D. R., I. R. Fillery, and G. P. Marx, Effect of temperature on the gaseous nitrogen products of denitrification in a silt loam soil, *Soil Sci. Soc. Am. J., 43, 1124-1128, 1979*

[77] Keeney and Nelson, Nitrogen-inorganic forms, in *Page, A.L. et al. (eds), Methods of soil analysis, Part 2, Chemical and Microbiological Properties, Second edition, Am. Soc. Agron., Madison, WI, 1986*

[78] Keller, M. and P. Matson, Biosphere-atmosphere exchange of trace gases in the tropics: evaluating the effects of land-use changes. In *Global Atmospheric-Biospheric Chemistry*, R. Prinn (ed.), Plenum Press, New York and London, pp. 103-118, 1994

[79] Kelly, C.A. and D.P. Chynoweth, The contributions of temperature and of the input of organic matter in controlling rates of sediment methanogensis, *Limnol. Oceanogr., 26, 891-897, 1981*

[80] Khalil, M.A.K., R.A. Rasmussen, Nitrous oxide: Trends and global mass balance over the last 3,000 years, *Annals of Glaciology, 10, 73-79, 1988*

[81] Khalil, M.A.K., R.A. Rasmussen, Nitrous oxide from coal-fired power plants: Experiments in the plumes, *J.G.R., 97, 14645-14649, 1992*

[82] Kim, K.R., and H. Craig, Two-isotope Characterization of N_2O in the Pacific Ocean and Constraints on Its Origin in Deep Water, *Nature, 347, 58-61, 1990*

[83] Knowles, R., Denitrification, *Ecol. Bull., 33, 315-329, 1981*

[84] Leemans, R. and Cramer, W.P., The IIASA climate database for land areas on a grid with 0.5° resolution, *WP-90-41, International Institute for Applied Systems Analysis (IIASA), Laxenburg, Austria, pp. 60, 1990*

[85] Leffelaar, P. A., and W. W. Wessel, Denitrification in a homogeneous, closed system: experiment and simulation, *Soil Sci., 146, 335-349, 1988*

[86] Letey, J., W.A. Jury, Aviva Hadas, and N. Valoras, Gas diffusion as a factor in laboratory incubation studies on denitrification, *J. Environ. Qual., 9, 223-227, 1980*

[87] Levitus, S., Climatological atlas of the World Ocean, NOAA Prof. Paper 13, US Gov't Printing Office, Washington, D.C., 1982

[88] Levy, H., J. Mahlman, and W. Moxim, Tropospheric N_2O variability, *J. Geophys. Res., 87, 3061-3080, 1982*

[89] Li, C., S. Frolking, and T. A. Frolking, A model of nitrous oxide evolution from soil driven by rainfall events, I, Model structure and sensitivity, *J. Geophys. Res., 97, 9759-9776, 1992a*

[90] Li, C., S. Frolking, and T. A. Frolking, A model of nitrous oxide evolution from soil driven by rainfall events, II, Model Application, *J. Geophys. Res., 97, 9777-9784, 1992b*

[91] Li, C., and S. Frolking, Simulation of N_2O emission from soil by DNDC model with generalized climate scenarios, Report, University of New Hampshire, Durham, New Hampshire, 1992

[92] Linak, W.P., J. A. McSorley, R. R. Hall, J. V. Ryan, R. K. Srivastava, J. O. L. Wendt, and J.B. Mereb, Nitrous oxide emissions from fossil fuel combustion, *J. G. R., 95, 7533-7541, 1990*

[93] Liss, P.S. and L. Merlivat, Air-sea gas exchange rates: Introduction and synthesis, In P.B. Menard (Ed.), *The role of air-sea exchange in geochemical cycling, D. Reidel, Hingham, Mass, 1986*

[94] Mahowald, N., Development of a 3-Dimensional Chemical Transport Model Based on Observed Winds and Use in Inverse Modeling of the Sources of CCl_3F, Ph.D. thesis, MIT, Cambridge, MA, 1996

[95] Marland, G., Fossil fuels CO_2 emissions: Three countries account for 50 % in 1986, In: *CDIAC Communications, Winter, 1989*

[96] Matthews, E. and L. Fung, Methane emissions from natural wetlands : global distribution, area, and environmental characteristics of sources,*Global Biogeochemical Cycles, 1, 61, 1987*

[97] Matthews, E., Global vegetation and land use: New high-resolution data bases for climate studies, *J. Clim. Appl. Meteorol., 22, 474-487, 1983*

[98] McConnanghey, P.K., and D.R. Bouldin, Transient microsite models of denitrification, I, Model development, *Soil Sci., Soc., Am., J., 49, 886-891, 1985*

[99] Melillo, J. M., A. David McGuire, David W. Kicklighter, Berrien Moore III, Charles J. Vorosmarty and Annette L. Schloss, Global climate change and terrestrial net primary production, *Nature, 263, 234-239, 1993*

[100] Mitchell, J.F.B., The greenhouse effect and climate change, *Rev. Geophys., 24, 115-139, 1989*

[101] Molina, J.A.E., C.E. Clapp, J.J. Shaffer, F.W. Chichester, and W.E. Larson, NCSOIL, a model of nitrogen and carbon transformations in soil: description, calibration, and behavior, *Soil Sci. Soc. Am. J., 47, 85-91, 1983*

[102] Moore, T. R. and R. Knowles, Influence of water table levels on methane and carbon dioxide emissions from peatland soils, *Can. J. Soil Sci., 69, 33-38, 1989*

[103] Moore, T.R., N. Roulet and R. Knowles, Spatial and temporal variations of methane flux from subarctic/northern boreal fens, *Global Biogeochem. Cycles, 4, 26-49, 1990*

[104] Moore, T.R. and N.T. Roulet, Methane flux: Water table relations in Northern Wetlands, *G. Res. Lett., 20, 587-590, 1993*

[105] Mosier, A., D. Schimel, D. Valentine, K. Bronson, and W. Parton, Methane and Nitrous Oxide fluxes in Native, Fertilized and Cultivated Grasslands, *Nature, 350, 330-332, 1991*

[106] Munch, J.C., Nitrous oxide emissions from soil as determined by the composition of denitrifying microbial population, *In: Diversity of environmental biogeochemistry, Elsevier, Amsterdam, pp. 308-315, 1991*

[107] Muzio, L., and J. Kramlich, An artifact in the measurement of N_2O from combustion sources, *Geophys. Res. Lett., 15, 1369-1372, 1988*

[108] Najjar, R.G., Marine Biogeochemistry, in K. E. Trenberth (ed), *Climate System Modeling, Cambridge University Press, 241-280, 1992*

[109] Neue, H.U., and H.W. Scharpenseel, Gaseous products of decomposition of organic matter in submerged soils, in *Organic matter and Rice*, pp. 311-328, International Rice Research Institute, Manila, Philippines, 1984

[110] Nevison, C.D., G. Esser and E.A. Holland, A global model of changing N_2O emissions from natural and perturbed soils, *Climatic Change, 32, 327-378, 1996*

[111] Nommik, H., Ammonium fixation and other reactions involving a nonenzymatic immobilization of mineral nitrogen in soil, *Agronomy, 10, 198-251, 1965*

[112] Nyhan, J. W., Influence of soil temperature and water tension on the decomposition rates of carbon-14 labelled herbage, *Soil Sci., 121, 288-293, 1976*

[113] Oort, A. H., Global Atmospheric Circulation Statisics, *NOAA Professional Paper, 14, U.S. Government Printing Office, Washington, D.C., 1983*

[114] Oremland, R. and C. Culbertson, Importance of methane oxidizing bacteria in the methane budget as revealed by use of s specific inhibitor, *Nature, 356, 421-423, 1992*

[115] Parashor, D.C., P.K. Cupta, J. Rai, R.C. Sharma, and N. Singh, Effects of soil temperature on methane emissions from rice paddy fields, *Chemosphere, 26, 247-250, 1993*

[116] Poth, M., and D. D. Focht, ^{15}N kinetic analysis of N_2O production by *Nitrosomonas europaea*: An examination of nitrifier denitrification, *Appl. Environ. Microbiol., 49, 1134-1141, 1985*

[117] Press, W.H., S.A. Teukolsky, W.T. Vetterling, and B.P. Flannery, *Numerical Recipes in FORTRAN, The Art of Scientific Computing*, Second Edition, Cambridge University Press, 1992

[118] Prinn, R., D. Cunnold, R. Rasmussen, P. Simmonds, F. Alyea, A. Crawford, P. Fraser, and R. Rosen, Atmospheric emissions and trends of nitrous oxide deduced from ten years of ALE/GAGE data, *J. G. R., 95, 18369-18385, 1990*

[119] Prinn, R.G., R.F. Weiss, B.R. Miller, J. Huang, F.N. Alyea, D.M. Cunnold, P.J. Fraser, D.E. Hartley, and P.G. Simmonds, Atmospheric trends and lifetime of CH_3CCl_3 and global OH concentrations, *Science, 269, 187-192, 1995*

[120] Prinn, R., H. Jacoby, A. Sokolov, C. Wang, X. Xiao, Z. Yang, R. Eckaus, P. Stone, D. Ellerman, J. Melillo, J. Fitzmaurice, D. Kicklighter, Y. Liu, G. Holian, Integrated global system model for climate policy analysis: I. Model framework and sensitivity studies, MIT Joint Program on Science and Policy of Global Change, Report No. 7, June 1996

[121] Raich, J.W., E.B. Rastetter, J.M. Melillo, D.W. Kicklighter, P.A. Steudler, B.J. Peterson, A.L. Grace, B. Moore III and C.J. Vorosmarty, *Ecological Applications, 1, 399-429, 1991*

[122] Reeburgh, W. S., N. T. Roulet, and B. H. Svensson, Terrestrial biosphere-atmosphere exchange in high latitudes. In *Global Atmospheric-Biospheric Chemistry*, R. Prinn (ed.), Plenum Press, New York and London, pp. 165-178, 1993

[123] Roulet, N., R. Ash, and T. Moore, Low boreal wetlands as a source of atmospheric methane, *J. G. R., 97, 3739-3749, 1992*

[124] Rudd, J. W. M., and C. D. Taylor, Methane cycling in aquatic environments, *Adv. Aq. Microbiol. 2:77-150,1980*

[125] Schmidt, E.L., Nitrification in soil, in *Nitrogen in Agricultural Soils, Agron. Monogr., Vol.22*, edited by F.J. Stevenson, pp. 253-288, American Society of Agronomy, Madison, Wis., 1982

[126] Schutz, H., W. Seiler and R. Conrad, Processes involved in formation and emission of methane in rice paddy fields. *Biogeochemistry, 7, 33-53, 1989*

[127] Sebacher, D.I., R.C. Harriss, K. B. Bartlett, S. M. Sebacher and S. S. Grice, Atmospheric methane sources: Alaskan tundra bogs, an alpine fen, and a subarctic boreal marsh, *Tellus 38B, 1-10, 1986*

[128] Seiler, W., and R. Conrad, Contribution of tropical ecosystems to the global budgets of trace gases, especially CH_4, H_2, CO and N_2O, in *Geophysiology of Amazonia: Vegetation and climate interaction, edited by R.E. Dickinson, Wiley and Sons, NY, 1987*

[129] Shea, D. J., Climatological atlas: 1959-1979, *NCAR Technical Note, TN-269+STR, 1986*

[130] Sloan, S. A., and C. K. Laird, Measurements of nitrous oxide emissions from p.f. fired power stations, *Atmos. Environ., 24 (A), 1199-1206, 1990*

[131] Sokolov, A. P. and P. H. Stone, Description and validation of the MIT version of the GISS 2D Model. MIT Joint Program on the Science and Policy of Global Change, Report No. 2, MIT, 1995

[132] Steele, L.P., P.S.Fraser, R.A. Rasmussen, M.A.K. Khalil, I.J. Conway, A.J. Crawford, R.H. Gammon, K. A. Masarie, and K.W. Thoning, The global distribution of methane in troposphere, *J. Atmos. Chem., 5, 125-171, 1987*

[133] Swift, M.J., *Decomposition in Terrestrial Ecosystem*, Berkeley, Uniersity of California Press, 1979

[134] Takai, Y. and E. Wada, 1990. Methane formation in waterlogged paddy soils and its controlling factors. In: *Soils on a warmer Earth (eds H.W. Scharpenseel, M. Schomaker and A. Ayoub). Developments in Soil Science 20, Elsevier, Amsterdam. pp. 101-107*

[135] Tans, P. P., I. Y. Fung, and T. Takahashi, Observational constraints on the global atmospheric CO_2 budget, *Science, 247, 1431-1438, 1990*

[136] Taylor, J.A., G. Brasseur, P. Zimmerman, and R. Cicerone, Study of the sources and sinks of methane and Methyl Chloroform using a global 3-D Lagrangian tropospheric tracer model, *J.G.R., 96, 3013-3044, 1991*

[137] Taylor, J.A., A global three-dimensional lagrangian tracer transport modelling study of the sources and sinks of nitrous oxide, *Mathematics and Computers in Simulation, 33, 597-602, 1992*

[138] Thiemens, M.H., W.C. Trogler, Nylon Production: An unknown source of atmospheric nitrous oxide, *Science, 251, 932-934, 1991*

[139] Thornthwaite, C. W., An approach toward a rational classification of climate, *Geogr. Rev., 38, 55-89, 1948*

[140] Trenberth, K. E., W. G. Large, and J.G. Olson, The effective drag coefficient for evaluating wind stress over the oceans, *J. Clim., 2, 1507-1516, 1989*

[141] Wang, C., R. Prinn, and A. Sokolov, A global interactive chemistry and climate model, manuscript in preparation, 1996

[142] Wanninkhof, R., Relationship between wind speed and gas exchange over the ocean, *J. G. R., 97, 7373-7382, 1992*

[143] Watson, R. T., L.G. Meira Filho, E. Sanhueza, and A. Janetos, Sources and sinks, in Climate Change 1992, The Supplementary Report to the IPCC Scientific Assessment, edited by J. T. Houghton, B. A. Callander, and S.K. Varney, pp. 25-46, University Press, Cambridge, Mass., 1992

[144] Watts, D. G., and R. J. Hanks, A soil-water-nitrogen model for irrigated corn on sandy soils, *Soil Sci. Soc. Am. J., 42, 492-499, 1978*

[145] Whalen, S. C., and W. S. Reeburgh, A methane flux time-series for tundra environments, *Global Biogeochemical Cycles, 2, 399-410, 1988*

[146] Whalen, S. and W. Reeburgh, A methane flux transect along the trans-Alaskan pipeline haul road, *Tellus, 42B, 237-249, 1990*

[147] Whalen, S. and W. Reeburgh, Interannual variations in tundra methane emissions: A four-year time series at fixed sites, *Global Biogeochemical Cycles, 6, 139-159, 1992*

[148] Weiss, R.F., and B.A. Price, Nitrous oxide solubility in water and seawater, *Marine Chemistry, 8, 347-359, 1980*

[149] Weiss, R.F., The temporal and spatial distribution of tropospheric nitrous oxide, *J. G. R., 86, 7185-7195, 1981*

[150] Weiss, R.F., F.A. Van Woy, and P.K. Salameh, Surface Water and Atmospheric Carbon Dioxide and Nitrous Oxide Observations by Shipboard Automated Gas Chromatography: Results from Expeditions Between 1977 and 1990, ORNL/CDIAC, NDP-044, Oak Ridge National Laboratory, U.S. Dept. of Energy, 1992

[151] Wetherald, R. T. and Manabe, S., Cloud feedback processes in a general circulation model, *J. Atmos. Sci., 45, 1397-1415, 1988*

[152] Williams, E.J., G.L. Hutchinson and F.C. Fehsenfeld, NO_x and N_2O emissions from soil, *Global Biogeochemical Cycles, 6, 351-388, 1992*

[153] Williams, R.J. and R. L. Crawford, Methane production in Minnesota peatlands, *Applied and Environmental Microgiology, 47, 1266-1271, 1984*

[154] Woldendorp, J.W., Nutrients in the rhizosphere, Agricultural yield potentials in continental climates, *Proc. Coll. Intl. Potash Institute, 16th, Bern, 99-125, 1981*

[155] Wu, J., Wind-induced drift currents, *J. Fluid Mech., 68, 49-70, 1975*

[156] Xiao, X., D.W. Kicklighter, J.M. Melillo, A.D. McGuire, P.H.Stone and A.P. Sokolov, Linking a global biogeochemical model with a 2-dimensional climate model: Implications for the global carbon budget, *Tellus, B, in press, 1996*

[157] Yamane, I., and K. Sato, Effect of temperature on the formation of gases and ammonium nitrogen in the waterlogged soils, *Sci. Rep. Res. Inst., 12, 31-46, 1961*

[158] Yavitt, J.B., G.E. Lang and R. K. Wieder, Control of carbon mineralization to CH_4 and CO_2 in anaerobic Sphagnum-derived peat from Big Run Bog, West Virginia, *Biogeochemistry, 4, 141-157, 1987*

[159] Yokoyama, T., S. Nishinomiya, and H. Mastsuda, N_2O emissions from fossil fuel fired power plants, *Environ. Sci. Technol., 25, 347-348, 1991*

[160] Yoshida, N., ^{15}N–depleted N_2O as a Product of Nitrification, *Nature, 335, 528-529, 1988*

[161] Yoshida, et al., Nitrification Rates and ^{15}N Abundances of N_2O and NO_3^- in the Western North Pacific, *Nature, 342, 895-897, 1989*

[162] Zardini, D., D. Raynaud, D. Scharffe and W. Seiler, N_2O measurements of air extracted from Antarctic ice cores: implications on atmospheric N_2O back to the last glacial-interglacial transition, *Journal of Atmospheric Chemistry, 8, 189-201, 1989*